

Chamber Investigations of Secondary Organic Aerosol Formation

Thesis by
David Rea Cocker III

In Partial Fulfillment of the Requirements
for the Degree of
Doctor of Philosophy

California Institute of Technology
Pasadena, California

2001

(Defended November 27, 2000)

© 2001

David Cocker

All Rights Reserved

Dedicated with love to Kathy
and my Mom and Dad

Acknowledgements

While preparing to write this section of my thesis, I have had a chance to reflect on all of the people who have contributed to my research efforts and made life during my stay at Caltech more enjoyable. A lot of people have been a part of my graduate school experience, and I wish I had the time and space to thank everyone. However, in the interest of finishing my thesis by the end of the year, I'd like to highlight the people who have had the greatest impact.

Most graduate students are lucky to get a good advisor. I had two, both of which aided me tremendously both in the lab and out. Professor John Seinfeld gave me tremendous support and, though he was very busy, he always seemed to have time when I needed advice on a current chamber crisis. When I wanted to move the outdoor chamber lab indoors, he patiently listened to my reasoning and gave me the rare opportunity to build a new lab. And when we were through discussing the current research project, I could always discuss the latest softball highlights.

Professor Rick Flagan was my instrument guru as well as my second advisor. He always took the time to listen and reason out my latest concern over the instrument's operation—be it a charger, a Friday evening spike or some other mystery of the roof lab. He also exhibited patience, even late at night as Mother Nature was relocating my lab. All the conversations and advice to improve the lab and my life as a graduate student were greatly appreciated.

I would also like to acknowledge the support of the National Science Foundation for my first three years of graduate study.

Of course, thanks go out to all the members of the roof crew. Rob, for showing me the ropes of the roof lab as well as being a good friend. Jian, Markus and Brian--three great post-docs to share ideas and a lab with. Nathan, for helping me with the new lab and all of those circuits. Don, for providing the inversion routine and all the help with the DMAs. Jay, for loaning me bits and pieces of his projects. Thanks also to the new roof crew--Hong, Roya and Keith, who aided in my final experiments. To the rest of the Seinfeld-Flagan group, especially Peter and Thanos, thanks for giving me the modeler's point of view. Although not part of the group, I would like to thank Professor Simon Clegg for his work on modeling the α -pinene/ozone experiments.

Other people in the Caltech community I would like to thank include my classmates—Dan, Yael, Tina, and Catherine—we all had a lot of fun. All the members of the “A” league teams who made softball (and the summer) great and played well enough to keep the trophy TWICE. Elizabeth, Ann, and Maria, for putting up with all my purchase requests, reimbursement requests, requests to talk to John...thanks for taking such good care of a graduate student. Rich, thanks for building me all those contraptions.

A lot of support from friends and family helped make this thesis a reality. Mom and Dad, while you may not have understood exactly what I was doing, I could not have gotten here without your support. Thanks for all the stress relief golf breaks, dinners, and a retreat when it was necessary to get away. Thanks to all my family for calling me up for barbecues and get-togethers to get me out of the lab (Grandma and the Fernholtzs). Albert, thanks for all the encouragement, basketball, movies, dinners, hearts and spades...Thanks also to the Smihula family for support, wiring, and coming out for the radiator games.

To my loving wife, Kathy, I cannot possibly begin to acknowledge all the ways you have been a part of this work. You have truly supported me in every way imaginable. You have been an editor, a lab assistant, a GC technician, a wiring expert, and so much more. You have listened and endured with me as my instruments quit and experiments failed and somehow always provided me with the encouragement I needed. Most of all, you have provided me with many laughs and great times helping make this all possible. Thank you. I love you.

Abstract

Hydrocarbons in the atmosphere undergo oxidation that can lead to the formation of semi-volatile products. These products undergo gas-to-particle conversion to form secondary organic aerosol (SOA). Reaction chambers provide a controlled environment in which gas-to-particle conversion is investigated. First, an extensive investigation into the aerosol forming potential of 14 biogenic hydrocarbons is reported.

Traditionally, chamber experiments have been performed at relative humidity levels such that the aerosol investigated is water-free. However, atmospheric conditions are typically such that ambient aerosol contains water. A new facility to improve measurement of SOA formation under humid conditions is described. A comprehensive study on how the presence of water affects gas-to-particle partitioning in the α -pinene ozonolysis and m-xylene and mesitylene photooxidation systems is reported.

The diurnal trends in the hygroscopic nature of Pasadena, CA, aerosol is reported for late summer, 1999. Presented are additional investigations into the identification of products resulting from ozonolysis of α -pinene, β -pinene, sabinene, Δ^3 -carene, and cyclohexene. A field campaign to identify similar monoterpene oxidation products in a forest environment is presented. Finally, an estimate of the global aerosol burden from biogenic hydrocarbons is provided.

Table of Contents

Acknowledgements	iv
Abstract	vii
List of Tables	xiii
List of Figures	xvi
1. Introduction	1
2. Aerosol formation from the oxidation of biogenic hydrocarbons	7
2.1 Introduction	8
2.2 Mechanism of secondary organic aerosol formation	11
2.3 Fractional aerosol yield	12
2.4 Chamber studies	15
2.5 Experimental procedure	16
2.6 Yields of biogenic organics in photooxidation experiments	21
2.7 Yields of biogenic organics in ozonolysis and nitrate radical experiments	23
2.8 Contribution of individual oxidants to aerosol formation	24
2.9 Conclusions	27
2.10 References	28
3. Hygroscopic Properties of Pasadena, California Aerosol	52
3.1 Introduction	53
3.2 Experimental Procedure	55
3.3 Analysis of 50 nm and 150 nm particle data	57

3.3.1	Hygroscopic behavior of 50 nm particles	62
3.3.2	Hygroscopic behavior of 150 nm particles	63
3.4	Summary and conclusions	64
3.5	References	65
4.	State-of-the-art chamber facility for studying atmospheric aerosol chemistry	80
4.1	Introduction	81
4.2	Facility overview	83
4.3	System preparation	86
4.3.1	Reactant injection	86
4.3.2	Seed generation	86
4.4	Gas-phase instrumentation	87
4.5	Aerosol instrumentation	88
4.5.1	Size distribution measurements	88
4.5.2	Number concentration	91
4.5.3	Hygroscopicity measurements	91
4.6	Aerosol formation and evolution experiments	93
4.6.1	Dry nucleation	93
4.6.2	Humid nucleation	93
4.6.3	Dry seed, dry conditions	94
4.6.4	Dry seed, elevated relative humidity	94
4.6.5	Aqueous seed, elevated relative humidity	95
4.7	Aerosol dynamics	96

4.8	References	98
5.	The effect of water on gas-particle partitioning of secondary organic aerosol: I. α -pinene/ozone system	114
5.1	Introduction	115
5.2	Experimental description	117
5.3	Aerosol Yield	120
5.4	Experimental Protocol	121
5.4.1	Dry nucleation	122
5.4.2	Humid nucleation	122
5.4.3	Dry seed, dry conditions	123
5.4.4	Dry seed, elevated relative humidity	123
5.4.5	Aqueous seed, elevated relative humidity	124
5.5	Effect of relative humidity on SOA formation in the α -pinene/ozone system	125
5.5.1	Dry seed vs. dry homogeneous nucleation	126
5.5.2	Dry seed with humid conditions	126
5.5.3	Aqueous salt solutions effect on SOA yield	127
5.5.4	Hygroscopic properties of α -pinene/ozone aerosol products	128
5.6	Thermodynamic modeling of organic-inorganic-water equilibria	130
5.6.1	Salt aerosols	130
5.6.2	Water uptake by condensed organic material	132

5.6.3	Two-component aerosol model	134
5.6.3.1	Two-product aerosol model	135
5.6.3.2	Multi-product aerosol model	139
5.7	Existence of multiple phases	145
5.8	Aerosol-phase chemistry—another potential salting effect	146
5.9	Conclusions	147
5.10	References	148
6.	The effect of water on gas-particle partitioning of secondary organic aerosol:	
II.	<i>m</i> -xylene and 1,3,5-trimethylbenzene photooxidation systems	175
6.1	Introduction	176
6.2	Experimental description	177
6.3	Hygroscopic properties of <i>m</i> -xylene and 1,3,5-TMB aerosol oxidation products	178
6.4	Effect of relative humidity on SOA formation for <i>m</i> -xylene and 1,3,5-TMB photooxidation	182
6.5	Product identification	185
6.5.1	Sampling techniques	185
6.5.2	Sample extraction and derivatization	186
6.5.2.1	Impactor samples	186
6.5.2.2	Impinger samples	187
6.5.3	GC/MS analysis	187
6.5.4	Identification of products in the <i>m</i> -xylene and 1,3,5-TMB photooxidation experiments.	187

6.5.5	<i>m</i> -Xylene photooxidation	188
6.5.5.1	Aerosol-phase composition	188
6.5.5.2	Gas-phase composition	189
6.5.6	1,3,5-TMB photooxidation experiments	189
6.5.6.1	Aerosol-phase composition	189
6.5.6.2	Gas-phase composition	190
6.5.7	Implications of the molecular identification results	190
6.6	Conclusions	191
6.7	References	192

A. Appendix

A.1	Gas-phase ozone oxidation of monoterpenes: gaseous and particulate products	204
A.2	Aerosol formation in the cyclohexene-ozone system	286
A.3	Observation of gaseous and particulate phase products of monoterpene oxidation in forest atmospheres	315
A.4	Estimate of global atmospheric organic aerosol from oxidation of biogenic hydrocarbons	333

List of Tables

2.1	Reaction rate constants for the oxidation of biogenic hydrocarbons	34
2.2a	Initial conditions and data for photooxidation experiments.	35
2.2b	Initial conditions and data.	38
2.3	Aerosol yield parameters for the photooxidation of biogenic hydrocarbons.	40
2.4	Aerosol yield parameters for the ozone and nitrate radical oxidation of biogenic hydrocarbons.	41
2.5	Simulations of gas-phase chemistry.	42
2.6	Individual contributions to aerosol formation.	44
3.1	Available data on hygroscopic aerosol growth.	69
4.1	Instrumentation summary.	100
4.2	Calculated ratios of rate constants for photolysis reaction for selected light sources.	101
4.3	Characteristic time scales for processes occurring in the chamber.	102
5.1	Experimental results.	154
5.2	Empirically fit partitioning coefficients.	156
5.3	Hygroscopic growth factors obtained from TDMA measurements.	157
5.4	Phase partitioning predicted from equation (5.1).	158
5.5	Products of the oxidation of α -pinene by ozone.	159
5.6	UNIFAC (Fredensland <i>et al.</i> , 1975) group compositions of the oxidation products.	160
5.7	Predicted phase partitioning.	161

6.1	Conditions for <i>m</i> -xylene photooxidation experiments.	195
6.2	Conditions for 1,3,5-trimethylbenzene experiments.	196
6.3	Carbonyl, alcohol, and carboxylic acid products detected in impactor samples.	197
6.4	Carbonyl, alcohol, and carboxylic acid products detected in impinger samples.	198
A.1.1	Initial conditions and results ozone-terpene reactions.	244
A.1.2	Denuder and filter collection efficiencies of selected products.	244
A.1.3	Relative recoveries of select multifunctional compounds vs. recovery standard.	245
A.1.4	Products from ozone oxidation of β -pinene.	246
A.1.5	Products from ozone oxidation of sabinene.	248
A.1.6	Products from ozone oxidation of α -pinene.	250
A.1.7	Products from ozone oxidation of Δ^3 -carene.	251
A.1.8	Products and their surrogates for quantification.	253
A.1.9	Gaseous and particulate product yields in the β -pinene/O ₃ reaction.	254
A.1.10	Gaseous and particulate product yields in the sabinene/O ₃ reaction.	256
A.1.11	Gaseous and particulate product yields in the α -pinene/O ₃ reaction.	257
A.1.12	Gaseous and particulate product yields in the Δ^3 -carene/O ₃ reaction.	258
A.1.13	Gas-particle partitioning coefficients (m ³ μ g ⁻¹) of individual products at 306-308 K.	259
A.1.14	Sub-cooled liquid vapor pressure estimates.	260
A.2.1	Experimental conditions.	302
A.2.2	Denuder collection efficiencies for individual cyclohexene/ozone reaction products.	303

A.2.3	Chemical structures of products of the cyclohexene-ozone reaction.	304
A.2.4	Chemical compounds used as standards or surrogates for quantification.	306
A.3.1	Monoterpene oxidation products detected at forest sites.	327
A.3.2	Monoterpene oxidation products in filter samples collected in Kejimikujik National Park, Nova Scotia.	330
A.3.3	Gaseous and particulate monoterpene oxidation products in samples collected in San Bernardino National Forest, California.	331
A.4.1	Aerosol yield parameters for biogenic organics.	346
A.4.2	OH and O ₃ oxidation patterns for bicyclic alkenes.	346
A.4.3	Estimated species contributions to global emissions.	347

List of Figures

2.1	Chemical structures of the biogenic hydrocarbons investigated.	46
2.2	Secondary organic aerosol yields for the bicyclic olefins tested as a function of organic mass concentration in photooxidation experiments.	47
2.3	Secondary organic aerosol yields for the cyclic diolefins tested as a function of organic mass concentration in photooxidation experiments.	47
2.4	Secondary organic aerosol yields for the sesquiterpenes tested as a function of organic mass concentration in photooxidation experiments.	48
2.5	Secondary organic aerosol yields for the acyclic triolefins and oxygenated terpenes tested as a function of organic mass concentration in photooxidation experiments.	48
2.6	Possible ring-opening mechanism for the reaction between OH and sabinene.	49
2.7	Secondary organic aerosol yields for the bicyclic olefins tested as a function of organic mass concentration in ozonolysis experiments.	50
2.8	Secondary organic aerosol yields for the bicyclic olefins tested as a function of organic mass concentration in NO ₃ experiments.	50
2.9	Example output from SAPRC90b gas-phase chemical mechanism.	51
3.1	Experimental TDMA system.	73
3.2	Number of discernible peaks vs. time of day for the aerosol classified dry of 49.7 nm classified aerosol.	74
3.3	Measured growth factors for log-normally fit peaks of 49.7 nm dry particles humidified to 89% relative humidity for August 17 to August 23.	75

3.4	Typical size distributions from DMA1, classification set to 49.6 nm.	76
3.5	Typical size distributions from DMA1, classification set to 148.5 nm.	77
3.6	Cumulative distributions for the entire 49.7 nm classified aerosol, humidified to 89% relative humidity.	78
3.7	Cumulative distributions for the entire 148.5 nm classified aerosol, humidified to 89% relative humidity.	79
4.1	Absorption spectra for 2 mil FEP Teflon film.	103
4.2	Block diagram of gas- and aerosol-phase instrumentation.	104
4.3	Light spectrum from Carter <i>et al.</i> (1995).	105
4.4	Flow scheme for clean-air system.	106
4.5	Seed particle generation schematic.	107
4.6	Automated scanning electrical mobility spectrometer.	108
4.7	Condensation particle counter dilution system.	109
4.8	Tandem differential mobility analyzer schematic.	110
4.9	Sample TDMA size distribution spectrum.	111
4.10	Cyclohexene and total aerosol mass concentration as a function of time.	112
4.11	Illustration of different processes occurring within the chamber.	113
5.1	Summary of experimental yield data obtained.	162
5.2	Summary of experimental yield data taken under dry conditions (RH<2%) in the presence of dry (NH ₄) ₂ SO ₄ , dry (NH ₄)HSO ₄ and no seed present.	163
5.3	Aerosol yield corrected for water uptake of organics for the nucleation at RH = 50% and for (NH ₄) ₂ SO ₄ seed aerosol, dry, at RH = 50%.	164

5.4	Growth factors (G_F) for α -pinene/ O_3 SOA from dry conditions to 85% RH (Experiment 12/6/99) as a function of the organic fraction of the aerosol.	165
5.5	Equilibrium water activity, equal to RH (solid lines), and density (dashed lines) for three aqueous salt solutions as a function of aqueous-phase salt mole fraction.	166
5.6	Equilibrium water activity, equal to RH, for mixtures of α -pinene SOA and water as a function of liquid-phase mole fraction of SOA.	167
5.7	Measured and calculated growth factors (RH from 0 to 85%) at 301 K for aerosols containing a mixture of organic compounds and $(NH_4)_2SO_4$.	168
5.8	Measured and calculated yield for systems without seed aerosol at 2% and 50% RH.	169
5.9	Measured and calculated yield at 50% RH for systems including $1.9 \times 10^{-7} \text{ mol m}^{-3} (NH_4)_2SO_{4(aq)}$ seed aerosol.	170
5.10	Measured and calculated yield at 50% RH for systems including $1.98 \times 10^{-7} \text{ mol m}^{-3} CaCl_{2(aq)}$ seed aerosol.	171
5.11	Measured and calculated yields for systems without seed aerosol at 2% and 50% RH.	172
5.12	Aerosol- and gas-phase concentrations of α -pinene oxidation products, for systems without salt seeds at 2% RH, calculated using the multi-product model described in section 5.6.3.2.	173
5.13	Photograph of multiple phase system.	174
6.1a	Hygroscopic growth factors (0 to 85% relative humidity) for pure <i>m</i> -xylene (top) and 1,3,5-TMB (bottom) oxidation products as a function of time.	199

6.1b	Hygroscopic growth factors (0 to 85% relative humidity) for pure α -pinene oxidation products as a function of time.	199
6.2	SOA yield curves for <i>m</i> -xylene and 1,3,5-TMB photooxidation experiments.	200
6.3	Comparison of <i>m</i> -xylene SOA yield curve in current experiments (T = 293 K) to that obtained by Odum <i>et al.</i> (1996) (T = 307 K).	201
6.4a	Chromatogram of impactor sample of <i>m</i> -xylene photooxidation showing ions with m/z 181+73+75 with all carbonyl, carboxylic, and/or hydroxyl compounds identified.	202
6.4b	Chromatogram of impinger sample of <i>m</i> -xylene photooxidation showing ions with m/z 181+73+75 with all carbonyl, carboxylic, and/or hydroxyl compounds identified.	202
6.5a	Chromatogram of impactor sample of 1,3,5-TMB photooxidation showing ions with m/z 181+73+75 with all carbonyl, carboxylic, and/or hydroxyl compounds identified.	203
6.5b	Chromatogram of impinger sample of 1,3,5-TMB photooxidation showing ions with m/z 181+73+75 with all carbonyl, carboxylic, and/or hydroxyl compounds identified.	203
A.1.1	Chromatogram of products from β -pinene/O ₃ reaction.	261
A.1.2	Methane CI mass spectra for the derivatives of products from ozone oxidation of β -pinene.	262
A.1.3	Chromatogram of products from sabinene/O ₃ reaction.	268

A.1.4	Mass spectra for the derivatives of two products (S_8 and S_{12}) from ozone oxidation of sabinene.	269
A.1.5	Chromatogram of products from α -pinene/ O_3 reaction.	270
A.1.6	Mass spectra for the derivatives of products from ozone oxidation of α -pinene.	271
A.1.7	Chromatogram of products from Δ^3 -carene/ O_3 reaction.	275
A.1.8	Methane CI mass spectra for the derivatives of products from ozone oxidation of Δ^3 -carene.	276
A.1.9	Amount of nopinone formed versus the amount of β -pinene reacted.	278
A.1.10	Measured $\log(K_{om,i})$ versus estimated $\log p_L^o$ for the major products in the β -pinene/ O_3 and α -pinene/ O_3 systems.	278
A.1.11	Fraction of pinic acid in aerosol-phase as a function of organic aerosol mass concentration.	279
A.1.12	Top: Time-dependent secondary organic aerosol yields as a function of organic aerosol mass for two α -pinene/ O_3 experiments. Bottom: α -Pinene mixing ratio and organic aerosol mass concentration as a function of time.	280
A.1.13	Top: Time-dependent secondary organic aerosol yields as a function of organic aerosol mass for sabinene/ O_3 experiments. Bottom: Sabinene mixing ratio and organic aerosol mass concentration as a function of time.	281
A.1.14	Reaction mechanism of O_3/β -pinene reaction.	282
A.1.15	Reaction mechanism of O_3 /sabinene reaction.	283
A.1.16	Formation mechanism for A_3 and A_7 in the O_3/α -pinene reaction.	284
A.1.17	Reaction mechanism of O_3/Δ^3 -carene reaction.	285

A.2.1	Cyclohexene and total aerosol mass concentration ΔM_0 as a function of time.	307
A.2.2	Chromatogram of a filter sample.	308
A.2.3	Molecular distribution of the particle composition.	309
A.2.4	Proposed reaction mechanism of the cyclohexene-ozone reaction leading to the products observed in this study.	310
A.2.5	The Criegee biradical can react with aldehydes to form a second ozonide.	314
A.3.1	Chemical ionization mass spectrum for the derivative of a C ₉ dioxo carboxylic acid detected in aerosol samples.	332
A.3.2	Formation pathways for a C ₉ dioxo carboxylic acid from oxidation of limonene.	332

Chapter 1

Introduction

Photochemical smog is a complex mixture of gas-phase and aerosol-phase pollutants. Oxides of nitrogen (NO_x) are released to the atmosphere as a by-product of combustion. Hydrocarbons are released from biological, combustion and industrial processes. The coupled interactions between NO_x and hydrocarbons, driven by sunlight, lead to elevated levels of atmospheric ozone, a key component of photochemical smog. Other gas-phase pollutants may include SO_2 , an important precursor for acid rain, chlorofluorocarbons, associated with stratospheric ozone depletion and greenhouse gases such as CH_4 and CO_2 . Gas-phase pollutants may undergo gas-to-particle conversion to form atmospheric aerosol.

An aerosol is defined as a suspension of fine solid or liquid particles in a gas. Aerosols can be primary, i.e., particles directly emitted from a source such as brake dust or secondary, i.e., formed by gas-to-particle conversion processes. Aerosol formed from semi-volatile organic products is referred to as secondary organic aerosol (SOA). SOA can account for as much as 80% of the mass concentration of organic aerosol in the environment [Turpin & Huntzicker, 1995]. High concentrations of atmospheric aerosols are linked to cardiovascular and respiratory distress, increased morbidity and mortality, visibility degradation, plant and property damage. Aerosol can also act as cloud condensation nuclei affecting the earth's radiative balance directly by backscattering light as well as indirectly through increased cloud cover. Aerosols are therefore of urban, rural and global importance.

Chamber studies have been instrumental in the understanding of gas-phase atmospheric chemistry and atmospheric aerosol formation. Chambers provide a medium for a methodical investigation and isolation of key chemical and microphysical processes

occurring within the atmosphere. The key parameters and processes can then be incorporated into regional and global air-shed models used for design of air quality control strategies. Chamber systems also allow for research of individual hydrocarbon (or other gas-phase pollutants) oxidation processes so that key pollutants may be targeted for control.

A myriad of products are formed from the oxidation of hydrocarbons that, if their resulting vapor pressures are sufficiently low enough, can partition between the gas- and aerosol-phase [Odum *et al.*, 1996]. The SOA formation potential of a parent hydrocarbon is defined by its mass-based yield, Y , that, in turn is the sum of the individual SOA yields of each product, Y_i . The SOA yield of a single oxidation product is related to two key parameters: α_i , the mass-based stoichiometric fraction of product i produced from the oxidation of the parent hydrocarbon; and $K_{om,i}$, the gas-particle partitioning coefficient for product, i . Yield is then defined as

$$Y = \sum Y_i = M_o \sum \frac{\alpha_i K_{om,i}}{1 + K_{om,i} M_o} \quad (1)$$

where M_o ($\mu\text{g}/\text{m}^3$) is the organic mass concentration in the aerosol-phase. It has been found sufficient to assume a two-product distribution, one of relatively high volatility and one of relatively low volatility to empirically fit the experimental data obtained.

Natural and agricultural plant emissions of non-methane hydrocarbons (NMHC) are estimated at 491-1050 TgC/year, exceeding anthropogenic emissions of NMHC (80 TgC/year) by an order of magnitude [Muller, 1992; Guenther *et al.*, 1995]. Biogenic hydrocarbons react quickly with hydroxyl radicals, ozone, and nitrate radicals to form ozone and atmospheric aerosols. Isoprene (C_5H_8) and monoterpenes ($\text{C}_{10}\text{H}_{16}$) comprise

the bulk of biogenic emissions. Isoprene is a straight chain, five-carbon dialkene and is believed to be a by-product of photorespiration. Monoterpenes are comprised of two units of isoprene and are associated with biophysical processes occurring in plant leaves and as a defense against herbivory. Because of their volatility, isoprene and its oxidation products do not produce aerosol. Monoterpenes are large and less volatile and are expected to produce aerosol.

A comprehensive investigation of the SOA formation potential of 14 biogenic compounds is reported in Chapter 2. The 14 hydrocarbons include bicyclic alkenes, cyclic dialkenes, open chain trialkenes, sesquiterpenes (3 isoprene blocks) and two oxygenated terpenes. The three oxidation pathways studied in these experiments are reaction with ozone, hydroxyl radical, and nitrate radical. A series of experiments investigate the individual oxidant contribution to SOA formation. Due to their atmospheric abundance, the four monoterpenes chosen for this part of the study are α -pinene, β -pinene, sabinene, and Δ^3 -carene.

During the construction of a new indoor facility, the hygroscopic nature of Pasadena, CA, aerosol was examined for six weeks in August and September 1999. To do so, a tandem differential mobility analyzer (TDMA), capable of measuring the water uptake of a particle when relative humidity is increased, was designed based on the original design of Rader and McMurry [*Rader and McMurry*, 1986]. Particle hygroscopicity provides insight into the chemical composition of the aerosol. The results of this investigation are provided in Chapter 4.

After the biogenic study, the chamber was moved into an environmentally controlled laboratory. The new laboratory provided control of temperature, relative

humidity and UV irradiation intensity within the chamber. The accuracy and stability of the aerosol instrumentation was greatly enhanced by automating the equipment with feedback control using the Labview® software package. The new chamber facility, including the instrumentation package designed, is described in detail in Chapter 4.

It is expected that the aerosol-phase water will affect the gas-particle partitioning. α -Pinene, *m*-xylene and 1,3,5-TMB were studied to determine how their SOA yields are affected by the presence of water. α -Pinene was chosen from the monoterpene isomers as the α -pinene/O₃ system is well characterized. α -Pinene contains a single bond available for oxidation and can be investigated using only O₃ as the oxidizing agent. Aromatic species comprise a significant fraction of the gas-phase hydrocarbons in the urban atmosphere. *m*-Xylene and 1,3,5-TMB are investigated under full photooxidation conditions. Chapter 5 reports on the α -pinene/ozone system experiments and results, and Chapter 6 reports on the *m*-xylene and mesitylene systems.

Several other investigations are presented in the Appendices. In order to better understand gas-particle partitioning, it was important to identify the composition of the secondary aerosol produced in the chamber. Appendix I contains the results from an investigation into the gas- and aerosol-phase products of α -pinene, Δ^3 -carene, β -pinene and sabinene ozonolysis reactions. Appendix II is a similar study on the products of cyclohexene/O₃ reaction. Additionally, a field-campaign to Big Bear, CA, in which the composition of the gas- and aerosol-phase in a pine forest was investigated. The investigation found similar organic oxidation products to those identified from chamber experiments, as well as several monoterpenes and a sesquiterpene. This study is found in Appendix III.

Chamber measurements of the aerosol formation potential of the biogenic compounds were used to make an estimate of the global aerosol burden from a global emissions inventory. The biogenic emissions inventory was based on different ecosystems and aerosol formation was implemented in a 3-D transport model. The results of the model are found in Appendix IV.

References:

- Guenther, A., et al., A global model of natural volatile organic compound emissions, *J. Geophys. Res.*, 100, 8873-8892, 1995.
- Müller, J. F., Geographical distribution and seasonal variation of surface emissions and deposition velocities of atmospheric trace gases, *J. Geophys. Res.*, 97, 3787-3804, 1992.
- Odum, J.R., T. Hoffmann, F. Bowman, D. Collins, R.C. Flagan, and J.H. Seinfeld, Gas/particle partitioning and secondary organic aerosol yields, *Environ. Sci. Technol.*, 30, 2580-2585, 1996.
- Rader, D.J. and McMurry, P.H. (1986). Application of the tandem differential mobility analyzer to studies of droplet growth or evaporation. *J. Aerosol Sci.* 17:771-787.
- Turpin, B.J., and J.J. Huntzicker, Identification of secondary organic aerosol episodes and quantitation of primary and secondary organic aerosol concentrations during SCAQS, *Atmos. Environ.*, 29, 3527-3544, 1995.

Chapter 2

Organic Aerosol Formation from the Oxidation of Biogenic

Hydrocarbons

Reference: R.J. Griffin, D.R. Cocker III, R.C. Flagan, and J.H. Seinfeld, *J. Geophys. Res.*, *104*, 3555-3567, 1999.

2.1 Introduction

A variety of organic compounds are emitted to the atmosphere from both natural and agricultural plants [Isidorov *et al.*, 1985; Arey *et al.*, 1991b; Fehsenfeld *et al.*, 1992; Winer *et al.*, 1992; Arey *et al.*, 1995]. Isoprene (C_5H_8), monoterpenes ($C_{10}H_{16}$), and sesquiterpenes ($C_{15}H_{24}$) comprise the majority of these emissions, although oxygenated and sulfur-containing species have also been identified [Arey *et al.*, 1991a; König *et al.*, 1995; Puxbaum and König, 1997]. Estimates of biogenic organic emissions have been made on global, national (e.g., the United States), and regional (e.g., the South Coast Air Basin of California or the Mediterranean region) bases. Total annual global biogenic organic emissions are estimated to range from 491 to 1150 TgC, greatly exceeding the 98 TgC of total organics estimated to be emitted from anthropogenic sources [Müller, 1992; Guenther *et al.*, 1995]. Averaged over the United States, biogenic emissions are estimated to be of the same order of magnitude of those from anthropogenic sources [Lamb *et al.*, 1993].

Significant uncertainty exists concerning the atmospheric reaction mechanisms of biogenic organics. The presence of unsaturated carbon-carbon bonds in these molecules leads to high reactivities [Atkinson *et al.*, 1995; Shu and Atkinson, 1995; Atkinson, 1997]. Because of the large quantity of emission and because of their atmospheric reactivity, biogenic nonmethane hydrocarbons (NMHCs) are predicted to play an important role in tropospheric chemistry [Chameides *et al.*, 1988; McKeen *et al.*, 1991; Roselle *et al.*, 1991; Fehsenfeld *et al.*, 1992]. Numerous studies investigating the nature of both gas-phase and aerosol-phase products formed from the reactions between biogenic NMHCs and the hydroxyl radical (OH), ozone (O_3), the $O(^3P)$ atom, and the nitrate radical (NO_3)

have been performed [*Stephanou and Stratigakis*, 1993; *Hakola et al.*, 1994; *Calogirou et al.*, 1995, 1997; *Berndt et al.*, 1996; *Grosjean and Grosjean*, 1997; *Hallquist et al.*, 1997; *Shu et al.*, 1997, *Vinckier et al.*, 1997; *Wängberg et al.*, 1997; *Alvarado et al.*, 1998; *Aschmann et al.*, 1998; *Griesbaum et al.*, 1998; *Yu et al.*, 1998].

Went [1960] was apparently the first to suggest the role of biogenic hydrocarbons in the formation of tropospheric aerosols. Higher molecular weight tropospheric hydrocarbons have been shown, upon oxidation, to produce semivolatile products that partition between the gas and aerosol phases [*Pandis et al.*, 1991; *Zhang et al.*, 1992; *Odum et al.*, 1996, 1997ab; *Hoffmann et al.*, 1997]. In the aerosol phase, these products are referred to as secondary organic aerosol (SOA). Among anthropogenic NMHCs, aromatics are the most important source of SOA [*Odum et al.*, 1996, 1997ab]. Among biogenic hydrocarbons, isoprene, because of its small size and the high volatility of its oxidation products, has been shown not to produce SOA at atmospheric levels [*Pandis et al.*, 1991]. Biogenic NMHCs larger than isoprene, however, are effective sources of aerosol [*Pandis et al.*, 1991; *Zhang et al.*, 1992; *Odum et al.*, 1996; *Hoffmann et al.*, 1997].

The importance of biogenic NMHCs in tropospheric aerosol formation will vary from area to area depending on climate, amount and nature of vegetation, and other environmental factors. In a Canadian forest, formation and growth of new particles have been attributed to oxidation of biogenic organics [*Leaith et al.*, 1999]. It has been estimated that under peak photochemical conditions, anywhere from 20-80% of the organic aerosol burden in the South Coast Air Basin of California is secondary in nature [*Turpin and Huntzicker*, 1995; *Schauer et al.*, 1996] and that 16% of the SOA during a

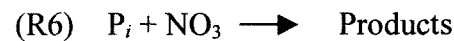
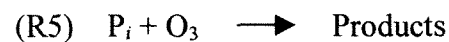
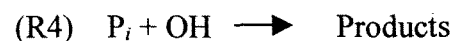
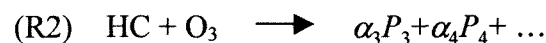
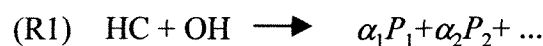
specific high-smog episode could be attributed to biogenic precursors [*Pandis et al.*, 1992]. Moreover, *Kaplan and Gordon* [1994] showed that a significant fraction of organic carbon associated with fine particulate matter in the Los Angeles area is not derived from fossil fuel precursors.

Previous experiments have provided limited information on the yields of SOA from α -pinene and β -pinene [*Pandis et al.*, 1991; *Zhang et al.*, 1992]. *Hoffmann et al.* [1997] reported the aerosol-forming potentials of a few other biogenic hydrocarbons, but too few experiments were performed to completely and quantitatively describe resulting aerosol formation. This study reports comprehensive outdoor chamber experiments on aerosol formation from 14 of the most prevalent biogenic organics. Differences in observed aerosol yields among compounds will be addressed on the basis of structural characteristics of the parent hydrocarbon. In sunlight-irradiated chamber experiments, OH, O₃, and NO₃ all contribute to hydrocarbon consumption and subsequent aerosol formation. To determine the individual contribution of each oxidant to aerosol formation for a parent hydrocarbon, gas-phase chemistry is modeled, from which the fraction of the parent hydrocarbon reacting with each oxidant can be determined. This is coupled with experiments in which O₃ or NO₃ is the only available oxidant. By deriving the quantitative parameters describing aerosol formation in these O₃-only or NO₃-only systems, it is possible to unravel the contribution to aerosol formation from each oxidant in full photooxidation experiments. An explanation of the mechanism of SOA formation, a derivation of the functional expression for aerosol yield, an expanded and specific list of the experiments performed, and a detailed experimental protocol all precede the

presentation of data from these experiments and the corresponding analysis and discussion.

2.2 Mechanism of Secondary Organic Aerosol Formation

Consider a parent hydrocarbon, HC, reacting with OH, O₃, and NO₃. A variety of products form:



While only two products are indicated for each reaction here, the actual number of products is much greater. (Later, a two-product model is used to quantitatively describe aerosol formation in full photooxidation experiments or ones in which a single oxidant is available.) The parameter α_i represents a stoichiometric factor relating the total amount of product i formed to the total amount of hydrocarbon that reacts. Later, this constant will be expressed on a mass basis, rather than the usual molar basis. As shown in (R4)-(R6), any of these products can, in principle, further react with any of the available oxidants, creating an even more complex and diverse mix of oxidation products.

For parent hydrocarbons containing roughly six or more carbon atoms, these products are semivolatile and, in the presence of sufficient organic aerosol, will partition between the gas and aerosol phases. The fraction of each product that partitions to the aerosol phase can be described on the basis of an equilibrium coefficient $K_{om,i}$. In principle, if the molecular nature of each product, as well as that of the aerosol organic phase, were known, $K_{om,i}$ could be calculated from first principles. In practice, such molecular-level information is not available, so $K_{om,i}$ values are determined experimentally.

2.3 Fractional Aerosol Yield

Secondary organic aerosol formation has been determined experimentally through investigation of the fractional aerosol yield Y [Pandis *et al.*, 1991; Zhang *et al.*, 1992; Odum *et al.*, 1996, 1997ab; Hoffmann *et al.*, 1997]. Because identification and quantification of individual oxidation products, for example, all the individual products in (R1)-(R6), are difficult, this yield is a convenient overall measure of the aerosol-forming potential of the secondary products of atmospheric oxidation of a parent organic molecule. This yield is defined as the ratio of the amount of SOA formed from the oxidation of a given parent compound to the amount of that compound that reacted:

$$Y = \frac{\Delta M_o}{\Delta HC} \quad (2.1)$$

where ΔM_o ($\mu\text{g m}^{-3}$) is the organic aerosol mass formed after the consumption of ΔHC ($\mu\text{g m}^{-3}$) of the given parent. The extent of gas/particle absorptive partitioning depends

on the amount of the condensed organic phase into which the products can be absorbed. Thus aerosol yield depends on the amount of organic matter present, M_o , into which the semivolatile products may partition. An outcome of this mechanism is that a secondary product can be absorbed into an organic phase, even if it exists in the gas phase below its own saturation concentration [Pankow, 1994ab; Odum *et al.*, 1996, 1997ab; Hoffmann *et al.*, 1997]. Pankow [1994ab] has defined an absorption equilibrium coefficient $K_{p,i}$ ($\text{m}^3 \mu\text{g}^{-1}$) for the partitioning of such a semivolatile component between the gas and particle phases as

$$K_{p,i} = \frac{F_{i,om}/(\text{TSP})}{A_i} = \frac{760RTf_{om}}{M_{om} 10^6 \zeta_i p_{L,i}^o} \quad (2.2)$$

where $F_{i,om}$ (ng m^{-3}) is the mass concentration of compound i in the absorbing organic matter (om) phase, A_i (ng m^{-3}) is its gas-phase mass concentration, TSP ($\mu\text{g m}^{-3}$) is the total suspended particulate concentration, R is the ideal gas constant, T (K) is the temperature, f_{om} is the fraction of the TSP that is absorbing om , M_{om} (g mol^{-1}) is the mean molecular weight of the absorbing phase, ζ_i is the activity coefficient of species i in the om phase, and $p_{L,i}^o$ (torr) is the vapor pressure (subcooled, if necessary) of compound i at temperature T . If only the absorbing organic phase is considered, a similar equilibrium constant can be defined as

$$K_{om,i} = \frac{F_{i,om}/M_o}{A_i} = \frac{K_{p,i}}{f_{om}} \quad (2.3)$$

simply by dividing $K_{p,i}$ by f_{om} . Equation (2.3) indicates that this new equilibrium constant is a function of the mass of the available organic phase into which a semivolatile product can be absorbed. Thus more of each product partitions to the organic aerosol phase as the total organic aerosol concentration increases. As a result, a parent compound that has undergone a certain amount of photooxidation, ΔHC , will exhibit a range of SOA yield values depending on the value of M_o . For the experiments described in this paper, $M_o = \Delta M_o$, since all organic aerosol mass is generated by the oxidation of the parent hydrocarbon. By combining the definitions of Y and $K_{om,p}$, a total mass balance, and a stoichiometric constraint, Y can be expressed as a function of ΔM_o by [Odum *et al.*, 1996]

$$Y = \Delta M_o \sum_i \left(\frac{\alpha_i K_{om,i}}{1 + K_{om,i} \Delta M_o} \right) \quad (2.4)$$

where ΔM_o , $K_{om,p}$ and α_i are defined as above. Yield data for over 30 individual parent compounds obtained in the Caltech outdoor chamber have been fit to (2.4) using a two product model, that is, with parameters, α_1 , α_2 , $K_{om,1}$ and $K_{om,2}$ [Hoffmann *et al.*, 1997; Odum *et al.*, 1996, 1997ab]. While it was given earlier that many products result from the atmospheric oxidation of a parent hydrocarbon, it has been shown that a two-product model is needed for most compounds to accurately describe the shape of the yield curve described by (2.4). Use of three or more products in the model has been proven to be superfluous. The four parameters derived in the two-product model can be seen as an adequate description of the stoichiometry and volatility of the complex mix of oxidation products.

It must be noted that this theory assumes that secondary products are unable to form a solution with existing seed aerosol. Accounting for the interactions between the organic compounds themselves allows it to be shown that such products can condense onto seed aerosol at concentrations lower than those predicted by saturation theory alone [Seinfeld and Pandis, 1998]. In this case, the threshold amount of the parent compound that must react to form SOA in the chamber is defined as ΔHC^* . After consumption of ΔHC^* , products condense onto seed aerosol to form an initial amount of SOA, which can then act as an absorptive medium. At this point, absorption becomes the dominant mechanism governing the partitioning of secondary products and, therefore, determining SOA yield, as in the atmosphere.

2.4 Chamber Studies

In this study the results of extensive outdoor chamber experiments on aerosol formation from 14 biogenic organic compounds are reported. These compounds include monoterpenes of chemical formula $\text{C}_{10}\text{H}_{16}$: α -pinene, β -pinene, Δ^3 -carene, and sabinene, bicyclic olefins that differ in the location of the double bond and the number of carbons associated with the secondary ring; limonene, α -terpinene, γ -terpinene, and terpinolene, cyclic diolefins that differ only in the location of a second double bond; and myrcene and ocimene, acyclic triolefins that differ only in the location of a third double bond. In addition, two sesquiterpenes of structure $\text{C}_{15}\text{H}_{24}$ (β -caryophyllene and α -humulene) and two oxygenated terpenes (linalool and terpinene-4-ol) are investigated. The structure of

each of these compounds is shown in Figure 2.1, and their reaction rate constants at 298K with OH, O₃, and NO₃ are given in Table 2.1.

As noted above, full sunlight-irradiated photooxidation experiments will have, in general, all three of OH, O₃, and NO₃ present, and, therefore, in general, aerosol yields will be the result of products generated in all three oxidation pathways. Experiments performed in a dark system with O₃ or NO₃ as the only available oxidants, in conjunction with results from gas-phase modeling, can then be used to determine the individual contributions to SOA formation from each oxidant. Experiments involving NO₃ as the only oxidant need be performed only for bicyclic olefins, as they are the slowest reacting of the compounds studied and will persist long enough for NO₃ to build up in the chamber. The other compounds are consumed completely by OH and O₃ in the sunlight-driven photooxidations prior to significant formation of NO₃.

2.5 Experimental Procedure

All experiments were performed in a sealed, 50-m³ Teflon chamber that has been described in detail previously [Odum *et al.*, 1996, 1997ab; Hoffmann *et al.*, 1997]. This chamber was normally divided in the center so that two experiments could be run under identical environmental conditions. Each resulting chamber had an estimated volume of 20 m³. Instruments for monitoring gas-phase components and a computer for acquiring aerosol data were operated from a laboratory adjacent to the chamber. Aerosol sampling instruments were operated directly next to the chamber in a closed cart that was maintained at a temperature of approximately 25°C. Between experiments, the chamber was continuously purged with compressed air and allowed to bake in sunlight for at least a

day. The compressed air was purified to remove organics, particulate matter, water, and NO_x species. Air in the chamber prior to the experiments contained no detectable hydrocarbons or particles and less than 5 ppb NO_x . Before entering the chamber, the air was passed through a rehumidifier containing distilled and deionized water so that the relative humidity during the experiments was approximately 5%.

At this time, it has not been determined how an increase in humidity influences the formation of SOA. Possible effects include differences in the chemical and physical nature of the absorbing phase such as a shift from an organic mixture to an aqueous-inorganic-organic mixture, a variation in the mean molecular weight of the absorbing phase, and a change in the activities of secondary products in the absorbing mixture. Deviation in any or all of these factors would affect the equilibrium partitioning coefficient of each product, thereby affecting the overall SOA yield. These issues are currently under study.

Gas-phase concentrations of the parent hydrocarbons in the chamber were monitored using a Hewlett Packard (Palo Alto, California) 5890 gas chromatograph (GC) equipped with a DB-5 column (J&W Scientific, Davis, California) and a flame ionization detector (FID). The temperature program for the GC began at -60°C , held for 1 min, ramped from -60°C to 150°C at a rate of $40^\circ\text{C min}^{-1}$, and then held for 1.5 min. Prior to each experiment, known volumes of a solution of the parent hydrocarbon and methylene chloride were vaporized into a small, 60-L Teflon bag filled with compressed air. Measurements from these bags were then used to calibrate the GC.

Following the GC calibration, seed particles of $(\text{NH}_4)_2\text{SO}_4$ were injected into the chamber to obtain initial particle concentrations of approximately 5,000-10,000 particles cm^{-3} . (Seed particles were not used in nitrate radical experiments.) The particles were

generated by atomizing a solution of $(\text{NH}_4)_2\text{SO}_4$ salt in deionized water. The particles flowed through a heated copper tube and a diffusion dryer, resulting in crystalline $(\text{NH}_4)_2\text{SO}_4$, and were then passed through a ^{85}Kr neutralizer before being injected into the chamber. The initial size distribution of the seed aerosol was centered around a diameter of approximately 100 nm.

Once the number concentration of particles on each side of the chamber had equilibrated, the chamber was divided and covered with a black polyethylene tarpaulin in order to prevent sunlight from irradiating the contents of the chamber. Propene, NO, NO_2 , hexafluorobenzene (C_6F_6), and hydrocarbon were then injected into each side of the chamber through Teflon lines. Propene was used as a photochemical initiator to provide sufficient levels of OH, and C_6F_6 was used as a nonreactive internal standard. NO and NO_2 are added primarily to facilitate the basic photochemical cycle involving O_3 and to participate in the reaction converting peroxy radicals (RO_2) to alkoxy radicals (RO). Therefore, it is expected that the NO_x level in the chamber will have little effect on aerosol yield except through the formation of O_3 and NO_3 . Propene and NO_x were injected from certified cylinders of approximately 500 ppm in nitrogen. The target initial mixing ratio of propene in each chamber was 250-300 ppb for each photooxidation experiment, and the amount of NO_x ($\text{NO}_x = \text{NO} + \text{NO}_2$) injected varied depending on the initial concentration of the parent hydrocarbon. The average hydrocarbon to total NO_x ratio (ppbC/ppb) was approximately 5 to 1, whereas the average ratio of NO to NO_2 was 1.5 to 1. The parent hydrocarbon and the C_6F_6 were injected by vaporizing microliter quantities in a heated

glass bulb that was diluted with compressed, purified air that flowed directly to the chamber.

After all of the injections to the chamber had been made and sufficient time had passed to allow mixing within each side of the chamber, measurements of hydrocarbon, O_3 , NO_x , and particle concentrations were taken in order to obtain initial values and to ensure that the contents of the chamber were well mixed. Typically, three hydrocarbon readings using the GC method described above were taken from each side of the chamber. Ozone was measured using a Dasibi Environmental Corporation (Glendale, California) Model 1008-PC O_3 analyzer that was calibrated at the beginning of the series of experiments by Dasibi. The estimated uncertainty in these readings is $\pm 4\%$; a drift of only a few percent in the monitor readings was seen over the course of several months. NO , NO_2 , and total NO_x concentrations were monitored using a Thermo Environmental Instruments (Franklin, Massachusetts) Model 42 chemilluminescence NO_x monitor. Prior to each experiment, zero and span checks were performed on this instrument using certified cylinders of NO , NO_2 , and N_2 . The estimated uncertainty in NO_x monitor readings are $\pm 4\%$ for NO and $\pm 7\%$ for NO_2 . After the initial readings were complete, the black tarpaulin was removed, exposing the chamber to sunlight and starting the experiment. During the experiments, O_3 and NO_x were sampled continuously from each side of the chamber in intervals of 10 min, and hydrocarbon samples were taken throughout the experiment from alternating sides of the chamber. Temperature was also tracked continuously throughout the course of each experiment.

Aerosol data included size distributions and total number concentrations for each side of the chamber at a 1-min frequency. Aerosol instrumentation consisted of a TSI (St.

Paul, Minnesota) Model 3071 cylindrical scanning electrical mobility spectrometer (SEMS) to measure the size distribution of particles and a TSI Model 3760 condensation nucleus counter (CNC) to count particles. SEMS voltages were ramped exponentially from 40 to 8500 V, and the classifier flows were 2.5 L min^{-1} for sheath and excess flows and 0.25 L min^{-1} for inlet and classified aerosol flows. This allowed for the measurement of particles in the diameter range of approximately 30-850 nm. A complete and detailed description of the SEMS operation that includes a description of data analysis techniques has been published previously [*Wang and Flagan*, 1990].

Experiments in which O_3 or NO_3 is the primary oxidant were performed at night to eliminate the possibility of photolysis of secondary products to form OH. (This also avoided high temperatures caused by keeping the chamber covered with the black tarpaulin in direct sunlight, as in the experiments of *Hoffmann et al.*, [1997].) In ozonolysis experiments, an appropriate concentration of 2-butanol was used to scavenge any OH formed in the hydrocarbon- O_3 reaction and to ensure that O_3 was the only oxidant present in the system [*Chew and Atkinson*, 1996].

To compare aerosol formation under the different conditions, it is important that the temperature in the chamber during the dark experiments be close to that of a typical afternoon smog chamber experiment because the partitioning coefficient $K_{om,i}$ is a function of temperature. To achieve this, the entire chamber was covered with an insulating cover as well as the black tarpaulin, neither of which was removed during the course of the experiment. This was done after the seed particles had been injected and the chamber had been divided as described above. In addition, four Holmes (Milford, Massachusetts) Model HFH-501FP space heaters were placed in the open area underneath the chamber.

the chamber. By varying the number of heaters used and their power settings, daytime temperatures of approximately 30°-35°C could be achieved and maintained throughout the course of an experiment.

Injectons of hydrocarbon, C_6F_6 , and 2-butanol (if needed) were then made to each side as described above. Once initial readings for both sides had been completed for ozonolysis experiments, O_3 was injected to each side using an Enmet Corporation (Ann Arbor, Michigan) Model 04052-011 O_3 generator until the Dasibi O_3 monitor read approximately 4 times the initial hydrocarbon concentration on the appropriate side. For NO_3 experiments, sufficient NO_3 was generated via the thermal decomposition of N_2O_5 synthesized by the combination of O_3 and NO_2 [R. Atkinson, personal communication, 1997]. Continuous aerosol, GC, and temperature readings were taken as described above. Initial conditions and resulting data are given for all experiments in Table 2.2.

2.6 Yields of Biogenic Organics in Photooxidation Experiments

Figures 2.2-2.5 show aerosol yields as a function of organic mass concentration for photooxidation experiments with the 14 biogenic compounds tested. Figures 2.2-2.5 also show the theoretical yield curves fit using (2.4) for each biogenic hydrocarbon. The parameters resulting from the fit of these curves are given in Table 2.3. As seen in Figures 2.2-2.5, there exists a wide range of aerosol yields for biogenic hydrocarbons. Sesquiterpenes have the highest yields of the compounds tested. This behavior is a consequence of the high carbon number of the parent compounds. Limonene, β -pinene, and sabinene are among the compounds with the highest yields, clearly indicating the effect of the presence of a $=CH_2$ group in a cyclic monoterpene structure. The yields of

limonene, Δ^3 -carene, α -pinene, and the terpinene isomers also indicate the significance of double bonds that are internal to ring structures. When oxidants attack unsaturated bonds, carbon atoms may be lost as a result of the decomposition of the resulting radical species [Atkinson, 1997]. However, the two trends noted above suggest that fewer carbon atoms are lost by oxidant attack on $=CH_2$ double bonds or double bonds that are internal to ring structures. The lower yields of ocimene, myrcene, linalool, and terpinolene also support this hypothesis since three or more carbon atoms can be cleaved by oxidant attack on these molecules. However, terpinene-4-ol, which has an OH group replacing the second double bond of the terpinene isomers, does not adhere to this trend, in that its yield is significantly lower than that of the terpinene isomers. This is likely a result of the fact that the OH group replaces the more reactive double bond.

For the bicyclic olefins, the number of carbon atoms associated with the secondary ring also seems to have an effect on SOA yield. Δ^3 -carene and α -pinene have an identical structure, outside of a difference in the number of carbon atoms in the secondary ring, yet Δ^3 -carene has a higher aerosol yield than α -pinene (Figure 2.2). Since many of the products of the oxidation of these parent hydrocarbons are expected to be similar and retain their secondary ring structures [Yu *et al.*, 1998], this difference in yield can be explained by the less volatile nature of Δ^3 -carene (boiling point 168°-169°C) compared to α -pinene (boiling point 155°-156°C). However, sabinene (boiling point 163°-164°C), which has an exocyclic methylene group and a secondary three-carbon ring, has lower yields than β -pinene (boiling point 165°-167°C), which has an external methylene group and a secondary four-carbon ring. This is the opposite of the trend seen with Δ^3 -carene

and α -pinene. This difference cannot be explained by the slight difference in boiling point of the parent compounds. However, it can possibly be explained by a mechanism that results in the cleavage of both rings in sabinene since open-chain compounds tend to be more volatile than cyclic ones. This mechanism, adapted from the H atom abstraction mechanism of *Aschmann et al.* [1998] for α -pinene, is shown in Figure 2.6. For illustrative purposes, only OH radical reaction is shown. The corresponding mechanism for β -pinene is much less likely to result in the cleavage of both rings.

2.7 Yields of Biogenic Organics in Ozonolysis and Nitrate Radical Experiments

In general, aerosol yields in ozonolysis of the biogenic hydrocarbons are less dependent on organic mass concentration when compared to those under sunlight-irradiated photooxidation, in which the parent hydrocarbon is oxidized by OH, O₃, and NO₃. This indicates that ozonolysis leads to secondary products that are less volatile than those in the full photooxidation system [*Hoffmann et al.*, 1997]. O₃ reactions with β -pinene and sabinene, however, produce significantly lower aerosol yields than the corresponding full photooxidation experiments. The opposite behavior is seen for α -pinene and Δ^3 -carene (Figure 2.7 and Table 2.4). This indicates that compounds with double bonds internal to ring structures are more likely to form condensable products when compared to compounds with external double bonds. (These results cannot be compared to those of *Hoffman et al.* [1997], since those experiments were performed without an OH scavenger and at considerably different temperatures.) Large yields of aerosol result from NO₃ reaction with β -pinene, Δ^3 -carene, and sabinene, indicating

possible formation of nitrated products in large yields (Figure 2.8 and Table 2.4). The olefin α -pinene shows insignificant aerosol formation from NO_3 oxidation. This can be explained by the creation in high yield of pinonaldehyde, which is too volatile to partition significantly to the aerosol phase [Wängberg *et al.*, 1997].

Some scatter can be seen in the data sets associated with each type of experiment. This is most likely linked to the uncertainty regarding charging of the aerosol generated in the chamber and slight variations in temperature between experiments.

2.8 Contribution of Individual Oxidants to Aerosol Formation

To identify the amount of parent hydrocarbon consumed by each of the three available oxidants in sunlight-driven photooxidation experiments, the SAPRC90b mechanism [Carter, 1990] was used to model the gas-phase chemistry of the photochemical smog chamber experiments for α -pinene [Odum *et al.*, 1996; Hoffmann *et al.*, 1997], β -pinene, sabinene, and Δ^3 -carene. By using initial concentrations of hydrocarbon, NO_x , and propene and varying model parameters such as sunlight intensity and temperature, it was possible to simulate experimental concentration profiles of hydrocarbon, NO_x , and O_3 , from which it was also possible to infer the amount of hydrocarbon consumed by each oxidant. A sample output is shown in Figure 2.9, and the results for the four hydrocarbons tested are summarized in Table 2.5. As shown in Table 2.5, the fraction of the parent hydrocarbon consumed by each oxidant varies among compounds and within a set of experiments for a single compound depending on initial concentrations of hydrocarbon and NO_x , sunlight intensity, and temperature. In addition,

concentrations of hydrocarbon and NO_x , sunlight intensity, and temperature. In addition, it is confirmed that OH is the primary oxidant for all compounds studied under full photooxidation conditions in the chamber.

The fraction of parent hydrocarbon consumed by each oxidant in each photooxidation experiment has been determined for α -pinene, β -pinene, Δ^3 -carene, and sabinene. Using experimental data from photooxidation experiments (total amount of organic mass formed and total amount of parent hydrocarbon reacted), yield parameters from ozonolysis experiments, and yield parameters from nitrate radical experiments in conjunction with these data, the contribution of each oxidant to aerosol formation in biogenic photooxidation experiments can be estimated.

By adding the contribution of OH, O_3 , and NO_3 to organic aerosol formation in equation (2.1),

$$Y = \frac{\Delta M_{o,\text{OH}+}}{\Delta \text{HC}} + \frac{\Delta M_{o,\text{O}_3}}{\Delta \text{HC}} + \frac{\Delta M_{o,\text{NO}_3}}{\Delta \text{HC}} \quad (2.5)$$

where OH+ represents OH reaction in addition to any cross reactions (e.g., the reaction of OH with products of initial O_3 reaction). By recognizing that

$$Y_i = \frac{\Delta M_{o,i}}{\Delta \text{HC}_i} \quad (2.6)$$

with i representing each oxidant, it can be shown that the overall yield is

$$Y_i = \frac{\Delta M_{o,OH+}}{\Delta HC} + \sum_i f_i Y_i \quad (2.7)$$

where f_i represents the fraction of the parent consumed by oxidant i ($\Delta HC_i/\Delta HC$) for O_3 and NO_3 , which has been determined from the gas-phase modeling. By applying (2.4) to each oxidant, it can be shown that

$$Y_i = \Delta M_o \sum_j \left(\frac{\alpha_{i,j} K_{om,i,j}}{1 + K_{om,i,j} \Delta M_o} \right) \quad (2.8)$$

where j now represents each product in the two-product model. Therefore, the overall yield is

$$Y = \frac{\Delta M_{o,OH+}}{\Delta HC} + \Delta M_o \sum_i f_i \sum_j \left(\frac{\alpha_{i,j} K_{om,i,j}}{1 + K_{om,i,j} \Delta M_o} \right) \quad (2.9)$$

with the only unknown being the amount of aerosol organic mass formed from OH reactions and cross reactions, which can be determined for each experiment. The fraction of aerosol derived from the reaction of the parent with each oxidant in photooxidation experiments can then be determined from (2.6), (2.8), and (2.9). The results for each experiment are given in Table 2.6. It can be seen that the contribution of each oxidant varies among compounds and within a set of compounds for each oxidant. This variation can be explained mechanistically by differences in temperature (affecting kinetics and gas-particle partitioning of secondary products), incident sunlight intensity (affecting

photolysis of NO_3), and initial concentrations (affecting the rate of O_3 and NO_3 formation).

2.9 Conclusions

The atmospheric aerosol forming potential of 14 of the most prevalent terpenoid biogenic hydrocarbons has been elucidated. Yield parameters for each compound tested show that these compounds have a greater potential to form secondary organic aerosol than typical aromatic constituents of gasoline. Although some degree of grouping of the biogenic hydrocarbons based on structural characteristics in terms of their aerosol forming potentials is possible, this is not uniformly the case at this time. As a result, it will be necessary to account individually for most biogenic hydrocarbons when modeling secondary organic aerosol formation in the ambient atmosphere.

Separate ozonolysis and nitrate radical experiments were performed for bicyclic olefins to investigate aerosol formation from reaction with individual oxidants. Yields in ozonolysis experiments are less dependent on organic mass concentration when compared to those in full sunlight-irradiated photooxidation. Sabinene and β -pinene have significantly lower yields from O_3 reaction alone than the corresponding sunlight-driven photooxidation experiments. However, the opposite behavior is seen for α -pinene and Δ^3 -carene. Reaction between NO_3 and β -pinene, Δ^3 -carene, or sabinene leads to high conversion to aerosol, indicating probable ambient aerosol formation at night when monoterpenes continue to be emitted and NO_3 accumulates.

It has been confirmed that OH, O₃, and NO₃ each contribute to parent hydrocarbon consumption and aerosol formation in chamber photooxidation. Gas-phase chemistry modeling, combined with yield parameters from individual oxidant experiments, allows for the determination of the contribution of each oxidant to aerosol formation.

2.10 References

- Alvarado, A., E.C. Tuazon, S.M. Aschmann, R. Atkinson, and J. Arey, Products of the gas-phase reactions of O(³P) atoms and O₃ with α-pinene and 1,2-dimethyl-1-cyclohexene, *J. Geophys. Res.*, *103*, 25,541-25,552, 1998.
- Arey, J., A.M. Winer, R. Atkinson, S.M. Aschmann, W.D. Long, and C.L. Morrison, The emission of (Z)-3-hexen-1-ol, (Z)-3-hexenylacetate, and other oxygenated hydrocarbons from agricultural plant species, *Atmos. Environ.*, *25*, 1063-1075, 1991a.
- Arey, J., A.M. Winer, R. Atkinson, S.M. Aschmann, W.D. Long, C.L. Morrison, and D.M. Olszyk, Terpenes emitted from agricultural species found in California's Central Valley, *J. Geophys. Res.*, *96*, 9329-9336, 1991b.
- Arey, J., D.E. Crowley, M. Resketo, and J. Lester, Hydrocarbon emissions from natural vegetation in California's South Coast Air Basin, *Atmos. Environ.*, *29*, 2977-2988, 1995.
- Aschmann, S.M., A. Reissell, R. Atkinson, and J. Arey, Products of the gas-phase reactions of the OH radical with α- and β-pinene in the presence of NO, *J. Geophys. Res.*, *103*, 25,553-25,561, 1998.
- Atkinson, R., Gas-phase tropospheric chemistry of volatile organic compounds, 1, Alkanes and alkenes, *J. Phys. Chem. Ref. Data*, *26*, 215-290, 1997.

- Atkinson, R., J. Arey, S.M. Aschmann, S.B. Corchnoy, and Y. Shu, Rate constants for the gas-phase reactions of *cis*-3-hexen-1-ol, *cis*-3-hexenylacetate, *trans*-2-hexenal, and linalool with OH and NO₃ radicals and O₃ at 296 +/- 2K and OH radical formation yields from the O₃ reactions, *Int. J. Chem. Kinet.*, **27**, 941-955, 1995.
- Berndt, T., O. Böge, I. Kind, and W. Rolle, Reaction of NO₃ radicals with 1,3-cyclohexadiene, α -terpinene, and α -phellandrene: Kinetics and products, *Ber. Bunsen-Ges. Phys. Chem.*, **100**, 462-469, 1996.
- Calogirou, A., D. Kotzias, and A. Kettrup, Atmospheric oxidation of linalool, *Naturwissenschaften*, **82**, 288-289, 1995.
- Calogirou, A., D. Kotzias, and A. Kettrup, Product analysis of the gas-phase reaction of β -caryophyllene with ozone, *Atmos. Environ.*, **31**, 283-285, 1997.
- Carter, W.P.L., A detailed mechanism for the gas-phase atmospheric reactions of organic compounds, *Atmos. Environ.*, **24**, 481-518, 1990.
- Chameides, W.L., R.W. Lindsay, J. Richardson, and C.S. Kiang, The role of biogenic hydrocarbons in urban photochemical smog: Atlanta as a case study, *Science*, **241**, 1473-1475, 1988.
- Chew, A.A., and R. Atkinson, OH radical formation yields from the gas-phase reactions of O₃ with alkenes and monoterpenes, *J. Geophys. Res.*, **101**, 28,649-28,653, 1996.
- Fehsenfeld, F., et al., Emissions of volatile organic compounds from vegetation and the implications for atmospheric chemistry, *Glob. Biogeochem. Cycles*, **6**, 389-430, 1992.
- Griesbaum, K., V. Miclaus, and I.C. Jung, Isolation of ozonides from gas-phase ozonolyses of terpenes, *Environ. Sci. Technol.*, **32**, 647-649, 1998.

- Grosjean, E., and D. Grosjean, The gas phase reaction of unsaturated oxygenates with ozone: Carbonyl products and comparison with the alkene-ozone reaction, *J. Atmos. Chem.*, 27, 271-289, 1997.
- Guenther, A., et al., A global model of natural volatile organic compound emissions, *J. Geophys. Res.*, 100, 8873-8892, 1995.
- Hakola, H., J. Arey, S.M. Aschmann, and R. Atkinson, Product formation from the gas-phase reactions of OH radicals and O₃ with a series of monoterpenes, *J. Atmos. Chem.*, 18, 75-102, 1994.
- Hallquist, M., I. Wängberg, and E. Ljungström, Atmospheric fate of carbonyl oxidation products originating from α -pinene and Δ^3 -carene: Determination of rate of reaction with OH and NO₃ radicals, UV absorption cross sections, and vapor pressures, *Environ. Sci. Technol.*, 31, 3166-3172, 1997.
- Hoffmann, T., J.R. Odum, F. Bowman, D. Collins, D. Klockow, R.C. Flagan, and J.H. Seinfeld, Formation of organic aerosols from the oxidation of biogenic hydrocarbons, *J. Atmos. Chem.*, 26, 189-222, 1997.
- Isidorov, V.A., I.G. Zenkevich, and B.V. Ioffe, Volatile organic compounds in the atmosphere of forests, *Atmos. Environ.*, 19, 1-8, 1985.
- Kaplan, I.R., and R.J. Gordon, Non-fossil-fuel fine-particle organic carbon aerosols in southern California determined during the Los Angeles aerosol characterization and source apportionment study, *Aerosol Sci. Technol.*, 21, 343-359, 1994.
- König, G., M. Brunda, H. Puxbaum, C.N. Hewitt, S.C. Duckham, and J. Rudolph, Relative contribution of oxygenated hydrocarbons to the total biogenic VOC

- emissions of selected mid-European agricultural and natural plant species, *Atmos. Environ.*, 29, 861-874, 1995.
- Lamb, B., D. Gay, H. Westberg, and T. Pierce, A biogenic hydrocarbon emission inventory for the U.S.A. using a simple forest canopy model, *Atmos. Environ.*, 27, 1673-1690, 1993.
- Leaitch, W.R., J.W. Bottenheim, T.A. Biesenthal, S.M. Li, P.S.K. Liu, K. Asalien, H. Dryfhout-Clark, F. Hopper, and F. Brechtel, A case study of gas-to-particle conversion in an eastern Canadian forest, *J. Geophys. Res.*, 104, 8095-8111, 1999.
- McKeen, S.A., E.Y. Hsie, and S.C. Liu, A study of the dependence of rural ozone on ozone precursors in the eastern United States, *J. Geophys. Res.*, 96, 15,377-15,394, 1991.
- Müller, J. F., Geographical distribution and seasonal variation of surface emissions and deposition velocities of atmospheric trace gases, *J. Geophys. Res.*, 97, 3787-3804, 1992.
- Odum, J.R., T. Hoffmann, F. Bowman, D. Collins, R.C. Flagan, and J.H. Seinfeld, Gas/particle partitioning and secondary organic aerosol yields, *Environ. Sci. Technol.*, 30, 2580-2585, 1996.
- Odum, J.R., T.P.W. Jungkamp, R.J. Griffin, R.C. Flagan, and J.H. Seinfeld, The atmospheric aerosol-forming potential of whole gasoline vapor, *Science*, 276, 96-99, 1997a.
- Odum, J.R., T.P.W. Jungkamp, R.J. Griffin, H.J.L. Forstner, R.C. Flagan, and J.H. Seinfeld, Aromatics, reformulated gasoline, and atmospheric organic aerosol formation, *Environ. Sci. Technol.*, 31, 1890-1897, 1997b.

- Pandis, S.N., S.E. Paulson, J.H. Seinfeld, and R.C. Flagan, Aerosol formation in the photooxidation of isoprene and β -pinene, *Atmos. Environ.*, 25, 997-1008, 1991.
- Pandis, S.N., R.A. Harley, G.R. Cass, and J.H. Seinfeld, Secondary organic aerosol formation and transport, *Atmos. Environ., Part A*, 26, 2269-2282, 1992.
- Pankow, J.F., An absorption model of the gas/aerosol partitioning of organic compounds in the atmosphere, *Atmos. Environ.*, 28, 185-188, 1994a.
- Pankow, J. F., An absorption model of the gas/aerosol partitioning involved in the formation of secondary organic aerosol, *Atmos. Environ.*, 28, 189-193, 1994b.
- Puxbaum, H., and G. König, Observation of dipropenyldisulfide and other organic sulfur compounds in the atmosphere of a beech forest with *allium ursinum* ground cover, *Atmos. Environ.*, 31, 291-294, 1997.
- Roselle, S.J., T.E. Pierce, and K.L. Schere, The sensitivity of regional ozone modeling to biogenic hydrocarbons, *J. Geophys. Res.*, 96, 7371-7394, 1991.
- Schauer, J.J., W.F. Rogge, L.M. Hildemann, M.A. Mazurek, G.R. Cass, and B.R.T. Simoneit, Source apportionment of airborne particulate matter using organic compounds as tracers, *Atmos. Environ.*, 30, 3837-3855, 1996.
- Seinfeld, J.H., and S.N. Pandis, *Atmospheric Chemistry and Physics*, Wiley-Interscience, New York, 1998.
- Shu, Y., and R. Atkinson, Atmospheric lifetimes and fates of a series of sesquiterpenes, *J. Geophys. Res.*, 100, 7275-7281, 1995.
- Shu, Y., E.S.C. Kwok, E.C. Tuazon, R. Atkinson, and J. Arey, Products of the gas-phase reactions of linalool with OH radicals, NO₃ radicals, and O₃, *Environ. Sci. Technol.*, 31, 896-904, 1997.

- Stephanou, E.G., and N. Stratigakis, Oxocarboxylic and α , ω -dicarboxylic acids: Photooxidation products of biogenic unsaturated fatty acids present in urban aerosols, *Environ. Sci. Technol.*, **27**, 1403-1407, 1993.
- Turpin, B.J., and J.J. Huntzicker, Identification of secondary organic aerosol episodes and quantitation of primary and secondary organic aerosol concentrations during SCAQS, *Atmos. Environ.*, **29**, 3527-3544, 1995.
- Vinckier, C., F. Compernelle, and A.M. Saleh, Qualitative determination of the non-volatile reaction products of the α -pinene reaction with hydroxyl radicals, *Bull. Soc. Chim. Belg.*, **106**, 501-513, 1997.
- Wängberg, I., I. Barnes, and K.H. Becker, Product and mechanistic study of the reaction of NO_3 radicals with α -pinene, *Environ. Sci. Technol.*, **31**, 2130-2135, 1997.
- Wang, S.C., and R.C. Flagan, Scanning electrical mobility spectrometer, *Aerosol Sci. Technol.*, **13**, 230-240, 1990.
- Went, F.W., Blue hazes in the atmosphere, *Nature*, **187**, 641-643, 1960.
- Winer, A.M., J. Arey, R. Atkinson, S.M. Aschmann, W.D. Long, C.L. Morrison, and D.M. Olszyk, Emission rates of organics from vegetation in California's Central Valley, *Atmos. Environ.*, **26**, 2647-2659, 1992.
- Yu, J., R.C. Flagan, and J.H. Seinfeld, Identification of products containing -COOH, -OH, and -C=O in atmospheric oxidation of hydrocarbons, *Environ. Sci. Technol.*, **32**, 2357-2370, 1998.
- Zhang, S.H., M. Shaw, J.H. Seinfeld, and R.C. Flagan, Photochemical aerosol formation from α -pinene and β -pinene, *J. Geophys. Res.*, **97**, 20,717-20,729, 1992.

Table 2.1. Reaction rate constants for the oxidation of biogenic hydrocarbons.

Parent			
Δ^3 -Carene	88	37	9.1
β -Caryophyllene	197	11600	19
α -Humulene	293	11700	35
Limonene	171	200	12.2
Linalool	159	430	11.2
Myrcene	215	470	11
Ocimene	252	540	22
α -Pinene	53.7	86.6	6.2
β -Pinene	78.9	15	2.5
Sabinene	117	86	10
α -Terpinene	363	21100	140
γ -Terpinene	177	140	29
Terpinene-4-ol	170	250	14.6
Terpinolene	225	1880	97

Units are $\text{cm}^3 \text{ molecule}^{-1} \text{ s}^{-1}$. Data are from *Atkinson et al.* [1995], *Shu and Atkinson* [1995], and *Atkinson* [1997].

Table 2.2a. Initial conditions and data for photooxidation experiments.

Date	Parent	<i>T</i> , K	Δ HC ppb	ΔM_o $\mu\text{g m}^{-3}$	<i>Y</i>	NO ppb	NO ₂ ppb
07/01/97a	Δ^3 -Carene	310.0	28.8	2.5	0.016	36.9	55.4
07/01/97b	Δ^3 -Carene	310.0	66.8	11.6	0.033	90.5	96.9
08/21/97b	Δ^3 -Carene	312.8	72.5	54.6	0.142	67.5	60.8
08/15/97b	Δ^3 -Carene	308.8	73.6	63.7	0.161	86.2	82.3
08/19/97b	Δ^3 -Carene	312.0	104.6	99.7	0.179	89.6	72.3
09/18/97b	β -Caryophyllene	308.3	5.9	17.6	0.369	18.7	9.4
09/16/97b	β -Caryophyllene	306.6	10.3	64.6	0.775	39.0	14.9
09/17/98b	β -Caryophyllene	308.6	12.9	82.3	0.790	13.1	11.1
09/18/97a	α -Humulene	308.3	5.0	12.9	0.319	16.2	7.8
09/15/97b	α -Humulene	309.3	5.4	28.2	0.648	30.8	23.8
09/16/97a	α -Humulene	306.6	8.6	59.2	0.845	37.6	14.8
09/17/97a	α -Humulene	308.6	9.2	54.2	0.732	19.5	13.5
08/26/97b	Limonene	313.4	20.6	9.5	0.087	43.1	61.8
08/26/97a	Limonene	313.4	35.2	49.6	0.266	17.4	62.8
08/17/97b	Limonene	309.4	49.5	79.1	0.298	73.6	65.8
08/17/97a	Limonene	309.4	65.1	120.2	0.344	75.7	64.4
08/28/97b	Linalool	312.4	71.6	26.7	0.056	164.7	130.1
09/19/97a	Myrcene	311.1	9.8	3.5	0.068	23.5	21.5
09/10/97b	Myrcene	311.9	77.5	57.5	0.168	117.9	79.9
08/24/97a	Ocimene	313.2	45.6	7.3	0.030	96.3	85.7
07/23/97a	Ocimene	315.7	76.5	17.6	0.043	49.0	94.0
07/23/97b	Ocimene	315.7	142.0	50.3	0.066	125.1	168.6

Table 2.2a. (continued) Initial conditions and data for photooxidation experiments.

Date	Parent	<i>T</i> , K	Δ HC ppb	ΔM_o $\mu\text{g m}^{-3}$	<i>Y</i>	NO ppb	NO ₂ ppb
08/15/97a	β -Pinene	308.8	32.3	20.4	0.118	81.4	53.4
07/15/97a	β -Pinene	313.6	33.7	14.6	0.080	49.2	62.5
07/17/97a	β -Pinene	316.2	42.0	7.2	0.032	15.6	43.4
07/27/97a	β -Pinene	313.3	45.0	34.2	0.144	53.1	58.6
07/15/97b	β -Pinene	313.6	62.2	51.4	0.153	87.0	79.7
08/19/97a	β -Pinene	312.0	79.0	109.4	0.260	88.8	64.8
07/21/97a	β -Pinene	313.5	85.5	100.1	0.221	93.7	63.6
07/21/97b	β -Pinene	313.5	96.5	141.6	0.272	93.0	67.0
07/09/97a	Sabinene	316.0	13.9	1.9	0.025	21.3	43.5
07/07/97a	Sabinene	310.3	34.9	14.3	0.076	50.2	52.2
07/05/97a	Sabinene	312.9	53.3	23.9	0.085	91.9	81.4
08/24/97b	Sabinene	313.2	74.0	48.7	0.124	115.3	96.5
07/05/97b	Sabinene	312.9	75.3	51.4	0.129	93.2	61.4
07/07/97b	Sabinene	310.3	77.7	53.4	0.129	106.0	77.9
07/09/97b	Sabinene	316.0	83.3	65.2	0.145	115.5	84.1
09/04/97a	α -Terpinene	316.0	47.0	20.2	0.082	87.1	51.3
09/08/97a	α -Terpinene	314.7	65.2	43.9	0.128	62.8	148.9
09/06/97a	α -Terpinene	313.3	79.6	73.8	0.175	106.0	53.0
09/11/97a	γ -Terpinene	312.4	40.9	21.3	0.098	44.7	45.0
09/10/97a	γ -Terpinene	311.9	77.5	65.9	0.160	132.2	82.7
09/06/97b	Terpinene-4-ol	313.3	116.2	42.6	0.056	216.3	132.2

Table 2.2a. (continued) Initial conditions and data for photooxidation experiments.

Date	Parent	T , K	ΔHC ppb	ΔM_o $\mu\text{g m}^{-3}$	Y	NO ppb	NO ₂ ppb
09/02/97a	Terpinolene	312.6	25.0	1.9	0.015	47.7	47.3
09/02/97b	Terpinolene	312.6	46.9	5.2	0.021	42.4	64.7
08/28/97a	Terpinolene	312.4	60.1	9.9	0.031	54.7	56.3
09/11/97b	Terpinolene	312.4	92.3	17.8	0.036	128.0	88.8
09/04/97b	Terpinolene	316.0	133.2	28.9	0.041	190.5	122.7

Read 09/18/97 as September 18, 1997.

Table 2.2b. Initial conditions and data.

Date	Parent	<i>T</i> , K	Δ HC ppb	ΔM_o $\mu\text{g m}^{-3}$	<i>Y</i>
<i>Nitrate Radical Experiments</i>					
05/20/98a	Δ^3 -Carene	308.0	36.2	24.4	0.125
06/03/98a	Δ^3 -Carene	308.2	51.6	178.8	0.643
05/28/98a	Δ^3 -Carene	310.1	70.2	267.7	0.713
05/18/98a	Δ^3 -Carene	309.2	80.1	310.5	0.722
06/01/98a	β -Pinene	309.9	18.8	32.4	0.322
05/09/98b	β -Pinene	304.0	19.7	46.1	0.428
06/01/98b	β -Pinene	309.9	54.7	243.2	0.830
05/13/98b	β -Pinene	302.0	96.4	467.3	0.891
05/20/98b	Sabinene	308.0	32.8	24.3	0.138
06/03/98b	Sabinene	308.2	41.5	151.5	0.677
05/28/98b	Sabinene	310.1	55.9	223.9	0.749
05/18/98b	Sabinene	309.2	68.2	276.5	0.755

Table 2.2b. (continued) Initial conditions and data.

Date	Parent	T , K	ΔHC ppb	ΔM_o $\mu\text{g m}^{-3}$	Y
<i>Ozone Experiments</i>					
06/19/98b	Δ^3 -Carene	308.6	11.8	5.5	0.086
06/21/98b	Δ^3 -Carene	309.3	29.9	18.7	0.117
06/23/98b	Δ^3 -Carene	307.0	47.7	33.1	0.129
06/15/98b	Δ^3 -Carene	306.2	89.9	64.4	0.132
06/05/98a	α -Pinene	309.9	16.7	7.4	0.083
06/05/98b	α -Pinene	309.9	18.2	8.5	0.087
06/07/98a	α -Pinene	303.3	31.0	30.3	0.179
06/07/98b	α -Pinene	303.3	45.5	46.0	0.184
06/09/98a	α -Pinene	308.0	57.0	52.3	0.170
06/09/98b	α -Pinene	308.0	65.0	65.1	0.186
06/13/98a	β -Pinene	308.4	11.9	0.0	0.000
06/13/98b	β -Pinene	308.4	35.2	1.8	0.009
06/11/98a	β -Pinene	306.9	57.6	9.2	0.030
06/11/98b	β -Pinene	306.9	80.1	22.5	0.052
06/19/98a	Sabinene	308.6	12.5	1.4	0.021
06/21/98a	Sabinene	309.3	34.0	5.1	0.028
06/23/98a	Sabinene	307.0	51.6	9.1	0.033
06/15/98a	Sabinene	306.2	92.4	17.9	0.036

Table 2.3. Aerosol yield parameters for the photooxidation of biogenic hydrocarbons.

Parent	α_1	α_2	$K_{om,1}$ $\text{m}^3 \mu\text{g}^{-1}$	$K_{om,2}$ $\text{m}^3 \mu\text{g}^{-1}$
Δ^3 -Carene*	0.054	0.517	0.043	0.0042
β -Caryophyllene*	1.000		0.0416	
α -Humulene	1.000		0.0501	
Limonene	0.239	0.363	0.055	0.0053
Linalool*	0.073	0.053	0.049	0.0210
Ocimene*	0.045	0.149	0.174	0.0041
α -Pinene*	0.038	0.326	0.171	0.0040
β -Pinene*	0.130	0.406	0.044	0.0049
Sabinene	0.067	0.399	0.258	0.0038
α - & γ -Terpinene	0.091	0.367	0.081	0.0046
Terpinene-4-ol*	0.049	0.063	0.159	0.0045
Terpinolene	0.046	0.034	0.185	0.0024

* Includes data from *Hoffmann et al.* [1997].

Table 2.4. Aerosol yield parameters for the ozone and nitrate radical oxidation of bicyclic hydrocarbons.

Parent	α_1	α_2	$K_{om,1}$ $\text{m}^3 \mu\text{g}^{-1}$	$K_{om,2}$ $\text{m}^3 \mu\text{g}^{-1}$
<i>Ozone</i>				
Δ^3 -Carene	0.128	0.068	0.337	0.0036
α -Pinene	0.125	0.102	0.088	0.0788
β -Pinene	0.026	0.485	0.195	0.0030
Sabinene	0.037	0.239	0.819	0.0001
<i>Nitrate Radical</i>				
Δ^3 -Carene	0.743	0.257	0.0088	0.0091
β -Pinene	1.000		0.0163	
Sabinene	1.000		0.0115	

Table 2.5. Simulations of gas-phase chemistry.

Date	Parent	Δ H ppb	%	%	%	ppb	ppb	ppb
07/01/97a	Δ^3 -Carene	28.8	66.4	13.0	19.3	19.1	3.7	5.6
07/01/97b	Δ^3 -Carene	66.8	68.1	14.6	13.7	45.5	9.8	9.2
08/21/97b	Δ^3 -Carene	72.5	66.0	14.2	18.0	47.8	10.3	13.1
08/15/97b	Δ^3 -Carene	73.6	65.9	15.3	15.9	48.5	11.3	11.7
08/19/97b	Δ^3 -Carene	104.6	63.4	15.3	19.0	66.3	16.0	19.8
08/17/95a	α -Pinene	73.1	38.3	35.1	24.5	28.0	25.6	17.9
09/22/95b	α -Pinene	90.8	46.0	31.5	21.2	41.7	28.6	19.2
09/22/95a	α -Pinene	94.6	47.4	30.9	20.1	44.8	29.3	19.0
09/25/95b	α -Pinene	94.7	47.8	32.7	18.1	45.3	31.0	17.1
09/25/95a	α -Pinene	96.7	53.0	31.3	14.0	51.3	30.3	13.6
08/15/97a	β -Pinene	32.3	79.6	8.0	9.8	25.7	2.6	3.2
07/15/97a	β -Pinene	33.7	69.0	9.4	19.9	23.2	3.2	6.7
07/17/97a	β -Pinene	42.0	56.6	11.2	31.6	23.8	4.7	13.3
07/27/97a	β -Pinene	45.0	71.4	9.3	17.5	32.1	4.2	7.9
07/15/97b	β -Pinene	62.2	68.6	10.0	18.4	42.7	6.2	11.4
08/19/97a	β -Pinene	79.0	72.0	9.5	15.7	56.9	7.5	12.4
07/21/97a	β -Pinene	85.5	64.3	9.9	23.6	54.9	8.5	20.2
07/21/97b	β -Pinene	96.5	62.9	10.2	24.7	60.7	9.8	23.9

Table 2.5. (continued) Simulations of gas-phase chemistry.

Date	Parent	Δ HC ppb	%	%	%	ppb	ppb	ppb
07/09/97a	Sabinene	13.9	69.4	13.5	16.5	9.6	1.9	2.3
07/07/97a	Sabinene	34.9	78.1	14.1	6.5	27.3	4.9	2.3
07/05/97a	Sabinene	53.3	72.4	14.8	10.9	38.6	7.9	5.8
08/24/97b	Sabinene	74.0	73.6	14.7	8.4	54.5	10.9	6.2
07/05/97b	Sabinene	75.3	71.0	14.7	12.7	53.5	11.1	9.6
07/07/97b	Sabinene	77.7	74.5	16.9	5.3	57.9	13.1	4.1
07/09/97b	Sabinene	83.3	71.1	15.0	11.3	59.3	12.5	9.4

Table 2.6. Individual contributions to aerosol formation.

Date	Parent	ΔM_o $\mu\text{g m}^{-3}$	Percent Contribution		
			OH	O ₃	NO ₃
07/01/97a	Δ^3 -Carene	2.5	24.14	49.92	25.93
07/01/98b	Δ^3 -Carene	11.6	12.48	48.02	39.50
08/21/97b	Δ^3 -Carene	54.6	45.23	13.24	41.53
08/15/97b	Δ^3 -Carene	63.7	51.52	12.82	35.65
08/19/97b	Δ^3 -Carene	99.7	38.25	12.04	49.71
08/17/95a	α -Pinene	22.7	11.75	88.25	0.00
09/22/95a	α -Pinene	33.0	21.04	78.96	0.00
09/25/95b	α -Pinene	34.2	18.70	81.30	0.00
09/22/95b	α -Pinene	38.2	33.48	66.52	0.00
09/25/95a	α -Pinene	39.3	29.34	70.66	0.00
08/15/97a	β -Pinene	7.2	0.00	7.94	92.06
07/15/97a	β -Pinene	14.6	47.66	4.62	47.72
07/17/97a	β -Pinene	20.4	75.86	3.34	20.79
07/27/97a	β -Pinene	34.2	51.97	4.40	43.63
07/15/97b	β -Pinene	51.4	39.62	5.76	54.62
08/19/97a	β -Pinene	100.0	27.78	6.13	66.09
07/21/97a	β -Pinene	109.4	55.97	5.28	38.76
07/21/97b	β -Pinene	141.6	30.30	6.34	63.36

Table 2.6. (continued) Individual contributions to aerosol formation.

Date	Parent	ΔM_o $\mu\text{g m}^{-3}$	Percent Contribution		
			OH	O ₃	NO ₃
07/09/97a	Sabinene	1.9	74.08	12.01	13.91
07/07/97a	Sabinene	14.3	81.75	6.35	11.90
07/05/97a	Sabinene	23.9	65.98	6.25	27.77
08/24/97b	Sabinene	48.7	71.35	4.41	24.24
07/05/97b	Sabinene	51.4	58.94	4.28	36.78
07/07/97b	Sabinene	53.4	79.33	4.91	15.76
07/09/97b	Sabinene	65.2	62.67	3.92	33.40

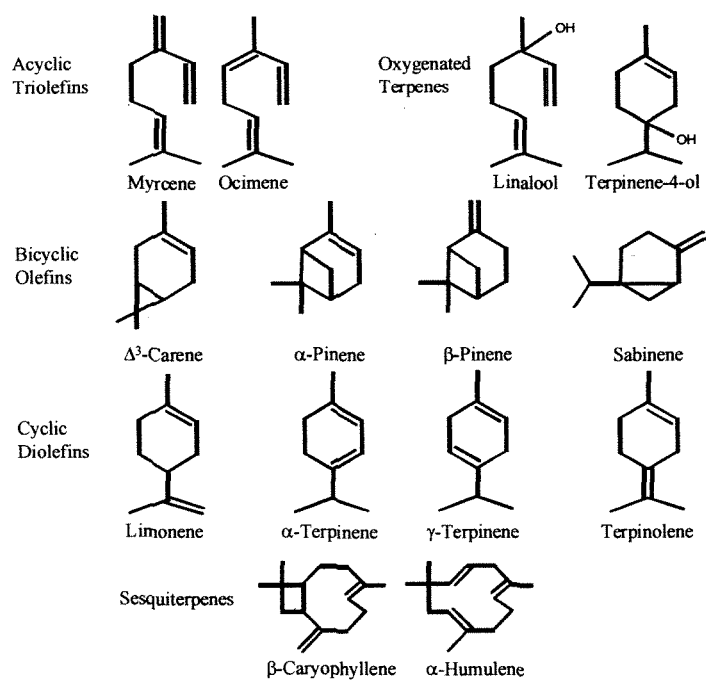


Figure 2.1. Chemical structures of the biogenic hydrocarbons investigated. Bonds between carbon atoms are shown with vertices representing carbon atoms; hydrogen atoms bonded to carbon are not explicitly shown.

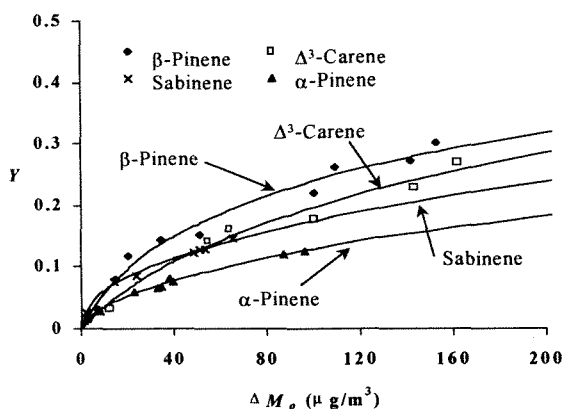


Figure 2.2

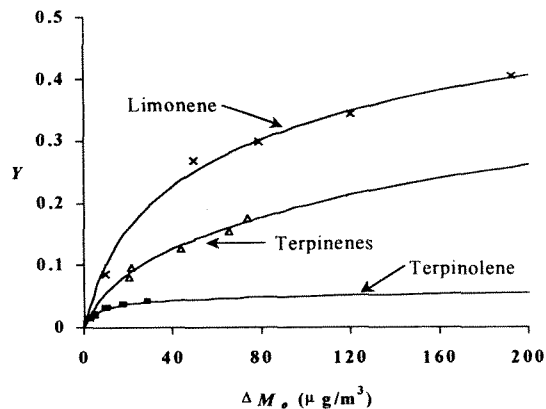


Figure 2.3

Figure 2.2. Secondary organic aerosol yields for the bicyclic olefins tested as a function of organic mass concentration in photooxidation experiments. Data are shown as filled triangles, plus signs, open circles, and filled diamonds for α -pinene, sabinene, Δ^3 -carene, and β -pinene, respectively. The α_1 , α_2 , $K_{om,1}$, and $K_{om,2}$ values used to generate the two-product model fitted curves are given in Table 2.3. Some data were taken from *Hoffmann et al.* [1997].

Figure 2.3. Secondary organic aerosol yields (data and fitted curves) for the cyclic diolefins tested as a function of organic mass concentration in photooxidation experiments. The α_1 , α_2 , $K_{om,1}$, and $K_{om,2}$ values used to generate the two-product model lines are given in Table 2.3. Some data were taken from *Hoffmann et al.* [1997].

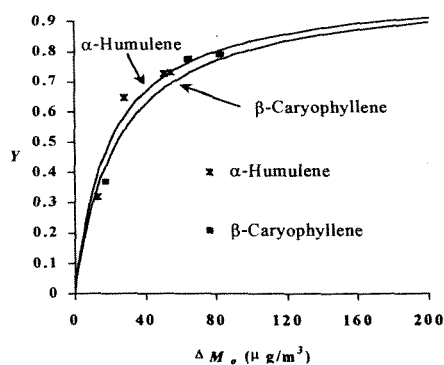


Figure 2.4

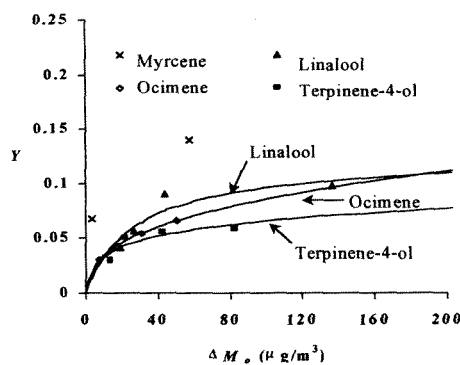


Figure 2.5

Figure 2.4. Secondary organic aerosol yields (data and fitted curves) for the sesquiterpenes tested as a function of organic mass concentration in photooxidation experiments. The α_1 , α_2 , $K_{om,1}$, and $K_{om,2}$ values used to generate the two-product model lines are given in Table 2.3. Some data were taken from *Hoffmann et al.* [1997].

Figure 2.5. Secondary organic aerosol yields (data and fitted curves) for the acyclic triolefins and oxygenated terpenes tested as a function of organic mass concentration in photooxidation experiments. The α_1 , α_2 , $K_{om,1}$, and $K_{om,2}$ values used to generate the two-product model lines are given in Table 2.3. Some data were taken from *Hoffmann et al.* [1997]. No curve is shown for myrcene as only two experiments with myrcene were performed.

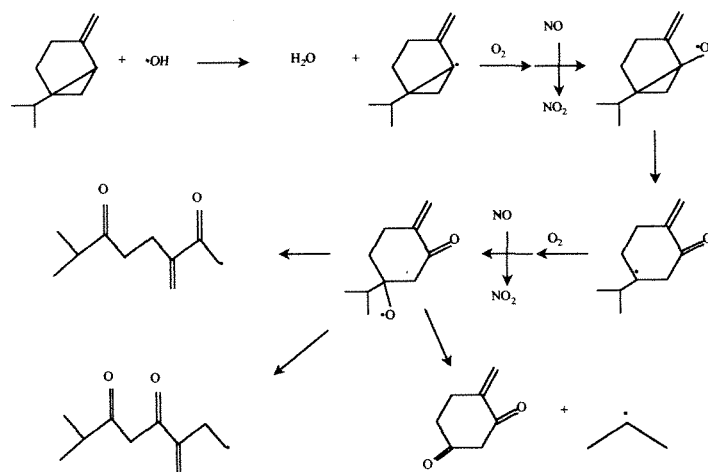


Figure 2.6. Possible ring-opening mechanism for the reaction between OH and sabinene.

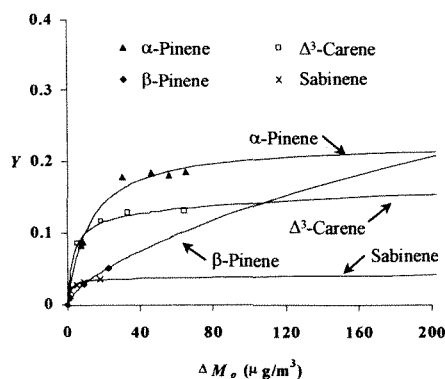


Figure 2.7

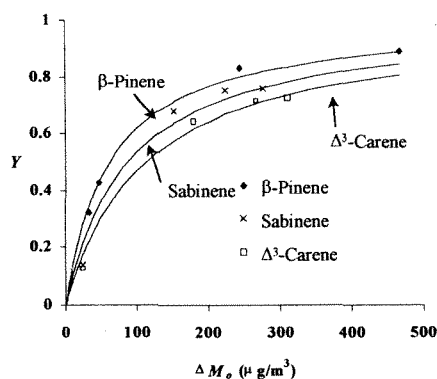


Figure 2.8

Figure 2.7. Secondary organic aerosol yields for the bicyclic olefins tested as a function of organic mass concentration in ozonolysis experiments. Data are shown as filled triangles, plus signs, open circles, and filled diamonds for α -pinene, sabinene, Δ^3 -carene, and β -pinene, respectively. The α_1 , α_2 , $K_{om,1}$, and $K_{om,2}$ values used to generate the two-product model fitted curves are given in Table 2.4.

Figure 2.8. Secondary organic aerosol yields (data and fitted curves) for the bicyclic olefins tested as a function of organic mass concentration in NO_3 experiments. The α_1 , α_2 , $K_{om,1}$, and $K_{om,2}$ values used to generate the two-product model lines are given in Table 2.4.

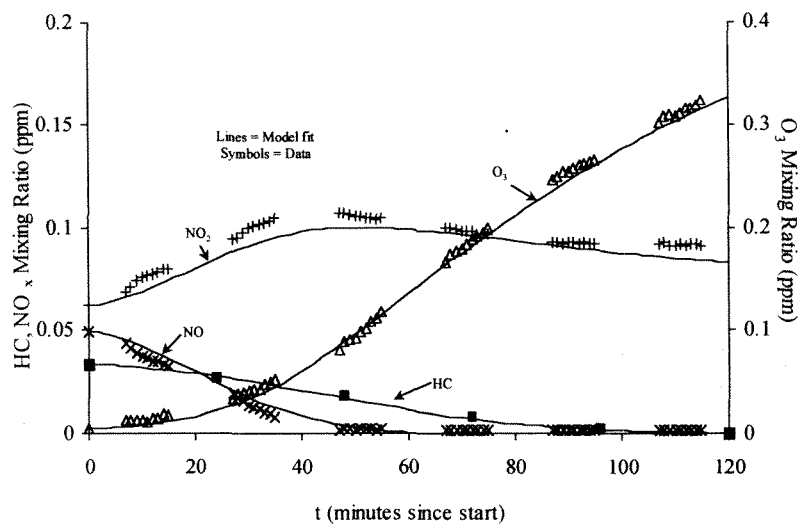


Figure 2.9. Example output (solid curves) from the SAPRC90b [Carter, 1990] gas-phase chemical mechanism. Data (dashes) are shown for the β -pinene experiment performed on July 15, 1997.

Chapter 3**Hygroscopic Properties of Pasadena, California, Aerosol**

3.1 Introduction

The response of atmospheric particles to changes in relative humidity (RH) is important in determining ambient particle size since water generally constitutes a substantial fraction of the atmospheric aerosol. This hygroscopic behavior is governed by the chemical composition of the aerosol. Since the detailed chemical composition of the atmospheric aerosol is rarely known, measurement of the hygroscopic behavior of the population allows one to infer indirectly important features indicative of the composition. Urban aerosols arise from a complex mix of anthropogenic and natural sources including marine layer salt, soot from combustion processes, primary and secondary organic products, and dust. During the day, primary aerosol is emitted from vehicle as well as commercial and industrial sources. Secondary aerosol is also created by the oxidation of gas-phase hydrocarbons to produce semi-volatile products.

Key studies of the hygroscopic behavior of atmospheric aerosols are summarized in Table 3.1. The most common approach utilizes the tandem differential mobility analyzer (TDMA), in which an aerosol, size classified in one differential mobility analyzer, is humidified, and the resulting size distribution is measured in the second analyzer. Hygroscopic growth data have been traditionally reported in terms of a less hygroscopic and a more hygroscopic peak growth mode. The shift of one or more modes upon humidification is usually reported in terms of a growth factor (GF), which is the ratio of the mean diameter of the humidified particles to that of the dry particles,

$$GF = \frac{D_p(RH)}{D_p(RH_{dry})}. \text{ Typical RHs used for humidification range from 80 to 90\%.}$$

Observed growth factors in the less hygroscopic mode of urban aerosol range from 1.0

(no growth) to 1.4; for the more hygroscopic mode, GF ranges from 1.1 to 1.8 (McMurry and Stolzenburg, 1989; Zhang *et al.*, 1996; Busch *et al.*, 1999; Ferron *et al.*, 1999). For marine boundary layer aerosols, growth factors range from 1.5 to 2.1 (Covert and Heintzenberg, 1993; Berg *et al.*, 1998; Massling *et al.*, 1999).

The splitting of a dry aerosol upon humidification into two modes reflects the chemical composition of the particles. In a study of aged continental aerosol, Swietlicki *et al.* (1999) observed two modes, a less hygroscopic mode with a GF of 1.12 and a more hygroscopic mode with GF between 1.44 and 1.65. They postulated that the hygroscopic growth could be attributed entirely to the inorganic content of the aerosol: sulfate, nitrate, and ammonium ions.

In laboratory studies of secondary organic aerosol formation by photochemical oxidation of monoterpenes, Virkkula *et al.* (1999) found growth factors of about 1.09. For experiments in which no seed aerosol was used, terpene oxidation products constituted the entire aerosol, and the hygroscopic growth factor remained nearly constant throughout the reaction. When ammonium sulfate seed aerosol was used, the growth factor decreased continually with the time of reaction, starting from about 1.5, a value typical of ammonium sulfate $((\text{NH}_4)_2\text{SO}_4)$, and dropping to 1.1 at the end of the experiment. All particle sizes studied exhibited this trend, although the process took more time with larger particles. These chamber-generated aerosols did not exhibit the two modes of growth often characteristic of ambient aerosols, because all the particles were generated from the same source. Several hygroscopic growth studies of mixtures of inorganic and organic aerosols (Hansson *et al.*, 1990, 1998; Xiong *et al.*, 1998) found that

organic layers on inorganic particles decreased the hygroscopic growth factor of the aerosol.

Assuming the atmosphere contains only two types of aerosol may, however, be an oversimplification. The age of the aerosol, the composition and amount of organic coating, the origin of the aerosol and its history are all expected to affect the hygroscopic nature of the particles. We report here nearly continuous measurement of the hygroscopic behavior of the Pasadena, CA, aerosol from August 15 to September 15, 1999. For most of the study, two dry sizes were studied, 50 nm and 150 nm diameter. We show the diurnal behavior of the observed growth factors for each particle size. During several days of the study, forest fires were burning in the adjacent mountains. Measured growth factors during that period appear to exhibit influence from the fire-generated particles. We first describe the experimental procedure, then present the measured hygroscopic growth data.

3.2 Experimental Procedure

The hygroscopic behavior of the atmospheric aerosol was measured using a TDMA (Rader and McMurry, 1986). The experimental system, illustrated in Figure 3.1, is similar to that employed by McMurry and Stolzenburg (1989) in previous studies of hygroscopic growth. Outdoor air was dried to a relative humidity of less than 10%. Using the model developed by Kreidenweis et al. (1987), the centerline residence time in the drying column was estimated to be at least ten times greater than the time necessary to completely dry the particles, barring any hysteresis effects. Once dried, the aerosol passes through a charger (Aerosol Dynamics, Berkeley, CA), equipped with ^{210}Po strips to produce the steady-state Fuchs charge distribution (Fuchs, 1963). The aerosol is then

classified using a TSI Model 3071 differential mobility analyzer (DMA; TSI, Inc., St. Paul, MN) operated at constant negative voltage to produce a monodisperse aerosol.

The excess air flow from DMA1 is filtered and then humidified by passing it through a heated flask saturator containing distilled deionized water and finally through a condenser that is held at 0.1°C below room temperature. The classified aerosol and saturated air are introduced coaxially into a humidification tube of 47 mm diameter and 1003 mm long. A flow straightener is used to ensure laminar flow. The Reynolds number of the flow in this tube was 90, so the length required to achieve fully developed flow and a uniform distribution of water vapor is approximately 150 mm. With particles introduced at the center of the flow, variations in the residence time caused by the parabolic velocity profile are minimized. The relative humidity in the tube is set at 89% by the ratio of dry to humid air flow rates. A water jacket around the humidification tube maintains its temperature.

The air exiting the humidifier enters a second DMA (DMA2) that operates as a scanning electrical mobility spectrometer (SEMS) with voltage scan times of 60 s. The flow from the outer annulus of the humidification tube is filtered before introduction into DMA2 as its sheath flow. The classified aerosol from DMA2 is mixed with filtered room air to produce the flow required for the TSI Model 3760 condensation particle counter (CPC) that is used to count the number of particles transmitted in 1 s time intervals. The particle size distribution is determined from particle counts after correction for the effects of multiple charging, diffusional broadening in the transfer function, and smearing due to the mixing effects within the CPC using the data inversion algorithm of Collins *et al.* (2001).

Precision TDMA measurements of particle growth require that all four flows entering and leaving each of the DMAs be accurately controlled. To achieve this degree of control continuously over weeks, all flow ratios were monitored by measuring pressure drops across calibrated capillaries using Dwyer (Michigan City, IN) Model 607-4 differential pressure transducers, interfaced to a personal computer with a National Instruments (Austin, TX) Model PC-LPM-16PnP data acquisition board that also records the number of particles from the CPC. A data acquisition and control program written in National Instruments LabView operates the five proportional flow control valves (Models 0248A-50000SV and 0248A-20000SV, MKS Instruments, Andover, MA) up to 100 times per second through an analog output card (Model PCI 6713, National Instruments). This control system maintains all of the flows at the desired levels without passing any aerosol through flow control valves.

The TDMA system sampled the Pasadena aerosol continuously from August 15, 1999, to September 15, 1999, with a gap from September 3 to 6. Prior to August 25, DMA1 was set to classify ambient particles at 50 nm diameter. Thereafter, it alternated between 50 and 150 nm, with three consecutive scans at each size. A delay was added before the first scan at a size to ensure that a representative sample was being attained. The entire cycle (six scans and two delays) required approximately 20 minutes. Additionally, an ozone detector (Model 1008-PC, Dasibi Environmental Corp., Glendale, CA) monitored ozone mixing ratios.

3.3 Analysis of 50 nm and 150 nm Particle Data

The data obtained were analyzed as two distinct sets: “normal” Pasadena summer aerosol and fire-influenced Pasadena summer aerosol. No fires were present from August

15 to August 28. Most days, the high temperatures were 35°C to 40°C. All days were clear by late morning after the marine layer burn-off. On August 29, a wildfire in the nearby San Gabriel Mountains broke out and was not contained until September 5. A major forest fire ignited in the San Bernardino Mountains (50 miles to the east) on August 29 and burned out of control until September 6 when it was contained. It was finally extinguished by September 15. On the days of August 30, August 31, and September 3, meteorological conditions were such that visibility decreased at the sampling site and a pervasive odor of smoke was present. For the entire period from August 29 to September 15 there were wildfires in other regions in the South Coast Air Basin, all within 50 miles of the sampling site in Pasadena. No TDMA data are available from noon September 3 until the morning of September 7 due to an operator error. A recurring computer error caused a number of small gaps in the data.

From August 15 to August 24, only the 50 nm aerosol (size exiting the first DMA) were sampled and analyzed. Starting on August 25, 150 nm and 50 nm sizes were sampled with three scans of each separated by a 3-minute delay. The calibrated size of the 50 nm and 150 nm data were 49.7 nm and 148.5 nm, respectively. The accumulation mode aerosols investigated (50 nm or 150 nm) are produced via evaporation of larger particles, by combustion, or by photochemical precursors. The aerosol is so fine that mechanical processes such as entrainment of mineral dust, construction artifacts, or tire or brake wear are unlikely to contribute significantly.

Virkkula *et al.* (1999) suggested that the hygroscopic growth of their smog chamber-generated aerosol could be separated into that attributed to organic and inorganic fractions. A seed aerosol composed of pure $(\text{NH}_4)_2\text{SO}_4$ was coated with the semi-volatile

organic products of the α -pinene/ozone reaction. The hygroscopic growth factor of the mixed chamber aerosol could then be estimated from the volume fraction of the organic (ε_o) and inorganic ($1-\varepsilon_o$) components:

$$GF = \sqrt[3]{\varepsilon_o GF_o^3 + (1 - \varepsilon_o) GF_i^3} \quad (3.1)$$

where GF_o and GF_i are growth factors of the organic and inorganic fractions, respectively.

Ambient air is more complex than that in a controlled chamber experiment, containing a much larger number of inorganic and organic compounds. The “history” of the ambient aerosol is also much more varied. However, particles that contain more organic compounds will generally exhibit lower growth factors than the pure inorganic salts. Particles containing substantial amounts of black carbon should exhibit very little, if any, hygroscopic uptake of water.

The 50 nm and 150 nm aerosol particles do not necessarily exhibit similar hygroscopic properties, since their organic – inorganic fractions may differ. A small organic layer on a 50 nm particle amounts to a significant organic volume fraction. Particles of 150 nm may have a significant inorganic fraction, which corresponds to a more hygroscopic fraction.

Primary aerosol particles of diameter 40 to 250 nm from anthropogenic sources typically contain a large fraction of organics. For example, Kleeman *et al.* (1999) found that the organic content of 40 to 250 nm diameter primary aerosol particles emitted by motor vehicles ranges from 85% to 95%. For wood smoke, aerosol in the 40 to 250 nm diameter size range, organic material constitutes between 65% and 95%, depending on the type of wood (Kleeman *et al.*, 1999b); char-broiling meat smoke and cigarette smoke

were found to have an organic content of about 67% and 98%, respectively. Therefore, primary aerosol released by these anthropogenic sources is expected to exhibit a relatively low growth factor.

Particles generated in the marine boundary layer are largely inorganic, composed primarily of sea-salt. These aerosols have measured water uptake factors of 1.5 to 2.1. Marine and anthropogenic aerosol should, therefore, be easily distinguished. However, atmospheric particles continuously change as semi-volatile secondary organic compounds, derived from oxidation of hydrocarbons in the atmosphere, coat the pre-existing sea-salt and anthropogenically derived aerosol. Both the time over which the particles may have been exposed to condensable vapors and the initial particle size influence the ultimate hygroscopic behavior of the aerosol.

For each 50 nm scan taken during the study, the number of discernible peaks was counted. Only peaks with an integrated number of greater than 1 count cm^{-3} were considered relevant. The number of peaks vs. time of day is displayed in Figure 3.2. Figure 3.2a gives a diurnal profile; 3.2b, a one week profile; and 3.2c the profile for the duration of the experiment. The solid line represents a five-point binomial smoothing algorithm. Each data point represents a single scan. Variability in the number of peaks on small time scales (scan to scan) are a result of the inability to distinguish individual peaks from scan to scan even though they may be present. The number of peaks produced by the humidified 50 nm aerosol exhibits a clear pattern with time of day throughout the experiment, with the smallest number of peaks present in the early afternoon (between 12 and 2 pm) and the most peaks present early morning (2-4 am). The pattern was not altered by emissions from the forest fires in the latter half of the study.

During the period from August 17 to August 23, only 50 nm aerosol was monitored. Over 3500 $89\% \pm 1\%$ humidity scans were obtained. Each scan was analyzed by first counting the number of peaks and then fitting the data to a multimodal log-normal size distribution, i.e.,

$$\frac{dN}{d \ln D_p} = \sum_i \frac{dN_i}{d \ln D_{p,i}} = \sum_i \frac{N_i}{(2\pi)^{1/2} \ln \sigma_{g,i}} \exp\left(-\frac{(\ln D_{p,i} - \ln \bar{D}_{pg,i})^2}{2 \ln^2 \sigma_{g,i}}\right) \quad (3.2)$$

by a least squares analysis. $\sigma_{g,i}$ is the standard deviation, $\bar{D}_{pg,i}$ is the mean aerosol diameter for the individual peak, $D_{p,i}$ is the diameter of each size bin, and N_i is the number of particles in the given peak.

Figure 3.3a displays the growth factors for each of the log normal distributions. Peak number 1 corresponds to the smallest diameter. Figure 3.3b shows the growth factor of the dominant peak, i.e., the one that contains the largest particle number concentration. Figure 3.3c shows the particle number concentration of each individually fit aerosol peak. Several trends are identifiable from careful consideration of these data. First, the locations of the first several peaks indicate that the hygroscopic growth factor of the aerosol does not vary much throughout the week for these modes. The first peak ranges from 1.0 to 1.1, the second from 1.04 to 1.2, and the third from 1.12 to 1.3. Only the last three peaks range more widely. Furthermore, most of the aerosol grows only slightly when exposed to high humidity. This suggests that the main fraction of the aerosol is composed of either organic material or soot, both of which have low hygroscopic growth factors. The hygroscopicity of the main fraction (based on number concentration) increases during the afternoon. This is also consistent with a mostly organic aerosol. This “peak” in the

hygroscopic growth factor in mid-afternoon corresponds to the peak in photochemical activity as measured by ozone concentration. This trend is consistent with chamber data, which shows an increase in the hygroscopic growth of organically coated aerosol as it becomes increasingly oxidized. The greater oxidation levels can lead to more acids and aldehydes, increasing the polar organic content and therefore its hygroscopicity.

3.3.1 Hygroscopic behavior of 50 nm particles

Figures 3.4a through 3.4i contain sample distributions taken from DMA2 for 50 nm diameter classified aerosol on August 26. These sample distributions are typical for the duration of the study. The timing of the monomodal distribution peak varies by 1-2 hours. The hygroscopic growth of the 50 nm particles increased slightly during the fires, but the size distribution pattern remained constant. Figure 3.4a shows the calibrated aerosol distribution that was obtained by maintaining the same relative humidity in the first and second DMA. Figures 3.4b – 3.4i show a sequence of humidified aerosol size distributions throughout the day, and reveal a pattern. Several peaks merge during the morning, becoming unimodal about 2:30 PM. The aerosol then separates into multiple modes throughout the rest of the day, as might be expected if the secondary aerosol were primarily organics. The hygroscopic particles that form multiple peaks in the early morning may grow out of the 50 nm size range as they are coated by secondary organic products, or the coating process may reduce the hygroscopicity by producing an aerosol that is mostly organic. In the late afternoon and evening, transport of aerosol dominated by inorganic salts increases the hygroscopicity of the Pasadena aerosol. The appearance of multiple peaks suggests that a variety of sources contribute to this aerosol. During the night, marine aerosol can be transported to the site without undergoing any photochemical

processes, as evidenced by the largest hygroscopic peaks appearing at night. Because the hygroscopic growth factors rarely reach 1.5, we may infer that few particles in the Pasadena aerosol are pure marine aerosols, even at night when the winds originate at the coast.

TDMA experiments performed on chamber aerosol at Caltech show that the $(\text{NH}_4)_2\text{SO}_4$ seed particles decrease in hygroscopic growth as they are coated with secondary organics. However, continued photochemical reactions after the primary hydrocarbon was reacted, led to an increase in the hygroscopic growth. Similar transformations of aerosol-phase organics may occur in the ambient aerosol, contributing to the increase in hygroscopicity later in the day as seen in the data.

3.3.2 Hygroscopic behavior of 150 nm particles

Figures 3.5a through 3.5i contain sample distributions taken from DMA2 for 150 nm classified aerosol on August 26. These sample distributions exhibit a pattern that is typical of that observed throughout the study. Figure 3.5a is the calibrated aerosol distribution, obtained by maintaining identical RH on the aerosol entering the first and second DMAs. Figures 3.5b through 3.5i illustrate that the size distributions differ substantially from those of the 50 nm particles. Fewer peaks are observed in the middle of the night, while the greatest number appears during the day. In spite of the obvious differences, this behavior suggests that the aerosol undergo similar atmospheric transformations as the 50 nm particles. The differences can be attributed to differences in the relative amounts of organic and inorganic aerosol in the two size fractions. Much more organic coating is necessary for the 150 nm aerosol to go from mostly inorganic, if marine in origin, to mostly organic by volume. At 1 AM, the distribution is clearly bi-

modal; one mode has a large growth factor of about 1.6, and the other mode is barely hygroscopic with a growth factor of 1.1. This is consistent with aerosol from two different sources, one a primary aerosol, probably anthropogenic in origin, while the other aerosol mode is most likely marine in origin and, therefore, mostly inorganic. During the day the splitting becomes more prevalent as the organic coats the aerosol leading to particles with lower inorganic fractions. However, because the particles start larger, the organic fraction is unable to dominate. A range of compositions or, perhaps, coating thickness causes the aerosol to separate into several modes.

3.4 Summary and Conclusions

Figures 3.6a and 3.6b show a compilation of all the 50 nm scans over the entire period of measurement. Figure 3.6a shows a one-week period to illustrate the diurnal cycle. Figure 3.6b shows the data for the entire experiment. The plots were generated by dividing the size distribution into 71 size bins where $\log(D_i/D_{i+1})$, D_i and D_{i+1} represent classified aerosol diameters in bin i and $i+1$, is constant for all size bins. The total number concentration of particles in each size bin was computed. The log (% number) in each bin was then plotted as the color axis, with blue being the largest and red being $<0.1\%$ by number. The ordinate is the growth factor for each bin, defined as the log averaged diameter of each size bin divided by the mean calibrated diameter exiting DMA 2. Figures 3.7a and 3.7b show the same type of plot for the 150 nm size aerosol.

Figures 3.6 and 3.7 indicate the duration of the fire periods. The hygroscopicity of the aerosol increased during the fire periods, but the general appearance of the diurnal cycle did not change. The 50 nm classified aerosol reduced to a single peak in the early afternoon, followed by a shift of the peak toward higher hygroscopic growth as the

afternoon progressed. The 150 nm classified aerosol remained bimodal at night and multimodal during the day, which was also the observable trend without the fire.

The hygroscopic growth behavior of Pasadena, CA, aerosol has been measured at 89% RH and reported. When humidified, both aerosol sizes, 50 nm and 150 nm diameter, separated into multiple distinct modes depending on the time of day and size of the particles. Diurnal patterns were observed for the hygroscopic growth with the largest modes present during the night and the lowest during the day. Differences in behavior of 50 nm and 150 nm particles were noted. The presence of wildfires in the vicinity of the sampling site led to an increase in aerosol hygroscopicity. In short, treating this complex urban aerosol as a combination of “less” and “more” hygroscopic fractions is an oversimplification.

3.5 References

- Baumgardner, D. and Clarke, A. (1998). Changes in aerosol properties with relative humidity in the remote southern hemisphere marine boundary layer. *J. Geophys. Res.* 103:16,525-16,534.
- Berg, O.H., Swietlicki, E., and Krejci, R. (1998). Hygroscopic growth of aerosol particles in the marine boundary layer over the Pacific and Southern Oceans during the First Aerosol Characterization Experiment (ACE 1), *J. Geophys. Res.* 103:16,535-16,545.
- Busch, B., Sprengard-Eichel, C., Kandler, K., and Schutz, L. (1999). Hygroscopic properties and water soluble fraction of atmospheric particles in the diameter range from 50 nm to 3.0 μm during the Aerosol Characterization Experiment in Lindenberg 1998. *J. Aerosol Sci.* 30:S513-S514.
- Collins, D.R., Flagan, R.C., and Seinfeld, J.H. (2001). Improved inversion of scanning

- DMA data. *Aerosol Sci. Technol.* In press.
- Covert, D.S., and Heintzenberg, J. (1993). Size distributions and chemical properties of aerosol at Ny Alesund, Svalbard. *Atmos. Environ.* 27A:2989-2997.
- Dua, S.K., and Hopke P.K. (1996). Hygroscopic growth of assorted indoor aerosols. *Aerosol Sci. Technol.* 24:151-160.
- Ferron, G.A., Karg, E., Busch, B., and Heyder, J. (1999). Hygroscopicity of ambient particles. *J. Aerosol Sci.* 30:S19-S20.
- Fuchs, N.A. (1963). On the stationary charge distribution on aerosol particles in a bipolar ionic atmospheric atmosphere. *Geofis. Pura. Appl.* 56:185-193.
- Hansson, H.-C., Rood, M.J., Rood, M.J., and Covert, D.S. (1990). Experimental determination of the hygroscopic properties of organically coated aerosol particles. *J. Aerosol Sci.* 21:S241-S244.
- Hansson, H.-C., Wiedensohler, A., Koloutsou-Vakakis, S., Hameri, K., Orsini, D., and Wiedensohler, A. (1998). NaCl aerosol particle hygroscopicity dependence on mixing with organic compounds. *J. Atmos. Chem.*, 31:321-346.
- Kleeman, M.J., Schauer, J.J., and Cass, G.R. (1999a). Size and composition distribution of fine particulate matter emitted from motor vehicles. In press.
- Kleeman, M.J., Schauer, J.J., and Cass, G.R. (1999b). Size and composition distribution of fine particulate matter emitted from wood burning, meat charbroiling and cigarettes. *Environ. Sci. Technol.* 33:3516-3523.
- Kreidenweis, S.M., Flagan, R.C., and Seinfeld, J.H. (1987). Evaporation and growth of multicomponent aerosols laboratory applications. *Aerosol Sci. Technol.* 6:1-14.
- Li, W., and Hopke, P.K. (1993). Initial size distributions and hygroscopicity of indoor

- combustion aerosol particles. *Aerosol Sci. Tech.* 19:305-316.
- Massling, A., Wiedensohler, A., and Busch, B. (1999). Hygroscopic growth of aerosol particles in the southern Atlantic Ocean and Indian Ocean. *J. Aerosol Sci.* 30:S837-S838.
- McMurry, P.H., and Stolzenburg, M.R. (1989). On the sensitivity of particle size to relative humidity for Los Angeles aerosols. *Atmos. Environ.* 23:497-507.
- McMurry, P.H., Litchy, M., Huang, P.-F., Cai, X., Turpin, B.J., Dick, W.D., and Hanson, A. (1996). Elemental composition and morphology of individual particles separated by size and hygroscopicity with the TDMA. *Atmos. Environ.* 30:101-108.
- Rader, D.J. and McMurry, P.H. (1986). Application of the tandem differential mobility analyzer to studies of droplet growth or evaporation. *J. Aerosol Sci.* 17:771-787.
- Svenningsson, I.B., Hansson, H.-C., Wiedensohler, A., Ogren, J.A., Noone, K.J., and Hallberg, A. (1992). Hygroscopic growth of aerosol particles in the Po Valley. *Tellus.* 44B:556-569.
- Swietlicki, E., Zhou, J., Berg, O.H., Martinsson, B.G., Frank, G., Cederfelt, S.-I., Dusek, U., Berner, A., Birmili, W., Wiedensohler, A., Yuskiewicz, B., and Bower, K.N. (1999). A closure study of sub-micrometer aerosol particle hygroscopic behaviour. *Atmos. Res.* 50:205-240.
- Virkkula, A., Dingenen, R.V., Raes, F., and Hjorth, J. (1999). Hygroscopic properties of aerosol formed by oxidation of limonene, α -pinene, and β -pinene. *J. Geophys. Res.* 104:3569-3579.
- Xiong, J.Q., Zhong, M., Fang, C., Chen, L.C., and Lippmann, M. (1998). Influence of organic films on the hygroscopicity of ultrafine sulfuric acid aerosol. *Environ. Sci.*

Technol. 32:3536-3541.

Zhang, X.Q., McMurry, P.H., Hering, S.V., and Casuccio, G.S. (1993). Mixing characteristics and water content of submicron aerosols measured in Los Angeles and at the Grand Canyon. *Atmos. Environ.* 27A:1593-1607.

Zhou, J., Swietlicki, E., Hansson, H.C., and Artaxo, P. (1999). Aerosol particle size distributions and hygroscopic growth in the Amazonian rain forest. *J. Aerosol Sci.* 30:S163-S164.

Table 3.1. Available data on hygroscopic aerosol growth.

#	Type of aerosol	Location	Dates	Technique	Conditions
1	Urban	Claremont, CA	Jun-Sep 1987	TDMA & impactor	Measured hygroscopic growth of 50, 200, and 500 nm particles.
2	Urban	Claremont, CA and Grand Canyon, AZ	1987 and 1990	TDMA & impactor	Measured hygroscopic growth of 50 to 500 nm particles.
3	Urban	Minneapolis, MN	Summers, 1993-94	TDMA & impactor	Separated more hygroscopic and less hygroscopic modes and determined composition.
4	Urban	Lindenberg, Germany	Jul-Aug 1998	TDMA	Tested hygroscopic growth of 50-250 nm particles.
5	Rural Semi-urban Urban	Germany	Winter, Summer, Fall, 1998	TDMA	Tested hygroscopic growth of 50-250 nm particles.
6	Marine boundary layer--ACE 1	Remote southern hemisphere ocean	Nov-Dec 1995	FSSP	Measured particle sizes as a function of ambient RH.
7	Marine boundary layer--ACE 1	Remote southern hemisphere ocean	Oct-Dec 1995	TDMA	Measured particles with dry diameters of 35, 50, 75 and 150 nm in the MBL of Southern Ocean.
8	Marine boundary layer and continental	Arctic--Norway	Mar-Apr 1989	TDMA	Measured hygroscopic growth of 110, 200, and 310 nm particles from 20% to 90% RH.
9	Marine and continental	Southern Atlantic and Indian Oceans	Jan-Apr 1999	TDMA	Tested hygroscopic growth of 50-250 nm particles.
10	Aged continental aerosol	Northern England	Mar-Apr 1995	TDMA & cascade impactors	Tested hygroscopic growth of particles between 35 and 265 nm.

Table 3.1. Available data on hygroscopic aerosol growth (continued).

11	Rain Forest	Amazon Rain Forest	Mar-Apr 1998	TDMA	Tested hygroscopic growth of 35-264 nm particles.
12	Fog	Po Valley, Italy	Nov 1989	TDMA	Tested hygroscopic growth of particles between 30 and 200 nm during fog episodes.
13	Secondary Organic Aerosol	N/A	1998	TDMA	Tested hygroscopic growth of SOA from smog chamber experiments. Used limonene, α -pinene, and β -pinene with and without seed.
14	Household primary aerosol	N/A	1996	TDMA	Measured hygroscopic growth of aerosols from deep frying oil, grilling sausages, burning wood.
15	Household primary aerosol	N/A	1993	TDMA	Measured hygroscopic growth of aerosols from incense, cigarettes, natural gas, propane, and candles.
16	Inorganic Salt: NaCl and $(\text{NH}_4)_2\text{SO}_4$	N/A	1990	TDMA	Tested hygroscopic growth with organic layers on particles.
17	Inorganic Salt (NaCl)	N/A	1998	TDMA	Tested hygroscopic growth with organic layers on particles.
18	Sulfuric acid	N/A	1998	TDMA	Tested hygroscopic growth with and without organic layers.

Table 3.1. Available data on hygroscopic aerosol growth (continued).

#	Findings	Reference	**
1	Aerosol split into two modes, non-hygroscopic and hygroscopic. Hygroscopic Growth Factors (GF): 1.12 for 50 nm particles, 1.19 for 200 nm particles, 1.46 for 500 nm particles.	McMurry and Stolzenburg, 1989	
2	Claremont: 'less hygroscopic' particles did not grow, 'more hygroscopic' had growth factors from 1.15 at 50 nm to 1.6 at 500 nm. Grand Canyon: 'less hygroscopic' GFs ranged from 1 (no growth) to 1.4, 'more hygroscopic' GFs were around 1.5.	Zhang, et al., 1993	a
3	Less hygroscopic: 55% chain agglomerates, 33% irregular shapes, <10% each spheres & flakes. More hygroscopic: liquid droplets that contained sulfur and sometimes carbon or ionic species (Na^+ or K^+).	McMurry et al., 1996	
4	Bimodal growth: Less hygroscopic: GF ranges from 1.0 to 1.2, More hygroscopic: GF ranges from 1.3 to 1.8.	Busch et al., 1999	
5	Bimodal growth: LH: GF=1.03, MH: GF=1.37.	Ferron et al., 1999	
	Bimodal growth: LH: GF=1.03, MH: GF=1.33.		
	Bimodal growth: LH: GF=1.00, MH: GF=1.30.		
6	Changes in particle volume, effective radius, and optical scattering are strongly related to RH.	Baumgardner and Clarke, 1998	b
7	Non-sea-salt sulfate (nss) GFs: 1.56-1.62, 1.59-1.66, and 1.63-1.78 for 35, 50, and 150 nm. Sea-salt particles: 2.12 and 2.14 for 50 and 150 nm.	Berg et al., 1998	c
8	Two modes: more hygroscopic, GF=1.45; Less hygroscopic showed very little growth (appeared only with continental aerosol). All aerosols tested showed some growth.	Covert and Heintzenberg, 1993	
9	Marine: Unimodal GF of 1.9, Continental: bimodal GF, MH=1.8, LH=1.4.	Massling et al., 1999	
10	Less hygroscopic GFs: 1.11 to 1.15, increasing slightly with particle diameter. More hygroscopic GFs: 1.38-1.69 increasing with particle diameter.	Swietlicki et al., 1999	d
**Notes:			
a	At Grand Canyon, growth factors varied from day to day, but did not vary significantly with size.		
b	FSSP=Forward Scattering Spectrometer Probe		
c	Particles with less hygroscopic growth only present during periods of anthropogenic influence		
d	Fitting a model to the data, the hygroscopic growth could be adequately described assuming only inorganic species interact with water vapor.		

Table 3.1. Available data on hygroscopic aerosol growth (continued).

11	Unimodal GFs from 1.2 to 1.4 when taken from a dry state to 90% RH.	Zhou et al., 1999	
12	Two modes: more hygroscopic mode had a mean GF of 1.44 ± 0.14 . Less hygroscopic mode had a mean GF of 1.1 ± 0.07 . GFs and LH fraction varied day to day, but no size dependence was seen.	Svenningsson, et al., 1992	
13	No seed: GFs of about 1.1 were observed. Ammonium sulfate seed: GFs started at about 1.5 before reaction, and diminished with time to ~ 1.1 . GFs did not vary much with size, but larger particles took longer to reach the final GF.	Virkkula et al., 1999	
14	Particles from wood smoke w/o flame were 92% soluble material, and had GFs of 1.5 to 2.5, depending on initial particle diameter.	Dua and Hopke, 1996	e
15	Average GFs: 1.36-1.85. For all types, GFs increased with increasing particle diameter. Tested room air as background: Growth ratio was 1.75 at 50 nm.	Li and Hopke, 1993	
16	Organic coating decreases hygroscopic growth, but non-uniform coatings cause large variations in GF.	Hansson, et al., 1990	
17	Organic coating decreases hygroscopic growth, but large concentration required to achieve the effect observed in field experiments.	Hansson, et al., 1998	
18	Organic layer on particles decreases hygroscopic growth of particles.	Xiong, et al., 1998	
**Notes:			
e	Particles from oil, sausages, and wood w/flame smokes did not grow, even though they were 8% to 46 % soluble material.		

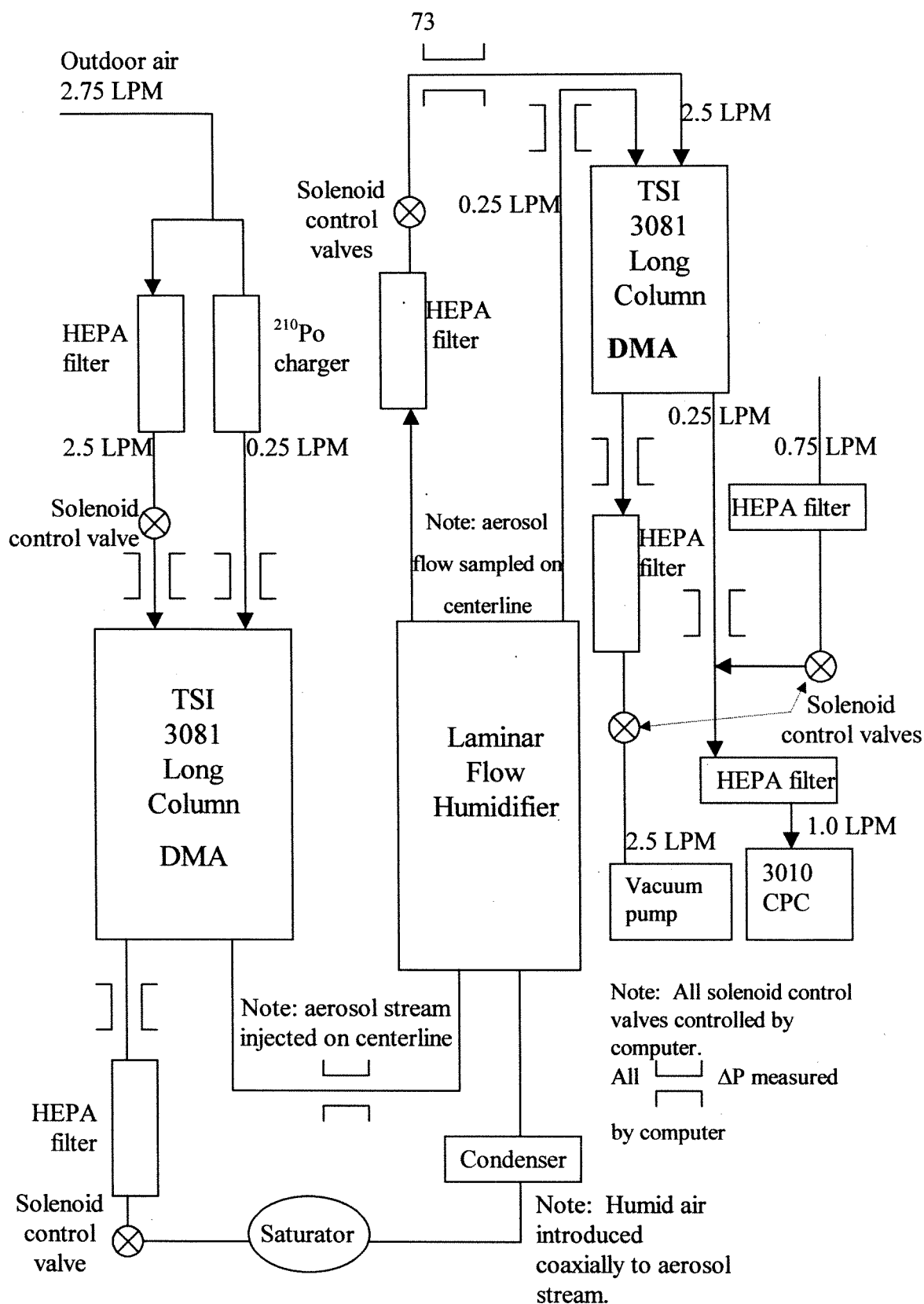


Figure 3.1. Experimental TDMA system

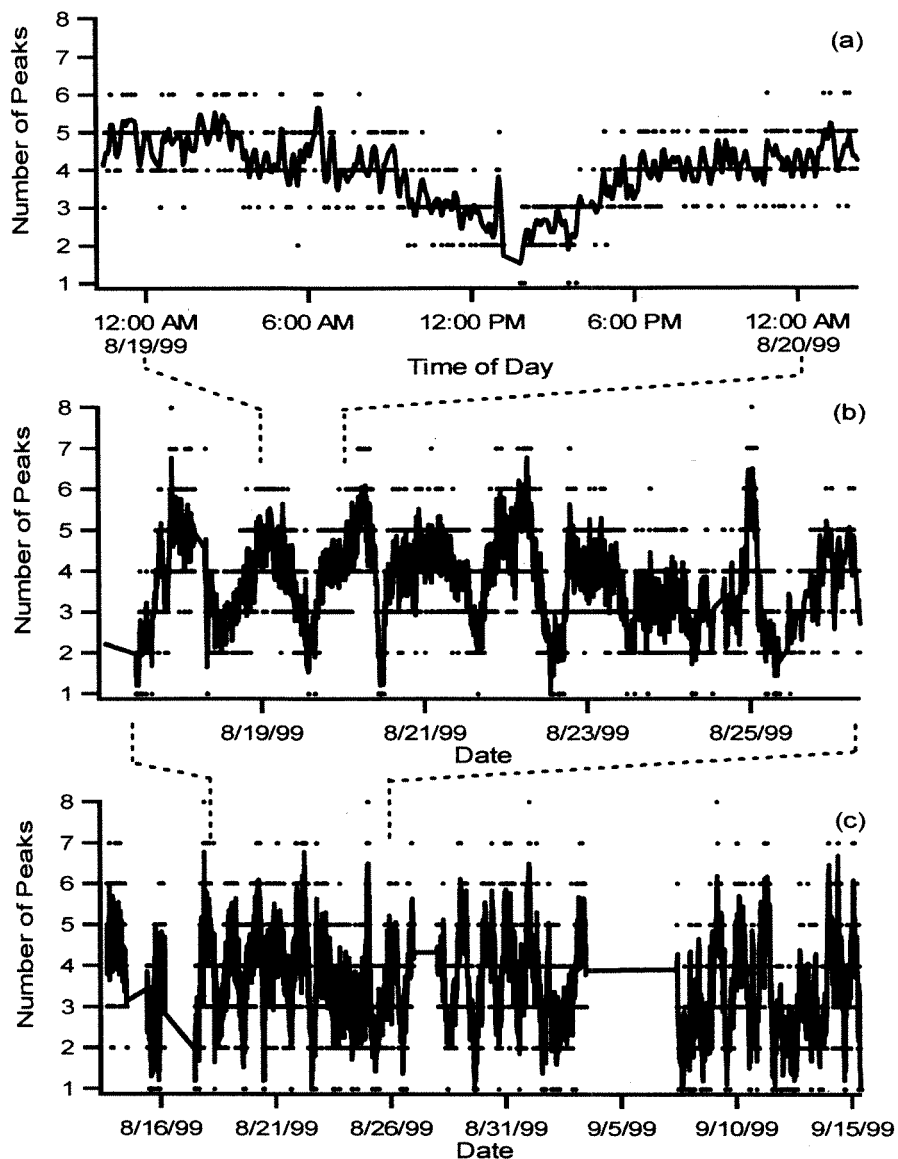


Figure 3.2. Number of discernible peaks vs. time of day for the aerosol classified dry of 49.7 nm classified aerosol. Points indicate individual peak observations. Line shows a five-point binomial smoothed fit through the data. (a) Diurnal cycle on August 19, 1999; (b) Weekly cycle from August 18 to August 26, 1999; (c) The complete study, spanning August 13 to September 15, 1999. Tickmarks (b,c) at midnight.

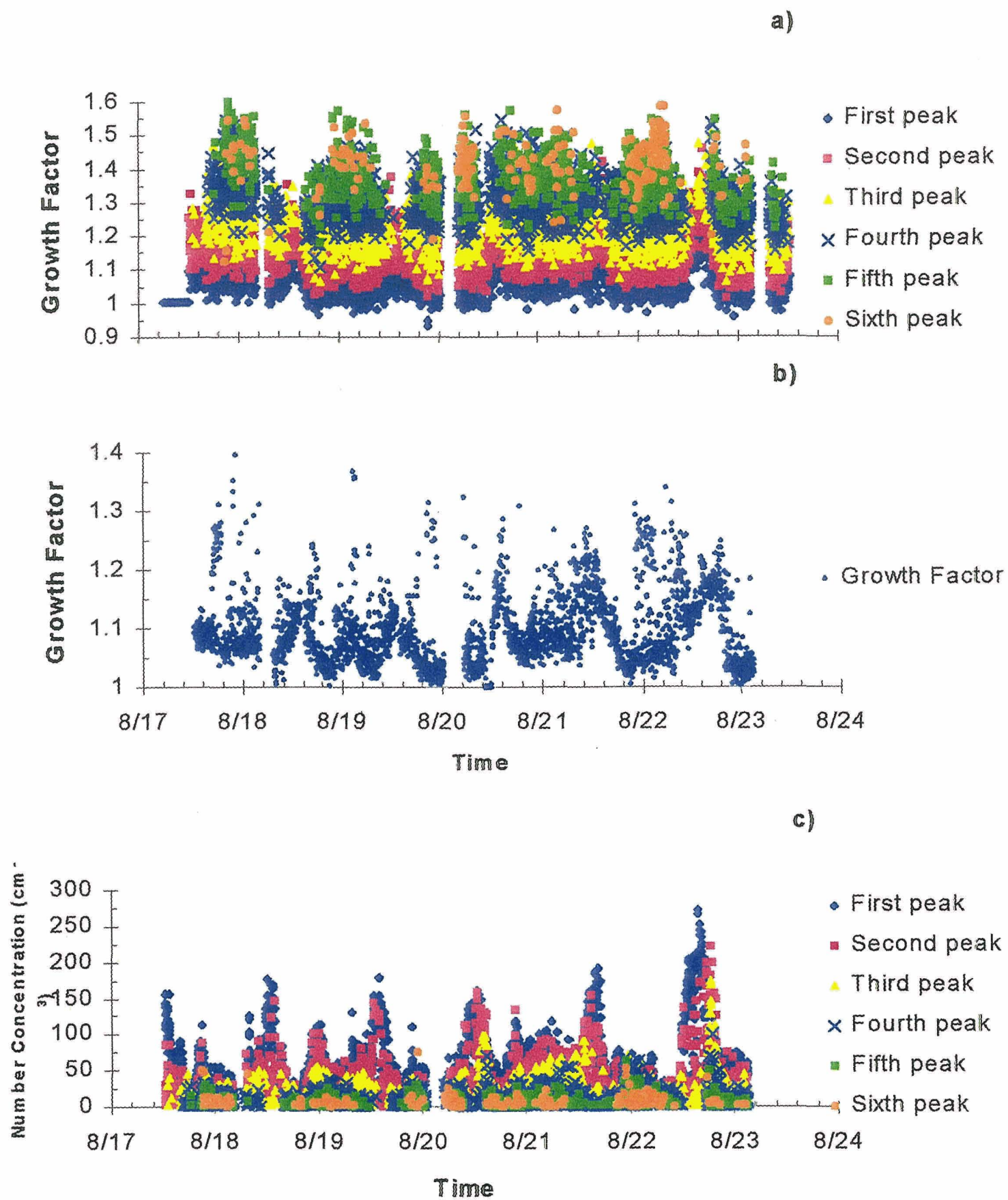


Figure 3.3. Measured growth factors for log-normally fit peaks of 49.7 nm dry particles humidified to 89% relative humidity for August 17 to August 23. (a) Growth factor for each peak. (b) Growth factor of the peak containing the greatest number percent of particles in the size distribution from DMA2. (c) Particle number concentration of each individually fit aerosol peak. Major tickmarks at midnight.

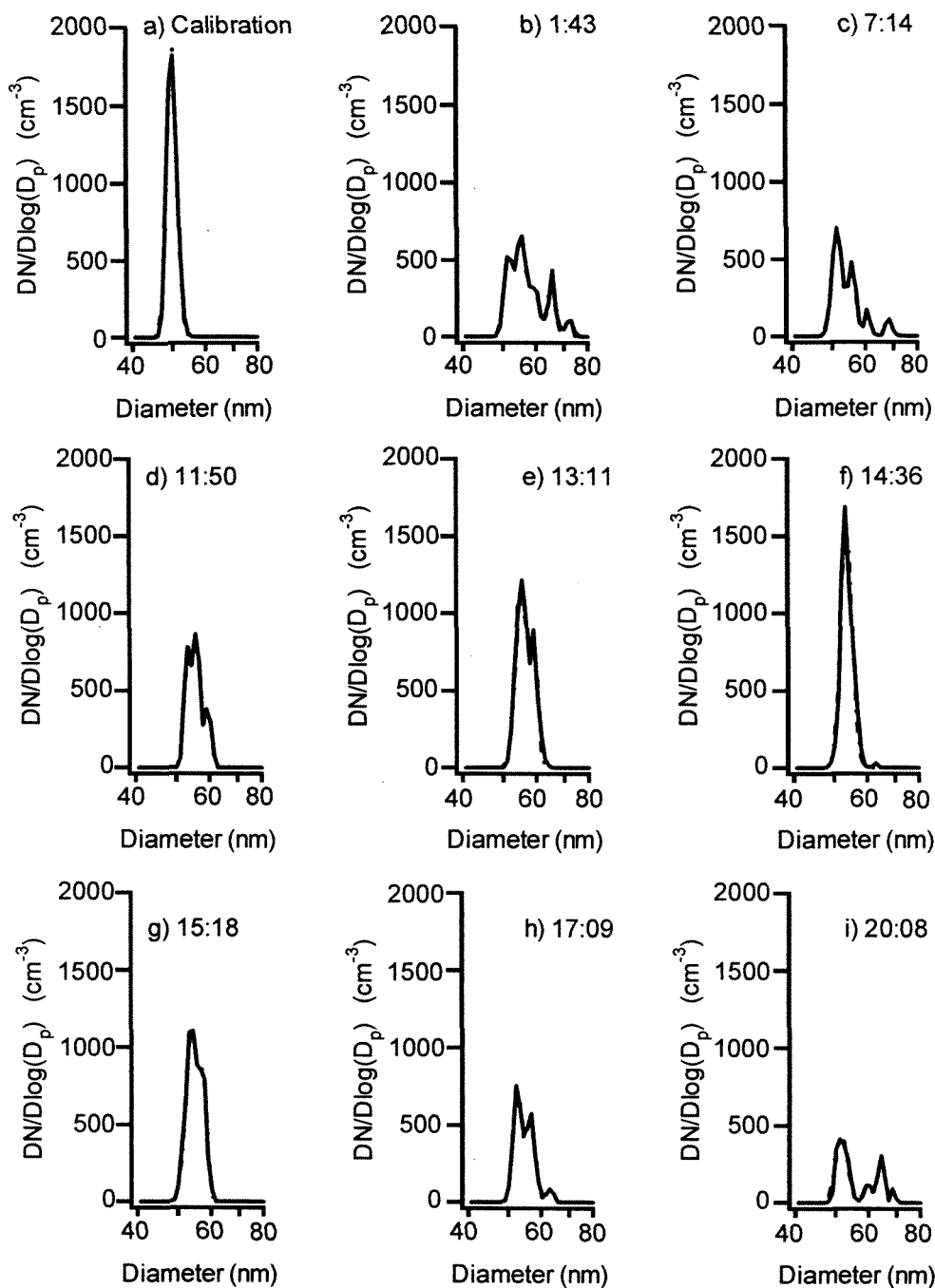


Figure 3.4. Typical size distributions from DMA1, classification set to 49.6 nm.

Solid line shows experimental data, dashed line shows a multimodal log-normal

fit. (a) Distribution before humidification. (b-i) Representative distributions on

August 26, 1999.

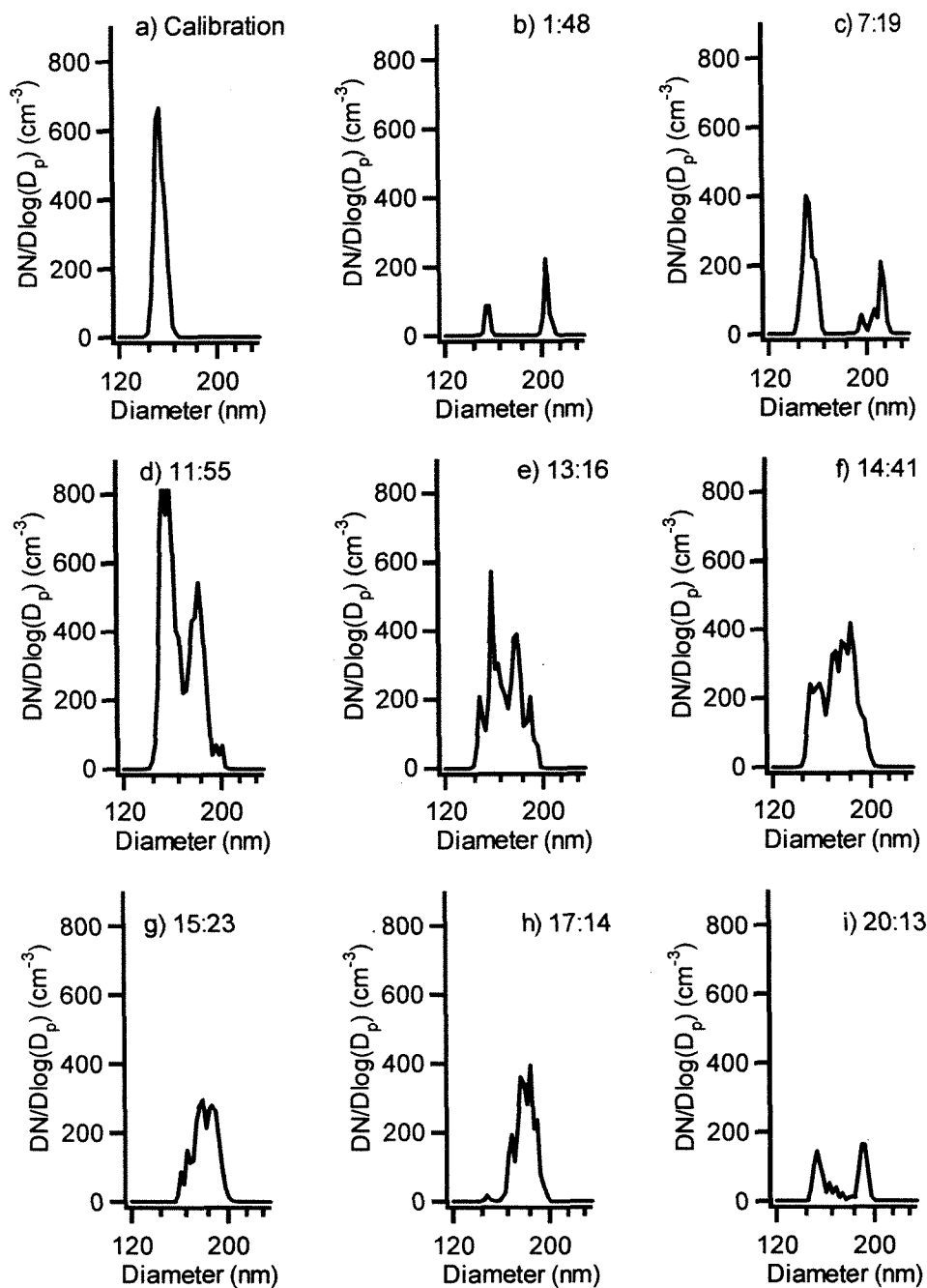


Figure 3.5. Typical size distributions from DMA1, classification set to 148.5 nm.

Solid line shows experimental data, dashed line shows a multimodal log-normal fit. (a) Distribution before humidification. (b-i) Representative distributions on August 26, 1999.

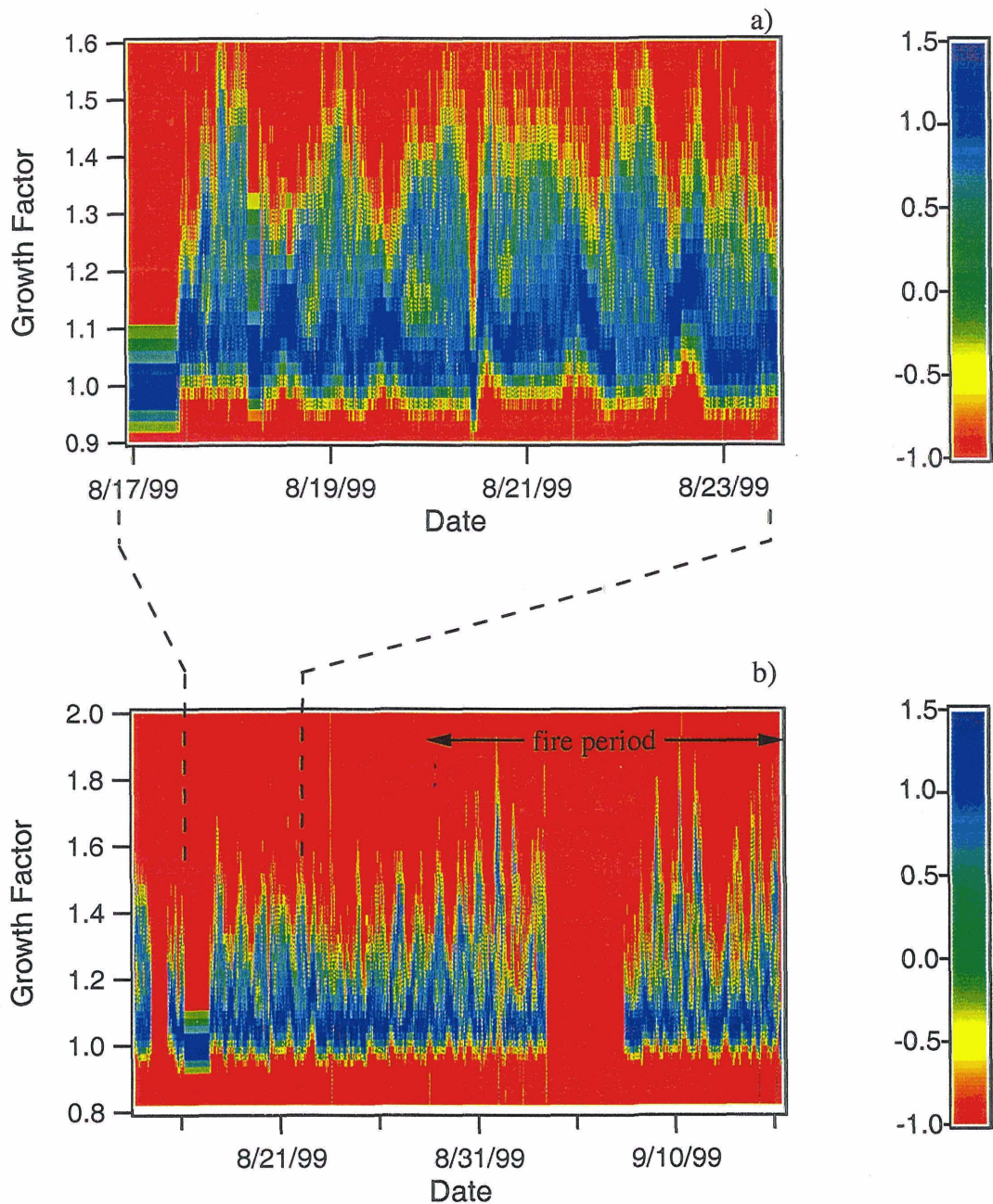


Figure 3.6. Cumulative distributions for the entire 49.7 nm classified aerosol, humidified to 89% RH. Color represents log of particle number concentration in each size bin. The period of influence is indicated. (a) Detailed data for the week of August 17 to August 23, 1999. (b) All data, August 13 to September 15, 1999. Tickmarks at midnight.

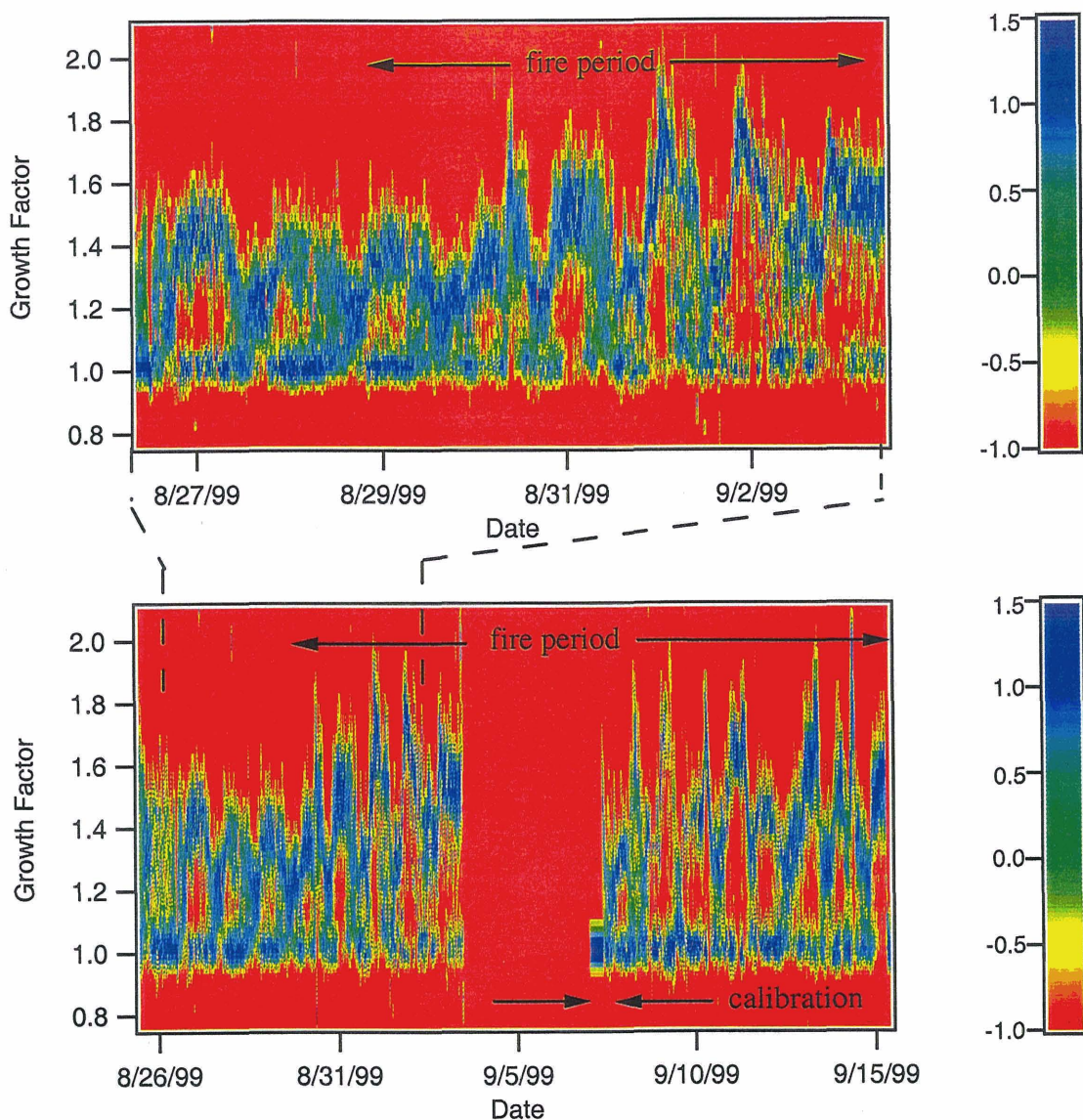


Figure 3.7. Cumulative distributions for the entire 148.5 nm classified aerosol, humidified to 89% RH. Color represents log of particle number concentration in each size bin. The period of fire influence is indicated. (a) Detailed data for the week of August 27 to September 3, 1999. (b) All data, August 26 to September 15, 1999. Tickmarks at midnight.

Chapter 4**State-of-the-Art Chamber Facility for Studying Atmospheric Aerosol
Chemistry**

4.1 Introduction

Laboratory chambers are indispensable in the study of gas-phase atmospheric chemistry and atmospheric aerosol formation and growth. Because of the difficulty of isolating chemical and microphysical processes in the atmosphere from flow and mixing effects, chamber studies provide a means to develop mechanistic understanding of such processes. In this context, a laboratory chamber constitutes a well-mixed batch reactor in which the chemical processes of interest can be isolated directly.

From the point of view of atmospheric chemistry where chemistry is generally driven by sunlight, chambers can be divided into two categories: those driven by natural sunlight and those driven by artificial sunlight. The principal advantage of outdoor chambers is the availability of natural sunlight; disadvantages arise from varying light intensity resulting from atmospheric conditions and clouds, as well as the general exposure to weather elements. Varying ambient conditions make replicate experiments difficult on a day-to-day basis and complicate temperature and relative humidity control. Indoor chambers afford precise control of temperature and humidity; but artificial lights may not simulate natural sunlight as closely as desired in portions of the solar spectrum, resulting in rates of certain photolysis reactions differing between the natural and artificial systems. Although not identical to natural sunlight, artificial light allows for experiments to be repeated.

Although a reaction vessel with a volume of a few liters strictly qualifies as a “chamber,” studies of atmospheric chemistry, especially involving aerosol formation, require systems of at least a few cubic meters in volume. Larger chambers reduce

chamber surface area-to-volume ratios, thereby minimizing wall effects such as removal of gas-phase species and deposition of particles on the wall of the chamber.

Chamber studies of aerosol formation and growth combine the challenges of both gas-phase chemistry and aerosol dynamics. It is to this area that the present paper is directed. A principal goal of chamber-based atmospheric aerosol research is to understand the fundamental mechanisms by which gas-phase atmospheric chemistry leads to aerosol formation and growth. Measurements required in such experiments include gas-phase species concentrations, and aerosol size distribution and composition. Measurements of aerosol microphysical properties, such as hygroscopic water uptake, are also useful.

We describe here a state-of-the-art indoor chamber facility for atmospheric aerosol research. Special emphasis has been placed on rapid, automated aerosol measurements. The system is particularly well suited for determination of the amount of secondary organic aerosol (SOA) formed from the oxidation of a single or group of parent hydrocarbons. Such experiments can be carried out in the absence or presence of a seed aerosol.

In this paper we describe the facility hardware and environmental controls. This is followed by a description of the gas-phase and aerosol-phase instrumentation. Details of aerosol formation and evolution experiments that probe the effects of relative humidity and the phase of the aerosol follow. Finally, a section is devoted to the aerosol dynamic processes occurring within the chamber.

4.2 Facility Overview

The indoor chamber facility comprises two 28 m³ Teflon chambers. The dimensions of each Teflon chamber are 2.5 x 3 x 3.7 m. The two chambers are suspended side-by-side in a 8.5 x 4.3 x 3.2 m room. Each chamber contains two Teflon ports, one port with a 0.3175 cm hole for gas chromatograph (GC) sampling and the other port with eight 0.9525 cm holes and one 2.54 cm hole that are used for sample injection and withdrawal. The chambers were manufactured by ATEC (Malibu, CA).

The chamber wall material is 2 mil (54 µm) FEP Teflon film, a transparent, non-reactive material. The wall material is flexible, enabling air extraction from the Teflon chamber without altering the pressure inside the reactor. The variation of light absorption by the Teflon material with wavelength is shown in Figure 4.1. A drawback of the use of Teflon film is static charge build-up on the FEP Teflon film surface that increases particle deposition to the walls.

Table 4.1 summarizes the instrumentation while Figure 4.2 shows a block diagram its configuration in the facility. Table 4.1 includes estimates of the accuracy and/or precision for each of the instruments. Each of the instruments are discussed in turn.

Three hundred 1.2m, 40 Watt Sylvania 350BL lights are used to illuminate the reaction chambers. The blacklight emission spectrum is displayed in Figure 4.3. To prevent heating at the surface of the Teflon film, the chamber is fixed at least 45 cm away from the chamber lights. To maximize the light intensity in the chamber, reflective Everbrite® (Alcoa, PA) aluminum sheeting (reflectance > 95%) covers all four walls, the ceiling, and the floor of the enclosure.

A Licor 1800 portable spectroradiometer is used to monitor the light spectrum emitted by the blacklights. The photolysis rate of NO_2 is estimated by steady-state actinometry, in which NO_2 is injected into a clean chamber, and irradiated, and the resulting NO , NO_2 , and ozone mixing ratios are measured. The photolysis rate constant, k_1 , is then estimated as $k_1 = k_3[\text{O}_3][\text{NO}]/[\text{NO}_2]$ where $[\text{O}_3]$, $[\text{NO}]$, and $[\text{NO}_2]$ are concentrations and k_3 ($\text{cm}^3/\text{molecule}/\text{min}$) is the rate constant of NO and ozone reaction. The measured k_1 value in the chamber at full light intensity is 1.1 min^{-1} , about twice that of natural sunlight at Pasadena, CA, at noon on a clear, summer day.

The artificial light produced by the blacklights is not representative of the entire ground-level solar light spectrum. A comparison of the relative light intensity of a typical fluorescent blacklight to ground-level solar radiation is given in Figure 4.3 (Carter *et al.*, 1995). The ultraviolet irradiation produced by the blacklight lamps corresponds to the wavelengths for maximum NO_2 photolysis. However, the longer wavelengths that can photolyze some organic compounds such as methyl glyoxal, in the range of 450-550 nm, are not emitted by the blacklight lamps. An extensive discussion of light sources and absorption cross sections for aldehydes and carbonyls is found in Carter *et al.* (1995). Table 4.2 is adapted from Carter *et al.* (1995) showing the relative rate of photolysis for several photolyzing species in the chamber when comparing blacklights to solar radiation. It is important to note that the irradiation produced by blacklight lamps vary with manufacturer.

Compressed house air is forced through a series of packed bed scrubbers containing activated charcoal, silica gel, Purafil (Purafil Inc., GA) and molecular sieve, followed by a filter to produce dry, particle- and hydrocarbon-free air. This system

supports flow rates in excess of 300 LPM producing particle-free air with NO_x , ozone, water vapor, and hydrocarbon levels below detection limits. A schematic of the system is shown in Figure 4.4. A Millipore deionized water system produces $18.2 \text{ M}\Omega\cdot\text{cm}$ (25°C) water containing less than 0.02 EU/mL pyrogens, 2-5 ppb TOC, < 0.1 ppb silicates, < 0.1 ppb heavy metals, < 1 cfu/mL microorganisms, and 1 particle larger than $0.2 \mu\text{m/mL}$ for use as a solvent in aerosol seed generation and for chamber humidification.

A 52.8 kW heat exchanger controls the temperature of the insulated room housing the instrumentation and Teflon chambers. The temperature can be set from 18°C to 50°C with the chamber lights on and 15°C to 50°C with the chamber lights off. Temperature drift during an experiment rarely exceeds $\pm 0.5^\circ\text{C}$ with a transient in temperature of less than 1°C for the time immediately following the blacklights being turned on. Heat generated by the blacklights is dispersed throughout the room using eight four-room ($14.2 \text{ m}^3\text{min}^{-1}$) circulating fans. The instrumentation and sampling lines must be maintained at the chamber temperature to prevent perturbation of the sample during measurement so the instruments are located within the controlled temperature environment.

A 1500 W immersion heater submersed in $>18.2 \text{ M}\Omega\cdot\text{cm}$ water in a 60 cm tall, 7.5 cm diameter glass cylinder fitted with a Teflon cap generates water vapor for chamber humidification. The steam passes through 2.5 cm diameter Teflon tubing into the chamber at a rate sufficient to achieve a relative humidity of 50% in approximately 40 min. A Vaisala (HMP233) capacitance meter measures relative humidity and temperature with stated temperature accuracy of $\pm 0.1\%$ and RH accuracy of $\pm 0.5\%$. The water vapor addition does not introduce detectable particles or hydrocarbons into the chamber.

4.3 System Preparation

Thoroughly flushing the chamber with at least 10 chamber volumes of clean air over 24 hours prior to the start of an experiment reduces ozone, NO_x, hydrocarbons, and particle concentrations below the detection limits of the instrumentation. Periodically the chamber walls are further cleaned by baking under blacklights at 50°C while flushing with clean air.

4.3.1 Reactant injection. Microliter syringes are used to measure and inject known volumes of liquid hydrocarbons (boiling point < 240°C) into a 250 mL glass bulb. Gently heating the glass bulb with a heat gun vaporizes the hydrocarbon into an ultra-pure air stream. The vapors pass through a FEP Teflon® transfer line and a stainless steel port for injection into the chambers. Compounds with b.p. > 240°C must be injected immediately adjacent to the injection port to minimize wall losses of the hydrocarbons before they reach the chamber.

Certified mixtures of gas-phase compounds in N₂ are introduced into the chamber using a mass-flow controller (Sierra Instruments Inc., CA) to maintain the flow-rate for a set period of time. The gas is then flushed into the chamber with ultra pure air through a FEP Teflon line and stainless steel port.

4.3.2 Seed generation. Aerosol growth experiments frequently employ inorganic electrolyte seed aerosol. A stainless steel constant-rate atomizer (Liu and Lee, 1975) generates the seed aerosol from a 0.005 M solution of salt in ultra-pure water. Dry (effloresced) aerosols are produced by passing the aerosol through a heated line and a Nafion® diffusion dryer. Wet, deliquesced aerosols are injected by maintaining the RH of the injection line and the chamber above the efflorescence RH of the salt. In each

case, the seed aerosol is mixed with air that has been passed through a ^{210}Po coated tube to eliminate the charge produced during atomization. The seed generation apparatus is shown in Figure 4.5.

4.4 Gas-Phase Instrumentation

A Hewlett-Packard 5890 series II Plus Gas Chromatograph (GC) equipped with a flame ionization detector (FID) monitors gas-phase hydrocarbon concentrations in the chamber. The GC employs a six-port gas injection valve for direct injection onto the GC column, DB-5 (J&W Scientific, CA) 60 m x 0.32 mm. A pump pulls the sample from the chamber through a 10 mL stainless steel sample loop at a rate of 0.4 LPM.

GC/FID measurements are taken every 11 minutes, alternating from one chamber to the other. The estimated uncertainty of the measurement is $\pm 2\%$. A hexafluorobenzene (C_6F_6) tracer provides an internal standard for the GC measurements and serves as an indicator of air leaks in the chamber. This stable tracer does not react with hydroxyl radical, nitrate radical, or ozone at an appreciable rate. To calibrate the GC/FID for the parent hydrocarbon and C_6F_6 , the parent hydrocarbons and C_6F_6 in a methylene chloride diluent are injected into a small Teflon chamber that is then filled with clean air at 5 LPM to a volume of 50 L. A minimum of three calibration measurements at each of four different concentrations is fit with a straight-line regression through zero.

A HP GCD (gas chromatograph with electron impact ionization, mass spectrometric detection) measures concentrations of vapor-phase hydrocarbons on samples collected downstream of a filter on Tenax TA adsorbent packed stainless steel tubes at a 5 LPM flow rate. A Tekmar-Dohrmann desorber instrument with cryofocusing

capabilities injects these samples into the GC column for gas-phase oxidation product identification and quantification of hydrocarbons that are difficult to introduce to the GC/FID through a conventional gas injection valve.

NO, NO₂ and NO_x mixing ratios are tracked using a Thermo Environmental Instruments Inc. (MA) Model 42 chemiluminescent NO-NO₂-NO_x analyzer. The analyzer continuously samples at a flow rate of 0.7 LPM, alternating between the chambers in ten-minute intervals. The instrument is calibrated weekly using a certified cylinder of NO. The accuracy of the measurement is $\pm 7\%$.

A Dasibi Environmental (CA) nondispersive ultraviolet ozone analyzer monitors the chamber ozone concentration. The ozone analyzer samples at a rate of 1 LPM, pulling from alternating sides of the chamber in ten-minute intervals. The stated accuracy of the ozone instrument is $\pm 4\%$.

4.5 Aerosol Instrumentation

The aerosol instrumentation for the chamber include a scanning electrical mobility spectrometer (SEMS), a tandem differential mobility analyzer (TDMA), and a condensation particle counter (CPC). Combined, these devices measure particle size distribution, aerosol number concentration, and the hygroscopic nature of the chamber aerosol. Duplicate aerosol-phase instruments continuously (except for the TDMA) sample from each side of the chamber at an average flow rate of 5.1 LPM.

4.5.1 Size Distribution Measurements. Particle size distributions and total number concentrations are obtained every 60 s using two scanning electrical mobility spectrometers (SEMS) (Wang and Flagan, 1989), one for each side of the chamber (Figure 4.6). Each SEMS is equipped with a TSI model 3077 ⁸⁵Kr neutralizer, a TSI

model 3081 long column cylindrical differential mobility analyzer (DMA) and a TSI model 3760 condensation particle counter (CPC). The DMAs operate with sheath and excess flows of 2.5 LPM, and sample inlet and classified aerosol outlet flows of 0.25 LPM. Raising the DMA column voltage exponentially from -30 V to -7000 V enables measurement of the mobility spectrum of the aerosol over the mobility diameter range, 25 nm to 700 nm.

The volumetric flow rates and the potential applied to the inner rod of the DMA must be controlled precisely for accurate mobility measurements. A Bertan (NY) 602C that has been modified for linear output from -10 V to -10000 V provides the rod potential. Laminar flow meters, consisting of a differential pressure transducer (Dwyer, IN, model 600-2) that measure the pressure drop across a laminar flow element, monitor the volumetric flow rates. 50 mL jars filled with silica gel isolate the pressure transducers from potentially humid flows. The measured pressure drop is proportional to the volumetric flow rate. Solenoid proportional control valves (MKS model 248A) are used to adjust the flow rates on the particle-free flows, while the flow rates of all DMA flows are measured. This arrangement eliminates variable particle losses associated with aerosol passage through valves at different settings, while still ensuring precise flow settings.

A personal computer (PC) using Labview software actively controls the volumetric flow rates and DMA voltage. An analog input board, a PC-LMP-16 PNP(National Instruments, Texas), monitors the flow rate, the column voltage (after a 2000:1 voltage divider), and the 3760 CPC counts. A digital/analog (D/A) output board, a PCI-6713 (National Instruments, Texas), controls the solenoid valves and the high

voltage supply. Software based proportional-integral-derivative (PID) control adjusts the three valves controlling the four DMA flows at a rate of 100Hz, enabling flow rate control to $\pm 0.2\%$. A log-ratio amplifier (Burr-Brown model JP100) operated in anti-log configuration, exponentiates the linear, 12-bit precision analog voltage to drive the high voltage supply over the entire DMA range (10-10000 V) with a precision of $\pm 0.5\%$. The sampling line and SEMS system temperatures are maintained within 0.2°C of the chamber temperature to prevent evaporation of, or condensation on the aerosol during sampling. The sheath flow passes through a Teflon filter (CPPK Gelman) to minimize perturbations to the RH and gas-phase hydrocarbon species concentrations so that the aerosol passing through the DMA column will remain at equilibrium with the surrounding gas-phase.

A data inversion routine converts the count versus time data obtained from the SEMS by the PC to a size distribution and number concentration (Collins *et al.*, 2000). The inversion routine accounts for the diffusional broadening of the DMA transfer functions, mixing-induced delays in counting particles by the CPC, the transmission efficiency of the aerosol stream through the sampling line and SEMS, and the charging efficiency of the neutralizer.

We have examined the reproducibility and stability of the SEMS measurement by continuously monitoring mobility classified (to eliminate solute particles) 198 nm polystyrene latex (PSL) spheres for 64 hours. The diameter reported fluctuated by ± 0.5 nm over the entire duration of this test. Currently there is no calibration standard for volume concentration so only the precision for such measurement is added. After correcting for atomizer output drift using a parallel CPC to monitor the particle

concentration variability in the aerosol volume concentration measurement was found to be less than 1%.

4.5.2 Number Concentration. Independent particle number concentrations are recorded using TSI model 3010 condensation particle counters to corroborate the DMA concentrations and to aid in estimating particle wall losses. Particle coincidence in the CPC was minimized by splitting the aerosol stream from the chamber, filtering 80% of the flow, and mixing the two streams so that only 1/5 of the aerosol stream reaches the CPC. This extends the measurement range of the CPC up to approximately 50,000 particles cm^{-3} . Figure 4.7 illustrates of the CPC system.

4.5.3 Hygroscopicity measurements. The tandem differential mobility analyzer (TDMA) provides a measure of the hygroscopic behavior of an aerosol. Figure 4.8 illustrates our experimental system based upon the original design of Rader and McMurry (1986). It consists of two TSI 3081 long column cylindrical DMAs, a laminar flow environmental chamber, a ^{210}Po stainless steel neutralizer (Aerosol Dynamics, CA) and a TSI Model 3760A CPC. Flow rates of 2.5 LPM are used for both the sheath and excess flows, and 0.25 LPM for both polydisperse and monodisperse flows. The ratio of the diameter of humidified aerosol to that of classified aerosol, $G_f = D_p(\text{humidified}) / D_p(\text{dry})$, defines a measure of the water uptake of an aerosol known as the hygroscopic growth factor.

The first DMA in the TDMA system operates at constant voltage to extract particles in a narrow size range from a polydisperse aerosol sample. This classified aerosol then passes through a flow straightening tube before entering at the center of a humidification tube. Humid air enters coaxially to the sample. The 1003 mm length of

the 47 mm diameter humidification tube is sufficient to ensure fully developed flow and a uniform distribution of water vapor across the tube. Centerline particle injection minimizes variations in the residence time, typically 10 s. An aerosol sample extracted from the centerline of the humidification tube then passes through a second DMA that is operated in scanning mode, i.e., as a SEMS, to measure the particle size distribution after humidification. Additional measurements made without humidification (bypassing the humidification tube) provide the data needed to calculate growth factor. Both size distributions are fitted to log-normal distributions to facilitate calculation of G_f .

To minimize perturbations in the particle size during TDMA measurements, the temperature of the sampling lines and the entire TDMA instrument are maintained within $\pm 0.2^\circ\text{C}$ of the chamber temperature. The sheath flow for the first DMA is taken from the chamber and filtered with a Gelman CPPK filter to minimize RH fluctuations and maintain the chamber gas-phase organic composition in the system. Excess air from DMA1 is filtered and humidified by passing through a heated flask saturator containing ultra-pure water and then through a condenser that controls the total gas-phase water concentration. Sheath air for the second DMA is filtered and taken from the laminar flow reactor to once again maintain RH and organic concentrations surrounding the particles. Flow and sizing calibrations account for the excess water-vapor volume added by humidification between the first and second DMA.

The system RH is controlled to within $\pm 0.5\%$ by a feedback loop between a digital hygrometer (Vaisala HMP233) and a refrigerated bath that controls the condenser temperature. A Labview-based PID controller maintains the flow within $\pm 0.5\%$. The larger uncertainty in flow rate results from simultaneous control of eight flows with five

valves, compared to four flows with three valves in the SEMS. The data inversion process corrects for diffusional broadening in the transfer function, particle transmission efficiency, charging efficiency, and mixing effects in the CPC (Collins *et al.*, 2001). A full scan takes 60 s. A typical size distribution is shown in Figure 4.9.

4.6 Aerosol Formation and Evolution Experiments

In the absence of seed particles, aerosol may form by homogeneous nucleation. The number of particles that results depends strongly upon the operating conditions. Moreover, the concentration is uncertain since nucleation produces particles that are, at least initially, too small to measure. For quantitative measurements of aerosol yield, we therefore turn to seeded chamber studies. As described below, the aerosol yield varies depending on whether the seed particles are dry or not.

4.6.1 Dry Nucleation. In experiments performed without seed particles and at low relative humidity, aerosol forms when a gas-phase organic product accumulates to a sufficient supersaturation to induce homogeneous nucleation. Condensation and subsequent absorption of oxidation products leads to particles that are 100% organic in composition. The quantity of aerosol produced in this case, estimated from the final aerosol volume after accounting for wall losses, provides a measure of the SOA formation potential in a clean, dry environment. TDMA measurements of the chamber aerosol produced in the absence of seed particles reveals the hygroscopic nature of the pure organic oxidation products.

4.6.2 Humid Nucleation. In experiments performed at elevated RH, but without seed particles, aerosol also forms by nucleation, but subsequent particle growth involves partitioning of both water and organic products into the aerosol. Used in conjunction

with a dry nucleation experiment, the humid nucleation experiment allows one to explore the effects of the presence of water on gas-particle conversion. The SOA yield of the wet nucleation experiments can be corrected for water uptake by estimating the water fraction as that obtained from TDMA analysis of dry nucleation particles. The SOA yield in the humid system can be calculated and compared to the dry nucleation experiments after accounting for wall losses.

4.6.3 Dry Seed, Dry Conditions. In experiments performed with sufficiently high concentrations of water-free inorganic seed particles in a dry chamber, the seed particles suppress nucleation and ensure that the chamber aerosol lies within the size range of the instrumentation throughout the experiment. SOA production commences when a sufficient supersaturation of oxidation products accumulates to induce the condensation onto the dry seed surface producing an initial organic layer. Further aerosol growth occurs by absorption of reaction products into the organic layer. The resulting aerosol contains both inorganic and organic species. With a non-volatile seed aerosol, the total suspended inorganic aerosol volume changes only by particle depositions onto the chamber walls. Therefore, the organic aerosol yield can be computed from the total aerosol produced less the initial amount of inorganic material present after correction for wall losses. Comparison of the results of these experiments to those of dry nucleation experiments allows one to estimate the influence of a dry, inert non-reactive surface on gas-particle partitioning.

4.6.4 Dry Seed, Elevated Relative Humidity. These experiments add the influence of water vapor to the previous experiments. To keep the seed particles dry, the RH in these experiments cannot exceed the deliquescence RH of the inorganic salt comprising the

seed particles. Aerosol growth takes place when a sufficient supersaturation of oxidation products leads to the production of an initial organic layer. Further aerosol growth occurs as water and organic material partition into the organic or organic-water phase. The resulting aerosol contains inorganic material, organic material, and, possibly, water. Several investigations have noted that the deliquescence RH of the inorganic salt is unperturbed by organic coatings (Cruz and Pandis, 2000). If, therefore, the inorganic core of the aerosol remains dry, SOA yield can be measured as the final aerosol volume less the initial seed volume and water content (all corrected for wall losses). Water content is again measured independently by TDMA analysis either using dry aerosol from dry nucleation or from dry seed, low RH experiments.

Care must be taken to ensure that the aerosol is dry when injected and is never exposed to RH higher than the particle deliquescence RH. The state of the seed aerosol is verified prior to the start of an experiment through TDMA analysis at an RH above the seed deliquescence RH. A G_f value lower than that for a dry seed aerosol indicates that the seed is not dry.

4.6.5 Aqueous Seed, Elevated Relative Humidity. In this case, experiments are performed at elevated RH with deliquesced (wet) seed aerosol. Generation of such aerosol requires that at no point does the RH surrounding the aerosol drop below its efflorescence RH. The state of the aerosol can be verified by TDMA measurements of the hygroscopic growth factor of the particles. The water content of the inorganic seed can be estimated based on thermodynamic theory (Nenes *et al.*, 1998). Oxidation products may partition into the aqueous phase or into a separate organic phase. The amount of water in the aerosol may either increase or decrease during growth. Because

the final aerosol water content cannot be independently determined, the total aerosol yield, including water and organic material, is reported.

4.7 Aerosol Dynamics

A major goal of the aerosol chamber experiments we have described is to determine the aerosol formation potential of either a single compound or a mixture. To do this, one must estimate the mass of aerosol produced over the course of an experiment. Figure 4.10 shows a typical set of data, including the hydrocarbon disappearance, the amount of suspended aerosol volume, and the number distribution of particles. The reaction is considered finished when the aerosol volume (corrected for wall processes) is no longer changing. Several microphysical processes occurring in the chamber must be considered in order to estimate the amount of organic aerosol produced (Bowman *et al.*, 1997).

The principal process that complicates the interpretation of measured aerosol data is loss of particles to the wall of the chamber. To determine the total amount of aerosol mass generated, one must estimate the quantity of the aerosol lost to the chamber walls over the course of the experiment and add that to that measured at the end of the run. Particles deposit on the wall at a rate that is proportional to the particle concentrations and depends on particle size, leading to first-order kinetics, i.e.,

$$\frac{dN(D_p,t)}{dt} = -\beta(D_p)N(D_p,t) \quad (4.1)$$

where $\beta(D_p)$ is the wall loss coefficient (Bowman *et al.*, 1997). Values of β for typical particle sizes in our chamber range from 0.0015 to 0.003 min⁻¹. The observed decay in total number concentration provides an estimate of the amount of aerosol lost to the wall over the course of an experiment. The only competing process that can confound this

interpretation is particle-particle coagulation that also reduces the particle number concentration. In seeded experiments, at typical seed aerosol size (about 100 nm in diameter) and number concentrations (about 10^4 cm^{-3}), the time scale for coagulation is about 74 hours; consequently, coagulation can be neglected as a cause of the decrease in the aerosol number concentration when seed aerosol is used.

In the absence of seed aerosol, initial particle formation occurs by nucleation. Typically, nucleation occurs in a brief burst that produces 10^4 to 10^7 particles cm^{-3} . At number concentrations of 10^7 , 10^6 , 10^5 , and 10^4 particles cm^{-3} , the time scale for coagulation is order 200 s, 33 min, 5.6 h, and 56 h respectively. Therefore, for large nucleation bursts, coagulation becomes a significant process to reduce the number concentration. Because coagulation is a second order process, the rate of reduction in the number concentration by coagulation decreases much more rapidly than does particle loss to the walls.

Table 4.3 gives characteristic times for chamber processes important in gas-to-particle conversion. Note that the only significant change in particle number concentration occurs through wall deposition processes (except when nucleation occurs). Therefore, the number of particles in the chamber can be described by the first-order wall loss rate as $N = N_0 e^{-\beta t}$. As the mass transfer rate to suspended particles greatly exceeds that of those deposited on the wall, the amount of organic material associated with each particle at the time of deposition is assumed to be constant. Thus, the total organic material produced is estimated to be the sum of that still suspended in the aerosol phase plus that deposited to the wall. The particle size increases due to condensation of organic vapors (and any nucleation products). The final size of the particles less the initial size

of the seed particles provides an estimate of the volume of organic material suspended in the chamber. Figure 4.11 illustrates the competing processes. Adsorption of gas-phase compounds on the wall might possibly decrease their concentrations since the characteristic time for diffusion to the wall of the present chamber is 1 min. However, FEP Teflon film is non-absorptive to most hydrocarbons; measured losses of C_6F_6 and m-xylene are 0.001 hr^{-1} (loss rate includes potential leaks).

4.8 References

- Bowman F. M., Odum J. R., Seinfeld J. H., and Pandis S. N. (1997) Mathematical model for gas-particle partitioning of secondary organic aerosols. *Atmos. Environ.* **31**:3921-3931.
- Carter W. P. L., Luo D., Malkina I. L., and Pierce J. A. (1995) Environmental chamber studies of atmospheric reactivities of volatile organic compounds. Effects of varying chamber and light source. Final report to National Renewable Energy Laboratory.
- Collins D. R., Flagan R. C., and Seinfeld J. H. (2001) Improved inversion of scanning DMA data. *Aerosol Sci. Technol.* In press.
- Cruz C. N., and Pandis S. N. (2000) Deliquescence and Hygroscopic Growth of Mixed Inorganic-Organic Atmospheric Aerosol. *Environ. Sci. Technol.* In press.
- Liu B. Y. H., and Lee K. W. (1975) An aerosol generator of high stability. *Amer. Ind. Hyg. J.* 861-865.
- Rader D. J., and McMurry P. H. (1986) Application of the tandem differential mobility analyzer to studies of droplet growth or evaporation. *J. Aerosol Sci.* **17**:771-787.
- Nenes A., Pandis S. N., and Pilinis C. (1998) ISORROPIA: A new thermodynamic equilibrium model for multiphase multicomponent inorganic aerosols. *Aquat.*

Geochem. 4:123-152.

Wang S. C., and Flagan R. C. (1989) Scanning electrical mobility analyzer. *J. Aerosol Sci.* 8:1485-1488.

Table 4.1. Instrumentation Summary

Instrument	Measures	LDL/Range	Accuracy	Flow Rate (LPM)	Dedicated/ Alternating
Gas chromatograph Flame Ionization Detector HP 5890 series II	Reactive Organic Gas (ROG)	1ppb ^x	2%	0.4	alternating
Chemiluminescent NO _x analyzer Thermoenvironmental Instruments, Model 42	NO, NO ₂	5ppb	7%	0.7	alternating
Ozone Dasibi Environmental	Ozone	1ppb	4%	1.0	alternating
Hygrometer (capacitance probe) Vaisala HMP 233	Temperature Relative humidity	5% - 95% -20 C to 50 C	0.50% 0.1 C	^c	alternating
Condensation particle counter TSI 3010 CPC	Volume Concentration	0.01 particles/cc	1% ^d	1.0	dedicated
Scanning electrical mobility spectrometer	Size Distribution and Number Concentration	25-700 nm ^b	0.3% ^e 1% ^e	2.75	dedicated
Tandem differential mobility analyzer	Hygroscopic Growth Factor	1.003	+/- .003 ^e	2.75	alternating
Portable spectroradiometer Licor - 1800	Light Spectrum	280 - 850 nm	0.1 nm	N/A	N/A
Gas chromatograph mass spectrometer HP GCD	ROG/gas-phase oxidation products	1 ppt ^a	5%	5.0	dedicated

^a will be a function of hydrocarbon^b as currently configured^c in series with ozone and NO_x instruments^d 500 - 30000 cm⁻³ as configured^e measured precision

Table 4.2*. Calculated ratios of rate constants for photolysis reaction for selected light sources. Wavelength regions affecting the various photolysis reactions are also shown.

Reaction or Species ^a	$k_{\text{rel}}(z=0)^b$	λ_{max}^c	λ_{char}^d	$(k_{\text{rel}}(z=60) / k_{\text{rel}}(z=0))^e$	$(k_{\text{rel}}(\text{black}) / k_{\text{rel}}(z=0))^f$
$\text{O}_3 \rightarrow \text{O}_2 + \text{O}^1\text{D}$	0.43	320	304	28	33
$\text{CH}_3\text{CHO} \rightarrow \text{CH}_3 + \text{HCO}$	0.067	330	310	46	49
$\text{CH}_3\text{COCH}_3 \rightarrow \text{Products}$	0.0093	335	310	43	49
Higher ketones: products	0.018	340	313	53	60
Higher aldehydes \rightarrow products	0.24	345	313	53	60
$\text{HCHO} \rightarrow \text{H} + \text{HCO}$	0.33	340	317	62	68
$\text{H}_2\text{O}_2 \rightarrow 2 \text{OH}$	0.084	355	322	69	104
CH_3OOH (absorption)	0.082	360	324	70	109
$\text{HCHO} \rightarrow \text{H}_2 + \text{CO}$	0.48	360	329	80	133
Acrolein (absorption)	5.2	380	339	87	165
Benzaldehyde \rightarrow products	0.48	385	345	89	159
CH_3ONO (absorption)	24.0	410	350	93	157
$\text{HONO} \rightarrow \text{OH} + \text{NO}$	18.0	390	356	97	156
$\text{NO}_2 \rightarrow \text{NO} + \text{O}_3\text{P}$	100.0	425	369	100	100
Glyoxal \rightarrow products	1.23	460	383	95	37
Methyl Glyoxal \rightarrow products	1.7	470	417	112	15
$\text{NO}_3 \rightarrow \text{NO}_2 + \text{O}_3\text{P}$	1900.0	635	548	124	2
$\text{NO}_3 \rightarrow \text{NO} + \text{O}_2$	207.0	640	592	126	0
$\text{O}_3 \rightarrow \text{O}_2 + \text{O}_3\text{P}$	5.2	900	647	114	13

*Adopted from Carter *et al.* (1995)

^aAbsorption cross sections and quantum yields.

^bPhotolysis rates relative to NO_2 , expressed as $k_{\text{rel}} = 100 \times (\text{Photolysis rate for reaction}) / (\text{Photolysis rate for } \text{NO}_2)$.

^cLongest wavelength where product of absorption cross sections and quantum yields are nonzero.

^dAverage wavelength weighed by $J_\lambda \sigma_\lambda \Phi_\lambda$.

^eRatios of k_{rel} calculated for the spectral distribution for zenith angle of 60 ($z=60$), to the k_{rel} calculated using the ground level solar spectral distribution for zenith angle of zero.

^fRatios of k_{rel} calculated for the spectral distribution for blacklights, to the k_{rel} calculated using the ground level solar spectral distribution for zenith angle of zero.

Table 4.3. Characteristic time scales for processes occurring in the chamber.

Process	Time constant	Typical chamber values
Formation of condensable gas	$\tau_F = \frac{1}{K_{OH}[OH]}$	2 hrs
Gas-particle transport (condensation)	$\tau_{GP} = \frac{1+8\lambda/\alpha D_p}{2\pi N D_p \lambda c}$	2 min
Particle-wall transport (wall deposition)	$\tau_{PW} = \frac{1}{(A_c/V_c)K_{MP}}$	5 hrs
Gas-deposited particle transport (absorption to deposited aerosol)	$\tau_{GD} = \frac{1}{\alpha(A_p/V_c)K_{MG}}$	3.5 days
Coagulation (no nucleation)	$\tau_{COAG} = \frac{2}{KN}$	3.1 days
Coagulation (nucleation)	$\tau_{COAG} = \frac{2}{KN}$	200 sec at 10^7 particle cm^{-3} to 56 hours at 10^4 particle cm^{-3}

*If transport to particle \gg formation of condensable gases

$$K_{OH} = 2 \times 10^{-11} \text{ cm}^3/\text{molecule}\cdot\text{s}$$

$$[OH] = 7 \times 10^6 \text{ molecule}/\text{cm}^3$$

$$N = 1 \times 10^4 \text{ cm}^{-3}$$

$$D_p = 100 \text{ nm}$$

$$\alpha = 1.0$$

$$\alpha_w = 1.0$$

$$(A_c/V_c) = 1.0 \text{ m}^{-1}$$

$$K_{MG} = 1.0 \text{ m}/\text{min}$$

$$K_{MP} = 1.5 \times 10^{-3} \text{ m}/\text{min}$$

$$A_p/V_c = 2 \times 10^{-4}$$

$$K_{ij} \text{ for } N = 1 \times 10^4 \text{ cm}^{-3}, D_p = 100 \text{ nm}$$

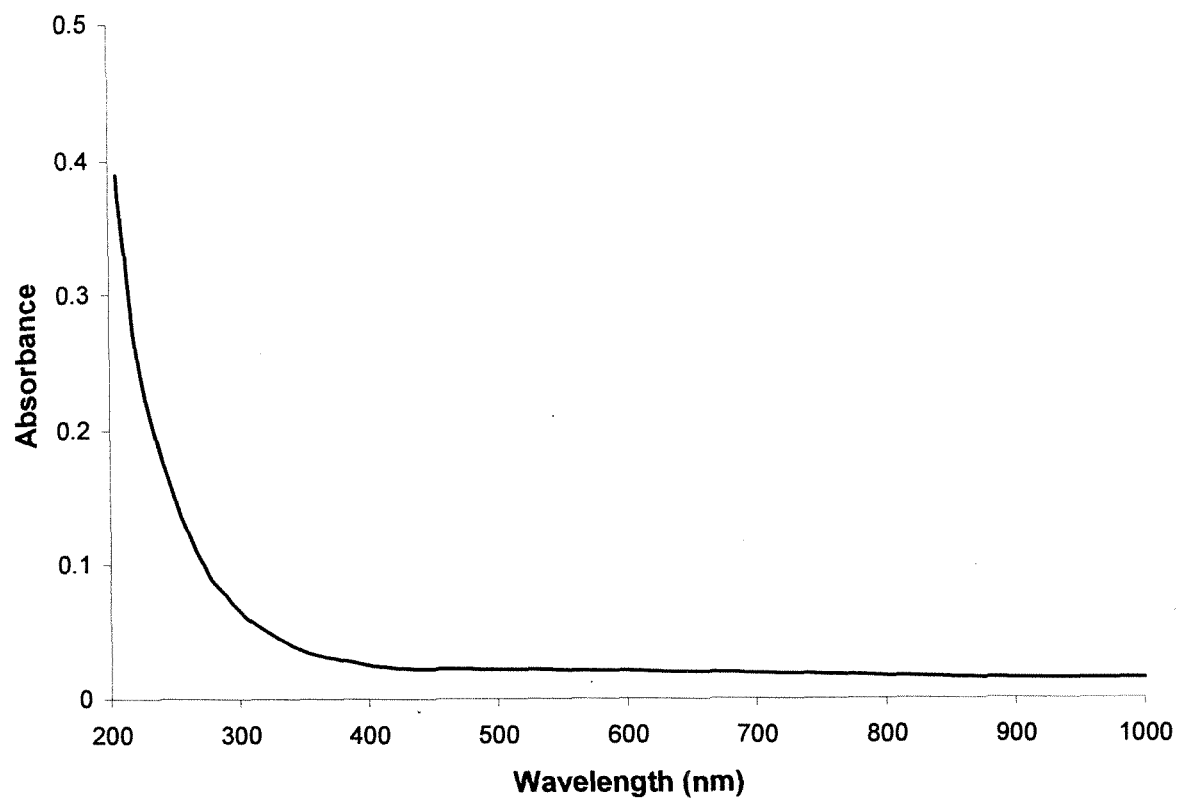


Figure 4.1. Absorption spectra for 2 mil FEP Teflon film.

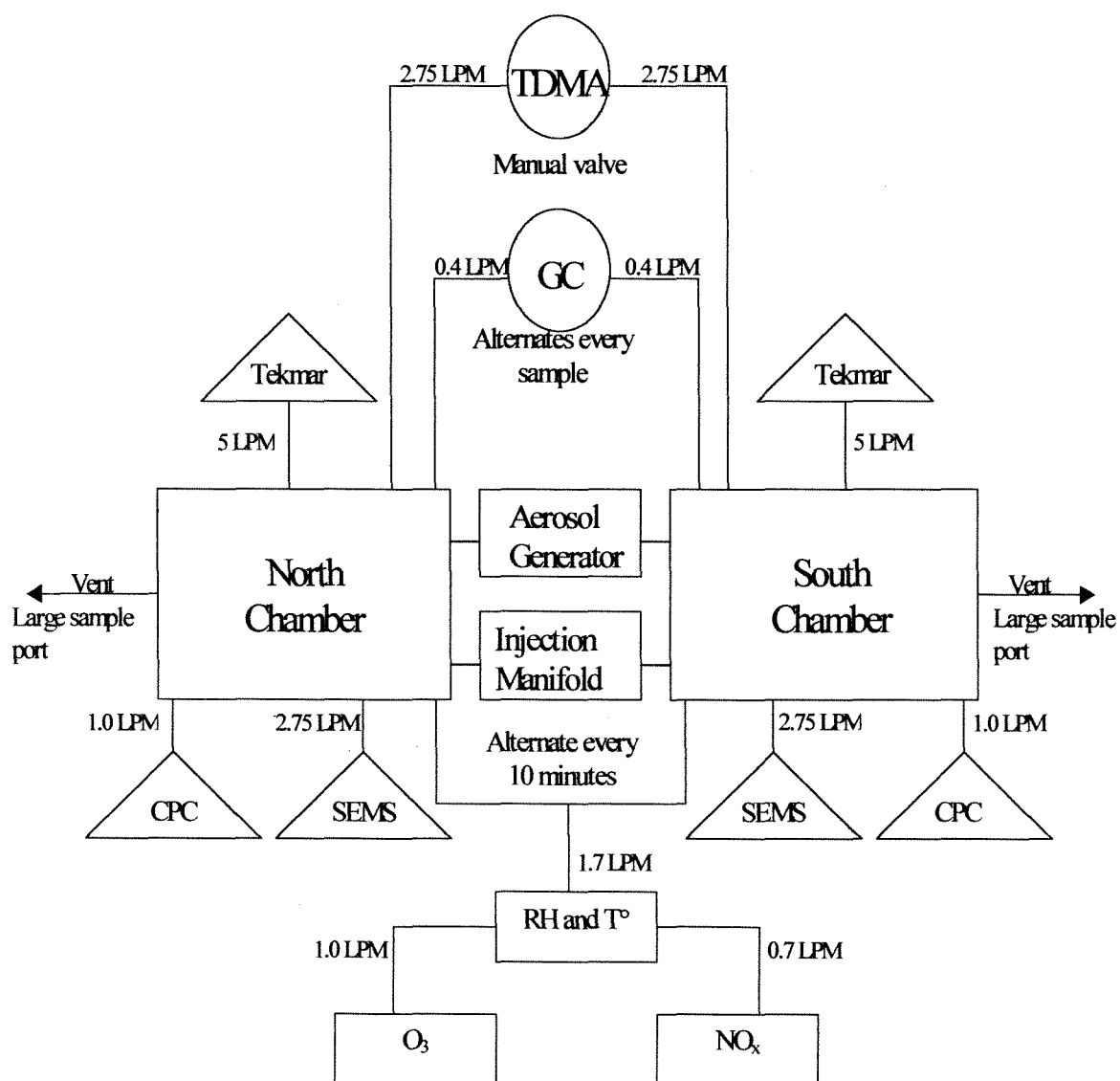


Figure 4.2. Block diagram of gas- and aerosol-phase instrumentation.

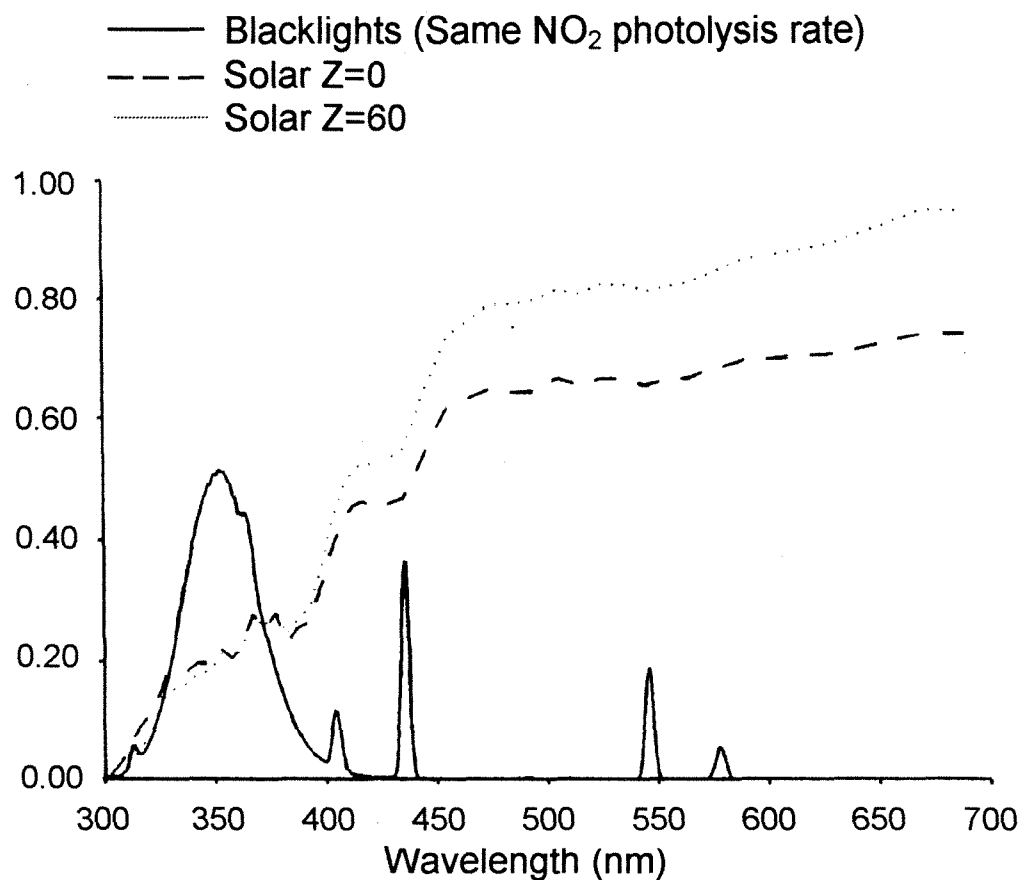


Figure 4.3. Light spectrum from Carter *et al.* (1995). Solid line represents Sylvania 350BL; dashed line is solar light intensity at zenith angle = 0; dotted line is solar light intensity at zenith angle = 60.

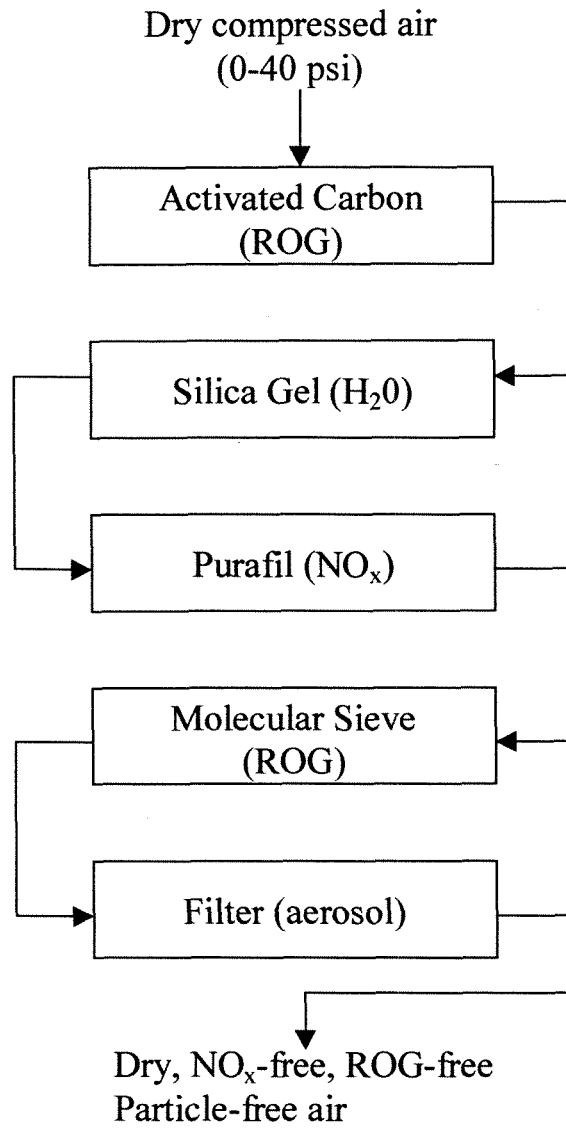


Figure 4.4. Flow scheme for clean-air system.

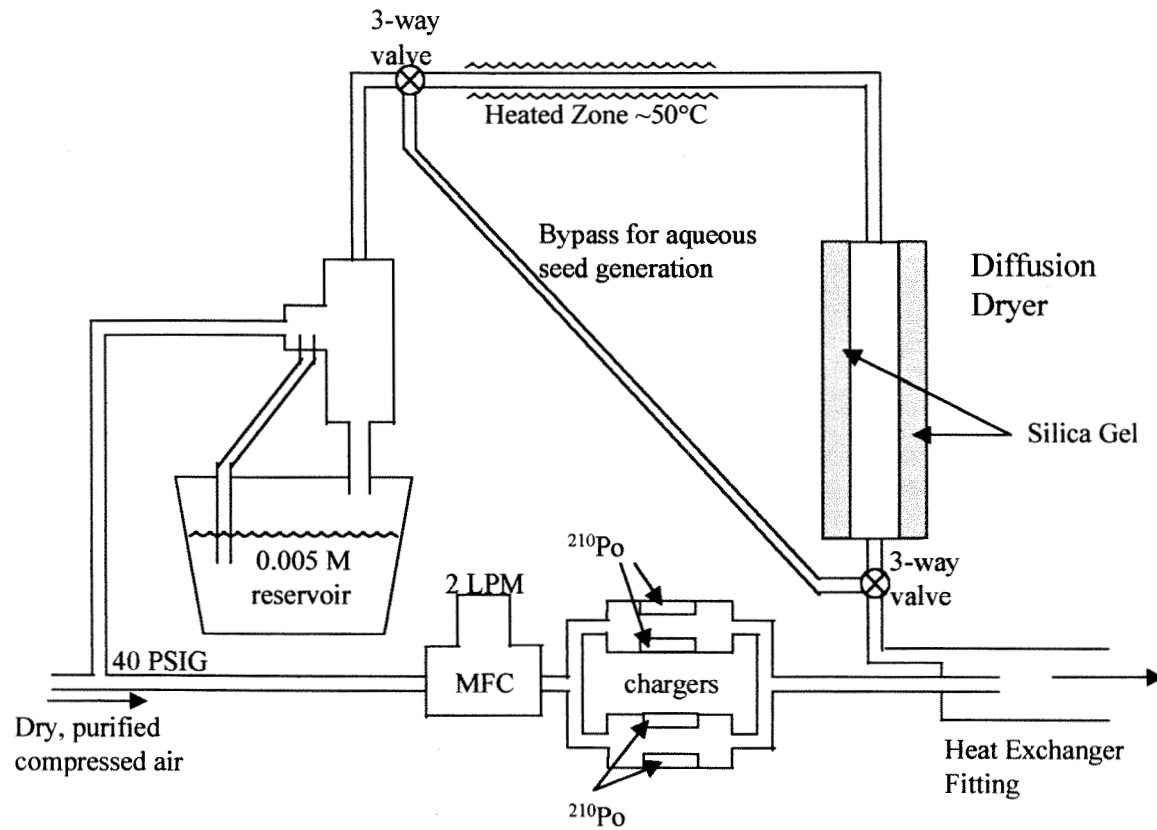


Figure 4.5. Seed particle generation schematic.

⊗ Pressure transducer

⊗ Solenoid valve

H HEPA filter

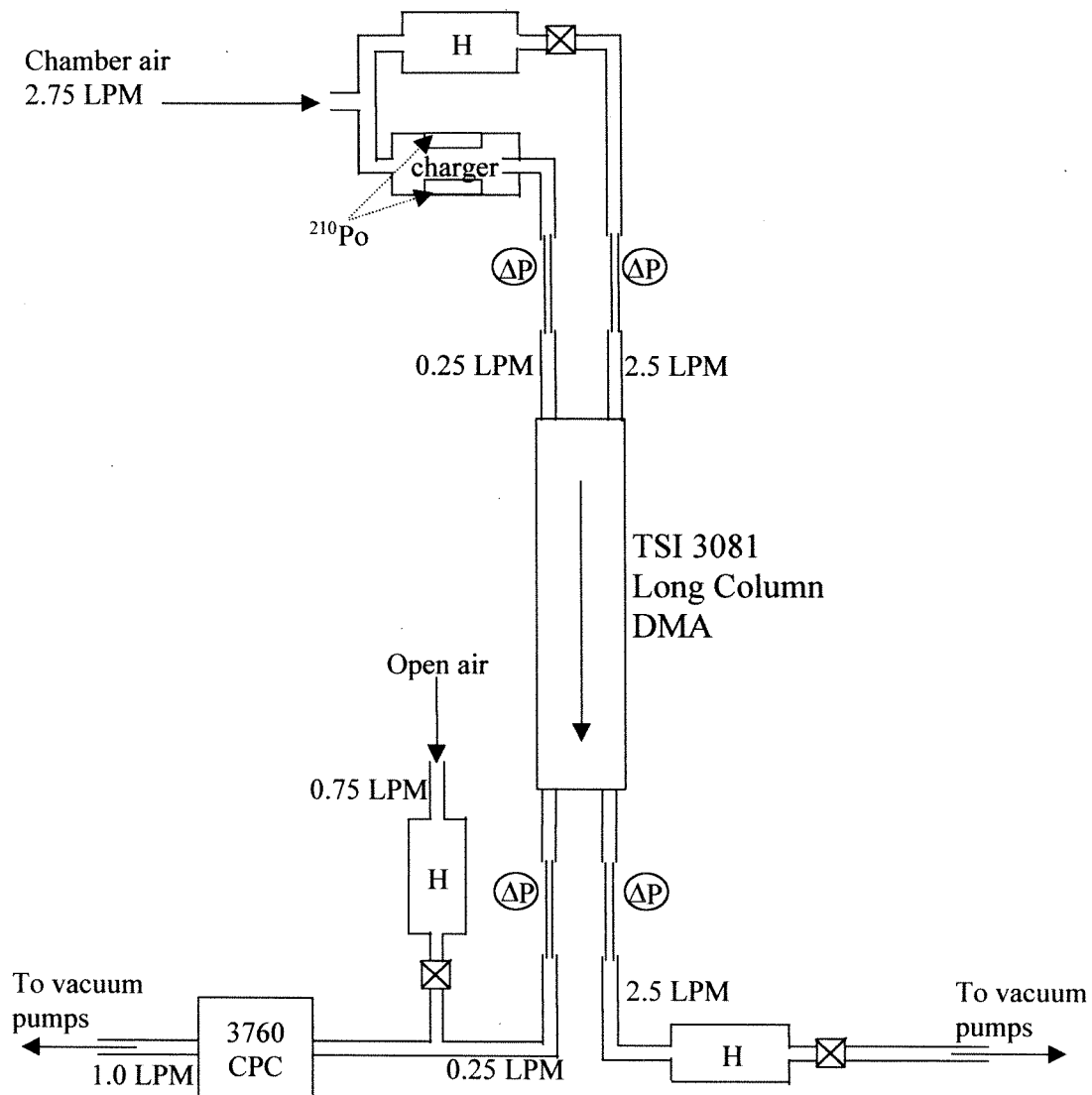


Figure 4.6. Automated scanning electrical mobility spectrometer. Pressure transducers monitored by computer; solenoid proportional control valves controlled by computer.

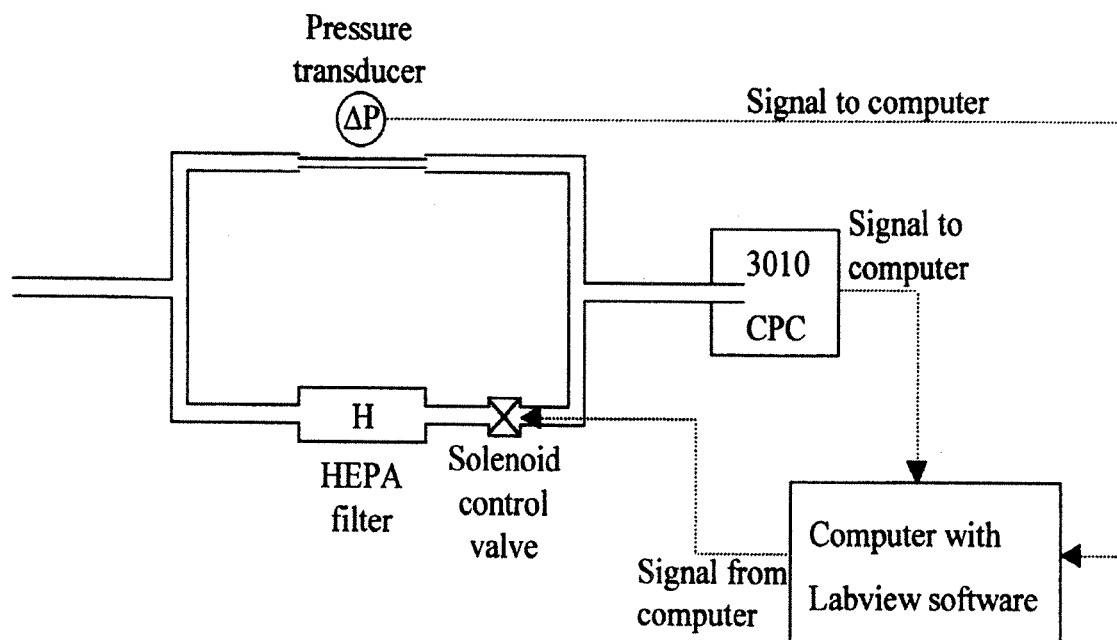


Figure 4.7. Condensation particle counter dilution system.

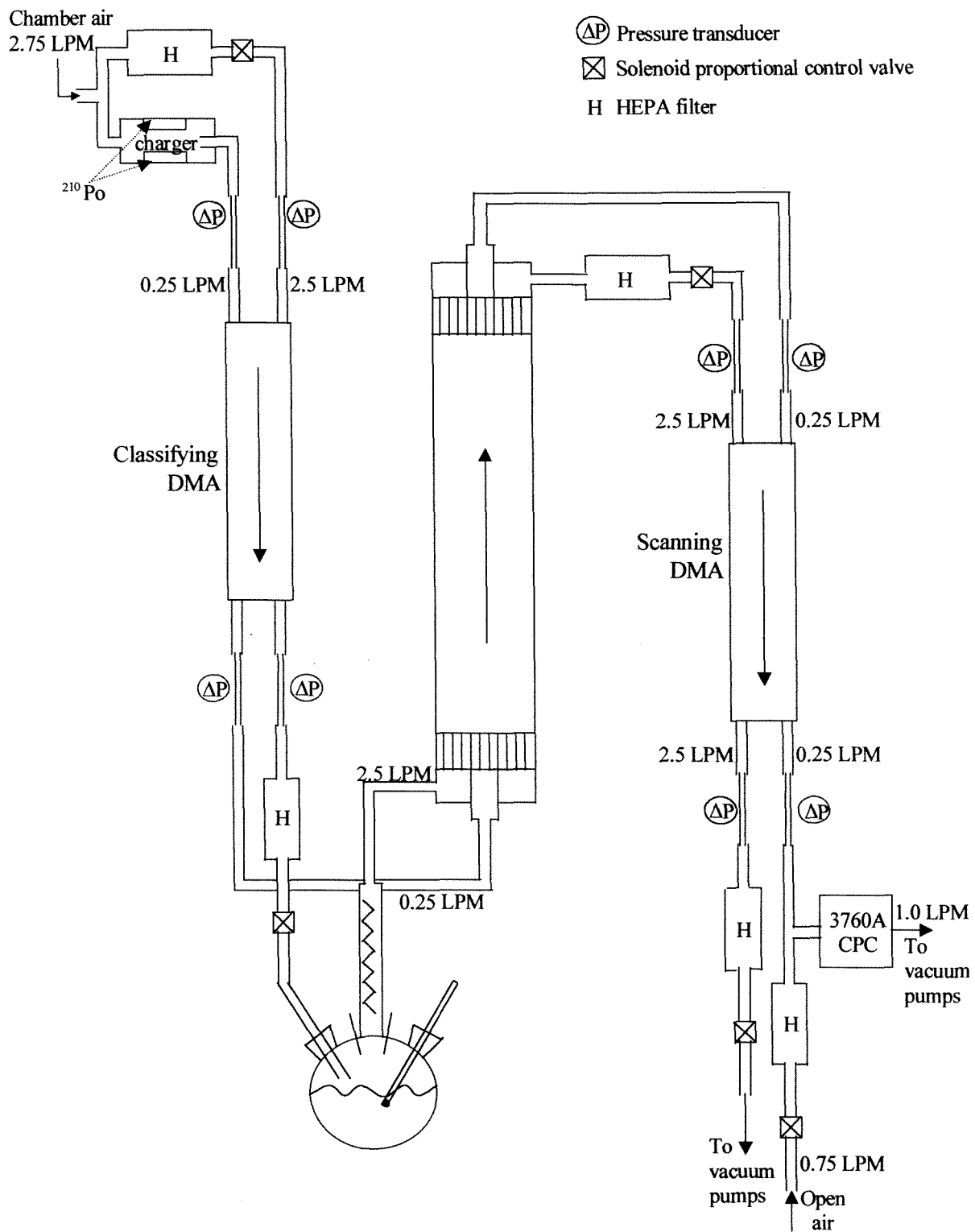


Figure 4.8. Tandem differential mobility analyzer schematic. Pressure transducers monitored by computer; solenoid proportional control valves controlled by computer.

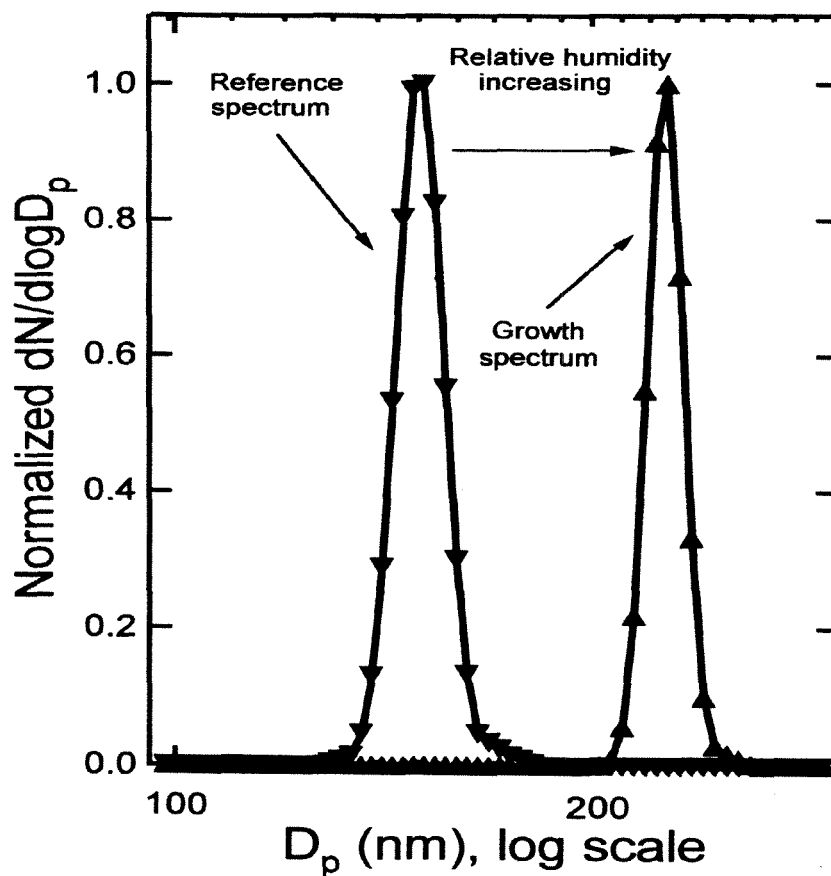


Figure 4.9. Sample TDMA size distribution spectrum. Left curve is output of second DMA for dry $(\text{NH}_4)_2\text{SO}_4$ seed particles classified to 136 nm by first DMA at RH = 0%. Right curve is output of second DMA for dry $(\text{NH}_4)_2\text{SO}_4$ seed particles classified to 136 nm by first DMA at RH = 85%.

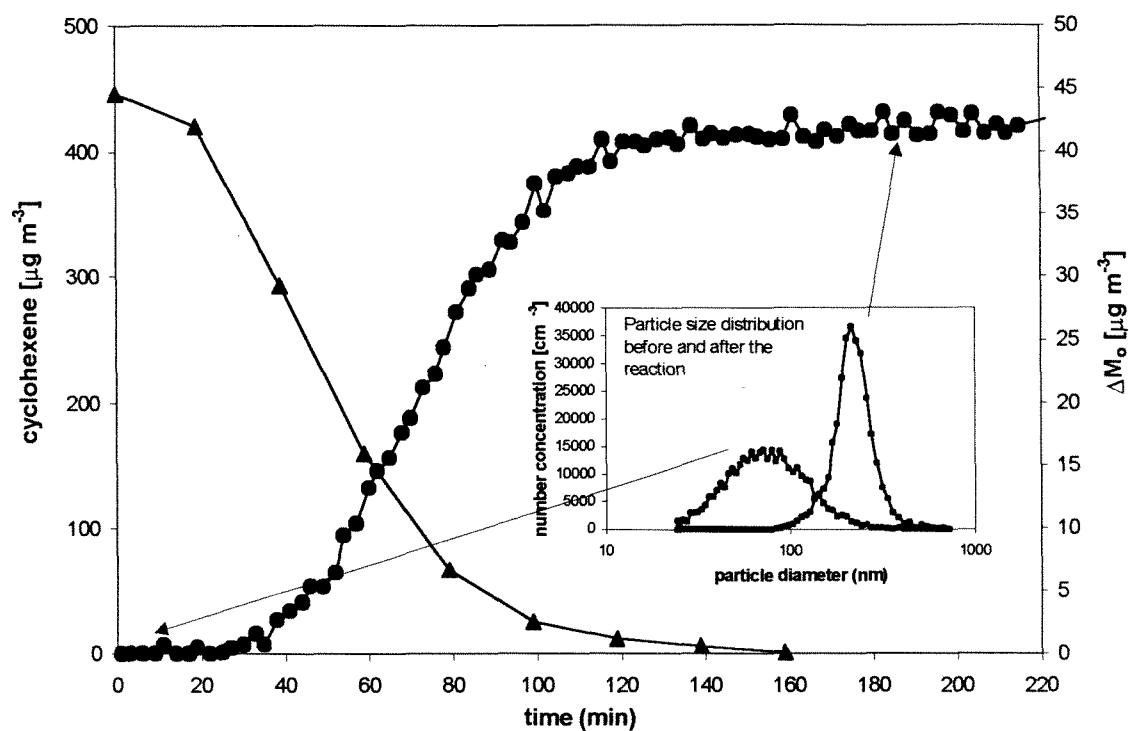


Figure 4.10. Cyclohexene and total aerosol mass concentration as a function of time. As the cyclohexene concentration decreases with time, the organic aerosol mass increases correspondingly. The organic aerosol mass, ΔM_o , is calculated from the difference of the aerosol size distributions at the beginning and end of the reaction, as shown in the insert.

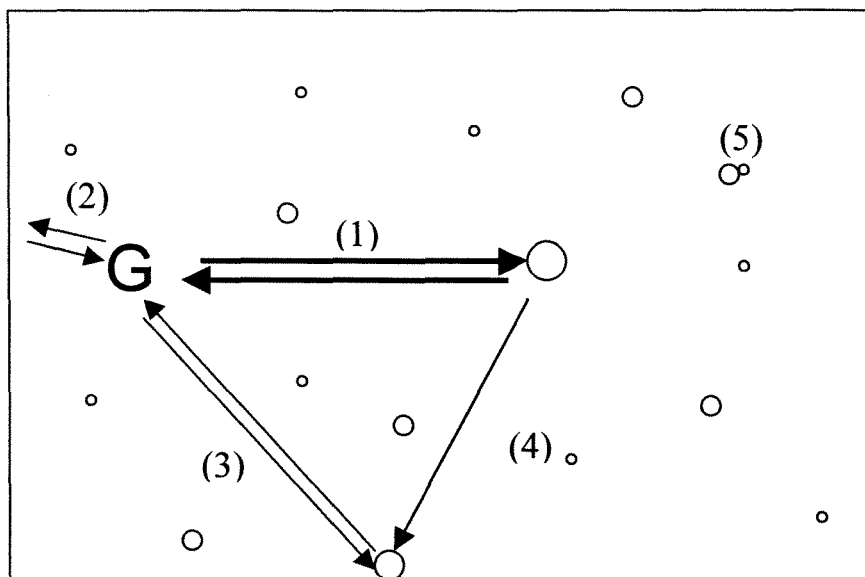


Figure 4.11. Illustration of different processes occurring within the chamber. Pathways include: (1) condensation, (2) gas-phase wall adsorption, (3) gas-deposited particle transport, (4) particle-wall transport, (5) coagulation.

Chapter 5**The Effect of Water on Gas-Particle Partitioning of Secondary Organic
Aerosol: I. α -Pinene Ozone System**

5.1 Introduction

Atmospheric oxidation of organic molecules containing six or more carbon atoms can lead to products of sufficiently low vapor pressure that they partition between the gas and aerosol phases. The aerosol fraction of these products is known as secondary organic aerosol (SOA). Over the last decade, there have been a number of laboratory studies of the SOA-forming potential of both anthropogenic and biogenic organics (Griffin *et al.*, 1999; Hoffmann *et al.*, 1997; Odum *et al.*, 1996, 1997; Edney *et al.*, 2000). This work has demonstrated convincingly that the mechanism of SOA formation is absorptive partitioning of the oxidation products between the gas-phase and a particulate organic absorbing phase. With few exceptions, laboratory and smog chamber studies on SOA formation have been carried out at relative humidity (RH) sufficiently low that the resulting aerosol is water-free. Experiments conducted under dry conditions are an essential first step in understanding the partitioning of organic products to the aerosol phase. Dry inorganic seed aerosol has frequently been used as an inert surface upon which SOA forms and grows. In experiments carried out under dry conditions in both the presence and absence of seed aerosol, it has been found that the amount of aerosol formed is the same (Odum *et al.*, 1996).

Ambient relative humidity is frequently high enough that atmospheric aerosols contain water. Understanding the water associated with inorganic atmospheric aerosols has occupied considerable attention in the literature over the past two decades (Pilinis and Seinfeld, 1987; Wexler and Seinfeld, 1990, 1991; Kim *et al.*, 1993a,b; Kim and Seinfeld, 1995; Jacobson *et al.*, 1996; Clegg *et al.*, 1992, 1998a,b; Nenes *et al.*, 1998; Zhang *et al.*, 2000). As a result of this body of work, that prediction of the liquid water content of

inorganic aerosols can now be made with considerable confidence. Atmospheric particles are, by and large, a mixture of both inorganic and organic components. Because of the wide variety of atmospheric organic compounds, the complex nature of organic-water molecular interactions, and the paucity of thermodynamic data on organic/water systems of atmospheric relevance, predicting how much water is associated with organic components of atmospheric aerosols is not yet possible on a general scale.

Water is likely to play a role in gas-particle partitioning of low vapor pressure oxidation products, potentially affecting the thermodynamic equilibrium achieved between gas- and aerosol- phase organics. Absorption of water into the organic phase of the aerosol may alter the activity of the organic constituents in solution, thus perturbing the fraction of organic material present at equilibrium in the aerosol from that in the absence of water. Inorganic particles, at sufficiently high relative humidity, can deliquesce, transforming the aerosol from a dry salt to an aqueous solution of high electrolyte concentration. The appearance of electrolytes could, in turn, alter the organic gas-particle thermodynamic equilibrium by changing the activity of the absorbing organic phase, especially if the water-electrolyte-organic mixture exists as a single phase in the aerosol. The goal of this work is to study experimentally how the yield of SOA is affected by the presence of liquid water in the aerosol phase. Upon atmospheric oxidation, each parent hydrocarbon yields its own characteristic set of oxidation products. As a result, it is likely that the presence of liquid water will not affect all SOA in the same manner. An appropriate system to begin a comprehensive study of the effect of RH on SOA formation is one that has been well-studied in the dry state and one for which, if possible, the molecular composition of the aerosol has been identified. The α -pinene/O₃ system

satisfies these conditions. We consider the relatively well-studied α -pinene/O₃ system (Hoffmann *et al.*, 1997; Virkkula *et al.*, 1999; Yu *et al.*, 1999; Griffin *et al.*, 1999) as a benchmark to study how the yield of SOA is affected by the presence of liquid water in the aerosol phase and the role of the inorganic seed aerosol in gas-particle partitioning.

We begin with a description of the experimental apparatus and procedures used to generate and measure α -pinene/O₃ SOA in the presence and absence of inorganic seed and water. Next, we discuss the experimental investigation of the role of water and the inorganic seed in aerosol formation and hygroscopic behavior. We then use a theoretical basis to attempt to explain the results obtained experimentally.

5.2 Experimental Description

Experiments were performed in indoor, dual, 28 m³ Teflon reactors. In this configuration, two experiments could be performed simultaneously under identical temperature conditions. Temperature and relative humidity in the system can be controlled from 20°C to 50°C at a precision of $\pm 0.5^\circ\text{C}$ and 1 to 85% at a precision of $\pm 0.5\%$, respectively.

Hydrocarbon measurements were carried out using a Hewlett-Packard (Palo Alto, CA) 5890 Series II Plus gas chromatograph (GC) utilizing a DB-5 60 meter column (J & W Scientific, Davis, CA) and a flame ionization detector (FID). The GC temperature program was as follows: -50°C for 1 minute, -50 to 150°C at $40^\circ\text{C min}^{-1}$, held at 150°C for 1 min. Estimated uncertainty of the hydrocarbon measurement is 2%.

Aerosol size distributions and number concentrations were obtained every 60 s using two cylindrical (TSI model 3071) scanning electrical mobility spectrometers (SEMS), one for each chamber. Each SEMS was equipped with a TSI model 3760

condensation particle counter (CPC). Sheath and excess flow was set to 2.5 LPM, with the inlet and classified aerosol flow set to 0.25 LPM. Voltages were ramped from 30 V to 7000 V, allowing for measurement of 25 nm to 700 nm diameter particles. Volumetric flow control to within $\pm 0.5\%$ was achieved by measuring the pressure drop of the gas flow across a laminar flow element and adjusting the flows with proportional control valves (MKS model 248A). These valves were then interfaced to Labview software (National Instruments, Houston, Texas) using proportional-integral-differential (PID) control that can update the flow at a rate of 100 s^{-1} . The data inversion routine accounts for charging and counting efficiency as well as particle loss (Collins *et al.*, 2001). Additional TSI 3010 CPCs were used to monitor the total number concentration in the chamber and for correction of SEMS generated number concentrations.

A tandem differential mobility analyzer (TDMA) was used to determine the hygroscopic uptake of water by the aerosol produced in the chamber. The TDMA follows the initial design of Rader and McMurray (1986) and includes the volumetric flow control of the SEMS mentioned above. The residence time of the TDMA humidification chamber is 10 s, and the relative humidity can be varied from 5% to 89% with approximately 0.5% accuracy. Hygroscopic growth data were obtained for chamber aerosol with initial classified diameters of 136 nm and 235 nm.

Prior to each experiment, the chambers were flushed with purified compressed laboratory air. The laboratory compressed air was processed via four packed bed scrubbers containing activated carbon, silica gel, Purafil, and 13x mol sieve, respectively, followed by a filter. The resulting air had no detectable reactive organic gases or particles, and less than 2 ppb NO_x .

Controlling the relative humidity of the Teflon chambers was achieved using a 1500 W immersion heater submersed into a 60 cm tall, 7.5 cm diameter glass cylinder fitted with a Teflon cap. Triple deionized water with a minimum conductivity of $18.2 \text{ M}\Omega^{-1}$ was added to the glass cylinder. The steam generated was passed through 2.5 cm diameter Teflon tubing into the chamber, allowing for a relative humidity of 50% to be achieved in approximately 40 min. Relative humidity and temperature were measured using a Vaisala (HMP233) capacitance meter with stated temperature accuracy of $\pm 0.1\%$ and RH accuracy of $\pm 0.5\%$. The process of adding gas-phase water did not introduce any detectable aerosol or organics into the chambers.

After allowing the humidity of the chamber to stabilize, initial seed aerosol was generated from 0.005 M solution of either $(\text{NH}_4)_2\text{SO}_4$, NH_4HSO_4 , or CaCl_2 using a stainless steel, constant rate atomizer to a number concentration of about $2 \times 10^4 \text{ cm}^{-3}$ of 80 nm mean diameter particles. Moist seed aerosol was generated by directly passing the aerosol to a previously humidified chamber; dry seed aerosol was generated by passing the atomized solution through a heated line and then a Nafion diffusion dryer with exiting RH $< 15\%$. In both cases, the aerosol stream was passed through Po-210 charge neutralizers before entering the chamber.

For the dark ozonolysis experiments, 2-butanol, which was used as a hydroxyl radical scavenger, and α -pinene were introduced at least 1.5 h before starting the experiment. 2-Butanol was injected at sufficient concentrations (680 times, by volume, of α -pinene injected) that the reaction rate of OH radicals (generated in the α -pinene/ O_3 reaction) with butanol exceeded that with α -pinene by a factor of 100. NO_x levels were kept below 2 ppb. Initial measurements of the α -pinene, 2-butanol, and ozone were made

prior to the start of the experiment. A minimum of three initial hydrocarbon measurements were taken for each chamber, and subsequently repeated every 11 min. Experiments commenced by injecting ozone into the reactor to a mixing ratio of approximately 10 ppm at a rate of 5 LPM for about 1 h. Ozone was monitored with a Dasibi Environmental Corp. (Glendale, CA) Model 1008-PC O₃ analyzer. Ozone measurements were taken in 10 min intervals for both chambers and have estimated uncertainties of +/- 4%. Temperature and relative humidity were monitored over the course of the reaction.

5.3 Aerosol Yield

Because of the difficulty associated with the molecular identification and quantification of secondary organic compounds derived from the oxidation of parent hydrocarbons, the aerosol yield has been used as a measure of the overall aerosol forming potential of various hydrocarbons (Griffin *et al.*, 1999). Aerosol yield, Y , is defined as the ratio of ΔM ($\mu\text{g m}^{-3}$), the aerosol mass concentration produced through oxidation of the parent hydrocarbon, to ΔHC ($\mu\text{g m}^{-3}$), the mass concentration of parent gas-phase organic reacted, $Y = \Delta M / \Delta HC$.

An absorptive partitioning model proposed by Pankow (1994a, 1994b) has been demonstrated extensively to describe SOA formation (Odum *et al.*, 1996, Griffin *et al.*, 1999). Gas-phase organic compounds partition into the aerosol phase below supersaturation through absorptive dissolution into the organic phase present. Once a threshold amount of secondary organic material is present to form an initial organic layer, gas-particle partitioning ensues. The aerosol yield Y resulting from the oxidation of a

single parent hydrocarbon can be described as the sum of the yields of each organic product Y_i as follows:

$$Y = \sum_i Y_i = \Delta M_o \sum_i \frac{\alpha_i K_{om,i}}{1 + K_{om,i} \Delta M} \quad (5.1)$$

where α_i is the mass-based stoichiometric fraction of species i formed from the parent hydrocarbon, $K_{om,i}$ is the gas-particle partitioning coefficient ($\text{m}^3 \mu\text{g}^{-1}$), which is inversely proportional to the compound's vapor pressure, and ΔM ($\mu\text{g m}^{-3}$) is the total mass concentration of organic material and associated water present in the aerosol phase. The fraction of secondary organic material condensing into the aerosol phase is seen to depend on the amount of organic aerosol mass present. Although numerous products are formed in the oxidation of a single parent hydrocarbon (Yu *et al.*, 1999; Forstner *et al.*, 1997), it has been shown that an empirical two-product model accurately represents yield data obtained for more than 30 parent hydrocarbons (Odum *et al.*, 1996; Hoffmann *et al.*, 1997; Griffin *et al.*, 1999). Essentially, one product represents the more volatile compounds while the other describes the products of lower volatility.

5.4 Experimental Protocol

Our goal is to gain a fundamental understanding of two phenomena: (1) the effect of water on the yield of SOA; and (2) the effect of the presence and nature of an aqueous inorganic electrolyte salt on the yield of SOA. Both phenomena are prevalent in the ambient atmosphere. Our approach is to address these issues both experimentally and theoretically. This section outlines the experimental protocol employed to isolate each of the phenomena. Five classes of experiments were conducted: (1,2) SOA formation in the

absence of a seed aerosol under humid and dry conditions; (3,4) SOA formation in the presence of a dry seed aerosol under humid and dry conditions; and (5) SOA formation in the presence of a wet (inorganic electrolyte) seed aerosol under humid conditions.

5.4.1 Dry Nucleation

SOA produced under dry conditions with no seed aerosol is 100% organic in content. Initial particle formation results from a sufficient supersaturation of low volatility organics to produce homogeneous nucleation followed by condensation to the aerosol. The organic aerosol produced is simply the final measured volume of the aerosol, after correcting for wall loss. The aerosol mass concentration is then estimated from the aerosol volume by assuming a density of 1 g cm^{-3} , consistent with the density of organic products of α -pinene/ O_3 oxidation as reported by Yu *et al.* (1999). The yield curve (Y as a function of ΔM_{org}) generated from such an experiment provides a pure “baseline” of the system—the amount of SOA formed in the absence of either inorganic constituents or water.

5.4.2 Humid Nucleation

SOA produced in the absence of seed aerosol but at elevated RH values, so-called humid nucleation experiments, consists of organic compounds and water. As in the dry, seed-free case, the initial aerosol is produced by nucleation of supersaturated oxidation products; however, the subsequent growth of the aerosol results from absorption of both organics and water (if the organic products are sufficiently hydrophilic). The total aerosol formed, in this case, will depend on organic-organic and organic-water interactions. The mass concentration of organic aerosol produced is the total aerosol mass concentration less the mass concentration of water associated with the aerosol. The water content of the

aerosol cannot be directly measured but may be inferred experimentally as follows.

Aerosol produced under dry nucleation conditions contains no water. The tandem differential mobility analyzer (TDMA) is used to measure the change in particle diameter that occurs when the relative humidity surrounding this pure organic aerosol is raised to RH conditions corresponding to the humid experiments. The water content of the wet aerosol is estimated from the dry and wet diameters measured in the TDMA as

$$M_{water} = M_{total} (D_{p,d}/D_{p,w})^3 \quad (5.2)$$

5.4.3 Dry Seed, Dry Conditions

In the experimental protocol most frequently followed in SOA formation studies, dry inorganic aerosol (inert, non-volatile, crystalline) is injected into the chamber to provide a surface upon which semi-volatile organic compounds condense. SOA initially forms via condensation onto the inorganic particles; subsequent growth occurs via absorption into the organic surface coating the inorganic core. The resulting aerosol composition is a mixture of organic and inorganic constituents, although in most experiments the amount of SOA ultimately deposited on the dry inorganic seed greatly exceeds the mass of initial seed, so the SOA yield is effectively equal to the final mass of the aerosol in the chamber, after wall losses have been accounted for. We will see that the inorganic seed aerosol does not affect the final yield attained; it acts simply as a substrate for aerosol condensation.

5.4.4 Dry Seed, Elevated Relative Humidity

Dry inorganic seed particles provide an inert crystalline surface upon which condensation of organic vapors occurs. Under humid conditions, but at an RH below the RH of deliquescence of the seed aerosol, condensed organic vapors create an organic layer

for further gas-phase absorption of both organic compounds and water. The inorganic salt is not expected to participate in the organic/water phase equilibrium since the RH is intentionally maintained below the RH of deliquescence of the seed aerosol. For example, Cruz and Pandis (2000) measured the deliquescence point of several salts with and without organic coatings and noted that there was no change in the deliquescence point relative humidity in the presence of organic coating. Thus, the gas-aerosol partitioning should be governed only by organic-organic and organic-water interactions. The volume concentration of SOA produced ($\mu\text{m}^3 \text{ m}^{-3}$), including any water taken up, is given by

$$V_{org+water} = V_{total} + V_{wall\ correction} - V_{salt} \quad (5.3)$$

The amount of water is estimated from TDMA measurements as follows. Aerosol generated in the dry seed experiments at zero RH is humidified up to 50% to determine the amount of water associated with the organic at 50% RH using equation (5.2). None of the water is associated with the seed since the RH is below the RH of deliquescence. The mass $\Delta M_{org+water}$ is equated to volume, as we assume unit densities of both the SOA and its mixtures with water.

5.4.5 Aqueous Seed, Elevated Relative Humidity.

For this system, the relative humidity of the chamber is raised prior to injection of seed aerosol. Seed aerosol, produced via a constant flow atomizer, is introduced to the chamber above its efflorescence point, resulting in an initial aqueous-phase electrolyte aerosol. Semi-volatile organic oxidation products generated by the reaction partition to the aqueous salt aerosol by condensation. The volume concentration of organic material present in the aerosol, including the change in water content in the aerosol, is given by

$$V_{org+water} = V_{total} + V_{wall\ correction} - V_{salt+water} \quad (5.4)$$

In the above equation $V_{salt+water}$ is the initial volume of aqueous salt seed aerosol, for which the water content can be calculated using an inorganic thermodynamic model. The volume $V_{org+water}$ therefore includes not only the amount of water taken up by the aerosol by the organic material but also any change in the total water content due to activity effects of the mixed organic/salt solution. Unit density of the volume element $V_{org+water}$ is again assumed when converting to mass, $\Delta M_{org+water}$.

5.5 Effect of Relative Humidity on SOA Formation in the α -Pinene/Ozone System

Forty-seven experiments were performed measuring the SOA yield of α -pinene in the dark reaction with ozone in the presence of 2-butanol as a hydroxyl radical scavenger. These experiments included ones in which no seed particles were initially present (where aerosol is formed by homogeneous nucleation), with ammonium sulfate present as either a dry inorganic seed or an aqueous inorganic seed, with ammonium bisulfate present as either a dry inorganic seed or an aqueous inorganic seed, and with calcium chloride as an aqueous seed. All experiments were performed at temperatures near 301 K. Table 5.1 summarizes the conditions for each of these experiments, including initial α -pinene and ozone concentrations, aerosol yields, relative humidity, and temperature. Figure 5.1 summarizes yield versus total aerosol mass concentration for all 47 α -pinene/O₃ experiments. Note that the yield includes both organic and water contributions for experiments carried out under humid conditions.

The data have been fit to a two-product absorptive partitioning model by minimizing the square of the residuals between the observed data and the curve described by equation (5.1). The parameters α_1 , α_2 , $K_{om,1}$, $K_{om,2}$ are given in Table 5.2. Note that the α and K_{om} values include the effect of relative humidity.

5.5.1 Dry Seed vs. Dry Homogeneous Nucleation.

Yields were determined for α -pinene oxidation by ozone in the absence and presence of initially dry seed to ascertain whether the presence or chemical composition of a dry inorganic salt affects SOA formation potential. Yield data and model fits for these experiments are given in Figure 5.2. It can be seen that neither the presence of the inorganic seed nor its chemical composition has any effect on the total aerosol yield. This observation is consistent with the hypothesis that the inorganic salt does not affect gas-particle partitioning into the organic layer and acts solely as a site upon which organic deposition occurs.

5.5.2 Dry Seed and No Seed With Humid Conditions.

Yield was determined at an elevated relative humidity in the presence and absence of a dry seed, yet at an RH below that of the deliquescence points of the seed compound, either ammonium sulfate or ammonium bisulfate. Therefore, water present in the aerosol is associated only with the organic phase of the aerosol. Figure 5.1 shows yield data obtained for these experiments, including the effect of aerosol water uptake.

Figure 5.3 shows the organic aerosol yield obtained under dry seed conditions at elevated relative humidity, as well as the aerosol yield obtained in the absence of seed aerosol at elevated relative humidity, all corrected for the water uptake of the organic phase of the aerosol. After correcting for water uptake, it can be seen that the measured yields in all of these experiments fall onto the same curve obtained for the dry experiments. This result demonstrates again that the dry inorganic seed aerosol does not influence the gas-particle conversion processes occurring, even at elevated relative humidity. This observation is further supported by the fact that there are no discernible

changes in the aerosol yield parameters between experiments in which the aerosol is produced by homogeneous nucleation and those with dry seed particles present. The fact that the organic aerosol yields are similar to those of the dry experiments implies that the distribution and volatility of the organic oxidation products have not been significantly altered by the presence of water. Aerosol yield formation parameters determined for α -pinene/O₃ under dry conditions are therefore sufficient to describe the gas-particle partitioning under humid conditions, as long as none of the water is associated with the inorganic seed aerosol.

5.5.3 Aqueous Salt Solutions Effect on SOA Yield

Aerosol formation potentials were measured at elevated relative humidity for α -pinene oxidation by ozone in the presence of aqueous (NH₄)₂SO₄, NH₄HSO₄, and CaCl₂ seed aerosol. Yields for all three salts are given by the lowest three curves in Figure 5.1. These curves include the total mass absorbed by the aerosol, which includes both organic and water constituents. Yield curves for all three aqueous salt systems were below those of the baseline dry curve as well as the yield curves at elevated humidity with dry seed.

Correction for water uptake of the aqueous aerosol is necessary to make a direct comparison of the organic aerosol formation in the dry and wet cases. Although the water associated with the salt alone can be calculated, and the water associated with the organic can be obtained through TDMA measurements, estimation of the water content of the composite aerosol is confounded by the organic-inorganic-water interaction. Several observations can be made even before attempting to remove the water content of the aerosol from the raw data. The presence of the electrolytes clearly reduces the fraction of organic aerosol partitioning from the gas to the aerosol phase. Secondly, the hygroscopic

water uptake by the organic compounds themselves is not sufficiently large to produce as much total aerosol (organic and water) as organic aerosol is formed in the dry experiments. Finally, and most interestingly, the reduction in aerosol production is compositionally dependent on the salt in aqueous form.

5.5.4 Hygroscopic Properties of α -Pinene/Ozone Aerosol Products

The hygroscopic behavior of an aerosol is typically reported in terms of a growth factor, G_f which is defined as the ratio of the humidified diameter ($D_{p,w}$) to the dry aerosol diameter ($D_{p,d}$), and conventionally measured using a tandem differential mobility analyzer (McMurry and Stolzenburg, 1989).

$$G_f = D_{p,w}/D_{p,d} \quad (5.5)$$

Table 5.3 reports the G_f values determined for each of the inorganic seed compounds at 85% RH, as well as literature values. The agreement with literature values provides confidence in our assignment of the state of the aerosol, i.e., deliquesced or effloresced. Also note that the G_f does not vary appreciably for pre-sized particles of 136 nm and 235 nm diameter.

Growth factors were measured for the dry seed (<2% RH) system during the course of reaction as ammonium sulfate became progressively coated with organic products of α -pinene/ O_3 oxidation. The TDMA was set to 85% RH with either 136 nm or 235 nm diameter chamber aerosol being selected for the hygroscopic growth. Analysis of the TDMA data followed that of Virkkula *et al.* (1999), where the hygroscopic uptake of the aerosol can be described by treating the inorganic and organic uptake of water separately,

$$G_f = \varepsilon_1 G_{f(1)}^3 + (1 - \varepsilon_1) G_{f(2)}^3 \quad (5.6)$$

where ϵ_1 , $G_{f(1)}$ and $G_{f(2)}$ refer to the fraction of organic present in the aerosol and the growth factors of the pure organic and inorganic portions, respectively. Figure 5.4 shows the evolution of G_f as a function of the organic volume fraction of the aerosol. Table 5.3 presents the growth factors of the organic and inorganic fractions at different relative humidities. The growth factors determined for the aerosol formed in α -pinene oxidation by ozone are similar with those of the less hygroscopic mode measured in ambient aerosols (Svenningsson *et al.*, 1992; Ferron *et al.*, 1999; Massling *et al.*, 1999; Swietlicki *et al.*, 1999; Cocker *et al.*, 2001). No discernible differences were seen in the growth factors of the 136 nm and 235 nm diameter particles. It was assumed that the growth factor of the organic fraction remains constant over the four-hour period of growth.

The TDMA data clearly demonstrate that the coating of inorganic particles with organic compounds reduces the hygroscopic nature of the aerosol. The close fit of the data to equation (5.6) shows that for the α -pinene/ozone system, accounting for the organic and inorganic water uptake separately can approximate the G_f of the organic-inorganic aerosol.

Growth factors determined in the TDMA experiments were used to estimate the volumetric fraction of water taken up by organic aerosol during experiments in which the relative humidity was 50% and the seed, when present, was dry. Aerosol produced during dry nucleation experiments (zero water, purely organic in content) was humidified in the TDMA as a surrogate for what occurs in the chamber during humid nucleation experiments. Aerosol produced during the dry seed, zero RH ($RH < 2\%$) experiments (zero water on aerosol) were humidified to 50% (below the deliquescence point of the seed) and the uptake of water by the organic was measured.

5.6 Thermodynamic Modeling of Organic-Inorganic-Water Equilibria

We now examine the possibility of explaining theoretically the experimental observations just presented. At the outset it should be noted that thermodynamic data for organic/inorganic/water systems of the type considered are scant; therefore, there is little at present on which to base a rigorous test of the accuracy of a thermodynamic theory. The UNIFAC model (Fredenslund *et al.*, 1975; Hansen *et al.*, 1991) has been used to estimate activity coefficients for organic/water aerosol mixtures (Saxena and Hildemann, 1997; Ansari and Pandis, 2000; Zhang *et al.*, 2000). The approach proposed by Clegg *et al.* (2000) is used here for predicting activity coefficients in solutions containing water, dissolved organic compounds, and salts. In this method, activity and osmotic coefficient (water activity) contributions are first calculated separately for the salt/water and organic/water components of the liquid-phase. These are combined with terms expressing mixture effects ("salting in" and "salting out") to produce thermodynamically self-consistent estimates of the activity and osmotic coefficients in the mixture.

The oxidation of α -pinene by ozone was previously studied by Yu *et al.* (1999) who determined the yields of the main products (see Table XI in that work). For aerosol composition we take the average of the results 6/9/98a,b. The total molar yields of each of the identified products are needed to calculate partitioning between the gas- and aerosol-phases where each of the compounds is assumed to exist in a liquid mixture. Compound vapor pressures have been estimated using the method of Myrdal and Yalkowsky (1997).

5.6.1 Salt Aerosols

For aqueous solutions of ionic compounds, the water activity of the solution, a_w , may be written as (Robinson and Stokes, 1959),

$$a_w = \exp\left[-\frac{M_w \nu \Phi m}{1000}\right] \quad (5.7)$$

where M_w is the molecular weight of pure water, ν is the total number of ions produced by the disassociation of one molecule of solute, Φ is the practical osmotic coefficient of the solution, and m is the solution molality. For droplets of size sufficiently large that corrections for surface curvature can be neglected, the relative humidity (in %) and the water activity are related by $RH = 100a_w$. The osmotic coefficient is represented by semi-empirical models (Pitzer and Mayorga, 1973); as m approaches zero, the ionic strength of the solution also approaches zero, and Φ approaches unity.

Water activities of aqueous solutions of the salts $(\text{NH}_4)_2\text{SO}_4$, NH_4HSO_4 and CaCl_2 are required and were obtained as follows. For $(\text{NH}_4)_2\text{SO}_4$, the model of Clegg *et al.* (1995) was used. This is based upon osmotic coefficients (measured for bulk solutions) up to saturation concentration of about 5.8 mol kg^{-1} (80% RH), and electrodynamic balance data to $>25 \text{ mol kg}^{-1}$ (about 40% RH). Osmotic coefficients of aqueous NH_4HSO_4 were calculated using the model of Clegg *et al.* (1998b) which is also based upon extensive measurements to very low RH. The equations of Ananthaswamy and Atkinson (1985) were used for aqueous CaCl_2 . Densities for aqueous CaCl_2 were calculated using the expression given by Sohnel and Novotny (1985); densities for aqueous $(\text{NH}_4)_2\text{SO}_4$ and NH_4HSO_4 were taken from Tang and Munkelwitz (1994). The dependence of water activity (equal to RH) and density on solution concentration at 301 K is shown in Figure 5.5 for the three salts.

5.6.2 Water Uptake by Condensed Organic Material

TDMA-measured growth factors for the α -pinene SOA and the three salts are listed in Table 5.3, and growth factors for mixtures of the organic products with $(\text{NH}_4)_2\text{SO}_4$ are shown in Figure 5.4. Measured growth factors for the pure salts can be compared directly with those calculated from literature osmotic coefficient and density data referred to above Table 5.3. There is reasonable agreement for all the salts. We note that, at 85% RH, the relative humidity in the TDMA is controlled to within $\pm 2\%$. This might be the cause of the small difference between the measured and calculated growth factor for $\text{CaCl}_{2(\text{aq})}$, for example.

We first consider water uptake by the α -pinene oxidation products alone. It is assumed that both the compounds themselves and their solutions in water have unit density, thus

$$M_{\text{org}+\text{water}} / M_{\text{org}} = G_f^3 \quad (5.8)$$

where $M_{\text{org}+\text{water}}$ is the total mass of organic material plus water, M_{org} is the mass of the organic material alone, and G_f is the growth factor from dry conditions to some known RH. Expressing the total mass as the sum of the organic and water masses, the number of moles of condensed water, $n_{\text{H}_2\text{O}}$, is

$$n_{\text{H}_2\text{O}} = (G_f^3 - 1)M_{\text{org}}/18.0152 \quad (5.9)$$

Assuming that the organic composition of the aerosol remains constant over the course of the oxidation, the mean molar mass of condensed-phase organic material is predicted to be 184 g mol^{-1} (see Section 5.6.4). Using this value enables the mean mole fraction of the

condensed organic material, and that of water, to be calculated from the measured growth factors using equation (5.9).

Experimentally inferred total mole fractions of dissolved organic material at 50% RH and 85% RH are shown in Figure 5.6 with predictions based on: (a) Raoult's law, (b) UNIFAC, and (c) a one parameter Margules model with $w = 1.0$. (see equations (5.11a) and (5.11b) in Section 5.6.3). Raoult's law is able to predict most closely the experimental observations, with the Margules equation underpredicting water uptake at 50% RH, and UNIFAC largely underpredicting water uptake at both RHs.

Next, we examine the extent to which measured growth factors for mixtures of α -pinene oxidation products and $(\text{NH}_4)_2\text{SO}_4$ (Figure 5.4) can be explained based on thermodynamic theory. Osmotic coefficients, Φ , of the mixture (hence, by iteration, the water content) are estimated using equation (5.3) of Clegg *et al.* (2000), which reduces to:

$$\Phi = 1 + \frac{3(\Phi' - 1)m_{\text{salt}}}{\sum_i m_i} + \frac{(\Phi'' - 1)m_{\text{org}}}{\sum_i m_i} + \frac{2m_{\text{salt}}m_{\text{org}}\lambda_{\text{org,salt}}}{\sum_i m_i} \quad (5.10)$$

where m indicates molality, Φ' is the osmotic coefficient contribution from the $(\text{NH}_4)_2\text{SO}_4$ /water component of the solution, and Φ'' is the contribution from the organic/water component. Φ'' is calculated from equation (5.12) below for the water activity coefficient. The last term in equation (5.10) is the contribution from ion-organic interactions ('salting in' or 'salting out'), characterized by the parameter $\lambda_{\text{org,salt}}$. The summation is equal to $(3m_{\text{salt}} + m_{\text{org}})$. It is also assumed that the apparent molar volumes of both the $(\text{NH}_4)_2\text{SO}_4$ and dissolved organic material are the same in their aqueous mixtures as in pure (single solute) solutions at the same molality.

It is important to realize that although the salt effect generally refers to the change in solubility of a volatile solute due to presence of salts in the solution, a corresponding influence on the osmotic coefficient exists which can be important when the concentration of the volatile solute in the condensed phase is comparable to that of the salt. Salting out, for which the parameter $\lambda_{\text{org,salt}}$ is positive, decreases the water activity of a solution, which has the effect of increasing water uptake into the condensed phase in a system at a fixed relative humidity. Consequently, because of a greater volume of solvent, the partitioning of the volatile compound into the liquid phase is enhanced, thus counteracting the decrease in its solubility. The extent to which these two effects cancel each other determines the overall amount of “salting out” that occurs in any given situation.

In Figure 5.7, growth factors predicted based on equation (5.9) are compared with the data in Figure 5.4 for three values of the salting coefficient $\lambda_{\text{org,salt}}$, 0, -0.1 (salting in), and 0.1 (salting out). First, it is clear that measured and predicted growth factors of the mixed solutions tend to agree best when $\lambda_{\text{org,salt}}$ is equal to zero. We note that this result is almost identical to that obtained using the much simpler assumption that the total amount of water in the condensed phase is equal to the sum of the amounts that would be taken up by the salt and organic compounds separately (not shown). The data are not consistent with salting in ($\lambda_{\text{org,salt}} = -0.1$).

5.6.3 Theoretical Analysis of Measured Aerosol Yields

We now address the extent to which it is possible to explain the observed aerosol yields using thermodynamic models. In doing so, we consider both a two-product model of the organic aerosol and a multi-product model based on product compounds identified by Yu *et al.* (1999). For each model, we first address the yields observed in the absence

of seed aerosol under dry conditions and at 50% RH. Then, for each model, we consider the yields observed in the presence of a wet seed aerosol.

5.6.3.1 Two-product Aerosol Model

In the two-product model given by equation (5.1), the organic compounds that form SOA are treated as just two classes: one that partitions chiefly into the particle phase (and is relatively involatile), and a second class of more volatile compounds that remain mainly in the gas phase. The two partition coefficients $K_{om,1}$ and $K_{om,2}$ are equivalent to equilibrium constants for the two compound classes, though with the use of mass fraction rather than mole fraction as the condensed phase concentration variable. It is clear from the fits in Figure 5.1 that equation (5.1) represents the experimental data well.

The model is based upon the $\alpha_{1,2}$ and $K_{om,1,2}$ values for dry nucleation without salts (Table 5.2). Mean molar masses of the involatile and volatile compound classes are taken as 184 g mol^{-1} and 169 g mol^{-1} , respectively (see Section 5.6.3.2 below). On a molar basis, α_1 is then equal to 0.177, and α_2 is 0.136, giving 0.313 moles of total organic products per mole of α -pinene. This is very close to the 0.309 average of the results 6/9/98a,b obtained by Yu *et al.* (1999). The partition coefficients are converted to mole-fraction based equilibrium constants by,

$$K_{x,i} = \frac{x_i f_i}{p_i} \quad (5.11)$$

where i represents each of the organic compound classes, distributed between the gas phase and a liquid aerosol phase that can also contain water and salts, x indicates the mole fraction, p_i the equilibrium partial pressure (atm), and f_i is the mole fraction based activity coefficient of i , which has a value of unity for pure i . The activity coefficients of the two

organic compound classes are assumed to be the same in all solutions, and both equal to unity in a mixture in which there are no other components.

Values of $K_{x,i}$ for each compound class were estimated by solving equation (5.1) to obtain the gas-phase and particulate amounts of both product classes (Table 5.4), and then converting condensed phase mass fractions to mole fractions and gas-phase amounts to partial pressures. Thus $K_{x,1}$ is equal to $3.1 \times 10^8 \text{ atm}^{-1}$, and $K_{x,2}$ is equal to $7.6 \times 10^6 \text{ atm}^{-1}$.

First, we consider the effect of water on the partitioning of the organic compounds. Calculations using UNIFAC for a mixture of water and the product compounds listed in Table 5.5 suggest that the activity coefficient of water is increased in the organic/water mixture. This would result in a lower mole fraction of water in the aerosol phase than predicted by Raoult's law. We have used equation (5.10) above to estimate total condensed phase yields for nucleation without salt seeds at 50% relative humidity. Activity coefficients of water (f_w) and organic compounds (f_i) were calculated using the following one-parameter Margules equation in which the value of the parameter w was adjusted to obtain agreement with the measurements:

$$\ln f_w = w x_{i(T)}^2 \quad (5.12a)$$

$$\ln f_i = w x_w^2 \quad (5.12b)$$

where x_w is the mole fraction of water in the aerosol phase, and $x_{N(T)}$ is the total mole fraction of both organic components. The results of this optimization are shown in Figure 5.8 for w equal to 1.0, together with a calculation in which both activity coefficients are equal to unity (Raoult's law). In the latter case, the yield is overestimated by about 15%, whereas the inclusion of the activity coefficients calculated by equation (5.12) above gives

excellent agreement. We note, however, that these activities are less consistent with the growth factor measurement for 50% RH than the Raoult's law assumption (Figure 5.6). It is important to bear in mind the assumptions being made here: first, that the aerosol consists of a single homogeneous phase. Second, the equilibrium constants K_x , which are determined for essentially dry conditions in which the true physical state of the aerosol is not known, are also applicable to a system in which water is a major constituent and for which we assume the physical state is liquid. If this were not so, then the equilibrium constants would differ by some factor which, in the present analysis, would be subsumed into the activity coefficient.

Next, we consider the effect of water on SOA yield in the presence of an initially wet seed aerosol. The effect of organic partitioning to a pre-existing aqueous salt aerosol at 50% relative humidity is to reduce the yield – by almost a third in the case of aqueous $(\text{NH}_4)_2\text{SO}_4$ (Figure 5.1). If we assume a fully liquid aerosol containing the salt, dissolved organic compounds, and water, can this salt effect be explained by salting out of the organic compounds (an increase in the value of f_i)? We have calculated yield curves for 50% relative humidity and 1.932×10^{-7} moles m^{-3} $(\text{NH}_4)_2\text{SO}_4$, for salting coefficients $\lambda_{\text{org,salt}}$ equal to 0 and 0.1. In these calculations, equation (5.10) is used to determine the partitioning of the two organic compound classes, and equations (5.9) and (5.11a) to determine the osmotic coefficient (hence water activity) of the liquid aerosol. The salt effect on the logarithm of the activity coefficient f_i is given by (Clegg *et al.*, 2000):

$$\ln(f_i) = \ln(f_i'') + \lambda_{\text{org,salt}} m_{\text{salt}} + \ln(x_w''/x_w) \quad (5.13)$$

where $\ln(f_i'')$ is the activity coefficient of i in a solution containing only the aerosol water and dissolved organic compounds, x_w'' is the corresponding water mole fraction, m_{salt} is

the molality of the salt in the liquid aerosol, and x_w the true water mole fraction equal to $n\text{H}_2\text{O}/(n\text{H}_2\text{O} + n_1 + n_2 + 3n(\text{NH}_4)_2\text{SO}_4)$. Figure 5.9 shows that the predicted yields, for $\lambda_{\text{org,salt}} = 0.1$, are substantially higher than those measured. The positive value of the salting coefficient (corresponding to a “salting out” effect) causes a predicted reduction relative to $\lambda_{\text{org,salt}} = 0$ in the condensed yield for small amounts of α -pinene oxidized, but a predicted increase relative to $\lambda_{\text{org,salt}} = 0$ over most of the measured range. At low concentrations of organic compounds in the liquid aerosol, the increase in the activity coefficients of the organic compounds (which reduces their concentration in the liquid aerosol) is greater than the salt/organic influence on the osmotic coefficient (equation 5.9). At high concentrations of organic compounds, the water activity relative to $\lambda_{\text{org,salt}} = 0$ is reduced, leading to an increase in the amount of condensed phase water at equilibrium.

The primary explanation for the behavior of the predicted yields shown in Figure 5.9 is that the water associated with the salt seed provides a medium into which the organic compounds dissolve. This is also why the predicted yield remains high even for very small amounts of α -pinene oxidized: most of the products partition into the pre-existing aqueous salt aerosol. The predicted results are not sensitive to the approach used to calculate the amounts of aerosol water: the use of the Zdanovskii-Stokes-Robinson relationship in place of equation (5.10), for example, gives a yield very similar to that shown in Figure 5.9. Ignoring the effect of the parameter $\lambda_{\text{org,salt}}$ on only the osmotic coefficient reduces the predicted yield considerably (not shown), but the yield still remains higher than the measured values for all $\Delta M_{\text{org+water}}$.

Figure 5.10 shows similar calculations for aqueous CaCl_2 seed aerosol. The predicted yields differ little from those obtained for $(\text{NH}_4)_2\text{SO}_4$, although the predicted

yield varies less with the amount of α -pinene reacted than for $(\text{NH}_4)_2\text{SO}_4$. This is because, at 50% RH, the amount of water associated with the CaCl_2 per mole is about three times greater than that with $(\text{NH}_4)_2\text{SO}_4$. The salting coefficient of 0.1 has a smaller effect for CaCl_2 as its influence on the activity coefficient f_i is reduced due to the lower molality of the salt (equation 5.13).

5.6.3.2 Multi-product Aerosol Model

The two-product thermodynamic model based on the empirical fit of the observed data described above quantitatively reproduces the observed aerosol formation at 2% and 50% RH for systems without salt seed aerosol. We now construct a model based upon the identified products of α -pinene oxidation (Table 5.5). The model is used both to interpret the results of the two-product approach, in particular to determine which compounds comprise the “involatile” and “volatile” aerosol components, and to examine the results of experiments utilizing salt seeds including the effects of possible liquid/liquid phase partitioning within the aerosol.

The UNIFAC method is used to estimate the organic/water contributions to activity coefficients, (see Table 5.6 for UNIFAC group compositions) and the method of Clegg *et al.* (2000) is used to estimate salt effects (equation 5.13). The equilibrium composition of the system was determined by Gibbs energy minimization. Pure compound vapor pressures, p_i° , need to be estimated for each of the species listed in Table 5.5, as experimentally measured vapor pressures are not generally available for these compounds. Initial calculations showed that the estimated p_i° were too high as, for most experimental conditions, no aerosol phase was predicted to exist. Accordingly, all the p_i° in Table 5.5 were reduced by a constant factor which was adjusted (to a final value of 10^2) until

reasonable agreement with the experimental yield data for $RH < 2\%$ was obtained. We can compare the estimated p_i^o with recent measurements for a few compounds. Bilde and Pandis (2000) have determined the vapor pressures of pinic acid and trans-norpinic acid using a TDMA, obtaining values of 8.1×10^{-10} atm (pinic acid) and about 54×10^{-10} atm (trans-norpinic acid) at 301 K. The relative magnitudes of these vapor pressures agree well with the estimates in Table 5.5. However, for pinic acid, the value of p_i^o needed to reproduce the observed yield of pinic acid by Yu *et al.* (1999) is a factor of five lower than that of Bilde and Pandis (2000), and for norpinic acid a factor of almost 7. In drawing conclusions about the behavior of individual compounds, we are implicitly assuming that the relative values of p_i^o , which vary over a four order of magnitude range, are better predicted than the absolute values. Comparisons made above for pinic and trans-norpinic acid are consistent with this assumption.

Condensed phase yields calculated using the multi-product model are shown in Figure 5.11 for both 2% and 50% RH. There is good agreement with the measurements over the full range of $M_{org+water}$ at the lower relative humidity, as expected, but at 50% RH, the predicted yield is somewhat low. This is because the water uptake calculated using UNIFAC to obtain water activities is too low, as suggested by the growth factor measurement at 50% RH (see Figure 5.6).

We next compare the results of this model with the two-product model based on equation (5.1). The partitioning of the product classes predicted by equation (5.1) for α -pinene reacted equal to $888.5 \mu\text{g m}^{-3}$ and $236.6 \mu\text{g m}^{-3}$ is summarized in Table 5.4. For the higher α -pinene concentration, about 87 wt.% of the condensed phase is predicted to be composed of the mainly non-volatile component 1, while component 2 makes up 81

wt.% of the total organic products present in the gas phase. For $\Delta\alpha$ -pinene equal to $236.6 \mu\text{g m}^{-3}$, the smaller amounts of the two product components reflect that partitioning is shifted towards the gas-phase; here only 59.5% of component 1 is predicted to reside in the condensed phase, while 96.6% of component 2 is predicted to exist in the gas phase.

Figure 5.12a shows the calculated gas/aerosol partitioning of all product compounds, by mass, for the $888.5 \mu\text{g m}^{-3}$ case. The calculated total condensed phase mass agrees closely with the measured value, and the mass of vapor phase products of $144 \mu\text{g m}^{-3}$ is also very close to the $142.5 \mu\text{g m}^{-3}$ predicted by equation (5.1). This degree of agreement is encouraging given that in the calculations the gas-phase product concentrations are derived essentially from the molar yields measured by Yu *et al.* (1999), giving the total quantities per m^3 . By contrast in the two-product model (equation 5.1) the same information is obtained indirectly from the variation of ΔM_{org} with $\Delta(\alpha\text{-pinene})$. How consistent is the 12-product model with the two-product approach in equation (5.1), and can the products be assigned unambiguously to the two classes? Some 84.5% of the predicted gas-phase mass of $98.8 \mu\text{g m}^{-3}$ for $\Delta(\alpha\text{-pinene})$ equal to $888.5 \mu\text{g m}^{-3}$ is accounted for by compounds A9 and A10, of which only $5.7 \mu\text{g m}^{-3}$ occurs in the condensed phase. Also, 91% ($193 \mu\text{g m}^{-3}$) of the condensed phase is accounted for by compounds A2, A5, A6, A7, and A12, of which some $32 \mu\text{g m}^{-3}$ (mostly A5) is predicted to occur in the gas phase. The remaining products (A1, A3, A8, A13, and A14) are generated only in small amounts and contribute little to either phase. The only compound that occurs to a significant extent in both phases is A5. Adding this compound to A9 and

A10 we obtain a total gas-phase organic concentration of $121.1 \mu\text{g m}^{-3}$, which agrees closely with $121.8 \mu\text{g m}^{-3}$ predicted by equation (5.1).

We can also carry out a similar comparison for $\Delta(\alpha\text{-pinene})$ equal to $236.6 \mu\text{g m}^{-3}$. Figure 5.12b shows the calculated gas/aerosol partitioning of all product compounds, by mass, for the $236.6 \mu\text{g m}^{-3}$ case. For a condensed phase component, again consisting of A2, A5, A6, A7, and A12, a total aerosol amount of $34.6 \mu\text{g m}^{-3}$ is predicted by the present model, in essentially exact agreement with the $35 \mu\text{g m}^{-3}$ observed and the $33.65 \mu\text{g m}^{-3}$ obtained from equation (5.1). For this case, in which ΔM_{org} is smaller by a factor of >6 , the amount of the mainly condensed phase component that also exists in the gas phase is larger: $20.7 \mu\text{g m}^{-3}$ is predicted by equation (5.1), which is very close to the $22.7 \mu\text{g m}^{-3}$ obtained by the multi-product model. Most of this amount ($14.1 \mu\text{g m}^{-3}$) is contributed by compound A5. A total of $26.2 \mu\text{g m}^{-3}$ is contributed by compounds A9 and A10 to the gas phase, rising to $40.3 \mu\text{g m}^{-3}$ if A5 is included, agreeing closely with equation (5.1), which yields $38.6 \mu\text{g m}^{-3}$. The amount of mainly gas-phase component occurring in the aerosol phase is only $1.35 \mu\text{g m}^{-3}$ from equation (5.1), which lies between the values predicted by the more complex model: $6.5 \mu\text{g m}^{-3}$ (A5 + A9 + A10) and $0.26 \mu\text{g m}^{-3}$ (A9 + A10 only).

In summary, comparison of the multi-product model with equation (5.1) shows that for values of ΔM_{org} encompassing the measured range the two models agree closely in their predictions of gas-phase and particulate organic concentrations for aerosol systems under dry conditions. This suggests that the assumption underlying both models – equilibrium partitioning between a vapor phase and an aerosol phase in which the

compounds are fully mixed – is correct. The result also implies that the molar yields of the product compounds obtained by Yu *et al.* (1999) are reasonable. This is because, if the total amounts used in the present model were significantly in error, then the model would not reproduce measured condensed phase amounts at the lower ΔM_{org} value, nor agree with the total masses of material predicted by equation (5.1) for both the examples examined above. The results of these calculations show that the primary condensed phase compounds are A2, A6, A7, and A12, and the gas-phase components are A9 and A10. The partitioning of compound A5 varies with the total amount of material present and can exist in significant quantity in both phases.

Next, the multi-product model was applied to two experimental results including wet salt seed aerosol: 12/21a for $(\text{NH}_4)_2\text{SO}_4$ at 45.1% RH and $\Delta(\alpha\text{-pinene})$ equal to $365.5 \mu\text{g m}^{-3}$, and 01/25b for CaCl_2 at 50% relative humidity and $\Delta(\alpha\text{-pinene})$ equal to $623.7 \mu\text{g m}^{-3}$. Calculations were carried out for both $\lambda_{org,salt} = 0$ and a range of positive values that correspond to a “salting out” effect. It was found that in all cases involving the CaCl_2 salt seed, and all except $\lambda_{org,salt} = 0$ for $(\text{NH}_4)_2\text{SO}_4$, the equilibrium system was predicted to contain an aerosol in which two liquid phases co-exist. The results of the calculations are summarized in Table 5.7a,b. The predicted total aerosol volume of about $1.0 \times 10^{-4} \text{ cm}^3 \text{ m}^{-3}$ for the $(\text{NH}_4)_2\text{SO}_4$ salt seed experiment is almost invariant with the value of the salting coefficient. The calculated total aerosol volume for the same conditions, but without the $(\text{NH}_4)_2\text{SO}_4$ seed, is $0.75 \times 10^{-4} \text{ cm}^3 \text{ m}^{-3}$ and the volume of the aqueous salt seed alone is estimated to be $0.25 \times 10^{-4} \text{ cm}^3 \text{ m}^{-3}$. Thus, subtracting the volume for the salt seed aerosol from the total to obtain $\Delta M_{org+water}$, we obtain almost exactly the value predicted for the system containing organic material and water alone. The same is true for the system

containing aqueous CaCl_2 seed: here the total aerosol volume is calculated to be about $2.0 \times 10^{-4} \text{ cm}^3 \text{ m}^{-3}$, and that of the salt seed alone $0.51 \times 10^{-4} \text{ cm}^3 \text{ m}^{-3}$. The same system, but not including the salt seed, is calculated to have a total aerosol volume of $1.51 \times 10^{-4} \text{ cm}^3 \text{ m}^{-3}$. Thus, again $\Delta M_{\text{org}+\text{water}}$ is predicted to be unaltered by the presence of the salt. The primary reason for this is that, for both cases, the liquid aerosol phase that contains the highest concentration (and largest amount) of organic material also contains only a very small fraction of the salt. The second liquid phase, by contrast, contains most of the salt but very little organic material. Consequently, the phase partitioning behavior differs little from that of salt/water and organic/water systems considered independently. We note similar behavior in the $\text{NaCl}_2/\text{C}_3\text{H}_7\text{COOH}/\text{H}_2\text{O}$ system modeled by Clegg *et al.* (2000): the formation of two liquid phases, one containing most of the salt, and the second containing most of the organic material. For these mixtures, for which the model was based on extensive vapor pressure and phase partitioning data, the calculated deliquescence behavior was found to be very similar to that for the sum of two separate $\text{NaCl}_2/\text{H}_2\text{O}$ and $\text{C}_3\text{H}_7\text{COOH}/\text{H}_2\text{O}$ phases.

How realistic is the model? It has already been shown in Figure 5.6 that the water activity/concentration relationship predicted by UNIFAC for the organic products of α -pinene oxidation is not consistent with the two growth factor measurements. Also, the present calculations assume a liquid mixture in which the organic compounds are soluble. The model does not allow for the formation of solids – either salt or one or more organic compounds – with experiments including aqueous salt seed. Additionally, there are a number of uncertainties in the parameters used in the model. Thermodynamic properties

had to be estimated for each oxidation product in the aerosol. Little data are available for estimation of $\lambda_{\text{org,salt}}$ for complex multifunctional organic products.

5.7 Existence of Multiple Phases

Until now we have assumed that the aerosol produced forms a single-phase water/salt/organic mixture. Pinic acid (Aldrich rare chemicals), a significant component of α -pinene/ O_3 SOA, was obtained to investigate the phenomena of “salting out” and whether the presence of the electrolytes could produce a multiple phase solution. First, the solubility of the pinic acid in H_2O was estimated to be between 4.7 mol kg^{-1} and 7.4 mol kg^{-1} at 25°C . Next, a saturated aqueous solution of $(\text{NH}_4)_2\text{SO}_4$ was added to a 3.4 mol kg^{-1} solution of pinic acid and water. Initial precipitation of a white solid was seen upon addition of $(\text{NH}_4)_2\text{SO}_4$. However, agitating the solution resulted in a single-phase solution containing 0.35 mol kg^{-1} $(\text{NH}_4)_2\text{SO}_4$ and 3.4 mol kg^{-1} pinic acid. Addition of further $(\text{NH}_4)_2\text{SO}_4$ solution lead to the precipitation of $(\text{NH}_4)_2\text{SO}_4$, and separation into two liquid phases as shown in Figure 5.11. The total molar quantities of material present was 6.3×10^{-4} moles pinic acid, 8.4×10^{-5} moles $(\text{NH}_4)_2\text{SO}_4$, and $0.19 \text{ g H}_2\text{O}$. (If only a single phase had formed, the composition would have been 3.4 mol kg^{-1} H_2O and 0.45 mol kg^{-1} $(\text{NH}_4)_2\text{SO}_4$.) The experiment was repeated, with two liquid phases and solid $(\text{NH}_4)_2\text{SO}_4$ being obtained at the interface, with molar quantities of 3.52×10^{-5} moles $(\text{NH}_4)_2\text{SO}_4$, 4.6×10^{-4} moles pinic acid, and $0.105 \text{ g H}_2\text{O}$. (Again, if a single-phase were present, the final solution composition would have been 4.4 mol kg^{-1} pinic acid and 0.34 mol kg^{-1} $(\text{NH}_4)_2\text{SO}_4$.)

Could the observed yields be explained by two co-existing liquid phases in the aerosol, as suggested by the results of experiments adding aqueous $(\text{NH}_4)_2\text{SO}_4$ to pinic

acid solutions? If this were to occur, then each particle would likely consist of one phase that is chiefly aqueous salt solution, with the other phase being mostly condensed organic material and a low concentration of dissolved salt. It appears that a system of this kind ought to give a yield little different from the no seed case, at least with the water uptake behavior of the organic material embodied in equation (5.9). There is a further possibility: that the condensed organic compounds, or some fraction of them, are deposited as solids and do not uptake water. However, if this were the case, the yield ought to be similar to the results for 2% RH. These are still higher than the yields determined in the experiments with salt seeds.

5.8 Aerosol-phase Chemistry--Another Potential Salting Effect.

As discussed in the previous section, electrolytic solutions may affect organic-water interactions. It is clear that “salting in” or “salting out” are unable by themselves to explain the experimental results obtained. However, the above model has neglected one potentially major avenue to aerosol formation and total aerosol production—aerosol-phase chemistry; we have assumed that all oxidation occurs in the gas-phase, followed by subsequent gas-particle partitioning into the aerosol-phase.

There is some evidence in the literature that aerosol-phase chemistry may be occurring in similar systems. Products identified in the aerosol-phase for the toluene/ NO_x irradiation (Jang and Kamens, 2001) and for the *m*-xylene and 1,3,5-trimethylbenzene/ NO_x irradiation (see Part II) have vapor pressures that are too high to be found in the aerosol phase. Jang and Kamens (2001) suggest that chemical reactions in the particle phase may dramatically alter the oxidation products partitioning behaviour. Such reactions include the “zipping” reaction of two oxygenated products to form a hemiacetal or acetal in

solution of lower vapor pressure. Such hemiacetals and acetals readily hydrolyze and would not be detected using conventional sampling techniques such as those employed by Yu *et al.* (1999) for identifying the products of the α -pinene/O₃ reaction. Tobias and Ziemann (2000) have recently reported the identification of such products in the ozonolysis of 1-tetradecene using a thermal desorption mass spectrometer. The presence of electrolytes in the organic aerosol may reduce the propensity for such “zipping” reactions. (We already know that the presence of the salt can raise the activity of an organic in solution.) Reduction in the formation of these heavier organic compounds will effectively raise the vapor pressure of the aerosol when salts are present, leading to the measurable reduction in aerosol formation with electrolytes present. Such processes are expected to be compound-specific, as individual organic-salt interactions may vary as well as the barrier to formation of such products.

5.9 Conclusions

An extensive investigation into the aerosol forming potential of α -pinene/O₃ oxidation under dry and humid conditions is presented. The presence of a dry inorganic salt has no measurable effect on the aerosol formation potential of the α -pinene/O₃ system. The presence of water leads to an increase in the aerosol volume produced due to water uptake by the organic phase during α -pinene ozonolysis but only if any inorganic salts present remained in their dry, crystalline forms. When aqueous seed is present, the amount of SOA yield decreases.

A thermodynamic investigation of the α -pinene/O₃ system is also presented. First, the water uptake of the pure inorganic salt was reliably predicted. Next, the water uptake of the oxidation products of α -pinene/O₃ was predicted using Raoult’s law, the Margules

equation, and UNIFAC. The Margules parameterization was able to sufficiently describe the additional water uptake by the pure organic aerosol. Additionally, a multi-component aerosol model was able to predict aerosol formation potential of the α -pinene/O₃ system based on its known aerosol product distribution. Finally, the effect of salting out on aerosol formation potential was investigated. It was determined that salting out effect, by itself, was unable to predict the large reduction in the aerosol forming potential of α -pinene/O₃ in the presence of a strong electrolyte. Further phenomenological process must be explored, such as heterogeneous chemistry, to identify the main driving force for the reduction in the formation potential of the α -pinene/O₃ system in the presence of strong electrolytes.

5.10 References

- Anathaswamy J. and Atkinson G. (1985) Thermodynamics of concentrated electrolyte mixtures. 5. A review of the thermodynamic properties of aqueous calcium chloride in the temperature range 273.15-373.15 K. *J. Chem. Eng. Data* **30**, 120-128.
- Ansari A. A. and Pandis S. N. (2000) Water absorption by secondary organic aerosol and its effect on inorganic aerosol behavior. *Environ. Sci. Technol.* **34**, 71-77.
- Bilde M. and Pandis S. N. (2000) Evaporation rates of α -pinene photooxidation aerosol products. *J. Aerosol Sci.* **31**, Suppl. 1, S174-S175.
- Clegg S. L., Pitzer K. S., and Brimblecombe, P. (1992) Thermodynamics of multicomponent, miscible, ionic solutions. II. Mixture including unsymmetrical electrolytes. *J. Phys. Chem.* **96**, 9470-9479.
- Clegg S. L., Ho S. S., Chan C. K., and Brimblecombe P. (1995) Thermodynamic properties of aqueous (NH₄)₂SO₄ to high supersaturation as a function of temperature.

J. Chem. Eng. Data **40**, 1079-1090.

Clegg S. L., Brimblecombe P., and Wexler A. S. (1998a) A thermodynamic model of the system $\text{H}^+ - \text{NH}_4^+ - \text{Na}^+ - \text{SO}_4^{2-} - \text{NO}_3^- - \text{Cl}^- - \text{H}_2\text{O}$ at 298.15 K. *J. Phys. Chem.* **102**, 2155-2171.

Clegg S. L., Brimblecombe P., and Wexler A. S. (1998b) A thermodynamic model of the system $\text{H}^+ - \text{NH}_4^+ - \text{SO}_4^{2-} - \text{NO}_3^- - \text{H}_2\text{O}$ at tropospheric temperatures. *J. Phys. Chem.* **102**, 2137-2154.

Clegg S. L., Seinfeld J. H., and Brimblecombe P. (2000) Thermodynamic modeling of aqueous aerosols containing electrolytes and dissolved organic compounds. In Press, *J. Aerosol Sci.*

Cocker D. R., Whitlock N. W., Flagan R. C., and Seinfeld J. H. (2001) Hygroscopic properties of Pasadena, California aerosol. In press, *Aerosol Sci. Technol.*

Collins D. R., Flagan R. C., and Seinfeld J. H. (2001). Improved inversion of scanning DMA data. In press. *Aerosol Sci. Technol.*

Cruz N. C. and Pandis S.N. (2000). Deliquescence and hygroscopic growth of mixed inorganic-organic atmospheric aerosol. *Aerosol Sci. Technol.* **34**, 4313-4319.

Edney E. O., Driscoll D. J., Speer R. E., Weathers W. S., Kleindienst T. E., Li W., and Smith D. F. (2000). Impact of aerosol liquid water on secondary organic aerosol yields of irradiated toluene/propylene/ NO_x / $(\text{NH}_4)_2\text{SO}_4$ /air mixtures. *Atmos. Environ.* **34**, 3907-3919.

Ferron G. A., Karg E., Busch B., and Heyder J. (1999). Hygroscopicity of ambient particles. *J. Aerosol Sci.* **30**, S19-S20.

Forstner H. J. L., Flagan R. C., and Seinfeld J. H. (1997). Secondary organic aerosol from the photooxidation of aromatic hydrocarbons: Molecular composition. *Environ.*

Sci. Technol. **31**, 1345-1358.

Fredenslund Aa., Jones R. L., and Prausnitz J. M. (1975) Group-contribution estimation of activity coefficients in non-ideal liquid mixtures. *AIChE J.* **21**, 1086-1098.

Griffin R. J., Cocker III D. R., Flagan R. C., and Seinfeld J. H. (1999) Organic aerosol formation from the oxidation of biogenic hydrocarbons. *J. Geophys. Res.* **104**, 3555-3567.

Hansen H. K., Rasmussen P., Fredenslund Aa., Schiller M., and Gmehling J. (1991) Vapor-liquidequilibria by UNIFAC group contribution. 5. Revision and extension. *Ind. Eng. Chem. Res.* **30**, 2352-2355.

Hoffmann T. P. W., Odum J. R., Bowman F., Collins D. R., Klockow D., Flagan R. C., and Seinfeld J. H. (1997) Formation of organic aerosols from the oxidation of biogenic hydrocarbons. *J. Atmos. Chem.* **26**, 189-222.

Jacobson M. Z., Tabazadeh A., and Turco R. P. (1996). Simulating equilibrium within aerosols and nonequilibrium between gases and aerosols. *J. Geophys. Res.* **101**, 9079-9091.

Jang M. and Kamens R.M. (2001).

Kim Y. P. and Seinfeld J. H. (1995). Atmospheric gas-aerosol equilibrium, III, Thermodynamics of crustal elements Ca^{2+} , K^{+} , and Mg^{2+} . *Aerosol Sci. Technol.* **22**, 93-110.

Kim Y. P., Seinfeld J. H., and Saxena P. (1993a). Atmospheric gas-aerosol equilibrium, I, Thermodynamic model. *Aerosol Sci. Technol.* **19**, 157-181.

Kim Y. P., Seinfeld J. H., and Saxena P. (1993b). Atmospheric gas-aerosol equilibrium, II, Analysis of common approximations and activity coefficient calculation methods.

Aerosol Sci. Technol. **19**, 182-198.

- Massling A., Wiedensohler A., and Busch B. (1999). Hygroscopic growth of aerosol particles in the southern Atlantic Ocean and Indian Ocean. *J. Aerosol Sci.* **30**, S837-S838.
- McMurry P. H. and Stolzenburg M. R. (1989). On the sensitivity of particle size to relative humidity for Los Angeles aerosols. *Atmos. Environ.* **23**, 497-507.
- Myrdal P. B. and Yalkowsky S. H. (1997). Estimating pure component vapor pressures of complex organic molecules. *Industr. Eng. Chem. Res.* **36**, 2494-2499.
- Nenes A., Pandis S. N., and Pilinis C. (1998). ISORROPIA: A new thermodynamic equilibrium model for multiphase multicomponent inorganic aerosols. *Aqua. Geochem.* **4**, 123-152.
- Odum J. R., Hoffmann T. P. W., Bowman F., Collins D., Flagan R. C., and Seinfeld J. H. (1996) Gas/particle partitioning and secondary organic aerosol yields. *Environ. Sci. Technol.* **30**, 2580-2585.
- Odum J. R., Jungkamp T. P. W., Griffin R. J., Forstner H. J. L., Flagan R. C., and Seinfeld J. H. (1997) Gas/particle partitioning of semivolatile organic compounds to model inorganic, organic, and ambient smog aerosols. *Science*, **276**, 96-99.
- Pankow J. F. (1991) Common y-intercept and single compound regressions of gas-particle data vs. $1/T$. *Atmos. Environ.* **25A**, 2229-2239.
- Pankow J. F. (1994a) An absorption-model of gas-particle partitioning of organic-compounds in the atmosphere. *Atmos. Environ.* **2**, 185-188.
- Pankow J. F. (1994b) An absorption-model of the gas aerosol partitioning involved in the formation of secondary organic aerosol. *Atmos. Environ.* **2**, 189-193.

- Pilinis C. and Seinfeld J. H. (1987). Continued development of a general equilibrium model for inorganic multicomponent atmospheric aerosols. *Atmos. Environ.* **32**, 2453-2466.
- Rader D. J. and McMurry P. H. (1986). Application of the tandem differential mobility analyzer to studies of droplet growth or evaporation. *J. Aerosol Sci.* **17**, 771-787.
- Saxena P. and Hildemann L. M. (1997). Water absorption by organics: Survey of laboratory evidence and evaluation of UNIFAC for estimating water activity. *Environ. Sci. Technol.* **31**, 3318-3324.
- Sohnel O. and Novotny P. (1985) *Densities of Aqueous Solutions of Inorganic Substances*, Elsevier, Amsterdam.
- Svenningsson I. B., Hansson H. C., Wiedensohler A., Ogren J. A., Noone K. J., and Hallberg A. (1992). Hygroscopic growth of aerosol particles in the Po Valley. *Tellus.* **44B**, 556-569.
- Swietlicki E., Zhou J., Berg O.H., Martinsson B.G., Frank G., Cederfelt S.-I., Dusek U., Berner A., Birmili W., Wiedensohler A., Yuskiewicz B., and Bower K.N. (1999). A closure study of sub-micrometer aerosol particle hygroscopic behaviour. *Atmos. Res.* **50**, 205-240.
- Tang I. N. and Munkelwitz H. R. (1994). Water activities, densities, and refractive-indexes of aqueous sulfates and sodium-nitrate droplets of atmospheric importance. *J. Geophys. Res. – Atmos.* **99**, 18801-18808.
- Tobias H. J and Ziemann P. J. (2000). Thermal desorption mass spectrometric analysis of organic aerosol form from reactions of 1-tetradecene and O₃ in the presence of alcohols and carboxylic acids. *Environ. Sci. Technol.* **34**, 2105-2115.

- Virkkula A., Dingenen R. V., Raes F., and Hjorth J. (1999). Hygroscopic properties of aerosol formed by oxidation of limonene, α -pinene, and β -pinene. *J. Geophys. Res.* **104**, 3569-3579.
- Wexler A. S. and Seinfeld J. H. (1990). The distribution of ammonium salts among a size and composition dispersed aerosol. *Atmos. Environ.* **24A**, 1231-1246.
- Wexler A.S. and Seinfeld J.H. (1991). Second-generation inorganic aerosol model. *Atmos. Environ.* **25A**, 2731-2748.
- Yu J., Cocker III D. R., Griffin R. J., Flagan R. C., and Seinfeld J. H. (1999) Gas-phase oxidation of monoterpenes: gaseous and particulate products. *J. Atmos. Chem.* **34**, 207-258.
- Zhang Y., Seigneur C., Seinfeld J. H., Jacobson M., Clegg S. L., and Binkowski F. S. (2000). A comparative review of inorganic aerosol thermodynamic equilibrium modules: similarities, differences, and their likely causes. *Atmos. Environ.* **34**, 117-137

Table 5.1: Experimental Results

Date	$\Delta(\alpha\text{-pinene})$ ($\mu\text{g m}^{-3}$)	$\Delta M_{\text{org+water}}^a$ ($\mu\text{g m}^{-3}$)	O_3 (ppb)	RH (%)	Temp ($^{\circ}\text{C}$)	Yield (%)	Seed	condition	Amount ^b (mol m^{-3})
11/29a	411	82	280	<2	28	20.0	(NH_4) ₂ SO ₄	dry	
11/29b	792.8	190	360	<2	28	24.0	(NH_4) ₂ SO ₄	dry	
12/03a	223.3	34	370	<2	28	15.2	(NH_4) ₂ SO ₄	dry	
12/03b	398.1	79	315	<2	28	19.8	(NH_4) ₂ SO ₄	dry	
12/06b	125.8	10	280	<2	28	7.9	(NH_4) ₂ SO ₄	dry	
12/16b	562.1	83	580	62	29.3	14.8	NH ₄ HSO ₄	aqueous	1.2×10^{-7}
12/17a	204.9	10	242	54.9	28	4.9	NH ₄ HSO ₄	aqueous	1.4×10^{-7}
12/17b	404.8	53	258	56.6	28	13.1	NH ₄ HSO ₄	aqueous	2.9×10^{-7}
12/18a	416	51	255	45	27.3	12.3	NH ₄ HSO ₄	aqueous	4.1×10^{-7}
12/18b	659.7	108	410	52.5	27.3	16.4	NH ₄ HSO ₄	aqueous	2.2×10^{-7}
12/19a	90.9	3	201	56.3	26.8	3.3	NH ₄ HSO ₄	aqueous	2.2×10^{-7}
12/19b	828.5	175	452	53.9	26.8	21.1	NH ₄ HSO ₄	aqueous	2.4×10^{-7}
12/21a	365.5	9.9	233	45.1	27.6	2.7	(NH_4) ₂ SO ₄	aqueous	1.9×10^{-7}
12/21b	900.9	148	302	52.4	27.6	16.4	(NH_4) ₂ SO ₄	aqueous	1.9×10^{-7}
01/03a	69	1.5	330	48.5	27.6	2.2	(NH_4) ₂ SO ₄	aqueous	1.7×10^{-7}
01/03b	384.4	35	350	48.1	27.6	9.1	(NH_4) ₂ SO ₄	aqueous	1.9×10^{-7}
01/04a	753.8	125	310	48.5	29.2	16.6	(NH_4) ₂ SO ₄	aqueous	2.4×10^{-7}
01/04b	571.5	79	208	55.2	29.2	13.8	(NH_4) ₂ SO ₄	aqueous	1.8×10^{-7}
01/05a	1302.3	263	310	47.1	28	20.2	(NH_4) ₂ SO ₄	aqueous	2.5×10^{-7}
01/05b	1183.5	216	280	50	28	18.3	(NH_4) ₂ SO ₄	aqueous	1.5×10^{-7}
01/08a	398.5	80	270	<2	27.8	20.1	None	N/A	0
01/10a	225.2	35	278	<2	28.9	15.5	None	N/A	0
01/10a	512.5	110	499	<2	28.9	21.5	None	N/A	0
01/11a	386.3	86	250	41	28.8	22.3	None	N/A	0
01/11b	675	177	380	57.7	28.8	26.2	None	N/A	0
01/12a	235.9	45	205	31	29.5	19.1	None	N/A	0
01/12b	686.7	175	258	46	29.5	25.5	None	N/A	0
01/13a	396	79	244	14.1	29.5	19.9	NH ₄ HSO ₄	dry	
01/13b	648.4	145	352	14.4	29.5	22.4	NH ₄ HSO ₄	dry	
01/14a	265	48	402	14.6	29.6	18.1	NH ₄ HSO ₄	dry	
01/14b	541.1	115	313	16.6	29.6	21.3	NH ₄ HSO ₄	dry	
01/17a	986.5	281	324	37.3	29.7	28.5	None	N/A	0
01/18a	636.6	140	130	<2	29.1	22.0	(NH_4) ₂ SO ₄	dry	
01/19a	389.2	74	256	39	29.4	19.0	(NH_4) ₂ SO ₄	dry	

^a The increase in aerosol mass caused by the uptake of organic matter and net change in liquid water content. Calculated from equations 5.3 and 5.4.

^b Reported is that suspended in chamber 60 min after ozone injection, and was calculated from the observed size distributions and water activities and densities from sources given in Section 5.6.1.

Table 5.1: Experimental Results continued

Date	$\Delta(\alpha\text{-pinene})$ ($\mu\text{g m}^{-3}$)	$\Delta M_{\text{org+water}}^{\text{a}}$ ($\mu\text{g m}^{-3}$)	O_3 (ppb)	RH (%)	Temp ($^{\circ}\text{C}$)	Yield (%)	Seed	condition	Amount ^b (mol m^{-3})
01/19b	848.2	213	503	49	29.4	25.1	$(\text{NH}_4)_2\text{SO}_4$	dry	
01/20a	189.7	25	190	45.3	29	13.2	$(\text{NH}_4)_2\text{SO}_4$	dry	
01/20b	669.3	165.5	600	49.2	29	24.7	$(\text{NH}_4)_2\text{SO}_4$	dry	
01/21a	627.1	98	180	47.1	29.7	15.6	$(\text{NH}_4)_2\text{SO}_4$	aqueous	1.4×10^{-7}
01/21b	964.5	165	206	50.2	29.7	17.1	$(\text{NH}_4)_2\text{SO}_4$	aqueous	2.1×10^{-7}
01/22a	888.5	220	175	<2	29.6	24.8	None	N/A	0
01/22b	762.6	185	380	<2	29.6	24.3	None	N/A	0
01/24a	406	60	250	41.5	28.5	14.8	CaCl_2	aqueous	2.7×10^{-7}
01/24b	628.2	130	300	57.5	28.5	20.7	CaCl_2	aqueous	2.9×10^{-7}
01/25a	256.3	25	260	49.2	29.5	9.8	CaCl_2	aqueous	0.97×10^{-7}
01/25b	623.7	120	300	50	29.5	19.2	CaCl_2	aqueous	2.2×10^{-7}
01/26a	1204.3	295	153	43.9	29	24.5	CaCl_2	aqueous	1.6×10^{-7}
01/26b	933.9	215	246	51.2	29	23.0	CaCl_2	aqueous	1.5×10^{-7}

^a The increase in aerosol mass caused by the uptake of organic matter and net change in liquid water content. Calculated from equations 5.3 and 5.4.

^b Reported is that suspended in chamber 60 min after ozone injection, and was calculated from the observed size distributions and water activities and densities from sources given in Section 5.6.1.

Table 5.2: Empirically fit partitioning coefficients

Experimental conditions	α_1	α_2	$K_{om,1}$ ($\mu\text{g m}^{-3}$)	$K_{om,2}$ ($\mu\text{g m}^{-3}$)
Dry nucleation	0.239	0.169	0.042	0.0010
Wet nucleation before water correction	0.239	0.169	0.056	0.0019
Wet nucleation after water correction	0.239	0.169	0.042	0.0010
dry $(\text{NH}_4)_2\text{SO}_4$	0.239	0.169	0.042	0.0010
dry NH_4HSO_4	0.239	0.169	0.042	0.0010
RH 50%, dry $(\text{NH}_4)_2\text{SO}_4$ before water correction	0.239	0.169	0.046	0.0018
RH 50%, dry $(\text{NH}_4)_2\text{SO}_4$ after water correction	0.239	0.169	0.042	0.0010
RH 50%, aqueous $(\text{NH}_4)_2\text{SO}_4$	0.239	0.169	0.016	0.00013
RH 50%, aqueous NH_4HSO_4	0.239	0.169	0.020	0.00028
RH 50%, aqueous CaCl_2	0.239	0.169	0.028	0.00073

Table 5.3: Hygroscopic growth factors obtained from TDMA measurements

Compound	Initial RH	Final RH	Growth factor	
			Measured	Predicted
α -Pinene SOA ^b	<2%	50%	1.04	---
α -Pinene SOA ^b	<2%	85%	1.09 ^a	---
Dry (NH ₄) ₂ SO ₄	<2%	85%	1.58	1.58
Dry (NH ₄) ₂ SO ₄	50%	85%	1.59	1.58
Aqueous (NH ₄) ₂ SO ₄	50%	85%	1.31	1.28
Dry NH ₄ HSO ₄	<2%	85%	1.65	1.64
Aqueous NH ₄ HSO ₄	50%	85%	1.36	1.33
Aqueous CaCl ₂	50%	85%	1.31	1.29

^aVirkkula *et al.* (1999) reports a growth factor of 1.08 at 85%.

^bMeasured at 180 min after the start of the experiment.

Table 5.4: Phase partitioning predicted from equation (5.1)^a

Compound	Mass ($\mu\text{g m}^{-3}$)	Mass ($\mu\text{g m}^{-3}$)
$\Delta(\alpha\text{-Pinene})$	888.5	236.6
Component 1 ^b (aerosol)	191.6	33.7
Component 1 (gas)	20.7	22.9
Component 2 ^c (aerosol)	28.4	1.35
Component 2 (gas)	121.8	38.6

^aFor 2% RH and 301 K.^b"Involatile" products.^c"Volatile" products.

Table 5.5: Products of the oxidation of α -pinene by ozone

Compound ^a	Formula	Yield ^b	p^o (301 K) ^c
Pinic acid (A2)	C ₉ H ₁₄ O ₄	4.50	1.5 x 10 ⁻⁸
Norpinic acid (A1)	C ₈ H ₁₂ O ₄	0.10	8.1 x 10 ⁻⁸
Hydroxy pinonaldehyde (A12)	C ₁₀ H ₁₆ O ₃	2.85	7.7 x 10 ⁻⁷
Pinonic acid (A6)	C ₁₀ H ₁₆ O ₃	2.35	3.6 x 10 ⁻⁷
Norpinoic acid (A5)	C ₉ H ₁₄ O ₃	7.25	1.1 x 10 ⁻⁶
Pinonaldehyde (A9)	C ₁₀ H ₁₆ O ₂	8.20	3.7 x 10 ⁻⁵
Norpinonaldehyde (A9)	C ₉ H ₁₄ O ₂	1.45	1.6 x 10 ⁻⁴
2,2-Dimethyl-cyclobutyl-1,3-dicarboxaldehyde (A8)	C ₈ H ₁₂ O ₂	0.35	3.3 x 10 ⁻⁴
Hydroxy pinonic acid (A7)	C ₁₀ H ₁₆ O ₄	2.20	1.1 x 10 ⁻⁸
(2,2-Dimethyl-3-acetyl)- cyclobutyl formate (A3)	C ₁₀ H ₁₆ O ₃	1.05	6.1 x 10 ⁻⁶
A13 ^d	C ₁₀ H ₁₄ O ₄	0.12	3.2 x 10 ⁻⁷
A14 ^d	C ₁₀ H ₁₄ O ₄	0.55	3.2 x 10 ⁻⁷

^aThe numbers in parentheses refer to the product numbers of Yu *et al.* (1999).

^bThe product yield in mole % of the α -pinene reacted.

^cThe estimated vapor pressure (Myrdal and Yalkowsky, 1997), in atmospheres, of the pure compound as a supercooled liquid. These values were reduced by a factor of 100 in the calculations (see text).

^dIn Table VI of Yu *et al.* (1999) compound A13 has been erroneously assigned the same structure as A3. Here we assume that A13 is similar to A14, but with the C=O group next to the -CHO swapped with the CH₂ preceeding the -COOH. The UNIFAC group compositions of these minor oxidation products are the same.

Table 5.6: UNIFAC (Fredenslund *et al.*, 1975) group compositions of the oxidation products^a

Compound	CH ₃ ^b	CH ₂ ^b	CH ^b	C ^b	COOH ^c	CHO ^d	CH ₂ CO ^e	CH ₃ CO ^e	OH ^f	CH ₂ O ^g
A2	2	2	2	1	2					
A1	2	1	2	1	2					
A12	2	2	3	2		1	1		1	
A6	2	2	1	1	1			1		
A5	2	1	2	1	1			1		
A10	2	2	2	1		1		1		
A9	2	1	2	1		1		1		
A8	2	1	2	1		2				
A7	2	2	2	1	1		1	1	1	
A3	2	1	2	1		1				1
A13	2	2	1	1	1		1			
A14	2	2	1	1	1		1			

^aEach column lists the number of occurrences of the group in the molecule. See Table 5.5 for the chemical formulae of the compounds.

^balkanes, ^ccarboxylic acid, ^daldehyde, ^ecarbonyl, ^falcohol, ^gether.

Table 5.7: Predicted phase partitioning

(a) System including $(\text{NH}_4)_2\text{SO}_4$ seed at 45.1% RH^a

$\lambda_{\text{org,salt}}$	Phase 1			Phase 2			Volume ^b
	ΣOrg	$n(\text{NH}_4)_2\text{SO}_4$	$n\text{H}_2\text{O}$	ΣOrg	$n(\text{NH}_4)_2\text{SO}_4$	$n\text{H}_2\text{O}$	
	$\mu\text{g m}^{-3}$	mol m^{-3}	mol m^{-3}	$\mu\text{g m}^{-3}$	mol m^{-3}	mol m^{-3}	
0	8.3×10^{-5}	1.9×10^{-7}	5.8×10^{-7}	-	-	-	1.09×10^{-4}
0.01	7.8×10^{-8}	6.7×10^{-8}	1.9×10^{-7}	7.8×10^{-5}	1.3×10^{-7}	5.4×10^{-7}	1.06×10^{-4}
0.02	1.5×10^{-7}	1.6×10^{-7}	4.6×10^{-7}	7.5×10^{-5}	3.3×10^{-8}	3.1×10^{-7}	1.04×10^{-4}
0.05	5.4×10^{-8}	1.9×10^{-7}	5.5×10^{-7}	7.5×10^{-5}	2.5×10^{-11}	1.4×10^{-7}	1.03×10^{-4}
0.10	7.3×10^{-9}	1.9×10^{-7}	5.5×10^{-7}	7.5×10^{-5}	7.3×10^{-14}	1.4×10^{-7}	1.03×10^{-4}

^aConditions: experiment 12/21a, $\Delta(\alpha\text{-pinene}) = 365.5 \mu\text{g m}^{-3}$, $T = 301 \text{ K}$.Total $n(\text{NH}_4)_2\text{SO}_4 = 1.932 \times 10^{-7}$ moles.^bTotal volume of both phases was calculated assuming that the apparent molar volumes of the salt and organic compounds are the same in mixed solutions as in pure (single solute) solutions at the same molality.(b) System including CaCl_2 seed at 50.0% RH^c

$\lambda_{\text{org,salt}}$	Phase 1			Phase 2			Volume ^b
	ΣOrg	$n\text{CaCl}_2$	$n\text{H}_2\text{O}$	ΣOrg	$n\text{CaCl}_2$	$n\text{H}_2\text{O}$	
	$\mu\text{g m}^{-3}$	mol m^{-3}	mol m^{-3}	$\mu\text{g m}^{-3}$	mol m^{-3}	mol m^{-3}	
0	5.0×10^{-7}	1.1×10^{-7}	1.2×10^{-6}	1.6×10^{-4}	1.1×10^{-7}	1.2×10^{-6}	2.1×10^{-4}
0.01	5.4×10^{-7}	1.2×10^{-7}	1.3×10^{-6}	1.5×10^{-4}	1.0×10^{-7}	1.2×10^{-6}	2.1×10^{-4}
0.05	7.2×10^{-7}	1.6×10^{-7}	1.8×10^{-6}	1.5×10^{-4}	5.6×10^{-8}	9.3×10^{-7}	2.0×10^{-4}
0.10	6.1×10^{-7}	2.2×10^{-7}	2.4×10^{-6}	1.5×10^{-4}	1.1×10^{-11}	3.0×10^{-7}	2.0×10^{-4}
0.15	3.5×10^{-7}	2.2×10^{-7}	2.4×10^{-6}	1.5×10^{-4}	6.9×10^{-14}	3.0×10^{-7}	2.0×10^{-4}

^cConditions: experiment 01/25b, $\Delta(\alpha\text{-pinene}) = 623.7 \mu\text{g m}^{-3}$. $T = 301 \text{ K}$, total $n\text{CaCl}_2 = 2.191 \times 10^{-7}$ moles.

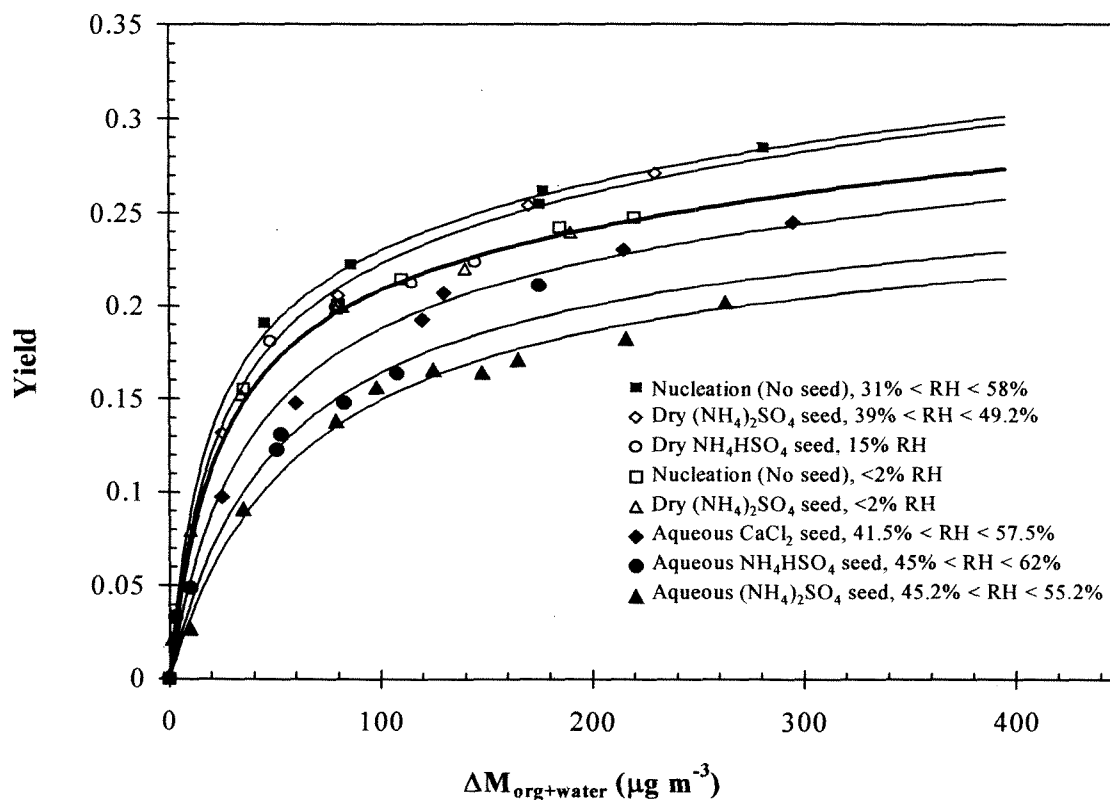


Figure 5.1. Summary of experimental yield data. Yields have not been corrected for water uptake, and the $\Delta M_{org+water}$ is the increase in mass of the aerosol in the chamber assuming the density of the aerosol is $1 g cm^{-3}$. Solid line is two-product fit through each data set. Exact humidities for each data point are given in Table 5.1. Thicker line is the “simple” dry aerosol yield.

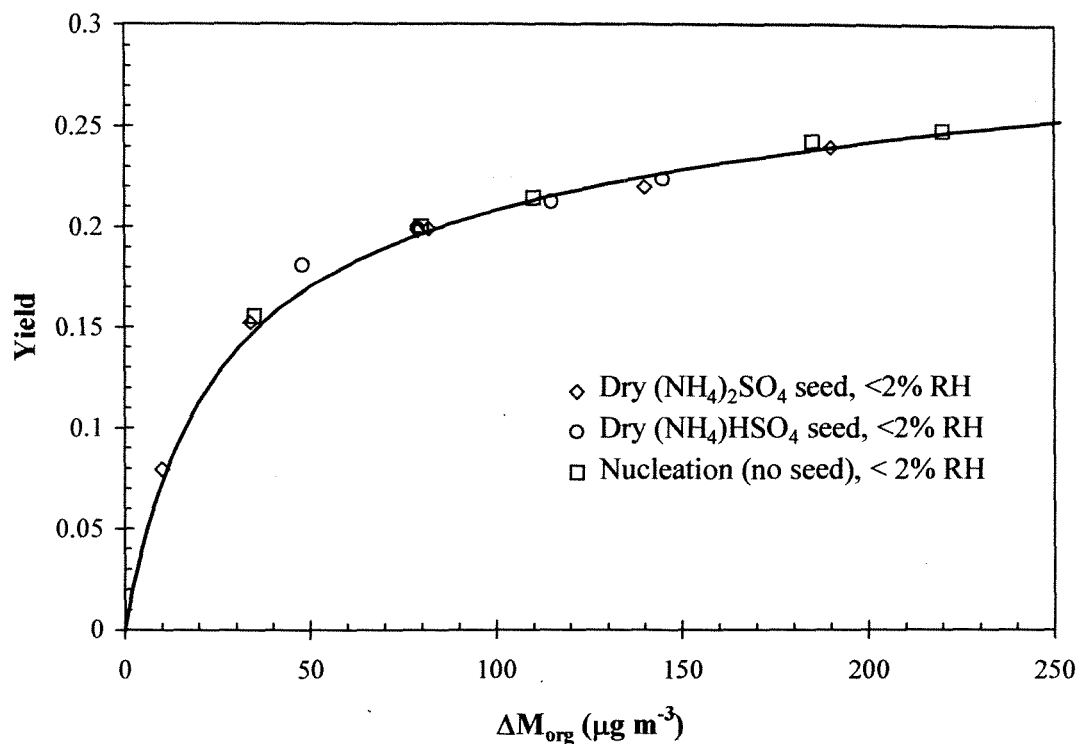


Figure 5.2. Summary of experimental yield data taken under dry conditions ($\text{RH} < 2\%$) in the presence of dry $(\text{NH}_4)_2\text{SO}_4$, dry NH_4HSO_4 , and no seed present. Solid line is two-product fit of data to equation (5.1): $\alpha_1 = 0.239$, $K_{om,1} = 0.042 \text{ m}^3 \mu\text{g}^{-1}$, $\alpha_2 = 0.169$, $K_{om,2} = 0.001 \text{ m}^3 \mu\text{g}^{-1}$.

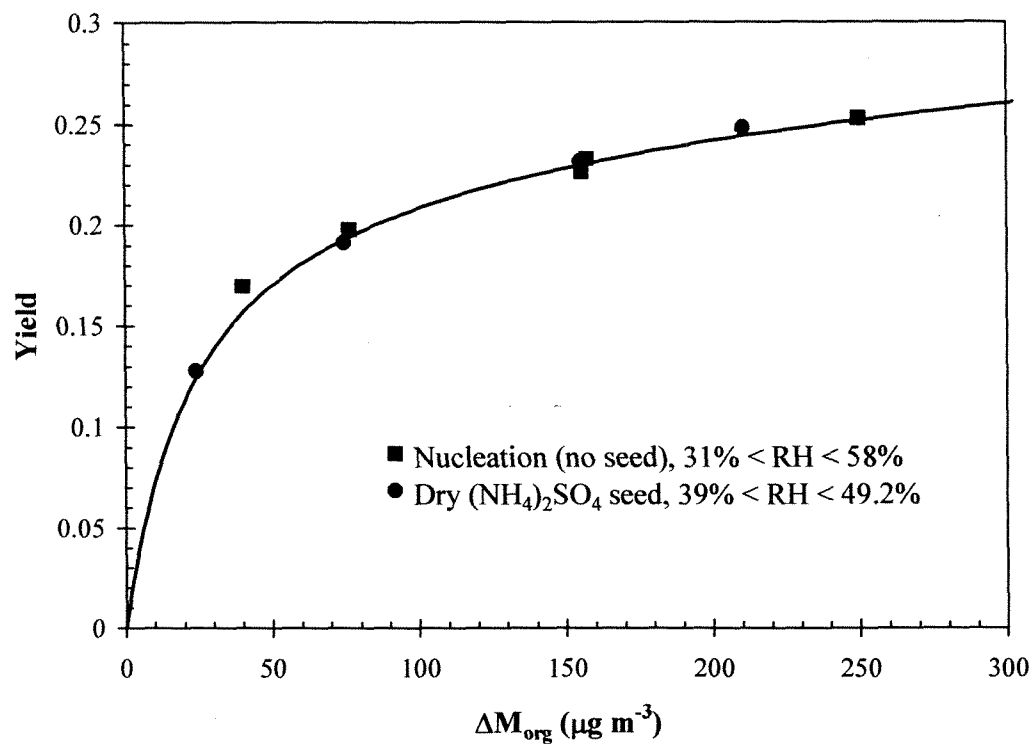


Figure 5.3. Aerosol yield corrected for water uptake of organics for nucleation at RH = 50% and for $(\text{NH}_4)_2\text{SO}_4$ seed aerosol, dry, at RH = 50%. Solid line is from Figure 5.2. Exact humidities for each data point are given in Table 5.1.

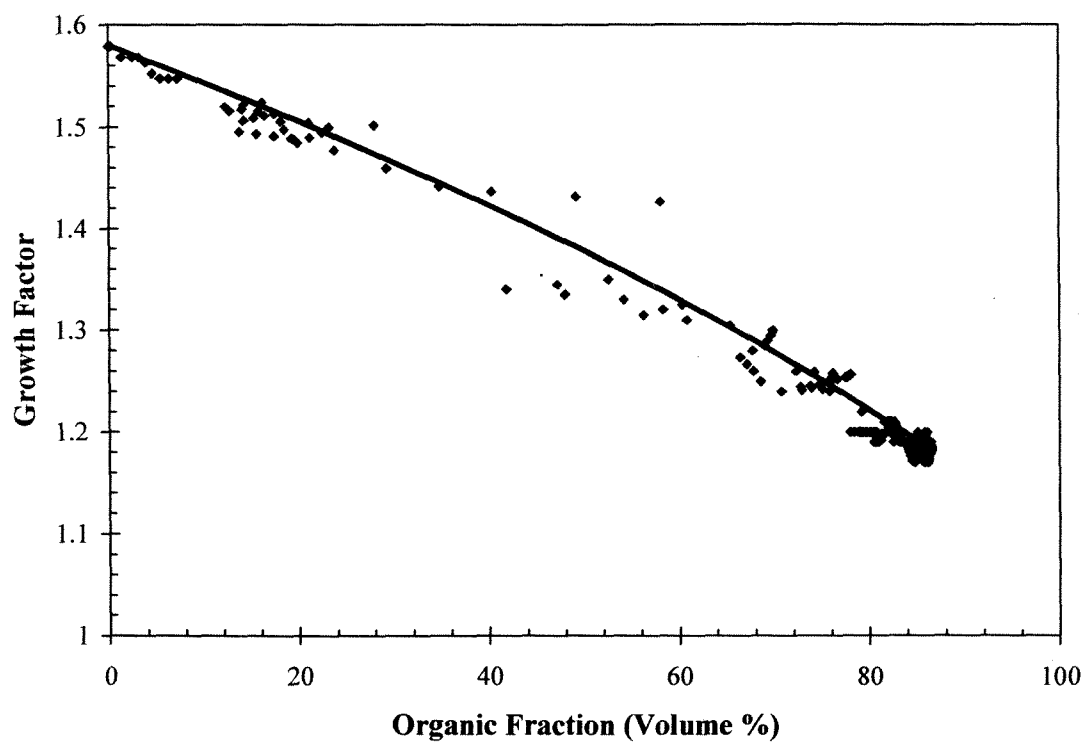


Figure 5.4. Growth factors (G_f) for α -pinene/ O_3 SOA from dry conditions to 85% RH (Experiment 12/6/99) as a function of the organic fraction of the aerosol.

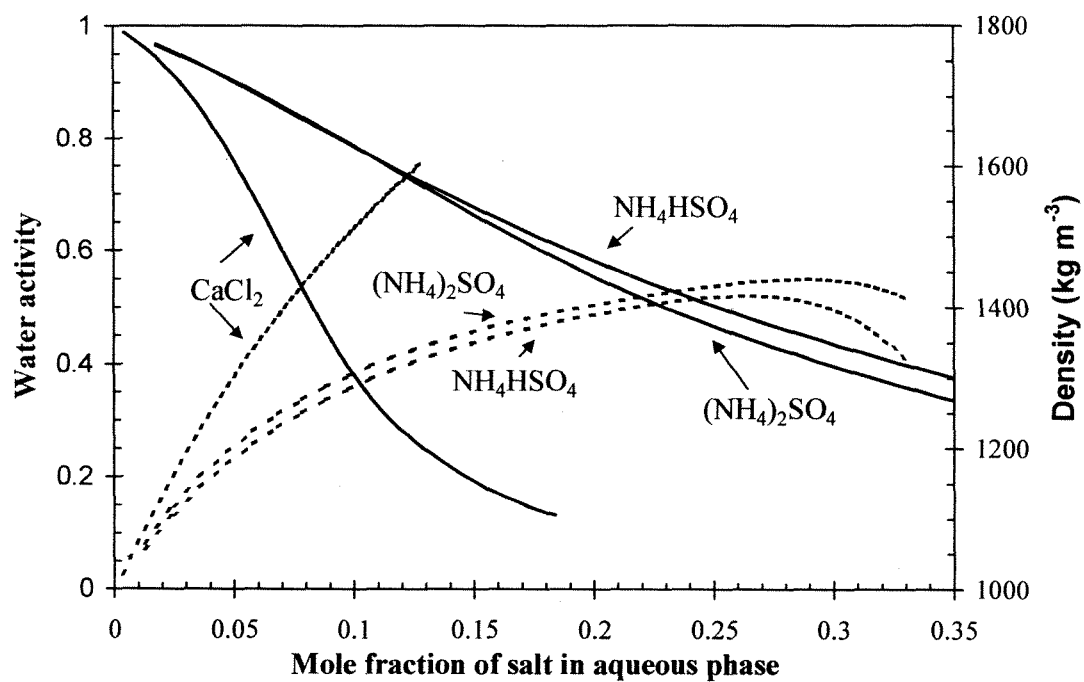


Figure 5.5. Equilibrium water activity, equal to RH (solid lines), and density (dashed lines) for three aqueous salt solutions as a function of aqueous-phase salt mole fraction.

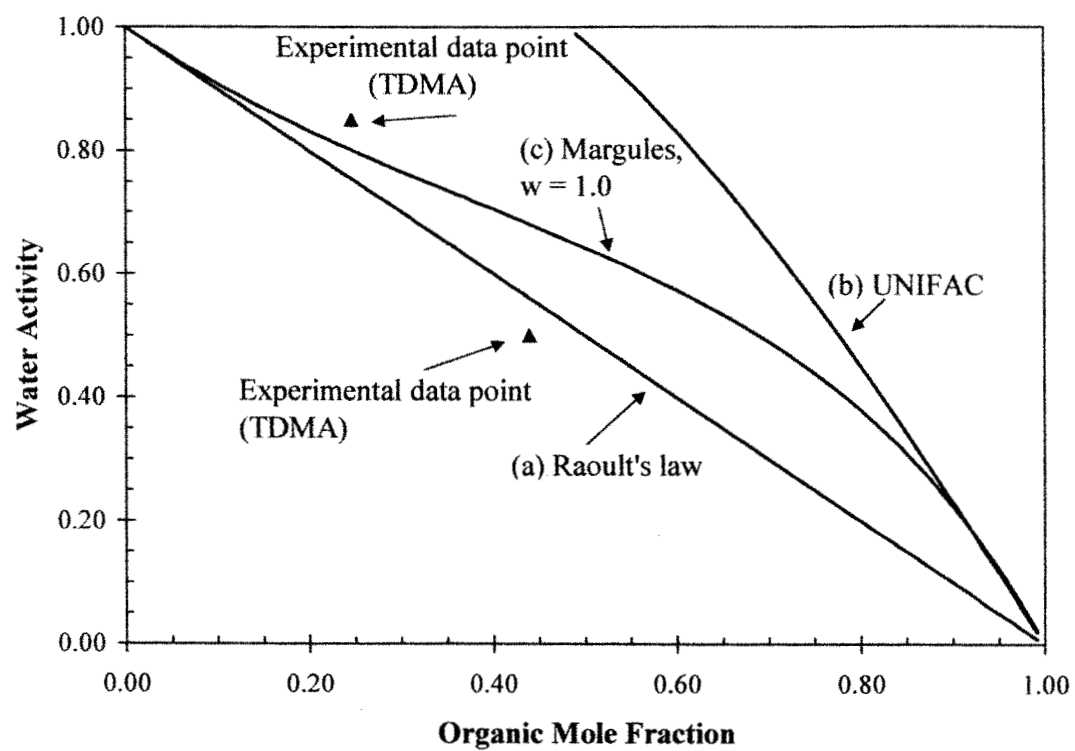


Figure 5.6: Equilibrium water activity, equal to RH, for mixtures of α -pinene SOA and water as a function of liquid-phase mole fraction of SOA.

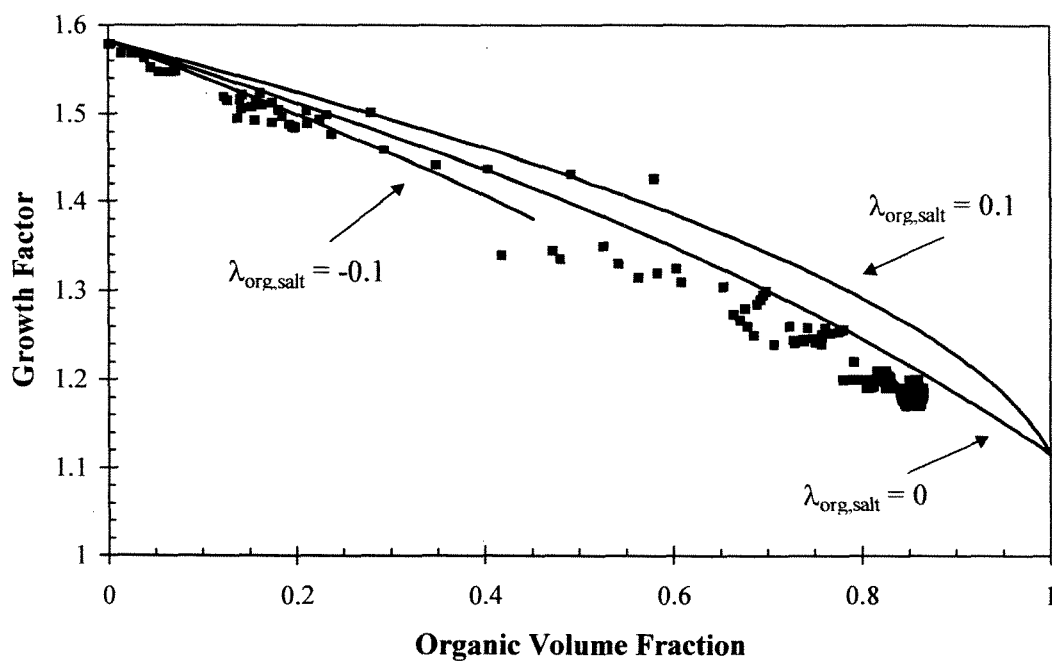


Figure 5.7. Measured and calculated growth factors (RH from 0 to 85%) at 301 K for aerosols containing a mixture of organic compounds and $(\text{NH}_4)_2\text{SO}_4$. Symbols – data from experiment 12/6/99 (Figure 5.4).

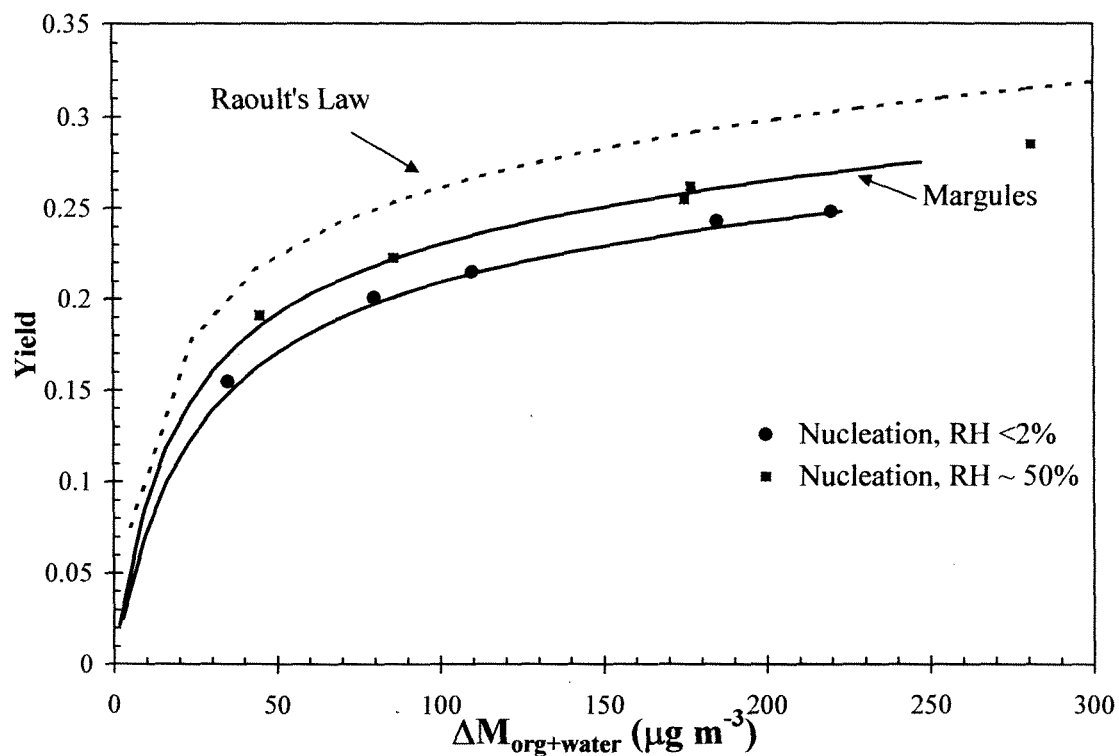


Figure 5.8. Measured and calculated yields for systems without seed aerosol at 2% and 50% RH. Symbols – all data under these conditions; solid lines – calculated using equations (5.9) to (5.11); dashed line – calculated using equations (5.9) to (5.11) and assuming unit activity coefficients of both the water and liquid phase compounds (Raoult's law).

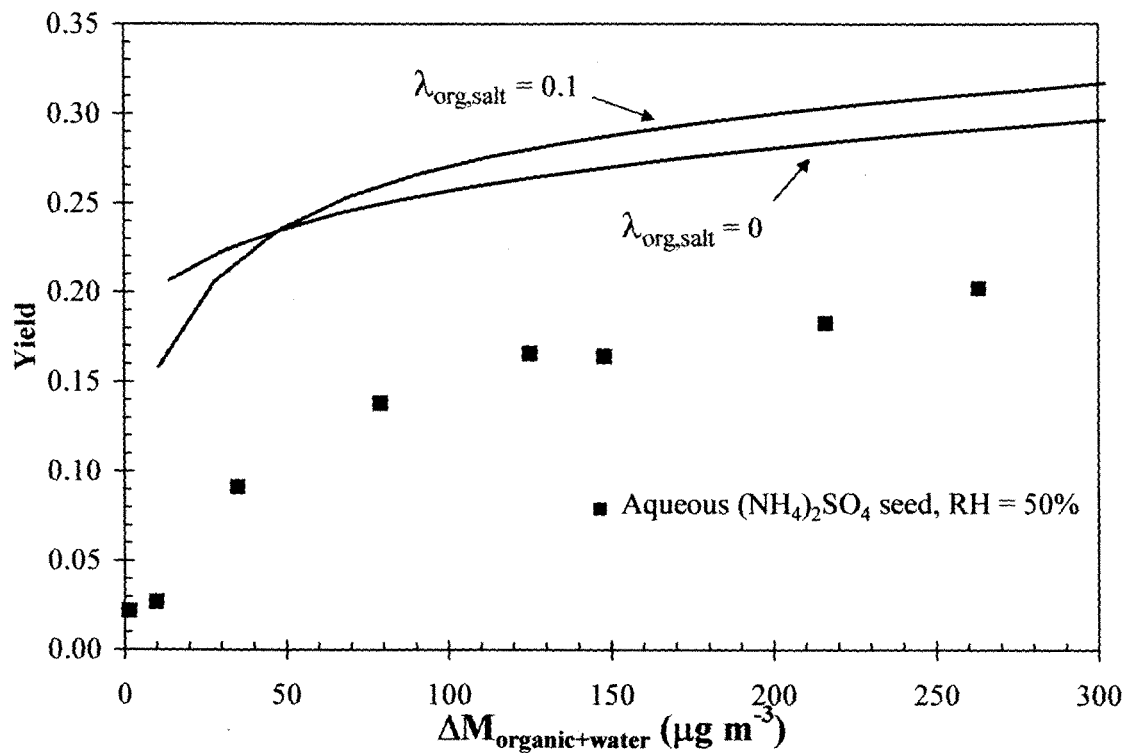


Figure 5.9. Measured and calculated yields at 50% RH for systems including $1.9 \times 10^{-7} \text{ mol m}^{-3} (\text{NH}_4)_2\text{SO}_{4(\text{aq})}$ seed aerosol. Symbols – all data under these conditions.

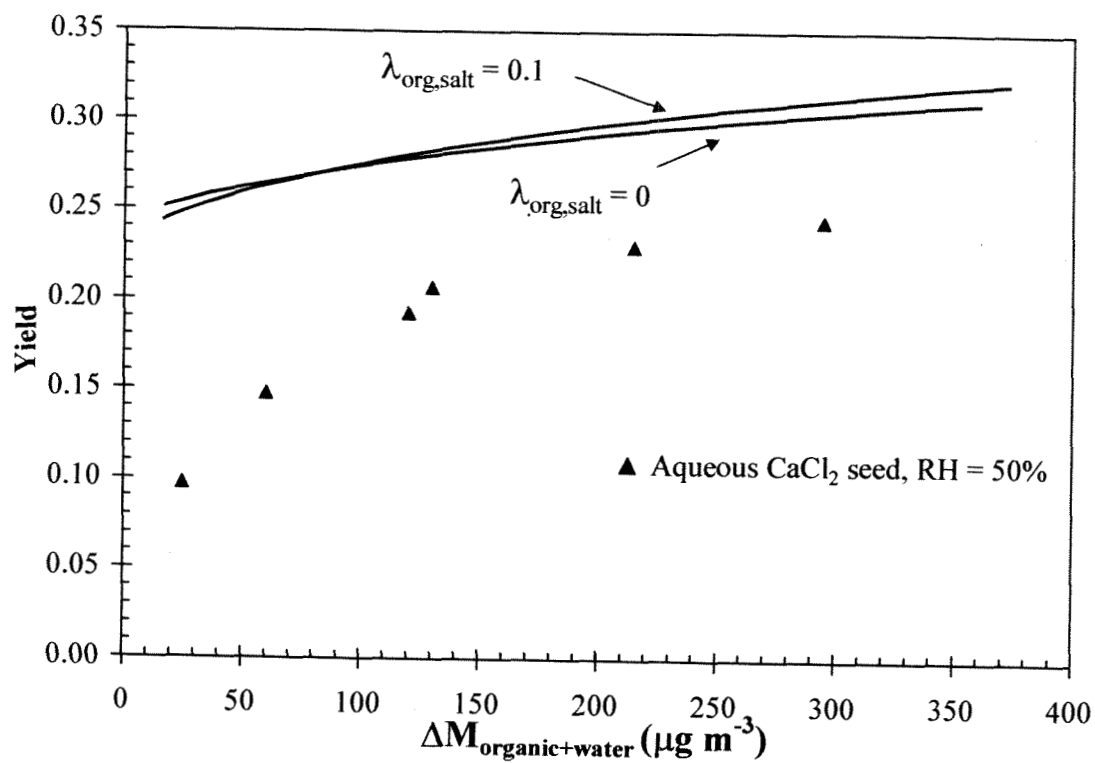


Figure 5.10. Measured and calculated yield at 50% RH for systems including $1.98 \times 10^{-7} \text{ mol m}^{-3} \text{ CaCl}_{2(\text{aq})}$ seed aerosol. Symbols – all data under these conditions.

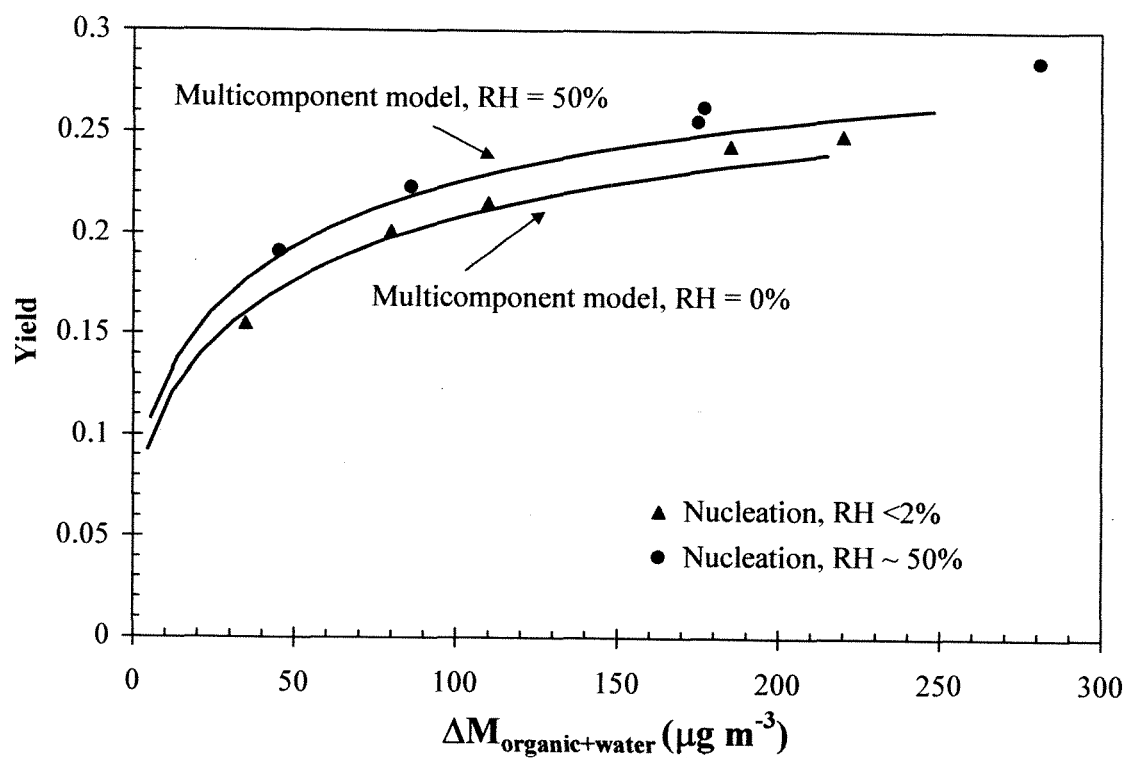


Figure 5.11. Measured and calculated yields for systems without seed aerosol at 2% and 50% RH. Symbols – all data under these conditions.

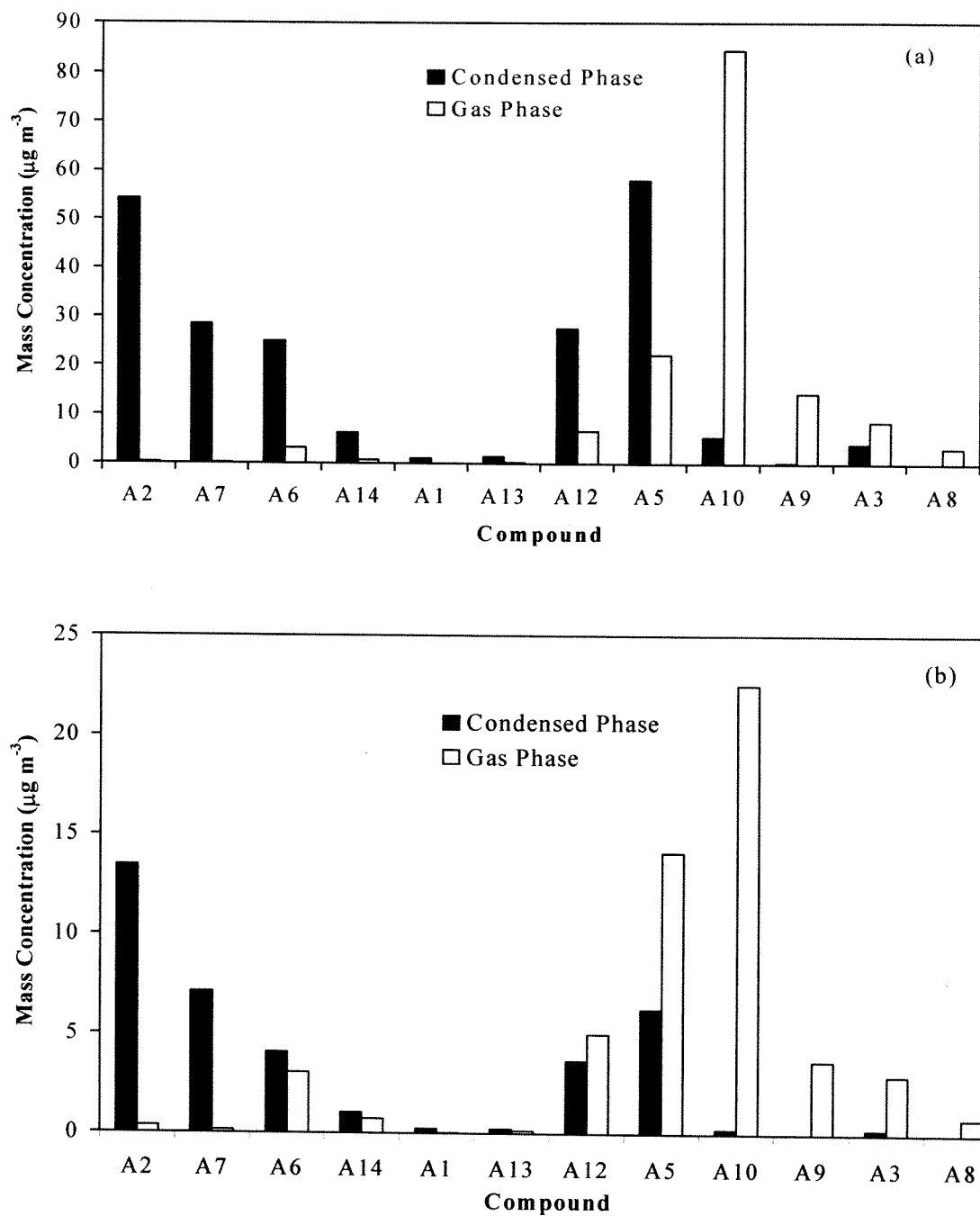


Figure 5.12. Aerosol- and gas-phase concentrations of α -pinene oxidation products, for systems without salt seeds at 2% RH, calculated using the multi-product model described in Section 5.6.3.2. (a) $\Delta(\alpha\text{-pinene}) = 888.5 \mu\text{g m}^{-3}$; (b) $\Delta(\alpha\text{-pinene}) = 225.5 \mu\text{g m}^{-3}$. Refer to Table 5.5 for notation identifying each compound.

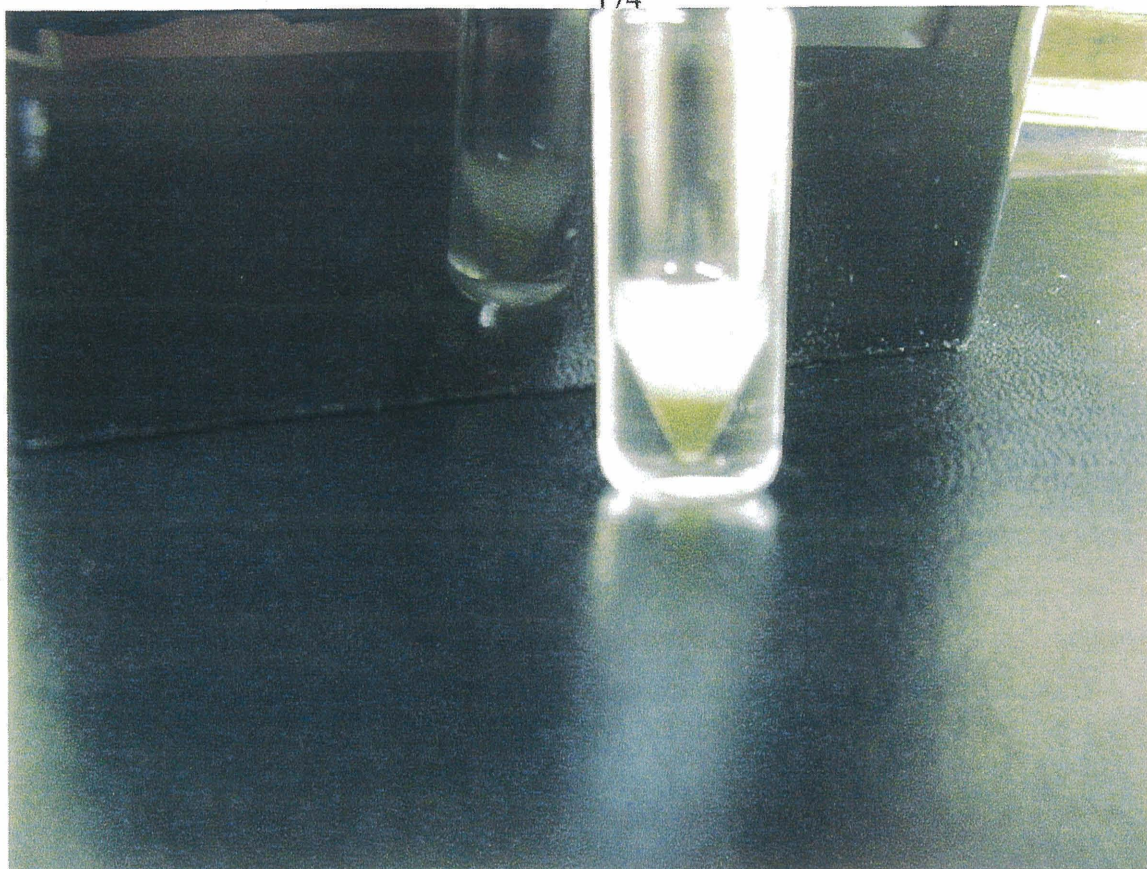


Figure 5.13: Multiple phase system. The bottom layer is pinic acid/water with trace of $(\text{NH}_4)_2\text{SO}_4$, precipitate at interface is $(\text{NH}_4)_2\text{SO}_4$, and top layer is $(\text{NH}_4)_2\text{SO}_4$ /water with trace of pinic acid.

Chapter 6**The Effect of Water on Gas-Particle Partitioning of Secondary Organic
Aerosol: II. *m*-Xylene and 1,3,5-Trimethylbenzene Photooxidation
Systems**

6.1 Introduction

Aromatic hydrocarbons, a significant component of the gas-phase organic compounds in the urban atmosphere, form ozone and secondary organic aerosol (SOA) upon oxidation. For example, Odum *et al.* (1997) determined that aerosols resulting from photooxidation of whole gasoline vapor could be attributed solely to the aromatic species in the gasoline. Until the recent work of Edney *et al.* (2000), the effect of relative humidity on the SOA yield from aromatic species had not been evaluated. Edney *et al.* estimated water uptake of the aerosol produced from toluene photooxidation using gravimetric analysis. Based on their results, they inferred that the presence of water does not affect SOA yield in the toluene system.

Part I reports an extensive investigation of the effect of relative humidity on the gas-particle partitioning of the oxidation products of the α -pinene/ozone reaction. In this system SOA yield is unaffected either in the presence or absence of a dry seed aerosol. After correction for aerosol water uptake, it was determined that gas-phase water does not affect the SOA yield whether or not dry seed particles are present. However, the presence of a strong aqueous electrolytic seed aerosol was found to decrease the SOA yield.

Identification of the aerosol molecular composition allows theoretical estimation of aerosol production, including the interaction with liquid water (Jang *et al.*, 1998; Ansari *et al.*, 2000). To date, only three studies identified molecular composition of aromatic oxidation products in conjunction with aerosol formation. Forstner *et al.* (1997) investigated seven aromatic compounds, toluene, *m&p*-xylene, *m&p*-ethyltoluene, ethylbenzene, and 1,2,4-trimethylbenzene. In these studies, aerosol products were

collected on quartz filters, extracted, and then analyzed using GC-MS. Only 15-30% of the mass collected and extracted was identified. Several identified compounds measured on the filter were believed to be a result of vapor adsorption to the quartz filter rather than aerosol-phase constituents. Jang and Kamens (2001) used a denuder/filter apparatus based on Yu *et al.* (1999) coupled with derivatization and GC-MS detection to identify a number of toluene photooxidation products. The authors also used a zinc selenide FTIR disc to collect SOA and analyze for functional group information. The vapor pressures of several aerosol products were higher than what is normally expected in the aerosol-phase. It was speculated that acetals or hemiacetals were formed in the aerosol-phase and that the derivatization process hydrolyzed them to form the higher vapor pressure products identified. Kleindienst *et al.* (1999) identified some gas-phase products of toluene, *p*-xylene, and 1,3,5-trimethylbenzene photooxidation in which aerosol was formed, but did not report specific molecular composition of the aerosol.

We report here the results of an investigation on the effect of relative humidity on SOA formation from *m*-xylene and 1,3,5-trimethylbenzene (1,3,5-TMB) photooxidation. First, we describe the experimental procedures used for these photooxidation experiments. Next, the hygroscopic nature of the oxidation products of *m*-xylene and 1,3,5-TMB is compared to that of α -pinene oxidation products. An evaluation of the SOA formation potential for *m*-xylene and 1,3,5-TMB for different experimental conditions follows. Finally, we report limited identification of the oxidation products of *m*-xylene and 1,3,5-TMB.

6.2 Experimental Description

The chamber facility and basic experimental procedures and protocols are outlined

in Part I. Those modifications and additions that are necessary specifically for photooxidation experiments are discussed below.

The indoor chamber is illuminated using three hundred 1.22 m GE350BL fluorescent blacklights. The integrated total light intensity is estimated by steady-state actinometry on NO₂. The photolysis rate of NO₂ in the current chamber configuration is measured at 1.1 min⁻¹. The chambers were flushed with purified air for a minimum of 24 h prior to the start of an experiment. 300 ppb propene (a photochemical initiator), NO, NO₂ and *m*-xylene or 1,3,5-TMB were introduced into the dark chamber. The total NO_x mixing ratio was set to a ppbC:ppb NO_x of 2:1. Hydrocarbon, NO_x, and ozone concentrations were measured prior to the start of the experiment. A minimum of three initial hydrocarbon measurements were taken for each chamber. Analysis were repeated every 11 min during the experiment. Ozone was monitored with a Dasibi Environmental Corp. (Glendale, CA) Model 1008-PC O₃ analyzer. NO and NO₂ were monitored with a Thermo Environmental Inc. (Woburn, MA) model 42 chemiluminescent NO-NO₂-NO_x analyzer. Ozone and NO_x measurements were taken during 10 min intervals, alternating between the two chambers. The estimated uncertainties are +/-4% and +/-7%, respectively. Temperature and relative humidity were monitored continuously.

6.3 Hygroscopic Properties of *m*-Xylene and 1,3,5-TMB Aerosol Oxidation Products

The hygroscopic behavior of an aerosol is a measure of its physical response to variation in the relative humidity surrounding the particle. The hygroscopic growth factor (G_f), conventionally measured using a tandem differential mobility analyzer (TDMA) (McMurry and Stolzenberg, 1989), is defined as the ratio of the particle diameter at a given RH ($D_{p,h}$) to the dry particle diameter ($D_{p,d}$), $G_f = D_{p,h}/D_{p,d}$. In the current study,

TDMA measurements were made on particles with dry diameters of 136 nm and 235 nm.

Growth factors for the nucleation products of *m*-xylene and 1,3,5-TMB photooxidation were obtained at 85% RH. Figure 6.1a shows G_f as a function of the time of oxidation for both parent hydrocarbons. At the onset of the experiment, the G_f of the condensing organic aerosol is 1.0, indicating that the initial condensing species are hydrophobic. However, as the photooxidation progresses, the aerosol becomes more hygroscopic; G_f eventually reaches values of 1.12 and 1.10 for *m*-xylene and 1,3,5-TMB, respectively.

The increase of G_f (85% RH) over the course of the photooxidation strongly suggests that the initial hydrocarbon oxidation products undergo continued oxidation throughout the experiment, leading to products more hygroscopic than those initially formed. These hygroscopic products then partition to the aerosol-phase, increasing its affinity for water. Alternatively, aerosol-phase oxidation might lead to the more hydrophilic aerosol-phase products. In either event, the changing water affinity clearly shows that the aerosol composition evolves over time. Therefore, it is critical, when performing molecular composition studies, that the extent of the oxidation be considered. It is not surprising that more highly oxidized species are more hygroscopic since further oxidation will likely lead to multiple oxygenated functional groups. These are expected to be more polar and have higher water affinity.

The increase in the hygroscopicity of the *m*-xylene and 1,3,5-TMB aerosol at 85% RH over the course of oxidation contrasts with that observed for α -pinene ozonolysis. Figure 6.1b shows G_f as a function of time of oxidation for α -pinene ozonolysis at 303 K. For α -pinene, the value of G_f early in the experiment is 1.065, indicating that the species

that condense initially are slightly hydrophilic. While the slight upward trend in G_f over the duration of the α -pinene oxidation may indicate some secondary chemistry, G_f never achieves the ultimate level observed for either aromatic system. It appears that the molecular composition of α -pinene oxidation products do not change significantly, as measured by water affinity, over the duration of the oxidation. This near constant value of G_f allows one to estimate the value of G_f based on the volume fractions of organic and inorganic constituents of the aerosol (see Part I) for the α -pinene system; however, for the aromatic systems it is necessary to know the instantaneous value of G_f for the organic portion as a function of time in order to compute the overall value of G_f at any time.

The G_f values obtained for *m*-xylene, 1,3,5-TMB, and α -pinene are consistent with those obtained at 89% RH for the less hygroscopic fraction of ambient urban aerosol. Measurements of the hygroscopic nature of Pasadena, California, aerosol (Cocker *et al.*, in press), carried out over the summer months of 1999, revealed that G_f for the less hygroscopic aerosol mode ranged from 1.03 to 1.17. In the Pasadena study, the lowest G_f values were noted in the early morning, while the highest ones were found in the late afternoon. This increase in G_f may result from increased organic oxidation as the day progresses. The less hygroscopic fraction of urban aerosol was attributed to SOA-coated aerosol. Since aromatic compounds constitute a significant fraction of gas-phase hydrocarbons in the urban atmosphere, our present results may help explain the measured increase in G_f over the course of a typical day in the Pasadena, California, aerosol.

Hygroscopic growth factors were obtained for *m*-xylene and 1,3,5-TMB also at 50% RH over the duration of the photooxidation. At this RH, the measured values of G_f never rose above their initial values ($G_f < 1.01$). The observed G_f values are lower than

those for α -pinene at 50% RH ($G_f = 1.04$), even though G_f at 85% RH for the two aromatics exceeds that for α -pinene ozonolysis. The marked increase in G_f for the aromatic compounds as RH increases from 50% to 85% is similar to, but smaller than, that observed for inorganic salts at their RH of deliquescence. Oxidation products of most hydrocarbons contain acids and diacids. It might be expected that an organic acid also deliquesces at sufficiently high RH, causing the weak acids in the aerosol phase to dissociate. Upon deprotonation, "charge" centers would be created about which water could cluster, drawing even more water into the aerosol and leading to measurable aerosol water uptake. If an α -pinene oxidation product contains a stronger acid than do the aromatic oxidation products, the α -pinene RH of deliquescence might be expected to be lower, possibly resulting in water uptake at 50% RH, while *m*-xylene and 1,3,5-TMB oxidation products do not.

When a seed aerosol was present, G_f values were obtained prior to the start of an experiment to verify the state of the seed particles as either deliquesced (aqueous) or effloresced (water-free). G_f for aqueous $(\text{NH}_4)_2\text{SO}_4$ seed upon humidification from RH 50% to 85% is 1.31, in contrast to the 1.59 G_f for dry $(\text{NH}_4)_2\text{SO}_4$ seed particles (Nenes *et al.*, 1998). Moreover, the liquid water content of the chamber aerosol can be estimated based on the measured G_f . The low G_f measured at 50% RH for particles generated by nucleation under dry conditions implies that very little water is associated with the organic at that humidity. Therefore, it can be assumed that only organic condensation contributes to the increase in the aerosol volume in the chamber; water uptake by the condensed organic is not significant.

6.4 Effect of Relative Humidity on SOA Formation for *m*-Xylene and 1,3,5-TMB

Photooxidation

The aerosol formation potential of a hydrocarbon is described by its mass-based aerosol yield. The protocols for specific experiments, i.e., dry nucleation runs, etc., and the corresponding methods for organic aerosol mass computation are also given in Part I.

Thirty-one and thirty-four experiments were performed measuring SOA yields from the photooxidation of *m*-xylene and 1,3,5-TMB, respectively. These experiments included ones in which no seed particles were initially present (where aerosol forms by homogeneous nucleation) and with $(\text{NH}_4)_2\text{SO}_4$ present as either dry inorganic seed particles or an aqueous inorganic seed aerosol. All experiments were performed at temperatures near 293 K. Table 6.1 summarizes the conditions for each *m*-xylene experiment, including initial *m*-xylene concentrations, NO_x concentrations, aerosol yields, relative humidity, and temperature. Table 6.2 summarizes the conditions for the 1,3,5-TMB experiments. Figure 6.2 shows the yield as a function of the total aerosol mass concentration for all *m*-xylene and 1,3,5-TMB photooxidation experiments. The data were fit with the two-product absorptive partitioning model, described in Part I assuming that aerosol growth is due solely to the uptake of organic compounds as indicated by the TDMA measurements.

The aerosol yield did not depend upon whether seed particles were, or were not, present on the physical state (aqueous or water-free) of the seed, or on RH. The empirical fits shown in Figure 6.2 are the best fits through all the data. Clearly, the water, either vapor or liquid water in the seed aerosol, does not affect the volume of SOA produced in the *m*-xylene and 1,3,5-TMB photooxidation systems investigated. The agreement

between SOA yields for the dry nucleation and the water-free $(\text{NH}_4)_2\text{SO}_4$ seed experiments confirms that water-free seed simply provides an inert surface upon which condensation can occur and does not affect the gas-particle equilibrium established. These findings are in agreement with Part I of this paper as well as those in Odum *et al.* (1996, 1997).

The agreement between the wet nucleation experiments and the water-free experiments demonstrates that increased RH does not increase the volume of aerosol produced from *m*-xylene and 1,3,5-TMB photooxidation. This is expected since gas-phase water is not expected to significantly alter the molecular composition of products. Moreover, TDMA measurements demonstrate that the organic compounds do not pick up significant water at a RH of 50%. These results agree with those obtained for α -pinene ozonolysis (Part I) after accounting for water uptake of the α -pinene oxidation products as measured by TDMA.

The yield data for aqueous seed at a RH of 50% and for dry seed are also in good agreement, suggesting that the presence of a strong $(\text{NH}_4)_2\text{SO}_4$ electrolyte solution does not significantly alter the gas-particle equilibrium established for *m*-xylene and 1,3,5-TMB. This result contrasts that obtained for α -pinene ozonolysis, described in Part I, where gas-particle partitioning was measurably reduced in the presence of a strong, electrolytic aerosol. The difference between α -pinene and the aromatics is not as surprising when one considers the water interaction at 50% RH based on TDMA measurement. *m*-Xylene and 1,3,5-TMB oxidation products do not uptake water, while α -pinene ozonolysis products exhibit a G_f of 1.04. Perhaps the *m*-xylene and 1,3,5-TMB hydrophobic interaction at 50% RH prevented the organic products from interacting with the aqueous solution,

resulting in a two-phase solution. Then, the resulting organic layer would be free to interact with the gas-phase as if the aqueous solution were not there, leading to similar SOA yields as measured for water-free and nucleation experiments.

Figure 6.3 compares the *m*-xylene SOA yield curve obtained here with that obtained in previous studies. The present SOA yields are higher than those in previous experiments, primarily as a result of the lower temperature used for the present experiments (293 K vs. 303 K for Kleindienst *et al.* (1999), 303 K for Izumi *et al.* (1990), and approximately 308 K for Odum *et al.* (1996)). Lower temperatures increase the partitioning coefficient of the products directly ($1/T$ dependence) and indirectly through lower vapor pressures of the semi-volatile oxidation products (exponential dependence of vapor pressure on temperature). Insufficient prior data on the aerosol yield of 1,3,5-TMB at these organic aerosol concentrations precludes comparison of this study with previous ones.

The conclusion that water vapor does not alter the gas-particle partitioning in *m*-xylene and 1,3,5-TMB systems is in agreement with the finding of Edney *et al.* (2000) that the hygroscopic nature of the photooxidation aerosol products of toluene could be explained by that of the inorganic seed alone.

The primary atmospheric oxidation pathway for the aromatic compounds investigated is through reaction with the hydroxyl (OH) radical. The rate constants for OH radical, O_3 , and NO_3 radical reactions with *m*-xylene at 298 K are $2.31 \times 10^{-11} \text{ cm}^3 \text{ molecule}^{-1} \text{ s}^{-1}$, $< 3 \times 10^{-21} \text{ cm}^3 \text{ molecule}^{-1} \text{ s}^{-1}$, and $2.6 \times 10^{-16} \text{ cm}^3 \text{ molecule}^{-1} \text{ s}^{-1}$, respectively (Calvert *et al.*, 2000). Similarly, the rate constants for OH radical, O_3 , and NO_3 radical reactions with 1,3,5-TMB at 298 K are $5.67 \times 10^{-11} \text{ cm}^3 \text{ molecule}^{-1} \text{ s}^{-1}$, $< 1 \times 10^{-20} \text{ cm}^3$

molecule⁻¹ s⁻¹, and 8.76×10^{-16} cm³ molecule⁻¹ s⁻¹, respectively (Calvert *et al.*, 2000).

Under chamber conditions, *m*-xylene and 1,3,5-TMB react only with the OH radical. As discussed above, the increase in hygroscopicity of the SOA produced over the duration of the photooxidation implies that secondary reactions of the first-generation of oxidation products are occurring. The relative abundances of OH, O₃, and NO₃ may be important in determining the final aerosol yield through further oxidation of products. As varying concentrations of NO_x and hydrocarbon are used, larger experimental scatter in the ultimate SOA yield than for the α-pinene ozonolysis (single oxidant) is expected. The blacklight lamps are unable to reproduce the entire solar spectrum at ground level and therefore some photolytic species may fail to photolyze in the chamber. A thorough comparison of fluorescent blacklight lamps to the solar spectrum and their effect on potential photolytic compounds is discussed in detail by Carter *et al.* (1995).

6.5 Product Identification

We attempted to identify and quantify the gas- and aerosol-phase products of *m*-xylene and 1,3,5-TMB under dry conditions. At the onset the goal was to identify enough oxidation products that aerosol yield could be predicted on a molecular basis (Part I). The following sections describe the sampling and identification techniques used, and present the compounds positively identified and quantified. We finish with a discussion of why this methodology failed to identify the vast majority of the products and the need for new techniques to progress in molecular species identification of aromatic oxidation products.

6.5.1 Sampling techniques. Aerosol-phase products were collected for 1.5 h to 6.0 h on the 56 nm stage of a MOUDI ten-stage impactor (MSP corporation, Minneapolis, MN) through a 1.5 m long, 2.2 cm diameter Teflon sampling port positioned in the center of the

chamber at a flow rate of 28 LPM. The impactor substrate, a pre-weighed 47 mm punch of aluminum foil, was pre-cleaned by baking at 550°C for 12 h. Gas-phase compounds were collected at a flowrate of 0.35 LPM downstream of the impactors using a series of three impingers pre-filled with 20 mL of de-ionized and organic-free Milli-Q treated water.

6.5.2 Sample extraction and derivatization.

6.5.2.1 Impactor samples. The impactor substrate was re-weighed after sampling to determine the mass of particulate material collected. A substrate was then loaded into a Soxhlet, spiked with 80 μ L of the perdeuterated C₂₄ *n*-alkane internal standard solution and extracted for 16-20 h using 100 mL of a 1:1 mixture (by volume) of dichloromethane and hexane. For each chamber experiment, a particle-free, blank impactor substrate was also extracted for quality assurance purposes. The sample was derivatized using PFHBA (O-(2,3,4,5,6-pentafluorobenzyl hydroxy amine)) and BSTFA (N,O-bis(trimethylsilyl)-trifluoro-acetamide) following the procedure of Yu *et al.* (1998). The derivatization reaction converts polar compounds into less polar derivatives enabling analysis by GC/MS. Carbonyl groups react with PFBHA to form oxime derivatives and carboxyl and hydroxy groups react with BSTFA to form trimethylsilyl derivatives. Briefly, the derivatization was carried out as follows: after Soxhlet extraction, 2.5 mg of PFBHA was added to the extract and the solution allowed to sit 12-16 h in the dark at room temperature (22-25°C). The extract was then rotary evaporated down to 4 mL, transferred to a 5 mL vial and blown down to 200 μ L using a gentle stream of ultra pure N₂. At this point 25 μ L of neat BSTFA was added to the extract and the solution allowed to react for 2 h at 75°C after which time the extract could be analyzed using GC/MS.

6.5.2.2 Impinger samples. Immediately after sampling, 2.5 mg of PFTBA was added to each impinger. The solution was then allowed to react for 12-16 h in the dark at room temperature. Next, the sample was acidified using 6 drops of a 36% HCl solution, and the aqueous phase extracted with three 5 mL aliquots of hexane. The sample was evaporated down to 1 mL using a gentle stream of ultra pure N₂, transferred to a 5 mL vial, and further evaporated down to 200 µL. At this point 25 µL of neat BSTFA was added to the extract, and the solution was allowed to react for 2 h at 75°C, after which time the extract was ready for GC/MS analysis.

6.5.3 GC/MS analysis. Derivatized sample extracts were analyzed using a Varian Star 3400/Saturn 2000 gas chromatograph/ion trap mass spectrometer operated in electron impact ionization mode. Separations were made using a HP-1 column (Agilent Technologies, Wilmington, DE). Identified compounds were quantified using authentic standards. Calibration mixtures included all identified compounds and were prepared at five concentrations over the relevant concentration ranges. Compound specific ions and/or mass fragments for the derivatized functional groups were used for quantification. Spiking blank impactor substrates and impingers with standard solutions allowed for recovery experiments of all compounds having authentic standards. The blanks were then extracted and derivatized using the same procedures employed for the actual samples.

6.5.4 Identification of products in the *m*-xylene and 1,3,5-TMB photooxidation experiments. Tables 6.3 and 6.4 summarize identified products in the *m*-xylene and 1,3,5-TMB photooxidation experiments. Derivatized compounds fragment in a characteristic way; compounds with a carbonyl functional group are identified by the mass *m/z* 181; those with a carboxyl or hydroxy group generally produce mass fragments at *m/z*

73 and m/z 75. In addition the fragments at m/z M-15, M-73, M-89 and M-117, which denote loss of $[\text{CH}_3]$, $[\text{Si}(\text{CH}_3)_3]$, $[\text{OSi}(\text{CH}_3)]$ and $[\text{C}(\text{O})\text{OSi}(\text{CH}_3)]$ from the derivatized molecule, respectively, are used for identification. Furthermore, the fragment at m/z M-117 is a characteristic ion only for carboxyl groups; the fragment m/z 147 $[(\text{CH}_3)_2\text{Si}=\text{OSi}(\text{CH}_3)]$ is associated with a compound with two carboxyl or hydroxy groups, and m/z 117 $[\text{C}(\text{O})\text{OSi}(\text{CH}_3)]$ is typically observed for compounds having only one carboxyl group. For compounds with carbonyl groups, the mass fragment M-197 $[\text{OCH}_2\text{C}_6\text{F}_5]$ is often observed.

6.5.5 *m*-Xylene photooxidation.

6.5.5.1 Aerosol-phase composition. Figure 6.4a shows a chromatogram of the m/z 181, m/z 75 and m/z 73 ions for a filter sample from a *m*-xylene photooxidation experiment. The compounds that are positively identified are indicated, as are those for which only the general structure can be elucidated. A total of 14 peaks are positively identified from the similarity of retention time and mass spectra to authentic standards. Positively identified compounds include: propionaldehyde and glycolaldehyde, whose mass spectra are dominated by a peak at m/z 181; hydroxyacetone, a hydroxyketone, whose mass spectra is also dominated by the m/z 181 ion; and glyoxal, a dicarbonyl, whose mass spectra is dominated by the m/z 147 peak. Three carboxylic acids are observed: glyoxalic acid, pyruvic acid, and a C_5 -oxo-carboxylic acid, with observed peaks at m/z 181, 117, 75, and 73, that indicate the presence of carbonyl, carboxyl, and hydroxy functional groups. The C_5 -oxo-carboxylic acid and methylglyoxal are quantified using the response factor for 4-oxo-pentanoic acid and glyoxal, respectively. Tentative identifications of 10 peaks are also made on the basis of the compounds' mass spectra. Table 6.3 summarizes the

retention time, identity, and corresponding percentage of the collected aerosol mass for peaks identified using authentic standards. Peaks with only tentative identifications are also included, but not quantified.

6.5.5.2 Gas-phase composition. Figure 6.4b shows a chromatogram combining the m/z 181, m/z 75 and m/z 73 ion peaks for an impinger sample from a *m*-xylene photooxidation experiment. Ten peaks are identified using authentic standards; only the general chemical structure could be elucidated for the other ten labeled peaks. Several compounds appear in both the gas and particle phases. The compounds identified using authentic standards are glycolaldehyde, hydroxyacetone, glyoxalic acid, pyruvic acid, glyoxal, and methylglyoxal. The particle phase contains a small quantity of propionaldehyde and a C₅-oxo-carboxylic acid that is not observed in the impinger extracts. This observation may result from the ten-times smaller volume of air sampled through the impingers than is sampled through the impactor. The volume of air collected by the impingers may be insufficient for the detection of propionaldehyde and the C₅-oxo-carboxylic acid. The results are summarized in Table 6.4.

6.5.6 1,3,5-TMB photooxidation experiments.

6.5.6.1 Aerosol-phase composition. Figure 6.5a shows a chromatogram of the m/z 181, m/z 75 and m/z 73 ions for a filter sample from a 1,3,5-TMB photooxidation experiment, and indicates the compounds that are positively identified, and those for which only the general structure can be elucidated. A total of 12 peaks were positively identified using authentic standards, and four peaks were tentatively identified on the basis of the mass spectra. Table 6.3 summarizes the retention time, identity, and corresponding percentage of the collected aerosols' mass for those peaks for which positive identification was

possible. Peaks with only tentative identifications are also included but are not quantified. The same products as positively identified for *m*-xylene photooxidation are also positively identified for 1,3,5-TMB photooxidation. Again, the C₅-oxo-carboxylic acid and methyl glyoxal were quantified using the response factor for 4-oxo-pentanoic acid and glyoxal, respectively.

6.5.6.2 Gas-phase composition. Figure 6.5b shows a chromatogram of the *m/z* 181, *m/z* 75 and *m/z* 73 ions from an impinger sample from a 1,3,5-TMB photooxidation experiment. Eight peaks were identified using authentic standards. Only tentative structures could be assigned to eight other peaks. Several compounds were observed in both gas and particle phases.

The compounds identified using authentic standards were glycolaldehyde, hydroxyacetone, glyoxalic acid, pyruvic acid, and methylglyoxal. Propionaldehyde and glyoxal were found in very small amounts in the particle phase but were not observed in the impinger extracts. Again, the smaller sample volume collected with the impingers may be insufficient to enable detection of propionaldehyde and glyoxal. The results are summarized in Table 6.4.

6.5.7 Implications of the Molecular Identification Results

Although the major peaks in the chromatogram of the filter samples have been identified, the sum of their masses represents only ~10% of the collected particle mass. It is unlikely that the small, unidentified peaks in the chromatographs constitute the remaining 90% of collected particle mass. Some GC runs were extended to 70 min, reaching column temperatures of 300°C for up to 10 min, but no significant peaks were observed. Furthermore, the compounds that are identified were mostly small, relatively

high vapor pressure compounds; it is expected that such compounds would comprise only a small percentage of the particle phase. Since Soxhlet extraction accounted for 96-110% of the collected mass of the impactor samples, it is likely that most of the compounds comprising the SOA do not pass through the GC liner or column. These compounds may have low vapor pressures that limit volatilization from the GC injector, or they may travel very slowly through the column. It is also possible that their polar functional groups do not quantitatively react with the derivatizing reagents; their vapor pressures may not decrease, and/or they may chemisorb on the surface of the GC injector.

Since GC/MS analysis with derivatization appears to be incapable of detecting most of the reaction products, it must be concluded that an alternate analytical technique will be required to make a substantial advance in molecular identification of aromatic aerosol photooxidation products. One such technique to analyze the oxidation products is liquid chromatography-mass spectrometry (LCMS) which minimizes product losses on the injection liners and eliminates the need to volatilize the products. Furthermore, derivatization is not necessary for transport of the product through the separation column. One major class of expected products is nitrated hydrocarbons for which GC/MS is not ideal.

6.6 Conclusions

The SOA formation potential of *m*-xylene and 1,3,5-TMB is unaffected by the presence of gas-phase and aerosol-phase water or the presence or lack of $(\text{NH}_4)_2\text{SO}_4$ seed at 50% relative humidity. Hygroscopic growth parameters for *m*-xylene and 1,3,5-TMB oxidation aerosol are found to be negligible at 50% RH and for the SOA produced early in the experiment at 85% RH. However, as the oxidation proceeds, the observed increase in

water affinity suggests that the hydrocarbon products undergo further oxidation, by either gas-phase oxidation or aerosol-phase oxidation. A number of the gas- and aerosol-phase photooxidation products were identified, but the majority of the products could not be identified using derivatization/GC-MS techniques. Other techniques will be needed to identify and quantify a significant fraction of the aerosol products of aromatic photooxidation.

6.7 References

- Ansari A. A. and Pandis S.N. (2000) Water absorption by secondary organic aerosol and its effect on inorganic aerosol behavior. *Environ. Sci. Technol.* **34**, 71-77.
- Calvert J. G., Atkinson R., Becker K. H., Kamens R. M., Seinfeld J. H., Wallington T. J., and Yarwood G. (2000) Mechanisms of atmospheric oxidation of aromatic hydrocarbons. Final report to Coordinating Research Council, Inc.
- Carter W. P. L., Luo D., Malkina I. L., and Pierce J. A. (1995) Environmental chamber studies of atmospheric reactivities of volatile organic compounds; effects of varying chamber and light source. Final report to: National Renewable Energy Laboratory; Coordinating Research Council, Inc.; California Air Resources Board; and South Coast Air Quality Management District.
- Cocker D. R., Whitlock N. E., Flagan R. C., and Seinfeld J. H. (in press) Hygroscopic properties of Pasadena, CA, aerosol. *Aerosol Sci. Technol.*
- Edney E. O., Driscoll D. J., Speer R. E., Weathers W. S., Kleindienst T. E., Li W., and Smith D. F. (2000) Impact of aerosol liquid water on secondary organic aerosol yields of irradiated toluene/propylene/NO_x/(NH₄)₂SO₄/air mixtures. *Atmospheric Environment* **34**, 3907-3919.

- Forstner H. J. L., Flagan R. C., and Seinfeld J. H. (1997) Secondary organic aerosol from the photooxidation of aromatic hydrocarbons: Molecular composition. *Environ. Sci. Technol.* **31**, 1346-1358.
- Izumi K., and Fukuyama T. (1990) Photochemical aerosol formation from aromatic hydrocarbons in the presence of NO_x . *Atmospheric Environment* **24A**, 1433-1441.
- Jang M. and Kamens R. M. (1998) A thermodynamic approach for modeling partitioning of semi-volatile organic compounds on atmospheric particulate matter: Humidity effects. *Environ. Sci. Technol.* **32**, 1237-1243.
- Kleindienst T. E., Smith D. F., Li W., Edney E. O., Driscoll D. J., Speer R. E., Weathers W. S. (1999) Secondary organic aerosol formation from the oxidation of aromatic hydrocarbons in the presence of dry submicron ammonium sulfate aerosol. *Atmospheric Environment* **33**, 3669-3681.
- McMurry P. H. and Stolzenburg M. R. (1989) On the sensitivity of particle size to relative humidity for Los Angeles aerosols. *Atmos. Environ.* **23**:497-507.
- Nenes A., Pandis S. N., and Pilinis C. (1998) ISORROPIA: A new thermodynamic equilibrium model for multiphase multicomponent inorganic aerosols. *Aquat. Geochem.* **4**, 123-152.
- Odum J. R., Hoffmann T., Bowman F., Collins D., Flagan R. C., and Seinfeld J. H. (1996) Gas/particle partitioning and secondary organic aerosol yields. *Environ. Sci. Technol.* **30**, 2580-2585.
- Odum J. R., Jungkamp T. P. W., Griffin R. J., Flagan R. C., and Seinfeld J. H. (1997a) The atmospheric aerosol-forming potential of whole gasoline vapor. *Science* **276**, 96-99.
- Odum J. R., Jungkamp T. P. W., Griffin R. J., Forstner H. J. L., Flagan R. C., and

- Seinfeld J. H. (1997b) Aromatics, reformulated gasoline, and atmospheric organic aerosol formation, *Environ. Sci. Technol.* **31**, 1890-1897.
- Yu J., Flagan R. C., and Seinfeld J.H. (1998) Identification of products containing -COOH, -OH, and -C=O in atmospheric oxidation of hydrocarbons. *Environ. Sci. Technol.* **32**, 2357-2370.

Table 6.1. Conditions for *m*-xylene photooxidation experiments.

Date	Seed Type	ΔHC $\mu\text{g}/\text{m}^3$	Initial N_0 cm^{-3}	$\Delta\text{M}_{\text{org}}$ $\mu\text{g}/\text{m}^3$	Yield %	NO ppb	NO ₂ ppb	T K	RH %
1/31b	dry	1364.2	14074	175	12.83	67.9	75.7	293.3	<2
1/31a	dry	260.5	16373	10.8	4.15	101.1	500	293.3	<2
3/13a	dry	976.7	9600	98	10.03	431.6	218.3	292.8	<2
3/13b	dry	1744	13200	230.9	13.24	241.2	123.5	292.8	<2
3/23a	dry	632.8	16372	81.6	12.90	234.4	101.1	293.2	<2
4/5a	dry	906.4	16842	113.9	12.57	310.1	160.6	293.2	<2
4/5b	dry	715.8	31861	70	9.78	197.3	106.4	293.2	<2
4/10a	dry	1332.2	17384	184.4	13.84	378.9	167.5	293.2	<2
4/18a	dry	382.7	16822	30.3	7.92	68.4	97.2	293.2	<2
4/27a	dry	1376.9	25028	192.1	13.95	431.2	186	293.2	<2
8/7b	dry	1253.9	19072	168.7	13.45	339.4	244.1	293.2	<2
8/7a	dry	1305.8	25516	163.9	12.55	214.4	331.5	293.2	<2
8/17a	dry	1253.9	16225	159.6	12.73	364.3	226.1	293.2	<2
8/17b	dry	1305.8	16240	160.2	12.27	346.7	228.5	293.2	<2
2/1b	aqueous	1887.8	8000	265	14.04	527.3	267.1	292.7	55.4
2/3b	aqueous	473.2	20560	28	5.92	145.5	169.9	293.7	45.3
2/4a	aqueous	972.6	30000	102	10.49	325.2	179.2	292.7	52.1
2/4b	aqueous	1244.8	33000	155.9	12.52	412.1	207.5	292.7	54.7
3/10a	aqueous	920.8	10920	71.3	7.74	309.1	163.6	292.9	49
3/10b	aqueous	1249.5	19780	157.3	12.59	384.3	196.3	292.9	50.5
3/15a	aqueous	255.8	13300	13.7	5.36	28.3	144.5	292.9	48.6
3/15b	aqueous	1581.5	23711	221.6	14.01	379.9	257.3	292.9	49.1
2/24a	none	788.8	0	81	10.27	268.1	181.2	294.3	<2
2/24b	none	1136.7	0	147.8	13.00	420.9	225.6	294.3	<2
4/3a	none	424.3	0	32.6	7.68	130.4	67.9	293.2	<2
4/3b	none	1424.8	0	215	15.09	414.6	200.7	293.2	<2
3/1a	none	1263.5	0	146.5	11.59	309.1	198.2	293.1	50.6
3/1b	none	1718.3	0	230	13.39	441.9	214.4	293.1	53.6
3/3a	none	711.8	0	47.7	6.70	200.7	161.1	292.9	51.5
3/3b	none	877	0	90.6	10.33	258.3	181.2	292.9	52.3

Table 6.2. Conditions for 1,3,5-trimethylbenzene experiments.

Date	Seed Type	ΔHC $\mu\text{g}/\text{m}^3$	Initial N_0 cm^{-3}	$\Delta\text{M}_{\text{org}}$ $\mu\text{g}/\text{m}^3$	Yield %	NO ppb	NO ₂ ppb	T K	RH %
2/11a	dry	1387	18113	61.1	4.41	345.7	299.8	292.5	<2
2/11b	dry	1696	22563	78.9	4.65	468.8	296.9	292.5	<2
2/19a	dry	1309	21335	60.1	4.59	323.2	414.6	294.3	<2
5/11b	dry	2730	19909	195.3	7.15	955.1	447.3	295.5	<2
5/17b	dry	3187	23950	249.7	7.83	951.2	453.1	293.2	<2
6/21b	dry	3298	14000	257.7	7.81	766.1	352.1	293.2	<2
6/26b	dry	3332	18089	257.4	7.73	775.4	391.6	293.2	<2
7/5b	dry	3085	18500	244	7.91	775.4	448.2	293.2	<2
8/9a	dry	1621	23100	95.7	5.91	448.2	328.6	293.2	<2
8/9b	dry	1651	13100	72.9	4.41	422.9	337.9	293.2	<2
8/11a	dry	1790	18227	89.2	4.98	455.6	371.1	293.2	<2
8/11b	dry	1707	16913	68.8	4.03	409.7	371.1	293.2	<2
8/14a	dry	1872	17566	98.9	5.28	507.8	301.8	293.2	<2
8/14b	dry	1801	15697	72.8	4.04	462.9	290	293.2	<2
2/12a	aqueous	920	13478	29.7	3.23	144.5	255.4	293.0	48.8
2/12b	aqueous	1332	21794	62.8	4.71	358.4	262.7	293.0	52.6
2/14a	aqueous	1669	16861	56.5	3.39	220.7	427.7	293.5	43.8
2/14b	aqueous	1806	25293	111.8	6.19	603	361.3	293.5	48.4
2/15a	aqueous	1969	15200	99.6	5.06	468.8	367.2	293.2	47.5
2/15b	aqueous	1728	30972	94.3	5.46	458	362.7	293.2	59.7
3/17a	aqueous	975	17611	27.4	2.81	289.1	204.1	293.7	43.7
3/17b	aqueous	1350	26000	53.9	3.99	382.8	250	293.7	43.4
3/29a	aqueous	954	13333	27.1	2.84	273.4	176.3	294.5	46
3/29b	aqueous	1353	18830	53.9	3.98	398.9	237.8	294.5	49.6
6/8a	aqueous	1920	25000	111.2	5.79	537.1	287.6	294.3	52.7
6/8b	aqueous	1780	23500	98.6	5.54	372.1	187	294.3	54.3
2/16a	none	2584	0	165	6.39	501	454.1	292.7	<2%
2/16b	none	3230	0	248.7	7.70	888.2	485.4	292.7	<2%
2/18a	none	2659	0	182.8	6.87	748	531.3	294.1	48.4
2/18b	none	3348	0	270.9	8.09	962.4	590.8	294.1	48.3
2/21a	none	1256	0	50.4	4.01	350.1	207	293.3	39.6
2/21b	none	2048	0	115.6	5.65	564.4	311.5	293.3	49.5
2/22a	none	1186	0	40.5	3.41	297.9	275.9	294.4	48.3
2/22b	none	1775	0	82.9	4.67	409.7	309.6	294.4	45

Table 6.3. Carbonyl, alcohol, and carboxylic acid products detected in impactor samples.

Peak	RT (min)	Identity	MW _{deriv.}	MW	<i>m</i> -xylene % of extracted mass	1,3,5-TMB % of extracted mass
	18.44/ 18.70	propionaldehyde	253	58	0.64	0.38
*PX1	21.10/ 21.35	C ₄ saturated carbonyl	267	72	detected	not detected
*PT1	21.63	C ₃ saturated triol or C ₂ saturated dihydroxy carboxylic acid	308	92	not detected	detected
*PX2	22.51/ 23.09	possible co-elution of two compounds	NA	NA	detected	not detected
*PX3	23.28/ 23.40	C ₂ hydroxy carbonyl	327	60	detected	not detected
	25.75/ 26.06	glycolaldehyde	327	60	2.91	6.18
	26.57	hydroxyacetone	341	74	0.12	0.02
	27.17	glyoxalic acid	341	74	0.09	0.51
	27.97	pyruvic acid	355	88	0.14	0.07
*PX4	29.34	compound with carbonyl and carboxylic acid groups	NA	NA	detected	not detected
*PT2	31.89	compound with carbonyl and hydroxy groups	NA	NA	not detected	detected
	32.66/ 32.76/ 33.00	C ₅ -oxo-carboxylic acid	383	116	1.05	2.11
	36.77/ 36.98	glyoxal	448	58	0.10	0.02
	37.12/ 37.43/ 37.73	methylglyoxal	462	72	2.24	0.72
*PX5	38.85	compound with carbonyl and carboxylic acid groups	NA	NA	detected	not detected
*PX6	39.81	compound with carbonyl group	NA	NA	detected	not detected
*PX7/ PT3	41.80	C ₅ trione	504	114	detected	detected
total % extracted mass identified					7.29	10.01

*Tentative identification

Table 6.4. Carbonyl, alcohol, and carboxylic acid products detected in impinger samples.

Peak	RT (min)	Identity	MW _{deriv.}	MW	present in <i>m</i> -xylene expts	present in 1,3,5- TMB experiments
*GX1	21.17	C ₄ saturated carbonyl	267	72	yes	no
*GT1	21.63	C ₃ saturated trialcohol or C ₂ saturated dihydroxy carboxylic acid	308	92	no	yes
*GX2	22.53	possible co-elution of two compounds	NA	NA	yes	no
	25.74/2 6.05/26 .61	glycolaldehyde	327	60	yes	yes
	26.48	hydroxyacetone	341	74	yes	yes
	26.61/2 7.18	glyoxalic acid	341	74	yes	yes
	27.98	pyruvic acid	355	88	yes	yes
*GX3	29.36	compound with carbonyl and carboxylic acid groups	NA	NA	yes	no
*GX4	31.74/3 3.05	C ₅ -mono-unsaturated- oxo-carboxylic acid	381	114	yes	no
*GT2	31.89	compound with carbonyl and hydroxy groups			no	yes
*GT3	32.53	dicarboxylic acid			no	yes
*GT4	32.78	dicarboxylic acid			no	yes
	36.76/3 6.98	glyoxal	448	58	yes	no
	37.14/3 7.76	methylglyoxal	462	72	yes	yes
*GX5/ GT5	37.42/3 8.85	compound with a carbonyl group	NA	NA	yes	yes
*GT6	40.03	compound with carbonyl and hydroxy groups	NA	NA	no	yes
*GX6	40.24	compound with carbonyl and carboxylic acid	NA	NA	yes	no
*GX7/ GT7	40.98	compound with carbonyl and hydroxy groups	NA	NA	yes	yes

*Tentative identification

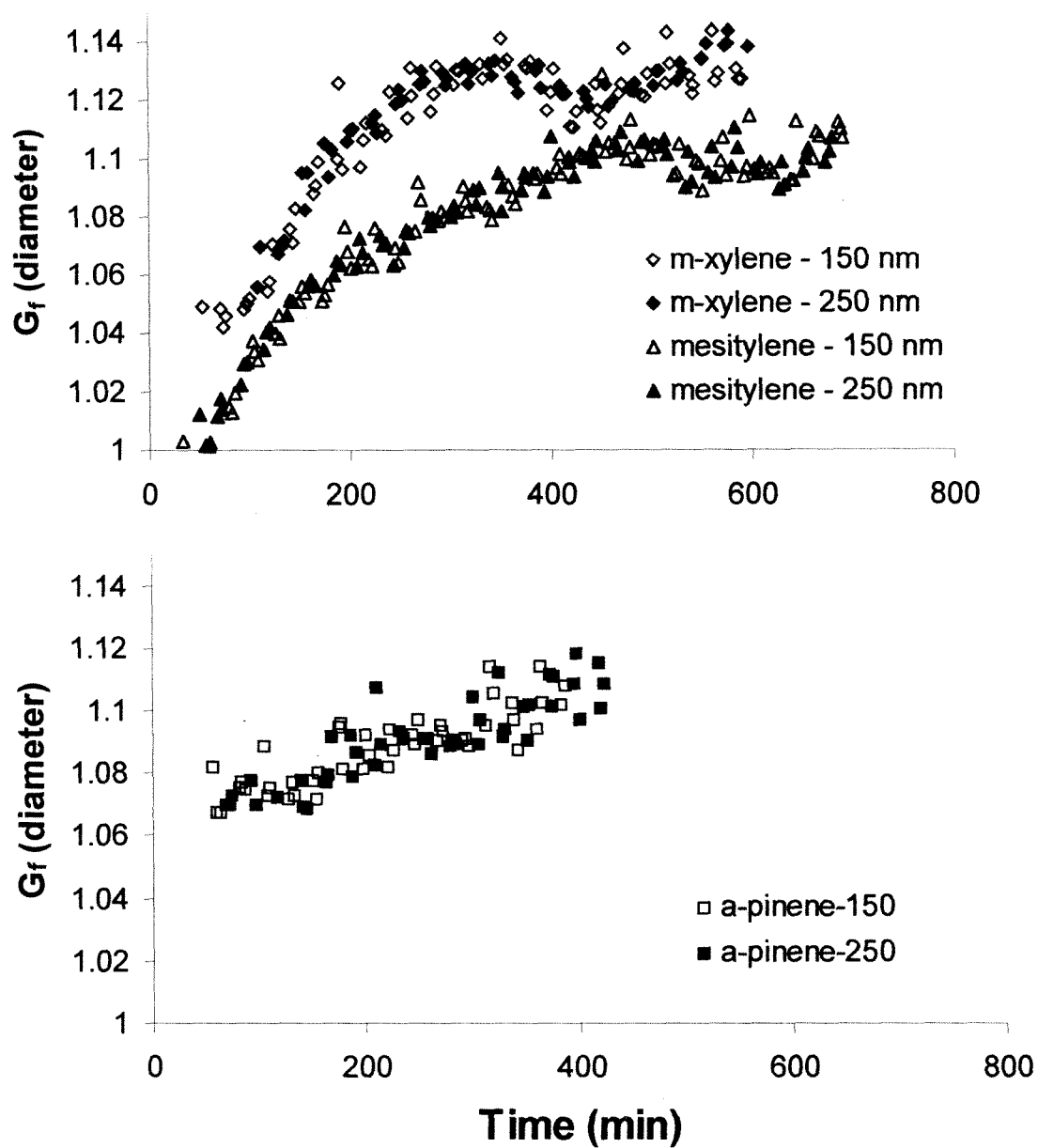


Figure 6.1. (a) Hygroscopic growth factors (0 to 85% relative humidity) for pure *m*-xylene (top) and 1,3,5-TMB (bottom) oxidation products as a function of time. (b) Hygroscopic growth factors (0 to 85% relative humidity) for pure α -pinene oxidation products as a function of time.

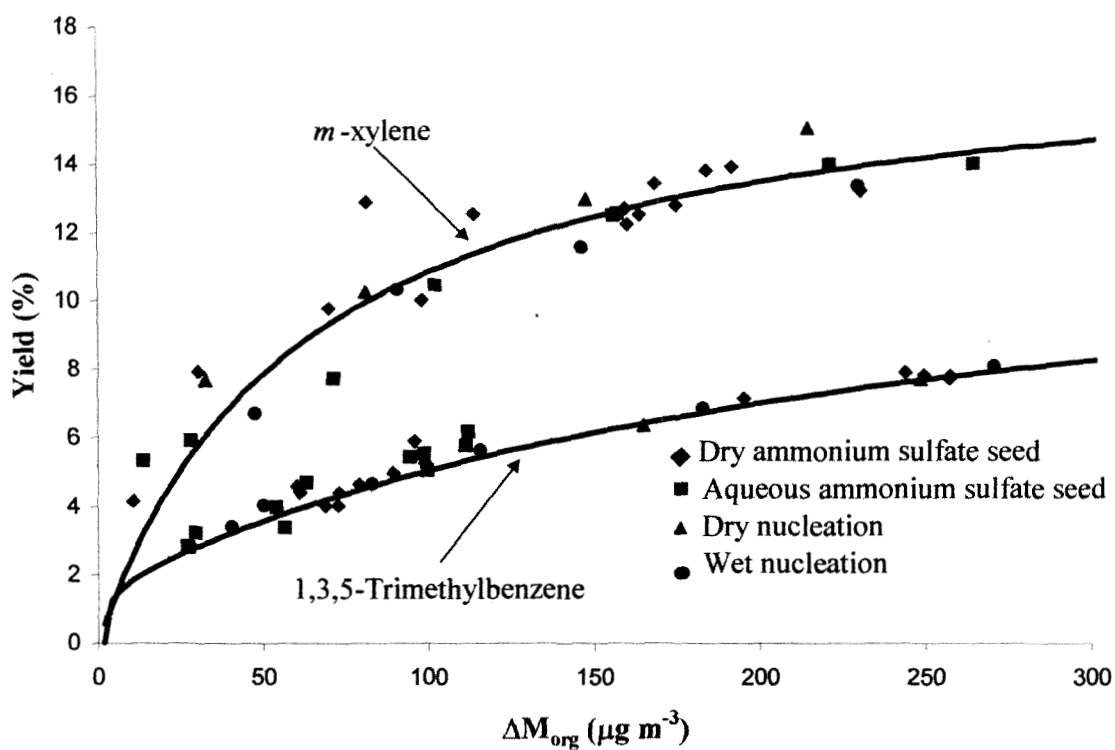


Figure 6.2. SOA yield curves for *m*-xylene and 1,3,5-TMB photooxidation experiments.

The α_1 , α_2 , $K_{om,1}$, and $K_{om,2}$ values used to fit *m*-xylene are 0.12, 0.019, 0.06, 0.01, respectively. The α_1 , α_2 , $K_{om,1}$, and $K_{om,2}$ values used to fit 1,3,5-TMB are 0.016, 0.50, 0.12, 0.004, respectively.

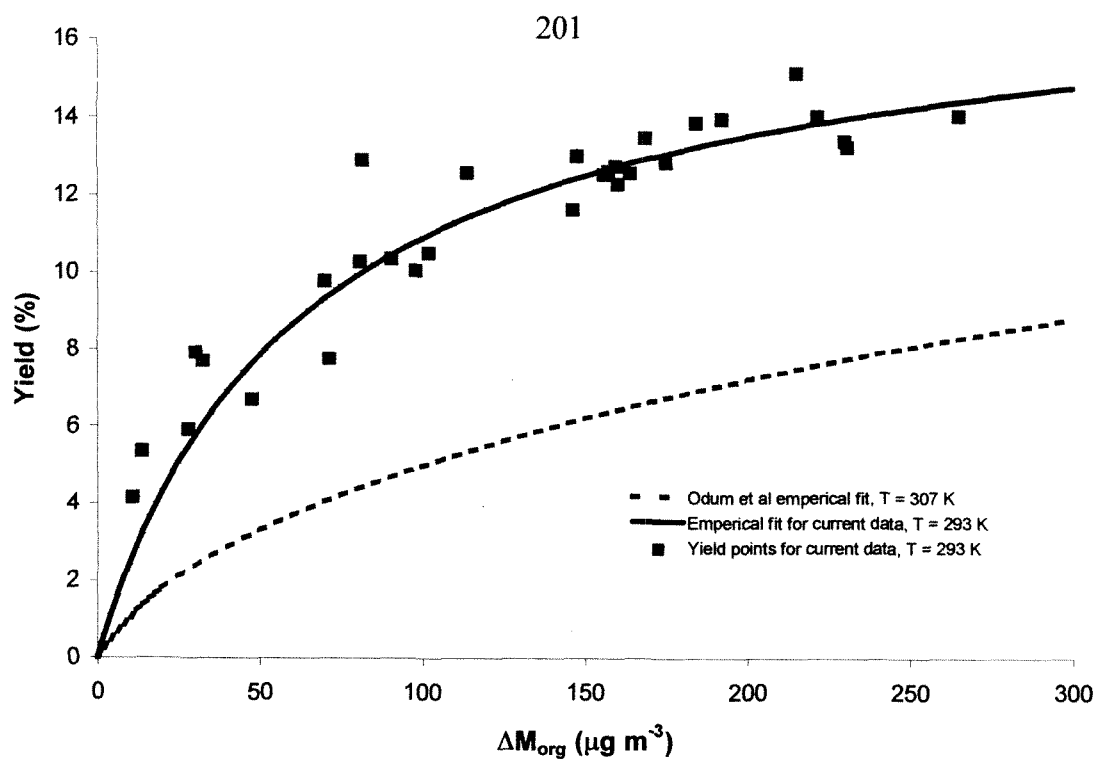


Figure 6.3. Comparison of *m*-xylene SOA yield curve in current experiments ($T = 293\text{ K}$) to that obtained by Odum *et al.* (1996) ($T = 307\text{ K}$). Izumi *et al.* (1990) data points ($T = 303\text{ K}$) are in agreement with Odum *et al.* yield curve.

Chromatogram Plots

Plot 1: c:\... \0305-mxyl-imp-w-1.sms Ions: 181+73+75 all
 Plot 2: c:\... \0305-mxyl-imp1-01.sms Ions: 73+75+181 all

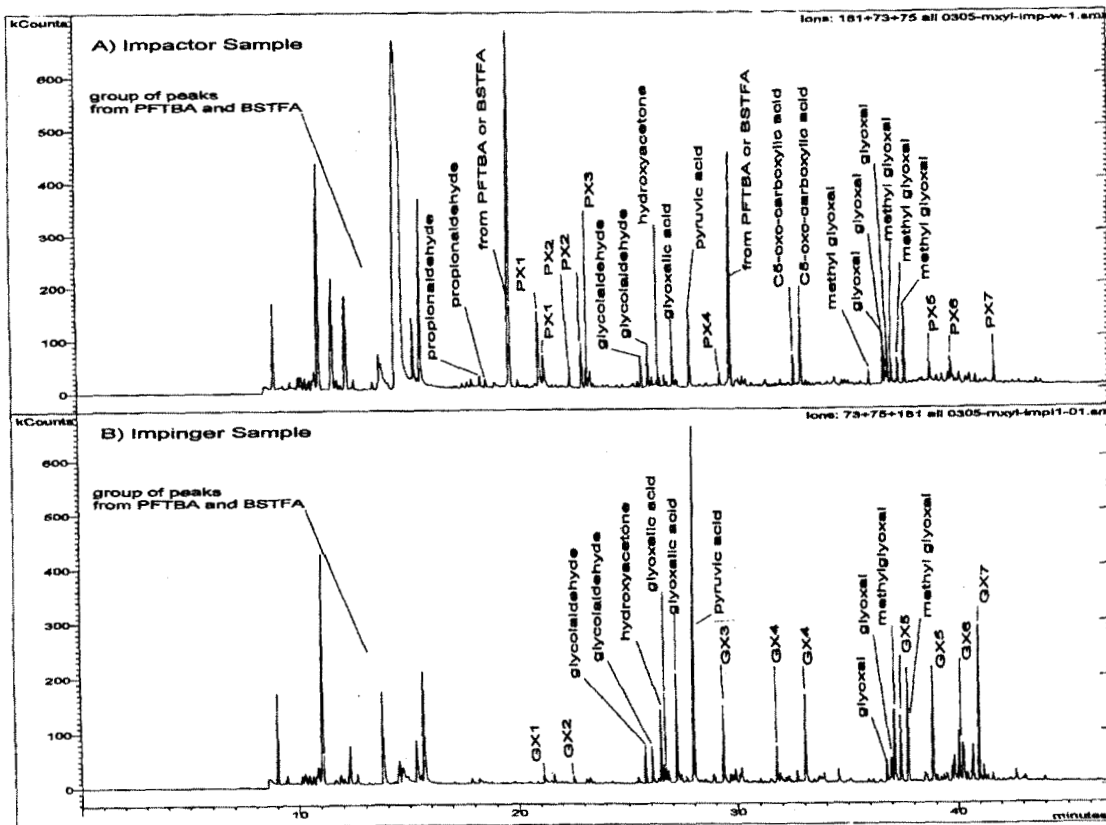


Figure 6.4. a) Chromatogram of impactor sample of *m*-xylene photooxidation showing ions with m/z 181+73+75 with all carbonyl, carboxylic, and/or hydroxyl compounds identified; b) chromatogram of impinger sample of *m*-xylene photooxidation showing ions with m/z 181+73+75 with all carbonyl, carboxylic, and/or hydroxyl compounds identified.

Chromatogram Plots

Plot 1: c:\...aromatics\135-tmb\51700particle1.sms Ions: 181+73+75 all
 Plot 2: c:\...markus\aromatics\135-tmb\51700gas1.sms Ions: 181+73+75 all

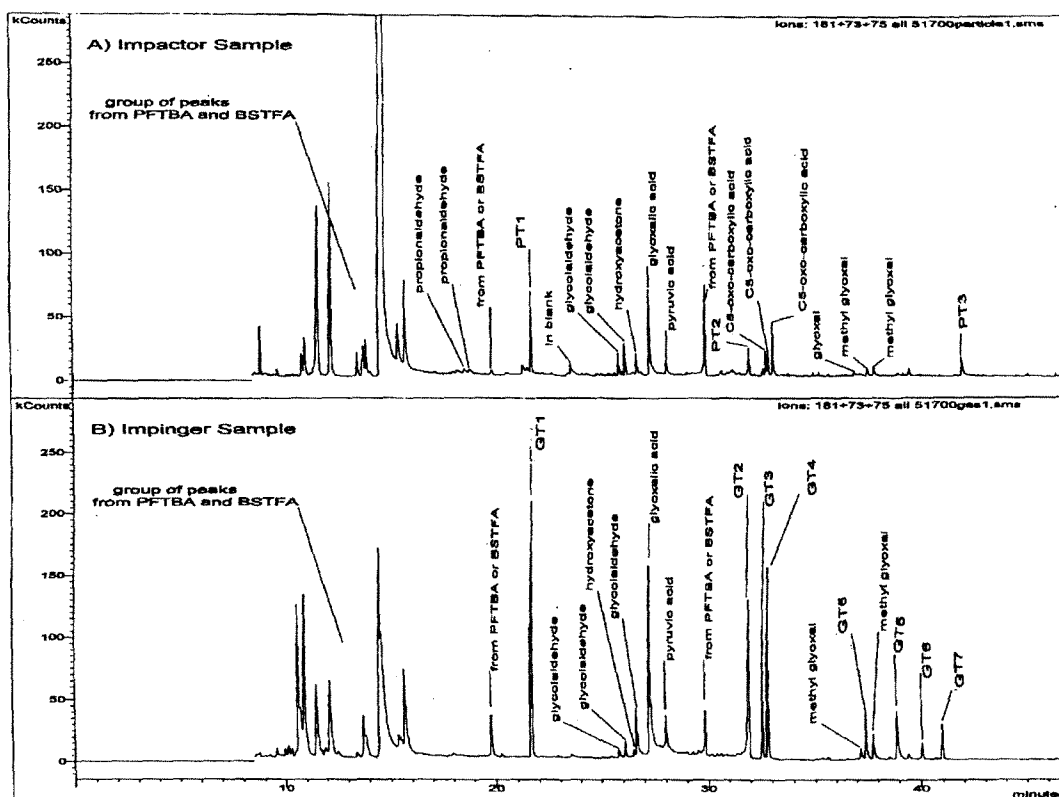


Figure 6.5. a) Chromatogram of impactor sample of 1,3,5-TMB photooxidation showing ions with m/z 181+73+75 with all carbonyl, carboxylic, and/or hydroxyl compounds identified; b) chromatogram of impinger sample of 1,3,5-TMB photooxidation showing ions with m/z 181+73+75 with all carbonyl, carboxylic, and/or hydroxyl compounds identified.

Appendix 1

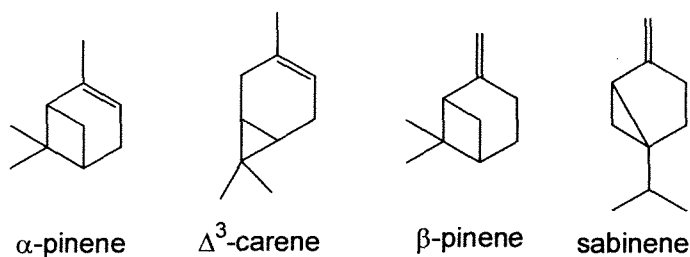
Gas-phase Ozone Oxidation of Monoterpenes: Gaseous and Particulate Products

Reference: J. Yu, D.R. Cocker III, R.J. Griffin, R.C. Flagan, and J.H. Seinfeld, *J. Atmos. Chem.*, 34, 207-258, 1999.

A.1.1. Introduction

Emissions of biogenic organic compounds have been estimated to dominate over those from anthropogenic sources on a global basis [Guenther *et al.*, 1995]. As important constituents of biogenic VOC emissions, the $C_{10}H_{16}$ monoterpenes contribute to formation of tropospheric ozone and secondary organic aerosol (SOA) [Kamens *et al.*, 1981; Chameides *et al.*, 1988; Pandis *et al.*, 1991; Zhang *et al.*, 1992; Hoffmann *et al.*, 1997; Griffin *et al.*, 1999]. Whereas the rate constants of monoterpenes with OH radicals, NO_3 radicals, and O_3 are reasonably well established, the reaction products are less well understood [Atkinson, 1997; Calogirou *et al.*, 1999]. Information on both gaseous and particulate products is important to elucidate the mechanism of oxidation and to understand the formation of secondary organic aerosol.

In a previous paper, we reported the identification of ozone oxidation products of α -pinene and Δ^3 -carene (see below for chemical structures) [Yu *et al.*, 1998]. In this work we have investigated ozone oxidation products of two additional bicyclic monoterpenes, β -pinene and sabinene, for which little product information is known.



At an initial β -pinene mixing ratio of several ppmv, nopinone is the only product that has previously been clearly identified from O_3 oxidation of β -pinene, besides low-molecular products such as formaldehyde, CO, and CO_2 [Hatakeyama *et al.*, 1989;

Grosjean et al., 1993; *Hakola et al.*, 1994]. For the sabinene/O₃ reaction, sabina ketone is the only known product [*Hakola et al.*, 1994].

Few studies have been carried out to determine yields of gaseous and particulate products from ozone oxidation of the monoterpenes, and to our knowledge, no study has been reported to examine gaseous and particulate oxidation products simultaneously. The semi-volatile nature of many of the oxidation products dictates that they partition between the gas and aerosol phases. The filter-only technique, which is the most common aerosol sampling method, results in positive artifacts from adsorption of gaseous semi-volatile compounds on the filter [*McDow and Huntzicker*, 1990; *Hart and Pankow*, 1994]. We have employed a denuder/filter pack system to separate gaseous and particulate semivolatile compounds and to minimize sampling artifacts. Using this sampling device, we have measured the product yields from the ozone oxidation of the four monoterpenes in both gas and aerosol phases and determined their gas-aerosol partitioning coefficients.

Detection and identification of products from oxidation of biogenic hydrocarbons are hindered by the fact that many contain functional groups such as carbonyl and carboxylic acids that are poorly resolved by standard gas chromatography. We have recently reported a method to detect and identify organics containing -C=O (aldehyde and ketone), -OH (hydroxy), and -COOH (carboxyl) groups [*Yu et al.*, 1998]. In this method, -C=O groups are derivatized using O-(2,3,4,5,6-pentafluorobenzyl) hydroxy amine (PFBHA) and -COOH and -OH groups are derivatized using a silylation reagent, N,O-bis(trimethylsilyl)-trifluoroacetamide (BSTFA), to give trimethylsilyl (TMS) derivatives. The resulting derivatives are easily resolved by a GC column and identified by their

chemical ionization (CI) and electronic ionization (EI) mass spectra. The CI mass spectra of these derivatives exhibit several pseudo-molecular ions, allowing unambiguous determination of molecular weights. The EI mass spectra allow functional group identification by exhibiting ions characteristic of each functional group: m/z 181 for carbonyl and m/z 73 and 75 for carboxyl and hydroxy groups. In addition, each functional group is associated with a unique set of pseudo-molecular ions in CI spectra. The PFBHA-carbonyl derivatives give rise to pseudo-molecular ions at m/z $M+181$, $M-181$ and $M-197$, whereas the TMS derivatives of OH/COOH containing compounds have pseudo-molecular ions at m/z $M+73$, $M-15$ and $M-89$. We refer the reader to *Yu et al.* [1998] for a detailed description of the mass spectra fragment patterns.

A.1.2. Experimental Section

A.1.2.1 Smog chamber experiments and sample collection

Samples were collected from a series of β -pinene/ O_3 , sabinene/ O_3 , α -pinene/ O_3 , and Δ^3 -carene/ O_3 experiments conducted in the dark in a 60-m³ Teflon reactor, which has been described previously [*Hoffmann et al.*, 1997; *Griffin et al.*, 1999]. When fully inflated, the reactor has a surface to volume ratio (S/V) of 1.8 m⁻¹. This reactor was normally divided in the center so that two experiments could be run under identical environmental conditions. The temperature in the reactor was maintained between 305 and 310 K to approximate that of a typical afternoon smog chamber experiment. To achieve this, the entire reactor was covered with an insulating cover as well as a black tarpaulin. In addition, four Holmes (Milford, MA) Model HFH-501FP space heaters were placed in the open area underneath the reactor. In a typical experiment, seed particles of (NH₄)₂SO₄ were injected into the chamber to obtain initial particle

concentrations of approximately 9,000-17,000 particle cm^{-3} . The initial size distribution of the seed aerosol was centered around 100 nm. The aerosol size distribution and total number concentrations of each side of the reactor were monitored at a one-minute frequency using a TSI (St. Paul, MN) Model 3071 cylindrical scanning electrical mobility spectrometer (SEMS) and a TSI Model 3760 condensation nucleus counter (CNC). Particle losses in the SEMS, SEMS response functions, particle charging efficiencies, CNC charging efficiencies, and particle deposition in the reactor have been taken into account in the analysis of the aerosol data [Wang *et al.*, 1992]. The initial monoterpene mixing ratio ranged from 50 to 110 ppbv, and an appropriate amount of 2-butanol was also added to the reactor to scavenge >95% of OH radicals produced from the monoterpene- O_3 reaction [Chew and Atkinson, 1996; Atkinson, 1997]. Finally, ozone was injected to the reactor using an Enmet Corporation (Ann Arbor, MI) Model 04052-011 O_3 generator until the O_3 mixing ratio reached approximately four times that of the initial hydrocarbon for all experiments except one α -pinene/ O_3 and one β -pinene/ O_3 experiment, in which excessive hydrocarbon was established in the reactor. Table A.1.1 summarizes the initial conditions of each experiment.

Reactor air was withdrawn through a sampling system consisting of a glass annular denuder (University Research Glassware, Chapel Hill, NC) followed by a 47 mm Pallflex Teflon impregnated glass fiber filter at a flow rate of 25 L min^{-1} for 1 h. The denuder is 40 cm long and consists of 5 annular channels with 2 mm space between channels. The sand-blasted denuder walls were coated with sub-micron XAD-4 particles beforehand using the procedure described by Gundel *et al.* [1995].

A.1.2.2 Sample treatment and analysis

Denuder and filter samples were spiked with 10 μL of 40 ng/ μL tricosane in dichloromethane (DCM) immediately after sample collection. Filters were soxhlet-extracted with 160 mL 1:1 acetonitrile and DCM solvents for 12-16 hrs. Before extraction, 150 μL of 19 mM PFBHA acetonitrile/aqueous solution (a minimum amount of water was used to dissolve PFBHA·HCl) was added to the soxhlet extractor along with the extraction solvents. Denuders were extracted with 4 x 40 mL of a solvent mix made of DCM, acetonitrile, and hexane (50%: 38%: 12%) by manually inverting the denuder 40 times. After addition of 150 μL of 19 mM PFBHA solution, the denuder extracts were left at room temperature overnight. Then both the filter and denuder extracts were reduced to *ca.* 5 mL by rotary evaporation. The extracts were blown to nearly dryness under a gentle N_2 stream, followed by reconstitution with 280 μL 1:1 hexane and DCM solvent mixture, and addition of 20 μL of BSTFA and 10 μL of 3 ng/ μL 1-phenyldodecane (injection internal standard). The mixtures were then heated at 70°C for 2.5 hrs. After cooling briefly, 20 μL of the mixture was injected for GC/MS analysis.

A Varian Saturn 2000 gas chromatograph/ ion trap mass spectrometer was used for both EI and methane CI analysis. The GC temperature was programmed at 60°C for 1 min, to 250°C at 10°C/min, to 300°C at 5°C/min, and held at 300°C for 10 min. Samples were injected in the splitless injection mode. The injector was switched to split mode 1 min after an injection was made. The injector port temperature was programmed at 60°C for 1 min, ramped to 320°C at 180°C/min, and held at 320°C until the end of the analysis.

The mass range was 50 - 650 amu. A 30m x 0.25 mm x 0.25 μ m DB-5 fused silica column was used for all samples.

A.1.2.3 Denuder and filter collection efficiencies

The collection efficiency of the 40-cm long denuder was determined by connecting this denuder and a 20-cm long denuder in series (the limited space between the sampling port and the ground can only accommodate a 20-cm long denuder). The collection efficiency was calculated as $A_L/(A_L+A_S)$, where A_L and A_S represent the amounts collected by the long and the short denuders, respectively. Semi-volatile products can volatilize from a filter due to changes in gas/particle equilibrium conditions as a result of the denuder stripping off gas-phase semi-volatiles. The filter "blow-off" was collected by a pre-baked glass fiber filter placed downstream from the Teflon filter. The filter collection efficiency was then calculated as $F_t/(F_t+F_g)$, where F_t and F_g represent the amounts collected by the front Teflon filter and the rear glass fiber filter, respectively. The collection efficiencies were computed using the photooxidation products of α -pinene/ NO_x in the outdoor reactor under sunlight irradiation. The reaction mixture contained pinic acid, pinonic acid, norpinonic acid, 2,2-dimethyl-3-formyl-cyclobutyl-methanoic acid, pinonaldehyde, and norpinonaldehyde. Table A.1.2 lists the denuder and filter collection efficiencies for each individual product. The results indicate that a 20-cm long denuder is sufficient to collect any breakthrough from the first denuder.

A.1.2.4 Recoveries of denuder and filter samples

Recoveries of select compounds were determined by spiking on filters and denuders known amounts of liquid standards and the recovery standard tricosane. The

same extraction and concentration procedures as those described in Section A.1.2.2 were then applied.

Relative recoveries for select multifunctional compounds versus the recovery standard tricosane are given in Table A.1.3. 2-Hydroxy-cyclohexanone is included to serve as a surrogate for hydroxy pina ketones and hydroxy sabina ketones, and the two dicarbonyls, 5-methyl-1,3-cyclohexanedione and 5-isopropyl-1,3-cyclohexanedione, act as surrogates for dicarbonyl compounds, such as pinonaldehyde and norpinonaldehyde. Two dicarboxylic acids, heptanedioic acid and octanedioic acid, and one keto acid, 7-oxo-octanoic acid, are included to test whether compounds with the same type of functional groups exhibit similar recoveries. Comparison of the recoveries of heptanedioic and octanedioic acid with that of pinic acid, a C₉ cyclic dicarboxylic acid, shows that the three dicarboxylic acids exhibit similar recoveries for both denuder and filter samples. The two keto acids, 7-oxo-octanoic acid and pinonic acid, also have similar recoveries. This adds confidence to the assumption that the recoveries for those compounds without available standards can be approximated with those of known standards that have similar functional groups.

For each compound tested, the denuder samples show lower recovery than filter samples. This indicates the mouth washing extraction technique performed on denuders is not as efficient in extracting the polar compounds as the soxhlet extraction method performed on filter samples. The large standard deviations associated with the recoveries are likely a result of a number of factors including extraction efficiency, volatilization during rotary evaporation, and losses from transfer and surface adsorption. Absolute recovery of a given compound is obtained by multiplying its relative recovery by that of

tricosane in individual samples. All the denuder and filter samples have been corrected with the recoveries determined here.

A.1.3 Product Identification

The newly developed analytical derivatization method [Yu *et al.*, 1998] allows for detection and identification of three types of products: (1) those containing only carbonyl group(s) (e.g., simple aldehydes, ketones and dicarbonyls), (2) those containing only OH/COOH groups (e.g., dicarboxylic acids), and (3) those containing both carbonyl and OH/COOH groups (e.g., oxoacids and hydroxy carbonyls). Here OH/COOH denotes the presence of hydroxy or carboxy functional groups since the mass spectra for the TMS derivatives often cannot differentiate between these two functional groups. Two types of ion chromatograms are constructed: m/z 181 ion chromatogram and m/z 73 and 75 ion chromatogram. Type (1) compounds show peaks only in the 181 ion chromatogram, type (2) compounds exhibit peaks only in the 73 and 75 ion chromatogram, and type (3) compounds show peaks in both chromatograms. The classification for each product is further substantiated by the unique pseudo-molecular ions in the CI mass spectra.

A.1.3.1 Products from ozone oxidation of β -pinene

Figure A.1.1a is the reconstructed m/z 181 ion chromatogram, showing carbonyl-containing products from the β -pinene/ O_3 reaction. Figure A.1.1b is the reconstructed m/z 73 and 75 ion chromatogram, displaying all products bearing OH/COOH groups. Table A.1.4 lists molecular weight (MW), chemical structure, and the pseudo-molecular ion fragments in the CI mass spectra that are used to obtain molecular weight for the products. Product names are derived using the newly proposed nomenclature for terpene oxidation products by Larsen *et al.* [1998].

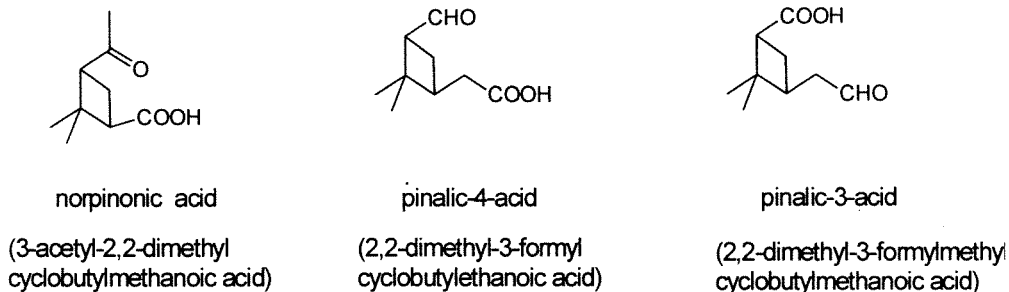
Among the products, compounds P₁ and P₂ are type (2) products, i.e., only contain OH/COOH groups. Compound P₁ is tentatively identified as norpinic acid (2,2-dimethylcyclobutane-1,3-dicarboxylic acid). The CI spectrum shows ions at m/z 389, 317, 301, 227, and 117, corresponding to M+73, M+1, M-15, M-89, and M-117 (Figure A.1.2- P₁). The m/z M+73 ion is an adduct ion resulting from the addition of the $[\text{Si}(\text{CH}_3)_3]^+$ fragment ion to a neutral molecule. The m/z M+1 ion is the protonated molecular ion. The ions at m/z M-15, M-89, and M-117 are fragment ions resulting from loss of CH₃, OSi(CH₃)₃ and C(O)OSi(CH₃)₃ from the neutral molecules. Compound P₂ is identified as pinic acid, which has been confirmed by comparison with an authentic standard obtained from Aldrich (Figure A.1.2-P₂).

Compounds P₃, P₁₀, and P₁₁ have carbonyl groups, but no OH/COOH groups (type 1 compounds), as indicated by their presence in Figure A.1.1a and absence in Figure A.1.1b. Compound P₃ is positively identified as nopinone (pina ketone) by comparison with an authentic standard. There are two GC peaks corresponding to nopinone, as PFBHA forms two geometric isomers with a given nonsymmetrical carbonyl [Le Lacheur *et al.*, 1993; Yu *et al.*, 1995]. The relative intensity of the pseudo-molecular ions from two isomers of a PFBHA derivative may vary, but the mass fragment patterns are similar. Therefore, only one spectrum is given to illustrate the identification of a given carbonyl-PFBHA derivative. Figure A.1.2-P₃ shows the CI spectrum of the second nopinone peak, with pseudo-molecular ions at m/z 514, 362, 334, 152 and 136, corresponding to M+181, M+29, M+1, M-181, and M-197. The m/z M+181 ion is an adduct ion formed between a neutral molecule and the fragment ion $[\text{C}_6\text{F}_5\text{CH}_2]^+$. The m/z M+29 ion is an adduct ion resulting from the addition of the

methane reagent ion $[\text{C}_2\text{H}_5]^+$ to a neutral molecule. The ions at m/z M-181 and M-197 are fragment ions arising from loss of $\text{C}_6\text{F}_5\text{CH}_2$ and $\text{C}_6\text{F}_5\text{CH}_2\text{O}$ fragments from the neutral molecules. Compound P_{10} is tentatively identified as 2,2-dimethyl-cyclobutane-1,3-dicarboxaldehyde, with a MW of 530 for its PFBHA derivative (Figure A.1.2- P_{10}). Compound P_{11} is tentatively identified as 3-oxo-pina-ketone, a diketone (Figure A.1.2- P_{11}). Its PFBHA derivative has a MW of 542 when both carbonyl groups are derivatized. In addition, two peaks in Figure A.1.1a are ascribed to the mono-derivative of 3-ketonopinone, with a MW of 347. For a dicarbonyl, PFBHA may derivatize only one of the two carbonyl groups and leave the other intact if unfavorable derivatization conditions occur. Among unfavorable conditions are steric hindrance and insufficient amount of derivatization agent and reaction time.

Compounds P_4 , P_5 , P_6 , P_7 , P_8 , and P_9 have both carbonyl and OH/COOH groups (type 3 compounds), indicated by their presence in both Figures A.1.1a and A.1.1b. Compound P_4 is tentatively identified as a hydroxy substituted nopinone, 3-hydroxy-pina ketone or 1-hydroxy-pina ketone. The derivatized form of P_4 has a MW of 421. (See Figure A.1.2- P_4 for its CI mass spectrum.) Compound P_5 is tentatively identified as 2,2-dimethyl-3-formyl-cyclobutyl-methanoic acid, having a MW of 423 for its derivatized form (Figure A.1.2- P_5). Three peaks, labeled P_6 in Figure A.1.1, are identified to have a MW of 437, indicated by the presence of several pseudo-molecular ions in their CI spectrum at m/z 510, 438, 348, 256, and 240, corresponding to $\text{M}+73$, $\text{M}+1$, $\text{M}-89$, $\text{M}-181$, and $\text{M}-197$ (Figure A.1.2- P_6). The observation of three peaks indicates that at least two isomers with the same number and type of functional groups are present. The

following three isomers are possible candidates with structures consistent with the EI and CI mass spectra fragment patterns:



Further differentiation among the three isomers is impossible on the basis of CI and EI mass spectra. Figure A.1.2-P₆ shows ion fragment patterns using pinalic-4-acid as an example. Compound P₇ is identified as *cis*-pinonic acid, and the identification has been confirmed by comparison with an authentic standard. The CI mass spectrum of its derivative is shown in Figure A.1.2-P₇. Compound P₈ is tentatively identified as hydroxy norpinonic acid, with a MW of 525 for its derivative (Figure A.1.2-P₈). Compound P₉ is tentatively identified as hydroxy pinonic acid, with a MW of 539 for its derivative (Figure A.1.2-P₉).

Some of the products observed here have been reported in previous studies. Nopinone has long been identified as a major product in the β -pinene/O₃ reaction [Hull, 1981; Hatakeyama *et al.*, 1989; Grosjean *et al.*, 1993, Hakola *et al.*, 1994]. Using GC/MS and nuclear magnetic resonance (NMR) analyses, Hull [1981] also positively identified 3-hydroxy-pina ketone and 3-oxo-pina ketone and had indirect evidence for the formation of 1-hydroxy-pina ketone. Products that are reported here for the first time include pinic acid, norpinic acid, 2,2,-dimethyl-3-formyl-cyclobutyl methanoic acid,

norpinonic acid and its isomers, pinonic acid, hydroxy norpinonic acid, hydroxy pinonic acid, and 2,2-dimethyl-cyclobutane-1,3-dicarboxaldehyde.

A.3.3.2 Products from ozone oxidation of sabinene

Carbonyl bearing products of the sabinene/O₃ reaction are shown in Figure A.1.3a, and OH/COOH bearing products are shown in Figure A.1.3b. Table A.1.5 lists the MWs and chemical structures of these products. Most products are analogous to those identified in the β -pinene/O₃ reaction, and their methane CI mass spectra are similar to those in the β -pinene/O₃ reaction. The CI mass spectra are given only for the products unique in the sabinene/O₃ reaction (Figure A.1.4). Interested readers can get from us the mass spectra data for those analogous products.

Among the products, compound S₁, S₂, and S₃ contain only OH/COOH groups (type 2 compounds). Compound S₁ is tentatively identified as norsabinic acid on the basis of that it shows a MW of 316 for its derivative, and elutes at an earlier retention time than that of norpinic acid. The CI spectrum of compound S₂ indicates a MW of 330 for its TMS derivative. S₂ elutes from the GC column earlier than pinic acid. It is tentatively identified as sabinic acid, the analogue of pinic acid derived from sabinene. Compound S₃ is pinic acid, confirmed by authentic standard. The observation of pinic acid as a product in the sabinene/O₃ reaction is also reported by *Glasius et al.* [1998]. It is not likely that pinic acid is a residue resulting from the previous chamber experiment, which was a β -pinene/O₃ experiment. Between chamber experiments, clean air of more than 15 times the bag volume passes through the reactor. More experiments are needed to verify this observation.

Compounds S₄ and S₁₁ are found to contain only carbonyl groups (type 1 compounds), indicated by their presence in Figure A.1.3a and absence in Figure A.1.3b. Both EI and CI spectra indicate a MW of 333 for compound S₄. It is tentatively identified as sabina ketone. This product is identified as a major product by *Hakola et al.* [1994]. Compound S₁₁ is tentatively identified as 3-oxo-sabina ketone. The mono-derivative of this diketone is also present.

Compounds S₅, S₆, S₇, S₈, S₉, S₁₀, and S₁₂ have both carbonyl and OH/COOH groups (type 3 compounds), indicated by their presence in both Figure A.1.3a and Figure A.1.3b. Compound S₅ is tentatively identified as 2-(2-isopropyl)-2-formyl-cyclopropyl-methanoic acid, as its CI spectrum shows a MW of 423 for its PFBHA and TMS derivative. Three peaks are ascribed to S₆, and their CI spectra indicate a MW of 421. S₆ is therefore tentatively identified as hydroxy sabina ketones (3-hydroxy and 1-hydroxy sabina ketone). Four peaks are assigned to S₇, which has a MW of 437. Similar to the P₇ peaks in the β -pinene/O₃ samples, S₇ could be two of the three isomers listed in Table A.1.5. Further differentiation is not possible based on the mass spectra data. Peak S₈ shows a MW of 495 (Figure A.1.4-S₈). Table A.1.5 lists one of the possible candidates that matches the MW and functional group types. Three peaks, with a MW of 525 determined from their CI mass spectra, are assigned to S₉. Three of all possible structures are listed in Table A.1.5. S₁₀ is determined to have a MW of 539 for its derivatized form. Two peaks are ascribed to compound S₁₂, with a MW of 590 for its derivatized forms. One EI spectrum is given in Figure A.1.4-S₁₂. Their CI spectra are weak, but the protonated molecular ion is present. One postulated structure is listed in Table A.1.5.

A comparison of the products from β -pinene/ O_3 and sabinene/ O_3 reveals that there are nine analogous product pairs in the two reaction systems: norpinic acid/norsabinic acid, pinic acid/sabinic acid, nopinone/sabina ketone, P_5/S_5 , hydroxy pina ketones/hydroxy sabina ketones, P_6/S_7 , P_8/S_9 , P_9/S_{10} , and 3-oxo-pina ketone/3-oxo-sabina ketone (Tables A.1.4 and A.1.5). These analogous products suggest that they are derived from a common moiety between the two parent reactants, i.e., an external unsaturated bond to the six-member ring. The sabinene/ O_3 reaction also produces two unique products (S_8 and S_{12}), correspondents of which are not observed in the β -pinene/ O_3 reaction.

A.1.3.3 Products from ozone oxidation of α -pinene

Identification of ozone oxidation products of α -pinene, based on a collection of $\sim 0.36\text{ m}^3$ reactor air in an impinger, has been described by *Yu et al.*[1998]. The collection of a larger air volume (1.5 m^3) by the denuder/filter system in this work allows detection of six additional minor products. For completeness, Table A.1.6 shows the structures of all the identified products. The six additional products identified include norpinic acid (A_1), (2,2-dimethyl-3-acetyl)-cyclobutyl formate (A_3), hydroxy pinonic acid (A_7), A_{11} , A_{13} , and A_{14} (See Table A.1.6.). Figures A.1.5a and A.1.5b are the GC chromatograms for carbonyl and COOH/OH bearing products, respectively. Some of the products in the α -pinene/ O_3 reaction are also observed in the β -pinene/ O_3 system, apparently as a result of the common moieties shared by α -pinene and β -pinene. Unique products in the α -pinene/ O_3 reaction include A_3 , and A_9 - A_{14} . Their CI spectra are displayed in Figure A.1.6.

The tentative identifications of (2,2-dimethyl-3-acetyl)-cyclobutyl formate (A_3), norpinonaldehyde (A_9), pinonaldehyde (A_{10}), and hydroxy pinonaldehydes (A_{12}) are based on their mass spectra and reasonable postulation of the gas-phase α -pinene/ O_3 reaction mechanism [Yu *et al.*, 1998]. A possible structure for A_{14} is suggested based on its mass spectrum. For A_{11} and A_{13} , only their MW and some functionality information are given in Table A.1.6, as it is difficult to suggest possible candidates.

A number of recent product studies of the α -pinene/ O_3 reaction have also revealed some of the products observed in this work [Hoffmann *et al.*, 1998; Glasius *et al.*, 1998,1999; Jang and Kamens, 1998]. Using HPLC/ atmospheric pressure chemical ionization (APCI) mass spectrometry, Hoffmann *et al.* [1998] reported the observation of pinic acid, norpinic acid, pinonic acid, and evidence for an adduct of pinic acid and norpinic acid. Such a binary diacid adduct, if existing, would likely dissociate when undergoing the heating treatment (70°C for 2.5 hrs) used for the silylation derivatization. Glasius *et al.* [1999], using HPLC/ electrospray ionization and APCI mass spectrometry, reported observation of pinonic acid, pinic acid, norpinic acid, hydroxy pinonic acid, and pinalic-4-acid. Jang and Kamens [1998], using derivatization techniques and GC/MS detection similar to this work, tentatively identified norpinic acid, pinic acid, norpinonic acid, pinonic acid, 2,2-dimethyl-3-formyl-cyclobutyl-methanoic acid, norpinonaldehyde, pinonaldehyde, pinalic-3-acid, hydroxy pinonic acid, and A_{14} . Compounds A_3 , A_{11} and A_{13} are reported here for the first time.

A.1.3.4 Products from ozone oxidation of Δ^3 -carene

Identification of ozone oxidation products of Δ^3 -carene based on impinger samples has been described by Yu *et al.* [1998]. Using the denuder/filter pack collection

system, we have identified additional products in small yields. Figures A.1.7a and A.1.7b are the GC chromatograms of the derivatized products in a denuder sample. Table A.1.7 lists the structures of these products and the pseudo-molecular ions in their CI mass spectra, which are used to determine MWs. Due to lack of authentic standards, all the products are tentatively identified on the basis of their mass spectra and possible reaction mechanism. Many of the products in the Δ^3 -carene/ O_3 reaction are analogous in structure to those in the α -pinene/ O_3 reaction. The CI mass spectra of the products that do not have analogous products in the α -pinene/ O_3 reaction are given in Figure A.1.8. The CI mass spectra for C_7 and C_8 have been shown in the previous paper [Yu *et al.*, 1998].

Additional products identified in the denuder sample include nor-caric acid (C_1), pinic acid (C_3), C_4 , C_5 , and C_{10} . For C_4 , C_5 , and C_{10} , we are not currently able to suggest possible chemical structures, so only their MW and the presence of functional group types are given in Table A.1.7. These three products do not have corresponding analogues in the α -pinene/ O_3 reaction. On the other hand, four products, A_3 , A_{11} , A_{13} , and A_{14} , are found unique to the α -pinene/ O_3 reaction. This is not unexpected as minor reaction pathways may take place at locations other than the C=C bond.

The observation of pinic acid in the Δ^3 -carene/ O_3 reaction is not expected. Glasius *et al.* [1998] also observed trace amount of pinic acid in their Δ^3 -carene/ O_3 reaction systems.

A.1.4. Product Yields

Yields of the above-identified products have been determined or estimated. For products with standards, the calibration factor, extraction recovery, and collection

efficiency have been determined using the standards. For products that do not have available authentic standards, their yields are estimated using the calibration factor, and the recovery and collection efficiency of surrogate compounds. The surrogate compounds are chosen to have the same type of functional groups and approximate carbon numbers as the products that the surrogates represent. Table A.1.8 lists the available standards and the products for which the standards serve as surrogates. For example, pinic acid serves as the surrogate for norpinic acid, 3-caric acid, nor-3-caric acid, sabinic acid, and norsabinic acid. Carbonyl bearing products (type 1 compounds) are quantified using the m/z 181 ion, products bearing COOH/OH groups (type 2 compounds) are quantified using the m/z 73 and 75 ions, and for those products that contain both carbonyl and COOH/OH groups (type 3 compounds), the sum of three ions at m/z 181, 73 and 75 is used for their quantification. The selection of surrogates on the basis of functional group types is justified by the use of the above functional group specific ions for quantification. The estimated calibration factors have a $\sim\pm 30\%$ uncertainty. The other sources that contribute to the uncertainty associated with product yields include uncertainties for collection efficiency ($\sim\pm 4\%$), extraction efficiency ($\sim\pm 15\%$) and sample volume ($\pm 5\%$). After considering all contributing sources, the uncertainty associated with product yields is estimated to be $\sim\pm 50\%$.

Our calculation of gaseous product yields ignores wall loss processes, as we estimate that the loss of an oxygenated product resulting from wall loss processes is likely less than 15% at 300 min after its formation. *Grosjean* [1985] measured the wall loss rates for five oxygenated species, biacetyl, pyruvic acid, *o*-cresol, benzaldehyde, and benzoic acid, in a Teflon chamber with a S/V of 3.8 m^{-1} . The first three compounds had

an unmeasurable wall loss rate while benzaldehyde and benzoic acid had wall loss rates of 3.4×10^{-4} and $10.8 \times 10^{-4} \text{ min}^{-1}$, respectively. *Hallquist et al.* [1997] measured the wall loss rates for pinonaldehyde and caronaldehyde to be $(2.4\text{-}4.2) \times 10^{-3} \text{ min}^{-1}$ in a borosilica glass reactor with a S/V of 14.3 m^{-1} . If one assumes wall loss processes are similar on borosilica glass and Teflon surfaces, one could calculate that the two dicarbonyls have a wall loss rate of $(3\text{-}5) \times 10^{-4} \text{ min}^{-1}$, comparable to that for benzoic acid ($5 \times 10^{-4} \text{ min}^{-1}$), in the present Teflon reactor with a S/V of 1.8 m^{-1} . Using the wall loss rate for benzoic acid, which has the highest wall loss rate among all the tested oxygenated species, we estimate that about 86% of an oxygenated product remains in the gas phase at 300 min after its formation, if we assume that wall loss is the only loss process. A more detailed study of gas-phase product yields needs experimentally determined wall loss rates for each product, which unfortunately cannot be readily accomplished as many products lack commercially available standards.

The organic aerosol mass generated in each experiment was obtained from the aerosol volume measured by SEMS/CNC and assuming a SOA density of 1 g cm^{-3} . The SOA yield (Y) was then calculated by

$$Y = \frac{\Delta M_o}{\Delta HC} \quad (\text{A.1.1})$$

where ΔM_o is the organic aerosol mass concentration ($\mu\text{g m}^{-3}$) produced for a given amount of hydrocarbon reacted, ΔHC ($\mu\text{g m}^{-3}$). The estimated uncertainty in the measured SOA yield is roughly $\pm 12\%$, with SOA density uncertainty assumed to be $\pm 10\%$.

A.1.4.1 β -Pinene

Table A.1.9 shows yields of individual products in gas and aerosol phases, as well as the total yields in two β -pinene/O₃ experiments. The yield of nopinone in the gas-phase is determined from measurements made by an on-line GC/FID, as GC/FID provides more accurate and frequent measurements of nopinone. As an example, Figure A.1.9 shows the amount of nopinone formed against the amount of β -pinene reacted for the experiment carried out on June 11, 1998 (side B). The gas-phase yield of nopinone was determined to be 17.0% and 15.8% in the 6/11/98b and 6/17/98b experiments, respectively. Nopinone resides almost exclusively in the gas phase; trace amounts were detected in the filter samples. Previously reported nopinone yields vary from 22% [Grosjean *et al.* 1993] and $23 \pm 5\%$ [Hakola *et al.*, 1994] to $40 \pm 2\%$ [Hatakeyama *et al.*, 1989]. The much higher nopinone yield in the study by Hatakeyama *et al.* [1989] is possibly due to the presence of other carbonyl products that were reported as nopinone, as their measurement of nopinone was based on FTIR absorption spectroscopy at the 1740 cm^{-1} -C=O stretch frequency.

Only one study in the literature [Hull, 1981] reported yields for individual products other than nopinone in the β -pinene/O₃ reaction. In this study, Hull [1981] estimated the total molar yields of three major products: nopinone (10%), 3-hydroxy-pina-ketone (28%), and 3-oxo-pina-ketone (7%). The total molar yield for 3-hydroxy-pina ketone in the present work is estimated to be 7.3% and 9.0% in the two experiments, lower than Hull's [1981] result. Our yield for 3-oxo-pina-ketone is estimated to be 1.8% and 7.7%. In his study, Hull [1981] used high mixing ratios for β -pinene (275 to 440

ppmv) and ozone (179 to 270 ppmv), and no OH scavenger. The very different reaction conditions may account for the different product yields.

The identified products account for 34% and 50% of the reacted β -pinene carbon mass in the 6/11/98b and 6/17/98b experiments, respectively. Products with a yield exceeding >1% include nopinone (15.8-17.0%), hydroxy pina ketones (7.3-9.0%), 3-oxo-pina-ketone (1.8-7.7%), norpinonic acid and its isomers (5.9-16.5%), and pinic acid (2.6-3.7%). The identified products are estimated to account for 98% and 83% of the organic aerosol mass formed in the two β -pinene/O₃ experiments. Norpinonic acid and its isomers, pinic acid, and hydroxy pina ketones are SOA components that contribute to more than 10% of the organic aerosol mass.

The 6/17/98b experiment has a much higher percentage of reacted β -pinene accounted for by the identified products than the 6/11/98b experiment, as two major products, norpinonic acid and its isomers and 3-oxo-pina-ketone, were observed to have much higher gas-phase yields in the 6/17/98b experiment (Table A.1.9). The two β -pinene/O₃ experiments were conducted under different initial conditions, i.e., ozone was present in an excess amount in the 6/11/98b experiment whereas β -pinene is in excess in the 6/17/98b experiment (Table A.1.1). The variation between the two experiments cannot be accounted for by measurement error alone. It is possible the different initial reaction conditions are responsible for the variation, but a satisfactory explanation is not possible without further experiments designed to systematically examine the effects of different reaction conditions on product yields.

The functional group distribution of SOA components from the β -pinene/O₃ experiments is comparable to results obtained by *Palen et al.* [1992] using Fourier

transform infrared spectrometry (FTIR). *Palen et al.* [1992] analyzed aerosol samples generated from an experiment with 8 ppmv O₃ and 14.5 ppmv β -pinene. Their results indicated that an average aerosol-phase product molecule contained one ketone group, 0.7 alcohol groups, and 0.4 carboxylic groups. For the 6/17/98 β -pinene/O₃ experiment where excessive β -pinene was used, our GC/MS analysis showed that the average aerosol molecule contained about one ketone group, 0.2 alcohol groups, and 0.8 carboxylic groups.

A.1.4.2 Sabinene

Table A.1.10 shows yields of individual products in the gas and aerosol phases, as well as the total yields of both phases in the sabinene/O₃ experiment. Identified products in both the gas and aerosol phases account for 57% of the reacted sabinene carbon mass. Products with a molar yield exceeding 1% include sabina ketone (47%), hydroxy sabina ketone (7%), norsabinonic acid and its isomers (5%), pinic acid (1%), and sabinic acid (1%).

All the products added together account for 100% of the organic aerosol mass formed. The 100% yield is rather fortuitous, and it is associated with an uncertainty factor resulting from the approximations made for response factors and SOA density. Aerosol components that make up more than 10% of the aerosol mass are norsabinonic acid and its isomers, hydroxy sabina ketones, sabinic acid, sabina ketone, and pinic acid.

The estimated yield of sabina ketone in this work is in agreement with that, $50 \pm 9\%$, measured by *Hakola et al.* [1994]. *Glasius et al.* [1998] reported molar yields of sabinic acid and pinic acid in aerosol phase at 1.1% and 1.4%. Our yields for the two dicarboxylic acids in the aerosol phase are 0.4% and 0.3%. As we will discuss in Section

A.1.5, the absolute aerosol yield of a particular product depends on the temperature and the organic aerosol mass concentration in each system in which SOA is generated.

Without the knowledge of the temperature and organic aerosol mass concentration in the system of *Glasius et al.* [1998], it is difficult to make a meaningful comparison.

A.1.4.3 α -Pinene

Table A.1.11 shows yields of individual products in the gas and aerosol phases, as well as the total yields of both phases, in three α -pinene/O₃ experiments. Identified products in both the gas and aerosol phases account for 29-67% of the reacted α -pinene carbon mass. Products with a molar yield exceeding 1% include pinonaldehyde (6-19%), norpinonic acid and its isomers (4-13%), hydroxy pinonaldehydes (2-11%), pinonic acid (2-8%), pinic acid (3-6%), hydroxy pinonic acid (1-4%), (2,2-dimethyl-3-acetyl)-cyclobutyl formate (1-4%), and norpinonaldehyde (1-3%).

In the 6/17/98a experiment, a much higher percentage of reacted α -pinene is accounted for by the identified products, as the four major products, pinonaldehyde, hydroxy pinonaldehydes, pinonic acid, and norpinonic acid and its isomers, are measured to have much higher yields than those in the experiments 6/9/98a and 6/9/98b. While measurement errors may account for part of the variation, the different reaction conditions also likely contribute to the variation. The 6/17/98a experiment is different from the experiments 6/9/98a and 6/9/98b in two aspects: 1) excessive α -pinene was used in the 6/17/98a experiment while excessive ozone was present in the prior two experiments, and 2) the denuder/filter sample was started 53 min after the initiation of the α -pinene/O₃ in the 6/19/98a experiment while in the other two experiments denuder/filter samples were collected more than 290 min after ozone oxidation of α -pinene started.

One explanation is that the polar nature of the products makes them susceptible to be lost to the reactor wall by adsorption, as demonstrated for pinonaldehyde and caronaldehyde by *Hallquist et al.* [1997] in their experimental chamber. Actual product yields may be higher after accounting for wall loss, but wall loss does not account for all the yield variation. It is noted that for both the α -pinene/O₃ and the β -pinene/O₃ experiments, higher gas-phase yields were measured when excess monoterpene was present in the reaction systems. Presently we do not have a satisfactory explanation for this observation.

Four previous studies have reported yields of some of the above products. The gas-phase yield of pinonaldehyde was measured to be $14.3 \pm 2.4\%$ [*Alvarado et al.*, 1998] and $19 \pm 4\%$ [*Hakola et al.*, 1994]. In this work, the yield is estimated to be 5.7-18.1%, in general agreement with the values reported in the two previous studies. *Hull* [1981] reported total yields in both phases for four major products: pinonic acid (27%), pinonaldehyde (15%), hydroxy pinonaldehyde (7%), and norpinonic acid (7%). We have measured or estimated the yields in both phases to be 2.1-7.9%, 6.5-19.0%, 1.8-11.2%, and 4.2-12.6%, respectively. The yield of pinonic acid measured by *Hull* [1981] is much higher than our yield. In *Hull's* [1981] study, no OH scavenger was added, and the mixing ratios of α -pinene used ranged from 110 to 509 ppmv, which is more than 1000 times higher than those in this work. It is difficult to make meaningful comparisons considering the very different reaction conditions investigated in the two studies. In the absence of OH scavengers, *Hatakeyama et al.* [1989] measured aldehyde yield in the gas-phase to be $51 \pm 6\%$ by FTIR absorption spectroscopy. In this study we have identified ten products with aldehyde functional group(s), i.e., pinonaldehyde, norpinonaldehyde,

hydroxy pinonaldehydes (A_{12}), norpinonic acid and isomers (A_5), A_4 , A_8 , A_{11} , A_{12} , A_{13} , and A_{14} . The sum of yields for all these aldehyde products in the gas phase ranges from 14-45%. If one considers that the absence of OH scavenger would increase yields of aldehyde products such as pinonaldehyde, yield data from this study may be consistent with the result obtained by *Hatakeyama et al.* [1989].

All the products added together account for 90-111% of the organic aerosol mass formed. The larger than 100% aerosol yield reflects the uncertainties associated with the estimated response factors for those products without available standards, and the assumption that SOA has a density of 1 g cm^{-3} . At 306-308 K, major aerosol components that make up more than 10% of the organic aerosol mass include pinic acid, hydroxy pinonaldehydes, pinonic acid, norpinonic acid and its isomers, and hydroxy pinonic acid.

Among all the monoterpenes, ozone oxidation of α -pinene is the most frequently studied reaction for its aerosol products. In previous studies, the molar yield of pinic acid and pinonic acid in the aerosol phase was measured to range from 0.2% to 1%, and 0.1-0.3%, respectively [*Christoffersen et al.*, 1998; *Glasius et al.*, 1998]. The temperature and organic aerosol mass in their systems were not reported.

A.1.4.4 Δ^3 -Carene

Table A.1.12 shows the gas and aerosol phase yields of the individual products, as well as the total yields of both phases in two Δ^3 -carene/ O_3 experiments. Identified products in both the gas and aerosol phases account for 24% of the reacted Δ^3 -carene carbon mass. Products with a molar yield exceeding 1% include caronaldehyde (8%), 3-caronic acid (4%), hydroxy caronaldehydes (3%), nor-3-caronic acid and isomers (2%), C_5 (2%), 3-caric acid (2%), hydroxy-3-caronic acid (1%), and pinic acid (1%).

Caronaldehyde has been identified as a major product in a previous study with a yield of $\leq 8\%$ in the gas phase [Hakola *et al.*, 1994]. Here the gas-phase caronaldehyde yield is estimated to be 7.8%.

All the products added together account for 61% of the organic aerosol mass formed. Major aerosol products that contribute to $>10\%$ of organic aerosol mass are 3-caronic acid and 3-caric acid. Glasius *et al.* [1998] reported three aerosol products, 3-caric acid, 3-caronic acid, and nor-3-caric acid, with aerosol phase yields of 0.5-5%, 0.1-0.7%, and 0.08-0.1%, respectively.

A.1.5 Gas-Particle Partitioning

Many products identified in this study are detected in both gas and aerosol phases. Gas-particle partitioning for semi-volatile organic compounds has been successfully described by the equilibrium relation:

$$K_{om,i} = \frac{F_i}{A_i \Delta M_o} \quad (\text{A.1.2})$$

where $K_{om,i}$ is the gas-particle partitioning coefficient of species i , A_i is the gas phase concentration ($\mu\text{g m}^{-3}$) of compound i , and F_i is the concentration of compound i ($\mu\text{g m}^{-3}$) in the aerosol phase [Odum *et al.*, 1996]. A_i and F_i can be determined directly from denuder and filter samples, and ΔM_o is obtained from aerosol size distribution measurements. Table A.1.13 lists the gas-particle partitioning coefficients of aerosol components generated in the ozone oxidation of the four monoterpenes.

Gas-particle partitioning coefficients of semi-volatile compounds depend on their vapor pressures [Pankow, 1987]:

$$K_{om,i} = \frac{760RT}{MW_{om} 10^6 \zeta_i p_{L,i}^o} \quad (\text{A.1.3})$$

where R is the ideal gas constant ($8.206 \times 10^{-5} \text{ m}^3 \text{ atm mol}^{-1} \text{ K}^{-1}$), T is temperature (K), MW_{om} is the number-averaged molecular weight of the organic matter (om) phase (g mol^{-1}), ζ_i is the molar fraction scale activity coefficient of compound i in the om phase, and $p_{L,i}^o$ is the sub-cooled liquid vapor pressure (mm Hg) of compound i . Sub-cooled liquid vapor pressures of the major products in the β -pinene/ O_3 and α -pinene/ O_3 systems have been estimated using a modification of the Clausius-Claperyron equation [Schwarzenbach *et al.*, 1993] (Table A.1.14). Measured $K_{om,i}$ values versus the estimated $p_{L,i}^o$ are shown in Figure A.1.10. As Figure A.1.10 illustrates, the lower the vapor pressure, the higher the corresponding $K_{om,i}$. For example, hydroxy pinonic acid, as a result of the presence of three polar functional groups, has the lowest vapor pressure ($\sim 10^{-5} \text{ mm Hg}$) among all identified products, and consequently exhibits the highest $K_{om,i}$ value. On the other hand, the vapor pressure of pinonaldehyde and 3-oxo-pina ketone are higher than the -COOH bearing products, which correlates with the lowest $K_{om,i}$ values (Table A.1.13). Nopinone has an even higher vapor pressure than 3-oxo-pina ketone and is, as a result, expected to reside mainly in the gas-phase. Only trace amounts of nopinone were detected in any filter samples, confirming the influence of vapor pressure on the partitioning between the gas and aerosol phases. Similar trends are observed for SOA products in the ozone oxidation of the other two monoterpenes.

The aerosol phase fraction ϕ_i of a semi-volatile product is given by

$$\phi_i = \frac{F_i}{F_i + A_i} = \frac{\Delta M_o K_{om,i}}{1 + \Delta M_o K_{om,i}} \quad (\text{A.1.4})$$

As equation (A.1.4) indicates, ϕ_i is controlled by the aerosol organic matter concentration ΔM_o available for absorption and the gas-aerosol partitioning coefficient $K_{om,i}$, which is a function of temperature and compound-dependent. Consequently, SOA chemical composition is a function of organic matter concentration and temperature. Figure A.1.11 illustrates the dependence of ϕ_i on ΔM_o , using pinic acid as an example. The temperature dependence of SOA chemical composition was demonstrated by *Jang and Kamens* [1998], who observed that for SOA generated in the α -pinene/ O_3 reaction, the more volatile SOA components reside in the particle phase to a much greater extent under cold conditions than warmer conditions. When reporting aerosol yield of an individual product and composition of SOA, it is necessary to include the organic aerosol mass concentration and associated temperature.

The yield of an individual product i in the aerosol phase (Y_i) can be expressed as:

$$Y_i = \Delta M_o \frac{\alpha_i K_{om,i}}{1 + K_{om,i} \Delta M_o} \quad (\text{A.1.5})$$

where α_i is the individual mass-based stoichiometric coefficient of i . The overall SOA yield Y is then just the sum of the individual yields,

$$Y = \sum_i Y_i = \Delta M_o \sum_i \left(\frac{\alpha_i K_{om,i}}{1 + K_{om,i} \Delta M_o} \right) \quad (\text{A.1.6})$$

Using equation (A.1.6), a two-product model has successfully described the overall SOA yield Y as a function of stoichiometric coefficient α_i and partitioning coefficients $K_{om,i}$ of two hypothetical products, and ΔM_o , the total organic aerosol mass concentration [Odum *et al.*, 1996, 1997ab; Hoffman *et al.*, 1997; Griffin *et al.*, 1999].

One of the major assumptions underlying the derivation of equations (A.1.5) and (A.1.6) is that the total amount of a product is proportional to the amount of the parent hydrocarbon reacted. If this assumption holds, the SOA yield at any time $Y(t)$, should be described by equation (A.1.6). Figure A.1.12a shows the $Y(t)$ values as a function of organic aerosol mass for the 6/09/98a and 6/09/98b α -pinene/ O_3 experiments. The experimentally determined time-dependent yield curves for both experiments can be closely represented by using equation (A.1.6) and assuming two hypothetical products with $\alpha_1 = 0.262$, $K_{om,1} = 0.030$, $\alpha_2 = 0.062$, and $K_{om,2} = 0.0028$ (Figure A.1.12a). On the other hand, a yield curve can also be constructed for each experiment by using equation (A.1.6) and the experimentally determined α_i and $K_{om,i}$ values for the individual aerosol-phase products. The resulting curves fit well the experimental SOA yield curves (Figure A.1.12a). Since the denuder/filter samples were taken at the end of the two experiments (Table A.1.1), the α_i and $K_{om,i}$ values obtained from these samples represent the SOA composition and product distribution between gas and aerosol phases at the end of the experiments. The fact that they also predict the SOA yields during earlier stages of the experiments indicates that in the α -pinene/ O_3 system, the SOA composition and product distribution between gas and particle phase remains relatively unchanged over time. This is in agreement with the time profiles of α -pinene mixing ratio and organic aerosol mass concentration ΔM_o (Figure A.1.12b). As Figure A.1.12b shows, after most of the α -

pinene is oxidized, the aerosol mass remains almost constant, which indicates that the SOA mass arises from either primary products or secondary products formed relatively rapidly.

Conversely, if the total amount of a product that is generated in the reaction is not proportional to the amount of the parent hydrocarbon reacted throughout an experiment, e.g., the relative chemical composition changes over the course of the experiment, one set of α_i and $K_{om, i}$ values will not describe the SOA yields over the reaction time. The time-dependent SOA yield in the sabinene/ O_3 reaction appears to be such an example (Figure A.1.13a). As shown in Figure A.1.13a, a two-product model, using equation (A.1.6) and assuming two hypothetical products with $\alpha_1 = 0.041$, $K_{om,1} = 0.154$, $\alpha_2 = 0.51$, and $K_{om,2} = 0.0005$, describes the time-dependent aerosol yield reasonably well up to $\Delta M_o \sim 15 \mu\text{g}/\text{m}^3$, which corresponds to a reaction time of ~ 100 min and 99% sabinene consumption. The $Y(t)$ curve computed using equation (A.1.6) and the α_i , and $K_{om, i}$ values for multiple actual products fits well the measured aerosol yields at the later stage, but represents poorly the early-stage yields. The denuder/aerosol sample was taken 232 minutes after the reaction started; therefore, the measured α_i , and $K_{om, i}$ values of individual products reflect the SOA composition in the later stage of the experiment. The above analysis suggests that slowly forming secondary or tertiary products play a role in the aerosol formation in the sabinene/ O_3 reaction. The contribution of secondary products is further evidenced by the time profiles of sabinene mixing ratio and organic aerosol mass concentration ΔM_o . As shown in Figure A.1.13b, at ~ 100 min, while nearly all the sabinene is reacted, the organic aerosol mass continues to grow.

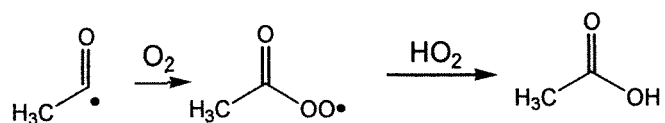
systems such as the sabinene/O₃ reaction, more than one set of α_i and $K_{om, i}$ values are necessary to describe the evolution of aerosol mass.

A.1.6. Mechanisms of product formation

Based on known reaction mechanisms for alkene-O₃ reactions, it is possible to propose reaction schemes to account for most of the observed products.

A.1.6.1 β -pinene / O₃ reaction

Figure A.1.14 shows reaction sequences leading to the products in the β -pinene/O₃ reaction. The reaction of β -pinene with O₃ proceeds by initial O₃ addition to the C=C bond to yield an energy-rich ozonide, which rapidly decomposes to form nopinone and a C₉ biradical. Many of the observed products are formed from the subsequent reactions of the C₉ biradical. The energy-rich C₉ biradical undergoes isomerization to give rise to two enehydroperoxides (EN₁ and EN₂) with excess energies. This is the so-called hydroperoxide channel. The formation of hydroxy pina ketones (P₄) are a result of stabilization of EN₁ and EN₂ through collision [Niki *et al.*, 1987; Martinez and Herron, 1987, 1988; Atkinson, 1997]. One additional pathway for EN₂ is to produce 3-oxo-pina ketone (P₁₁) by loss of a H₂ molecule. This pathway is not operative for EN₁ because the OH group is attached to a tertiary C, and no H-atom is available for loss of a H₂ molecule. It is postulated that the energized 3-hydroxy pina ketone could undergo unimolecular dissociation to form an acetyl-like radical I₁ and I₂. For the acetyl radical, it has been established that its subsequent reactions with O₂ and HO₂ radical lead to the formation of acetic acid [Niki *et al.*, 1985; Moortgat *et al.*, 1989].



Similarly, the reaction of I_1 and I_2 with O_2 and subsequently with HO_2 would lead to P_6 . I_2 can also lose a molecule of CO to form I_3 , which reacts with O_2 , and a peroxy radical RO_2 to form I_4 . It follows that I_4 loses one H-atom to an O_2 molecule to produce P_{10} . The formation of P_5 , norpinic acid (P_1), and pinic acid (P_2) is presupposed to result from oxidation of their corresponding aldehydes, P_{10} , P_5 and P_6 , respectively, although the explicit oxidation mechanism is unclear.

The formation pathway for a possible candidate of P_8 is proposed to arise from I_5 , which can be formed from isomerization of I_1 . It is difficult to construct plausible formation pathways for pinonic acid and hydroxy pinonic acid.

A.1.6.2 Sabinene / O_3 reaction

Figure A.1.15 depicts reaction pathways that account for most of the products observed from the sabinene/ O_3 reaction. The many pairs of analogous products in the sabinene/ O_3 and β -pinene/ O_3 reactions are easily explained by the same reaction pathways derived from O_3 attack of the external $\text{C}=\text{C}$ bond.

The observation of pinic acid in the sabinene/ O_3 reaction is difficult to explain in terms of plausible gas-phase reaction mechanisms. It is not clear whether aerosol surface plays a role in the formation of pinic acid via heterogeneous reactions. There is evidence that isomerization of monoterpenes can take place on acidic surfaces [*Pio and Valente*, 1998]. In addition, *Coeur et al.* [1997] observed that $\sim 70\%$ of sabinene isomerizes to other monoterpenes of lower ring tension when it is sampled onto Tenax TA or Carboxen

sorbents. Sabinic acid may undergo similar isomerization to pinic acid on particle surfaces.

As the chemical structures of the two unique products, S₈ and S₁₂, in the sabinene/O₃ reaction remain uncertain, we do not attempt to propose formation mechanisms for them.

A.1.6.3 α -Pinene / O₃ and Δ^3 -carene / O₃

The formation mechanisms of products from ozone oxidation of α -pinene have been described in an earlier paper [Yu *et al.*, 1998]. Here we only discuss the formation pathways for the newly identified products (Figure A.1.16). The formation of A₃ arises from isomerization of the Criegee biradical, known as the ester channel [Atkinson, 1997]. Hydroxy pinonic acid is postulated to result from its aldehyde precursor, 10-hydroxy-pinonaldehyde (A₁₂). We do not yet attempt to propose formation mechanism for A₁₁, A₁₃ and A₁₄, as their chemical structures are not yet known.

The formation pathways for most of the products in the Δ^3 -carene/O₃ reaction (Figure A.1.17) are similar to those in the α -pinene/O₃ reaction, as a result of the internal C=C bond common to both reactants. Those products unique to the Δ^3 -carene/O₃ reaction do not have obvious routes of formation. The presence of pinic acid in the Δ^3 -carene/O₃ reaction system may derive from similar routes to those responsible for the formation of pinic acid in the sabinene/ O₃ reaction system.

A.1.7. Summary and Conclusions

This study has identified a substantial fraction of the particulate products from ozone oxidation of each of the four monoterpenes: α -pinene, β -pinene, Δ^3 -carene, and sabinene. β -Pinene and sabinene are structurally analogous in that both are bicyclic and

have an external unsaturated bond where ozone oxidation takes place. α -Pinene and Δ^3 -carene also share one common structural moiety, an internal unsaturated bond. A number of analogous product pairs, including major products, have been identified for each pair of monoterpenes. These products are consistent with the established understanding of the mechanism of ozone-alkene reactions. In addition to expected products, a number of products having minor yields that are unique to each monoterpene have also been detected. One interesting finding that is yet to be explained is the presence of pinic acid in both the sabinene/O₃ and Δ^3 -carene/O₃ reactions.

Yields of individual products in both the gas and aerosol phases have been determined or estimated, thus providing a direct measure of the gas-particle partitioning of each product. The identified products account for a significant fraction of the secondary organic aerosol for each of the parent hydrocarbons. Identified products, in both gas and aerosol phases, are estimated to account for about 34-50%, 57%, 29-67%, and 24% of the total reacted carbon mass for β -pinene, sabinene, α -pinene, and Δ^3 -carene, respectively. Whereas these percentages exceed those of previous studies, a significant fraction of the monoterpenes reacted still remains unaccounted for. As the yields of many products are estimated using the response factor of surrogates, an improved mass balance awaits authentic standards or new analytical techniques that do not require authentic standards. Based on experimentally measured gas-particle partitioning coefficients of individual oxidation products, it is possible to evaluate the extent to which overall aerosol yields observed in smog chamber experiments can be represented by the stoichiometric yields and gas-particle partitioning of the individual products.

Based on the nature and yield of various aerosol components, products such as pinic acid, pinonic acid, norpinonic acid, hydroxy pinonic acid, and hydroxy pinonaldehydes can act as molecular markers for secondary organic aerosol derived from biogenic sources.

A.1.8 References

- Alvarado, A., E.C. Tuazon, S.M. Aschmann, R. Atkinson, and J. Arey, Products of the gas-phase reactions of O(³P) atoms and O₃ with α-pinene and 1,2-dimethyl-1-cyclohexene, *J. Geophys. Res.*, *103*, 25,541-25,551, 1998.
- Arey, J., R. Atkinson, and S.M. Aschmann, Product study of the gas-phase reactions of monoterpenes with the OH radical in the presence of NO_x, *J. Geophys. Res.*, *95*, 18,539-18,546, 1990.
- Atkinson, R., Gas-phase tropospheric chemistry of volatile organic compounds: 1. alkanes and alkenes, *J. Phys. Chem. Ref. Data*, *26*, 215-290, 1997.
- Atkinson, R., and W.P.L. Carter, Kinetics and mechanisms of the gas-phase reactions of ozone with organic compounds under atmospheric conditions, *Chem. Rev.*, *84*, 437-470, 1984.
- Calogirou, A., B.R. Larsen, and D. Kotzias, Gas phase terpene oxidation products: A review, *Atmos. Environ.*, *33*, 1423-1439, 1999.
- Chameides, W. L., R.W. Lindsay, J. Richardson, and C.S. Kiang, The role of biogenic hydrocarbons in urban photochemical smog: Atlanta as a case study, *Science*, *241*, 1473-1475, 1988.
- Chew, A. A., and R. Atkinson, OH radical formation yields from the gas-phase reaction of O₃ with alkenes and monoterpenes, *J. Geophys. Res.*, *101*, 28,649-28,653, 1996.

- Christoffersen, T. S., J. Hjorth, O. Horie, N.R. Jensen, D. Kotzias, L.L. Molander, P. Neeb, L. Ruppert, R. Winterhalter, A. Virkkula, K. Wirtz, and B.R. Larsen, *cis*-Pinic acid, a possible precursor for organic aerosol formation from ozonolysis of α -pinene, *Atmos. Environ.*, **32**, 1657-1961, 1998.
- Coeur, C., V. Jacob, I. Denis, and P. Foster, Decomposition of α -pinene and sabinene on solid sorbents, Tenax TA, and Carboxen, *J. Chromatogr.*, **786**, 185-187, 1997.
- Glasius, M., M. Duane, and B.R. Larsen, Analysis of polar terpene oxidation products in aerosols by liquid chromatography ion trap mass spectrometry (MS^n), *J. Chromatogr.*, **833**, 121-135, 1999.
- Glasius, M., M. Lahaniati, A. Calogirou, D. DiBella, N.R. Jensen, J. Hjorth, M. Duane, D. Kotzias, and B.R. Larsen, Carboxylic acids in secondary aerosols from O_3 and OH oxidation of cyclic monoterpenes, In Proceedings of the fifth EUROTRAC Symposium, Garmish-Partenkirchen, March 23-27, 1998.
- Griffin, R. J., D.R. Cocker III, R.C. Flagan, and J.H. Seinfeld, Organic aerosol formation from the oxidation of biogenic hydrocarbon, *J. Geophys. Res.*, **104**, 3555-3567, 1999.
- Grosjean, D., Wall loss of gaseous pollutants in outdoor Teflon chamber, *Environ. Sci. Technol.*, **19**, 1059-1065, 1985.
- Grosjean, D., E.L. William II, E. Grosjean, J.M. Andino, and J.H. Seinfeld, Atmospheric oxidation of biogenic hydrocarbons: reaction of ozone with β -pinene, D-limonene and *trans*-caryophyllene, *Environ. Sci. Technol.*, **27**, 2754-2758, 1993.
- Guenther, A., C.N. Hewitt, D. Erickson, R. Fall, C. Geron, T. Graedel, P. Harley, L. Klinger, and M. Lerdau, A global model of natural volatile organic compound emissions, *J. Geophys. Res.*, **100**, 8873-8892, 1995.

- Gundel, L.A., V.C. Lee, K.R.R. Mahanama, R.K. Stevens, and J.M. Daisey, Direct determination of the phase distributions of semi-volatile polycyclic aromatic hydrocarbons using annular denuders, *Atmos. Environ.*, **29**, 1719-1733, 1995.
- Hakola, H., J. Arey, S.M. Aschmann, and R. Atkinson, Product formation from the gas-phase reactions of OH radicals and O₃ with a series of monoterpenes, *J. Atmos. Chem.*, **18**, 75-102, 1994.
- Hallquist, M., I. Wängberg, and E. Ljungström, Atmospheric fate of carbonyl oxidation products originating from α -pinene and Δ^3 -carene: Determination of rate of reaction with OH and NO₃ radicals, UV absorption cross sections, and vapor pressure, *Environ. Sci. Technol.*, **31**, 3166-3172, 1997.
- Hart, K. M., and J.F. Pankow, High-volume air sampler for particle and gas sampling. 2. Use of backup filters to correct for the adsorption of gas-phase polycyclic aromatic hydrocarbons to the front filter, *Atmos. Environ.*, **28**, 655-661, 1994.
- Hatakeyama, S., K. Izumi, T. Fukuyama, and H. Akimoto, Reactions of ozone with α -pinene and β -pinene in air: Yields of gaseous and particulate products, *J. Geophys. Res.*, **94**, 13,013-13,024, 1989.
- Hoffmann, T., R. Bandur, U. Marggraf, and M. Linscheid, Molecular composition of organic aerosols formed in the α -pinene/O₃ reaction: Implication for new particle formation processes, *J. Geophys. Res.*, **103**, 25,569-25,578, 1998.
- Hoffmann, T., J.R. Odum, F. Bowman, D. Collins, D. Klockow, R.C. Flagan, and J.H. Seinfeld, Formation of organic aerosols from the oxidation of biogenic hydrocarbons, *J. Atmos. Chem.*, **26**, 189-222, 1997.
- Hull, L.A., Terpene ozonolysis products, in J.J. Bufalini and R.R. Arnts (eds),

Atmospheric Biogenic Hydrocarbons Vol. 2, Ambient Concentrations and

Atmospheric Chemistry, Ann Arbor Science, Ann Arbor, 161-185, 1981.

Jang, M., and R.M. Kamens, Newly characterized products and composition of secondary aerosols from the reaction of α -pinene with ozone, *Atmos. Environ.*, **33**, 459-474, 1998.

Kamens, R.M., H.E. Jeffries, M.W. Gery, R.W. Wiener, K.G. Sexton, and G.B. Howe, The impact of α -pinene on urban smog formation: an outdoor smog chamber study, *Atmos. Environ.*, **15**, 969-981, 1981.

Larsen, B.R., M. Lahaniati, A. Calogirou, and D. Kotzias, Atmospheric oxidation products of terpenes: a new nomenclature, *Chemosphere*, **37**, 1207-1220, 1998.

LeLacheur, R.M., L.B. Sonnenberg, P.C. Singer, R.F. Christman, and M.J. Charles, Identification of carbonyl compounds in environmental samples, *Environ. Sci. Technol.*, **27**, 2745-2753, 1993.

Martinez, R.I., and J.T. Herron, Stopped-flow studies of the mechanisms of ozone-alkene reactions in the gas-phase: Tetramethylethylene, *J. Phys. Chem.*, **91**, 946-953, 1987.

Martinez, R.I., and J.T. Herron, Stopped-flow studies of the mechanisms of ozone-alkene reactions in the gas phase: *trans*-2-Butene, *J. Phys. Chem.*, **92**, 4644-4648, 1988.

McDow, S.R., and J.J. Huntzicker, Vapor adsorption artifact in the sampling of organic aerosol: Face velocity effects, *Atmos. Environ.*, **24A**, 2563-2571, 1990.

Moortgat, G.K., B. Veyret, and R. Lesclaux, Kinetics of the reaction of HO₂ with CH₃C(O)O₂ in the temperature range 253-368K, *Chem. Phys. Lett.*, **160**, 443-447, 1989.

Niki, H., P.D. Maker, C.M. Savage, and L.P. Breitenbach, FTIR study of the kinetics and

- mechanism for Cl-atom-initiated reactions of acetaldehyde, *J. Phys. Chem.*, **89**, 588-591, 1985.
- Niki, H., P.D. Maker, C.M. Savage, L.P. Breitenbach, and M.D. Hurley, FTIR spectroscopic study of the mechanism for the gas-phase reaction between ozone and tetramethylethylene, *J. Phys. Chem.*, **91**, 941-946, 1987.
- Odum, J.R., T. Hoffmann, F. Bowman, D. Collins, R.C. Flagan, and J.H. Seinfeld, Gas/particle partitioning and secondary organic aerosol yields, *Environ. Sci. Technol.*, **30**, 2580-2585, 1996.
- Odum, J.R., T.P.W. Jungkamp, R.J. Griffin, R.C. Flagan, and J.H. Seinfeld, The atmospheric aerosol-forming potential of whole gasoline vapor, *Science*, **276**, 96-99, 1997a.
- Odum, J.R., T.P.W. Jungkamp, R.J. Griffin, H.J.L. Forstner, R.C. Flagan, and J.H. Seinfeld, Aromatics, reformulated gasoline, and atmospheric organic aerosol formation, *Environ. Sci. Technol.*, **31**, 1890-1897, 1997b.
- Palen, E.J., D.T. Allen, S.N. Pandis, S.E. Paulson, J.H. Seinfeld, and R.C. Flagan, Fourier transformation infrared analysis of aerosol formed in the photooxidation of isoprene and β -pinene, *Atmos. Environ.*, **26A**, 1239-1251, 1992.
- Pandis, S.N., S.E. Paulson, J.H. Seinfeld, and R.C. Flagan, Aerosol formation in the photooxidation of isoprene and β -pinene, *Atmos. Environ.*, **25A**, 997-1008, 1991.
- Pankow, J. F., Review and comparative analysis of the theories on partitioning between the gas and aerosol particulate phases in the atmosphere, *Atmos. Environ.*, **21**, 2275-2283, 1987.
- Pio, C.A., and A.A. Valente, Atmospheric fluxes and concentrations of monoterpenes in

resin-tapped pine forest, *Atmos. Environ.*, 32, 683-691, 1998.

Rechsteiner, C.E., Jr., Boiling Point, in Lyman, W.J., Reehl, W.F., and Rosenblatt, D.H. (eds), *Handbook of Chemical Property Estimation Methods*, American Chemical Society, Washington D.C., 1990.

Schwarzenbach, R.P., P.M. Gschwend, and D.M. Imboden, *Environmental Organic Chemistry*, John Wiley & Sons, New York, 70-75, 1993.

Wang, S-C., S.E. Paulson, D. Grosjean, R.C. Flagan, and J.H. Seinfeld, Aerosol formation and growth in atmospheric organic/NO_x systems- I. Outdoor smog chamber studies of C₇- and C₈-hydrocarbons, *Atmos. Environ.*, 26A, 403-420, 1992.

Yu, J., R.C. Flagan, and J.H. Seinfeld. Identification of Products Containing -COOH, -OH, and -C=O in atmospheric oxidation of hydrocarbons, *Environ. Sci. Technol.*, 32, 2357-2370, 1998.

Yu, J., H.E. Jeffries, and R.M. LeLacheur, Identifying airborne carbonyl compounds in isoprene atmospheric photooxidation products by their PFBHA oximes using gas chromatography/ion trap mass spectrometry, *Environ. Sci. Technol.*, 29, 1923-1932, 1995.

Zhang, S-H, M. Shaw, J.H. Seinfeld, and R.C. Flagan, Photochemical aerosol formation from α -pinene and β -pinene, *J. Geophys. Res.*, 97, 20,717-20,729, 1992.

Table A.1.1. Initial conditions and results of ozone-terpene reactions.

HC	Date	<i>T</i> (K)	O ₃ initial ppbv	HC initial ppbv	HC final ppbv	ΔHC ppbv	Sample start time (min)	Δ <i>M</i> _o μg m ⁻³	Aerosol yield
α-pinene	6/9/98a	308	237	59.2	2.2	57.0	291	54.2	0.176
	6/9/98b	308	269	67.2	2.1	65.1	339	65.1	0.186
	6/17/98a	306	74	107.1	62.0	45.1	53	38.8	0.159
β-pinene	6/11/98b	307	352	87.9	10.0	77.9	388	18.9	0.045
	6/17/98b	306	56	104.6	79.8	24.8	303	11.2	0.083
Δ ³ -carene	6/15/98b	306	360	89.9	0.4	89.5	299	63.3	0.130
sabinene	6/15/98a	306	370	92.4	0.0	92.4	232	17.6	0.035

Table A.1.2. Denuder and filter collection efficiencies of selected products.

Compound	Collection efficiency (%)	
	denuder	filter
pinic acid	98.7 ± 0.2	0.85
2,2-dimethyl-3-formyl-cyclobutyl methanoic acid	97.1 ± 1.9	NA*
norpinonic acid	94.0 ± 4.0	NA
pinonic acid	97.8 ± 1.3	0.59
norpinonaldehyde	95.8 ± 1.0	0.89
pinonaldehyde	97.7 ± 0.5	0.95

* Not available.

Table A.1.3. Relative recoveries of select multifunctional compounds vs. recovery standard.

Compound	Denuder samples	Filter samples
	N=6*	N=5*
pinic acid	0.66±0.04	0.80±0.07
pinonic acid	0.67±0.19	0.74±0.14
2-hydroxy-cyclohexanone	0.64±0.10	0.74±0.07
5-methyl-1,3-cyclohexanedione	0.41±0.06	0.61±0.08
5-isopropyl-1,3-cyclohexanedione	0.44±0.04	0.63±0.10
7-oxo-octanoic acid	0.66±0.12	0.83±0.07
heptanedioic acid	0.69±0.05	0.77±0.17
octanedioic acid	0.59±0.05	0.82±0.14

* Number of experiments conducted.

Table A.1.4. Products from ozone oxidation of β -pinene.

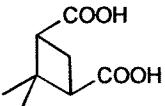
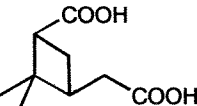
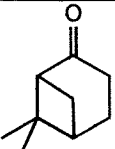
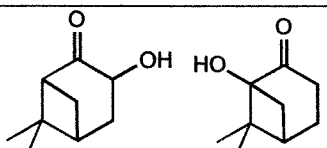
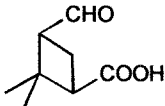
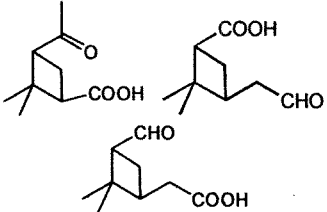
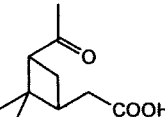
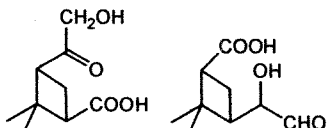
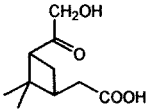
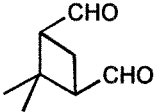
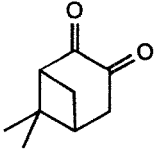
Name	Structure	Pseudo-molecular ions in CI mass spectrum
P ₁ : C ₈ H ₁₂ O ₄ norpinic acid MW=172 deri. MW=316 [‡]		M+73: 389 M+1: 317 M-15: 301 M-89: 227 M-117: 199
P ₂ : C ₉ H ₁₄ O ₄ [*] pinic acid MW=186 deri. MW=330		M+73: 403 M+1: 331 M-15: 315 M-89: 241
P ₃ : C ₉ H ₁₄ O [*] nopinone MW=138 deri. MW=333		M+181: 514 M+29: 362 M+1: 334 M-181: 152 M-197: 136
P ₄ : C ₉ H ₁₄ O ₂ hydroxy pina ketone MW=154 deri. MW=421		M+181: 602 M+1: 422 M-15: 406 M-89: 332 M-197: 224
P ₅ : C ₈ H ₁₂ O ₃ 2,2-dimethyl-3-formyl- cyclobutyl-methanoic acid MW=156 deri. MW=423		M+73: 496 M+1: 424 M-15: 408 M-89: 334 M-117: 306 M-181: 242 M-197: 226
P ₆ : C ₉ H ₁₄ O ₃ norpinonic acid and its isomers MW=170 deri. MW=437		M+73: 510 M+1: 438 M-15: 422 M-89: 348 M-117: 320 M-181: 256 M-197: 240
P ₇ : C ₁₀ H ₁₆ O ₃ [*] pinonic acid MW=184 deri. MW=451		M+73: 524 M+1: 452 M-89: 362 M-181: 270 M-197: 254 M-238: 213
P ₈ : C ₉ H ₁₄ O ₄ hydroxy norpinonic acids MW=186 deri. MW=525	e.g. 	M+73: 598 M+1: 526 M-15: 510 M-89: 436 M-181: 344 M-197: 328

Table A.1.4. (continued) Products from ozone oxidation of β -pinene.

Name	Structure	Pseudo-molecular ions in CI mass spectrum
P ₉ : C ₁₀ H ₁₆ O ₄ hydroxy pinonic acid MW=200 deri. MW=539		M+73: 612 M+1: 540 M-15: 524 M-89: 450 M-181: 358 M-197: 342 M-326: 213
P ₁₀ : C ₈ H ₁₂ O ₂ 2,2-dimethyl-cyclobutane- 1,3-dicarboxaldehyde MW=140 deri. MW=530		M+1: 530 M-181: 349 M-197: 333 M-224: 306
P ₁₁ : C ₉ H ₁₂ O ₂ 3-oxo-pina ketone MW=152 deri. MW=542 mono-deri. MW=347		M+29: 571 M+1: 543 M-197: 345

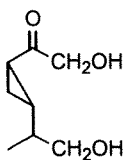
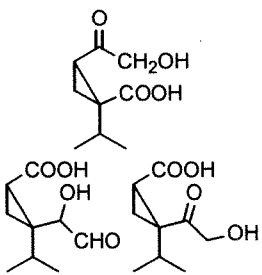
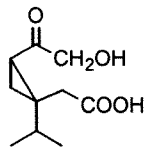
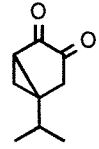
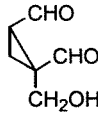
[†] deri. denotes derivative.

* identification confirmed with an authentic standard.

Table A.1.5. Products from ozone oxidation of sabinene.

Name	Structure	Pseudo-molecular ions in CI mass spectrum
S ₁ : C ₈ H ₁₂ O ₄ MW=186 deri. MW=330		M+73: 389 M+1: 317 M-15: 301 M-89: 227 M-117: 199
S ₂ : C ₉ H ₁₄ O ₄ sabinic acid MW=186 deri. MW=330		M+73: 430 M+1: 331 M-15: 315 M-89: 241 M-117: 225
S ₃ : C ₉ H ₁₄ O ₄ pinic acid MW=186 deri. MW=330		M+73: 403 M+1: 331 M-15: 315 M-89: 241
S ₄ : C ₉ H ₁₄ O sabina ketone MW=138 deri. MW=333		M+181: 514 M+29: 362 M+1: 334 M-181: 152 M-197: 136
S ₅ : C ₈ H ₁₂ O ₃ 2-(2-isopropyl)-2-formyl- cyclopropyl-methanoic acid MW=156 deri. MW=423		M+73: 496 M+1: 424 M-15: 408 M-89: 334 M-181: 242 M-197: 226
S ₆ : C ₉ H ₁₄ O ₂ hydroxy sabina ketones MW=154 deri. MW=421		M+181: 602 M+1: 422 M-15: 406 M-89: 332 M-197: 224 M-212: 210
S ₇ : C ₉ H ₁₄ O ₃ norsabinonic acid and its isomers MW=170 deri. MW=437		M+197: 634 M+181: 618 M+73: 510 M+1: 438 M-15: 422 M-89: 348 M-197: 240

Table A.1.5. (continued) Products from ozone oxidation of sabinene.

Name	Structure	Pseudo-molecular ions in CI mass spectrum
<p>S₈: C₈H₁₂O₃</p> <p>MW=156</p> <p>deri. MW=495</p>	<p>e.g.</p> 	<p>M+89: 584 M+1: 496</p> <p>M+29: 524 M-15: 480</p> <p>M-89: 406 M-147: 348</p> <p>M-197: 298</p>
<p>S₉: C₉H₁₄O₄</p> <p>hydroxy norsabinonic acid</p> <p>MW=186</p> <p>deri. MW=525</p>	<p>e.g.</p> 	<p>M+73: 598 M+1: 526</p> <p>M-15: 510 M-89: 436</p> <p>M-197: 328</p>
<p>S₁₀: C₁₀H₁₆O₄</p> <p>MW=200</p> <p>deri. MW=539</p>	<p>e.g.</p> 	<p>M+73: 612 M+1: 540</p> <p>M-15: 524 M-89: 450</p> <p>M-181: 358 M-197: 342</p>
<p>S₁₁: C₉H₁₂O₂</p> <p>3-oxo-sabina ketone</p> <p>MW=152</p> <p>deri. MW=542</p>		<p>M+29: 571 M+1: 543</p> <p>M-197: 345</p>
<p>S₁₂: C₆H₈O₃</p> <p>MW=128</p> <p>deri. MW=590</p>	<p>e.g.</p> 	<p>El spectrum</p> <p>M: 590 M-15: 575</p> <p>M-181: 409 M-197: 393</p>

* identification confirmed with an authentic standard.

Table A.1.6. Products from ozone oxidation of α -pinene.

Product	Structure	Product	Structure
A ₁ : C ₈ H ₁₂ O ₄ norpinic acid MW=172 deri. MW=316		A ₈ : C ₈ H ₁₂ O ₂ 2,2-dimethyl- cyclobutyl-1,3- dicarboxaldehyde MW=140	
A ₂ : C ₉ H ₁₄ O ₄ * pinic acid MW=186 deri. MW=330		A ₉ : C ₉ H ₁₄ O ₂ norpinonaldehyde MW=154 deri. MW=544	
A ₃ : C ₁₀ H ₁₆ O ₃ (2,2-dimethyl-3-acetyl)- cyclobutyl formate MW=184 deri. MW=379		A ₁₀ : C ₁₀ H ₁₆ O ₂ pinonaldehyde MW=168 deri. MW=558	
A ₄ : C ₈ H ₁₂ O ₃ 2,2-dimethyl-3-formyl- cyclobutyl-methanoic acid MW=156 deri. MW=423		A ₁₁ : C ₁₁ H ₁₈ O ₂ MW=182 deri. MW=572	two carbonyl groups
A ₅ : C ₉ H ₁₄ O ₃ norpinonic acid and isomer MW=170 deri. MW=437		A ₁₂ : C ₁₀ H ₁₆ O ₃ hydroxy pinonaldehydes MW=184 deri. MW=646	
A ₆ : C ₁₀ H ₁₆ O ₃ * pinonic acid MW=184 deri. MW=451		A ₁₃ MW=198 deri. MW=588	two carbonyl groups
A ₇ : hydroxy pinonic acid MW =200 deri. MW=539		A ₁₄ : C ₁₀ H ₁₄ O ₃ MW=198 deri. MW=660	e.g.

* identification confirmed with an authentic standard.

Table A.1.7. Products from ozone oxidation of Δ^3 -carene.

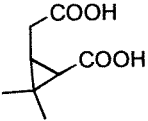
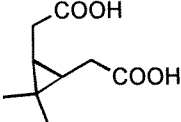
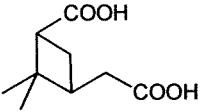
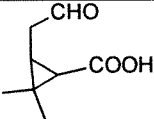
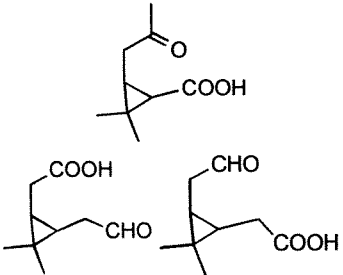
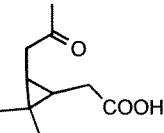
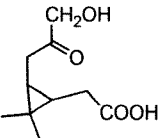
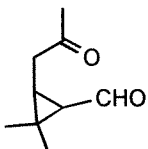
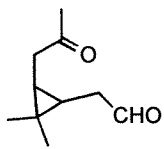
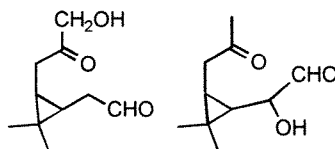
Product	Structure	Pseudo-molecular ions in CI mass spectrum
C ₁ : C ₈ H ₁₂ O ₄ nor-3-caric acid MW=172 deri. MW=316		M+1: 317 M-15: 301 M-89: 227 M-117: 199
C ₂ : C ₉ H ₁₄ O ₄ 3-caric acid MW=186 deri. MW=330		M+147: 477 M+73: 403 M+29: 359 M+1: 331 M-15: 315 M-89: 241 M-117: 213
C ₃ : C ₉ H ₁₄ O ₄ pinic acid* MW=186 deri. MW=330		M+73: 403 M+1: 331 M-15: 315 M-89: 241 M-117: 213
C ₄ : MW=118 deri. MW=457	one carbonyl and two OH/COOH groups	M+181: 638 M+1: 458 M-15: 442 M-89: 368 M-117: 340 M-197: 260
C ₅ : MW=142 deri. MW=337	one carbonyl group, no OH/COOH groups	M+181: 518 M+1: 338 M-17: 320 M-197: 140
C ₆ : C ₈ H ₁₂ O ₂ MW=140 deri. MW=423		M+1: 424 M-89: 334 M-197: 226
C ₇ : C ₉ H ₁₄ O ₃ 3-norcaronic acid and isomers MW=170 deri. MW=437		M+73: 510 M+1: 437 M-89: 348 M-181: 256 M-197: 240
C ₈ : C ₁₀ H ₁₆ O ₃ 3-caronic acid MW=184 deri. MW=451		M+73: 524 M+1: 452 M-89: 362 M-181: 270 M-197: 254 M-197: 254 M-211: 240

Table A.1.7. (continued) Products from ozone oxidation of Δ^3 -carene.

Product	Structure	Pseudo-molecular ions in CI mass spectrum
C_9 : $C_{10}H_{16}O_3$ hydroxy 3-caronic acid MW=184 deri. MW=539	e.g. 	M+1: 540 M-89: 450 M-197: 342
C_{10} : MW=128 deri. MW=518	two carbonyl groups, no OH/COOH groups	M+1: 519 M-181: 337 M-197: 321 M-224: 294
C_{11} : $C_9H_{14}O_2$ norcaronaldehyde MW=154 deri. MW=544		EI spectrum: M: 544 M-181: 363 M-197: 347
C_{12} : $C_{10}H_{16}O_2$ caronaldehyde MW=168 deri. MW=558		M+29: 587 M+1: 559 M-181: 377 M-197: 361 M-238: 320
C_{13} : $C_{10}H_{16}O_3$ hydroxy 3-caronic aldehydes MW=184 deri. MW=646		M+1: 647 M-197: 449

* identification confirmed with an authentic standard.

Table A.1.8. Products and their surrogates for quantification.

Standard	Products surrogated for			
	β -pinene/O ₃	sabinene/O ₃	α -pinene/O ₃	Δ^3 -carene/O ₃
pinic acid	norpinic acid	sabinic acid, norsabinic acid	norpinic acid	3-caric acid, nor-3-caric acid
pinonic acid	P ₅ , norpinonic acid and its isomers, hydroxy norpinonic acid, hydroxy pinonic acid	sabinonic acid, norsabinonic acid and its isomers, S ₈ , S ₉ , S ₁₀	A ₄ , norpinonic acid and its isomers, hydroxy pinonic acid,	3-caronic acid, nor-3-caronic acid and its isomers, C ₆ , C ₉
2-hydroxy-cyclohexanone	hydroxy pina ketones	hydroxy sabina ketones		
5-methyl-1,3-cyclohexanedione	P ₁₀ , 3-oxo-pina ketone	3-oxo-sabina ketone, S ₁₂	pinonaldehyde, norpinonaldehyde, A ₈ , A ₁₁ , hydroxy pinonaldehydes, A ₁₃ , A ₁₄	C ₁₀ , norcaronaldehyde, caronaldehyde, hydroxy caronaldehydes
nopinone		sabina ketone	A ₃	C ₅

Table A.1.9. Gaseous and particulate product yields in the β -pinene/O₃ reaction (6/11/98b).

Product	Molar yield (%)			Aerosol yield by mass (%)
	Gas	Aerosol	Total	
pinic acid	1.7	0.91	2.6	1.2
norpinic acid	0.23	0.11	0.35	0.17
pinonic acid	0.41	0.10	0.52	0.14
norpinonic acid and its isomer	4.6	1.3	5.9	1.7
hydroxy-pina-ketones	6.6	0.66	7.3	0.74
3-oxo-pina-ketone	1.8	0.02	1.8	0.02
2,2-dimethyl-cyclobutane-1,3-dicarboxaldehyde	0.35	ND	0.35	ND
nopinone	17.0	trace	17.0	trace
hydroxy norpinonic acid	0.58	0.1	0.68	0.14
hydroxy pinonic acid	0.26	0.17	0.43	0.25
total molar yield	33.5	3.4	36.9	4.4
carbon-based total yield	34.2			
Aerosol yield measured by SEMS and CNC				4.5

Table A.1.9. (continued) Gaseous and particulate product yields in the β -pinene/O₃ reaction (6/17/98b).

Product	Molar yield (%)			Aerosol yield by mass (%)
	Gas	Aerosol	Total	
pinic acid	2.5	1.2	3.7	1.6
norpinic acid	0.17	0.09	0.27	0.12
pinonic acid	0.56	0.19	0.74	0.25
norpinonic acid and its isomer	14.3	2.2	16.5	2.7
hydroxy-pina-ketones	7.9	1.1	9.0	1.3
3-oxo-pina-ketone	7.6	0.11	7.7	0.12
2,2-dimethyl-cyclobutane-1,3-dicarboxaldehyde	0.29	ND	0.29	ND
nopinone	15.8	trace	15.8	trace
hydroxy norpinonic acid	0.98	0.24	1.2	0.33
hydroxy pinonic acid	0.16	0.15	0.31	0.20
total molar yield	50.3	5.3	55.6	6.6
carbon-based total yield	50.1			
Aerosol yield measured by SEMS and CNC				8.3

Table A.1.10. Gaseous and particulate product yields in the sabinene/O₃ reaction.

Product	Molar yield (%)			Aerosol yield by mass (%)
	Gas	Aerosol	Total	
pinic acid	1.1	0.29	1.4	0.39
sabinic acid	0.80	0.39	1.2	0.53
norsabinic acid	0.18	0.07	0.25	0.09
norsabinonic acid and its isomers	3.6	1.1	4.7	1.4
hydroxy-sabina-ketones	6.6	0.43	7.0	0.53
3-oxo-sabina-ketone	0.50	0.01	0.51	0.01
S ₅ [*]	0.15	0.11	0.26	0.13
sabina ketone	46.2	0.43	46.6	0.43
S ₈ [*]	0.54	ND	0.54	ND
S ₉ [*]	0.75	ND	0.75	ND
S ₁₀ [*]	0.12	0.02	0.14	0.03
total molar yield	60.5	2.9	63.4	3.5
carbon-based total yield			57.0	
Aerosol yield measured by SEMS and CNC				3.5

* See Table A.1.5 for possible candidate structures.

Table A.1.11. Gaseous and particulate product yields in the α -pinene/O₃ reaction.

Product	Molar yield (%)									Aerosol yield		
	Gas			Aerosol			Total			(% by mass)		
Experiment	6/9a	6/9b	6/17	6/9a	6/9b	6/17	6/9a	6/9b	6/17	6/9a	6/9b	6/17
pinic acid	1.2	2.1	2.7	1.8	3.9	2.8	3.0	6.0	5.5	2.5	5.3	3.9
norpinic acid	0.04	0.03	0.04	0.08	0.09	0.05	0.1	0.1	0.09	0.1	0.1	0.06
hydroxy pinonaldehydes	1.4	0.8	9.2	2.4	1.1	2.0	3.8	1.9	11.2	3.3	1.4	2.8
pinonic acid	0.8	0.6	6.6	1.7	1.6	1.3	2.5	2.2	7.9	2.3	2.1	1.8
norpinonic acid & isomer	2.2	5.4	9.8	2.1	4.8	2.8	4.3	10.2	12.6	2.6	5.9	3.4
pinonaldehyde	9.6	5.7	18.1	0.8	0.3	0.9	10.4	6.0	19.0	1.0	0.4	1.1
nor-pinonaldehyde	1.1	1.5	2.4	0.1	0.2	0.2	1.2	1.7	2.6	0.2	0.2	0.2
2,2-dimethyl-cyclobutane-1,3-dicarboxaldehyde	0.4	0.3	1.6	ND	ND	ND	0.4	0.3	1.6	0	0	0
hydroxy pinonic acid	0.8	0.2	1.6	2.1	1.3	2.1	2.9	1.5	3.7	3.1	1.9	3.1
A ₃ *	1.5	0.6	3.8	ND	ND	ND	1.5	0.6	3.8	ND	ND	ND
A ₁₃ *	0.06	0.02	0.1	0.08	0.12	0.1	0.14	0.1	0.2	0.1	0.2	0.1
A ₁₄ *	0.03	trace	0.03	0.55	0.48	0.8	0.6	0.5	0.8	0.7	0.6	1.1
total molar yield	19.1	17.2	56.0	11.7	13.9	13.0	30.8	31.0	69.1	15.9	18.1	17.6
carbon-based total yield							29.9	29.1	66.8			
Aerosol yield measured by SEMS and CNC										17.6	18.6	15.9

* See Table A.1.6 for possible candidate structures.

Table A.1.12. Gaseous and particulate product yields in the Δ^3 -carene/O₃ reaction.

	Molar yield (%)			Aerosol yield
Product	Gas	Aerosol	Total	by mass (%)
pinic acid	0.83	0.33	1.2	0.46
3-caric acid	0.64	1.3	1.9	1.8
nor-3-caric acid	0.07	ND	0.07	ND
hydroxy caronaldehydes	3.0	0.19	3.2	0.25
3-caronic acid	2.7	1.5	4.2	2.1
nor-3-caronic acid and isomers	1.8	0.54	2.3	0.68
caronaldehyde	7.8	0.67	8.5	0.83
norcaronaldehyde	trace	trace	trace	trace
hydroxy 3-caronic acid	0.47	0.69	1.2	1.0
C ₄ [*]	0.31	0.39	0.70	0.54
C ₅ [*]	2.3	0.24	2.5	0.25
C ₁₀ [*]	0.22	ND	0.22	ND
total molar yield	20.1	5.9	26.0	7.9
carbon-based total yield			24.4	
Aerosol yield measured by SEMS and CNC				13.0

* See Table A.1.7 for possible candidate structures.

Table A.1.13. Gas-particle partitioning coefficients ($\text{m}^3 \mu\text{g}^{-1}$) of individual products at 306-308 K.

α -Pinene/ O_3		Δ^3 -Carene/ O_3		β -Pinene/ O_3		Sabinene/ O_3	
Compound	$K_{om, i}$	Compound	$K_{om, i}$	Compound	$K_{om, i}$	Compound	$K_{om, i}$
pinic acid	0.028 ± 0.001	3-caric acid	0.033	pinic acid	0.035 ± 0.009	sabinic acid	0.027
hydroxy pinon-aldehydes	0.019 ± 0.013	hydroxy caron-aldehydes	0.0010	hydroxy pina-ketones	0.0091 ± 0.0054	hydroxy sabina ketones	0.0037
pinonic acid	0.030 ± 0.005	3-caronic acid	0.0090				
norpinonic acid and its isomers	0.013 ± 0.005	nor-3-caronic acid	0.0047	norpinonic acid and its isomers	0.014 ± 0.001	nor-sabinonic acid and its isomers	0.018
pinon-aldehyde	0.0012 ± 0.0003	caronaldehyde	0.0014	3-oxo-pina ketone	0.0010 ± 0.0005	3-oxo-sabina ketone	0.0012
hydroxy pinonic acid	0.040 ± 0.010	hydroxy caronic acid	0.0231	hydroxy pinonic acid	0.066 ± 0.026	sabina ketone	0.00053
A_{13}	0.025 ± 0.003			hydroxy norpinonic acid	0.016 ± 0.009		

Table A.1.14. Sub-cooled liquid vapor pressure estimates.

Compound	T_b (K) ^a	Vapor pressure estimates at 306K ^b	
		mm Hg	ppmv
hydroxy pinonic acid	606	1.9×10^{-5}	0.048
pinic acid	601	5.1×10^{-5}	0.067
hydroxy pinonaldehydes	577	2.4×10^{-4}	0.32
pinonic acid	572	8.4×10^{-4}	0.45
norpinonic acid & isomers	558	8.4×10^{-4}	1.1
hydroxy pina ketone	542	2.2×10^{-3}	2.9
pinonaldehyde	530	4.4×10^{-2}	58
3-oxo-pina ketone	521	6.9×10^{-2}	91
nopinone	482	4.7×10^{-1}	620

^a T_b , boiling point at 1 atm if decomposition would not occur, estimated using Meissner's method [Reichsteiner, 1990]. T_b is needed to estimate vapor pressure. Meissner's method underestimates the T_b for each of C₅-C₁₀ *n*-alkanoic acids by ~6.5%; therefore, a correction formula is obtained by a linear regression ($r^2=0.994$) for C₅-C₁₀ *n*-alkanoic acids, and applied to the compounds of unknown T_b . This correction is also justified for carbonyl-containing compounds. For example, Meissner's method estimates that the T_b for nopinone is 453K before correction and 485K after correction, which agrees well with the experimental value 482K.

^b Sub-cooled liquid vapor pressures are estimated using a modification of the Clausius-Claperyron equation [Schwarzenbach *et al.*, 1993].

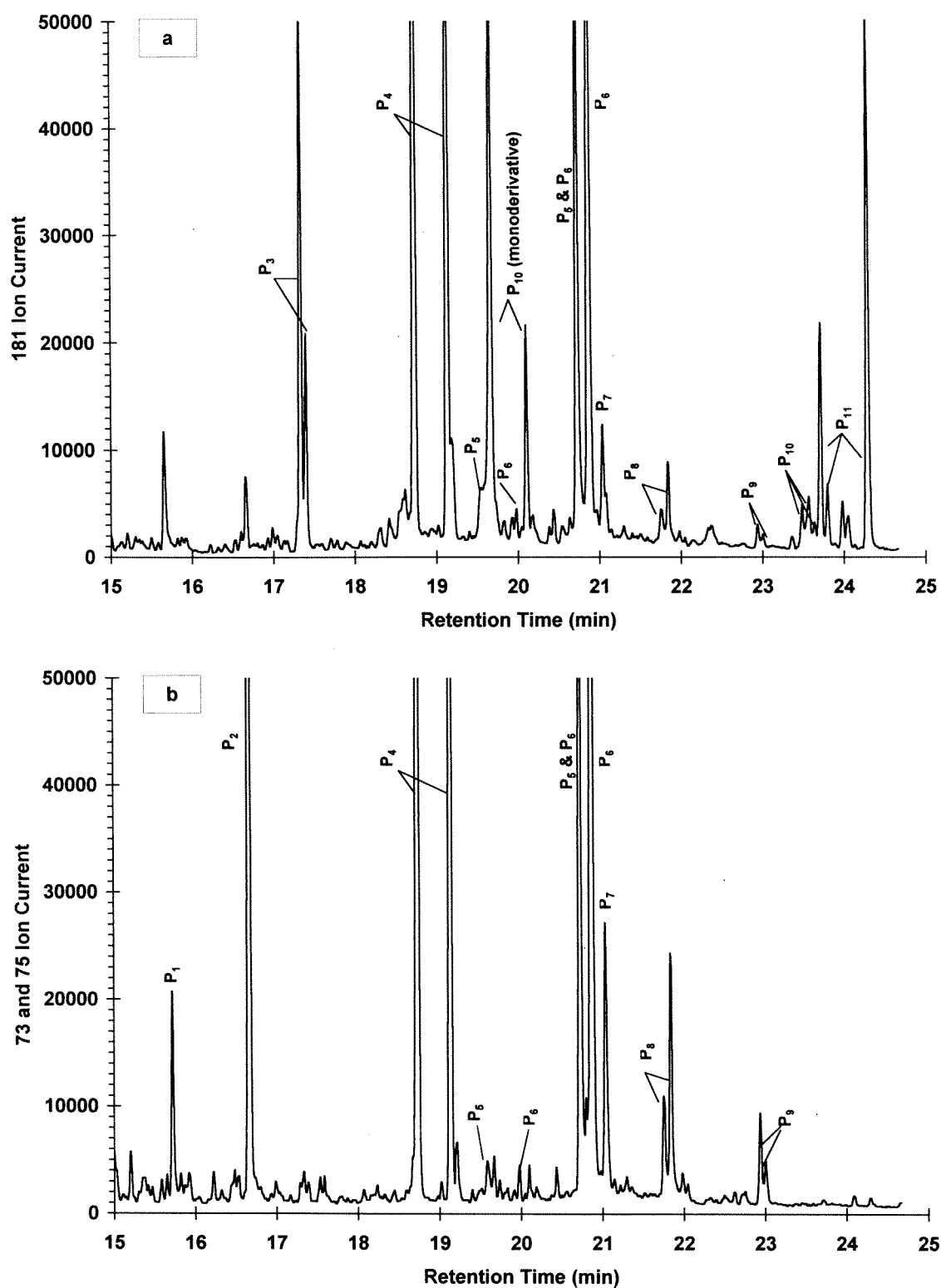


Figure A.1.1. Chromatogram of products from β -pinene/ O_3 reaction; see Table A.1.4 for peak identification. Top: Products containing carbonyl groups. Bottom: Products containing OH/COOH groups.

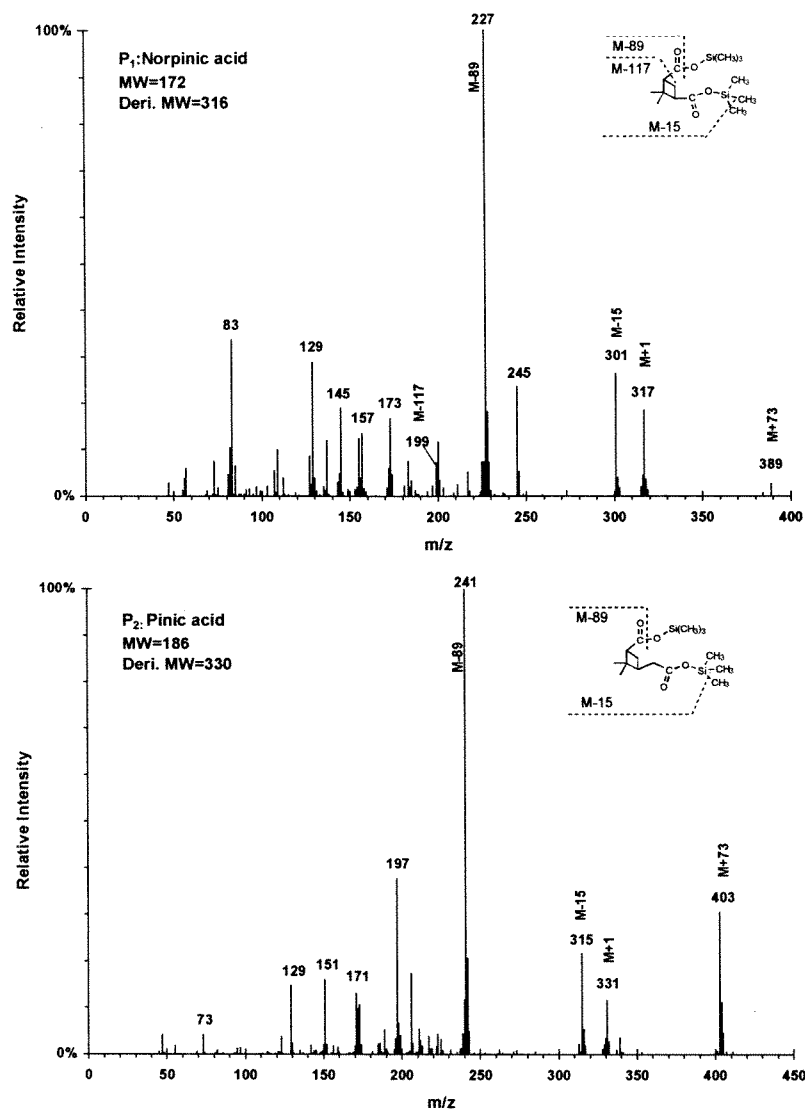


Figure A.1.2. Methane CI mass spectra for the derivatives of products from ozone oxidation of β -pinene.

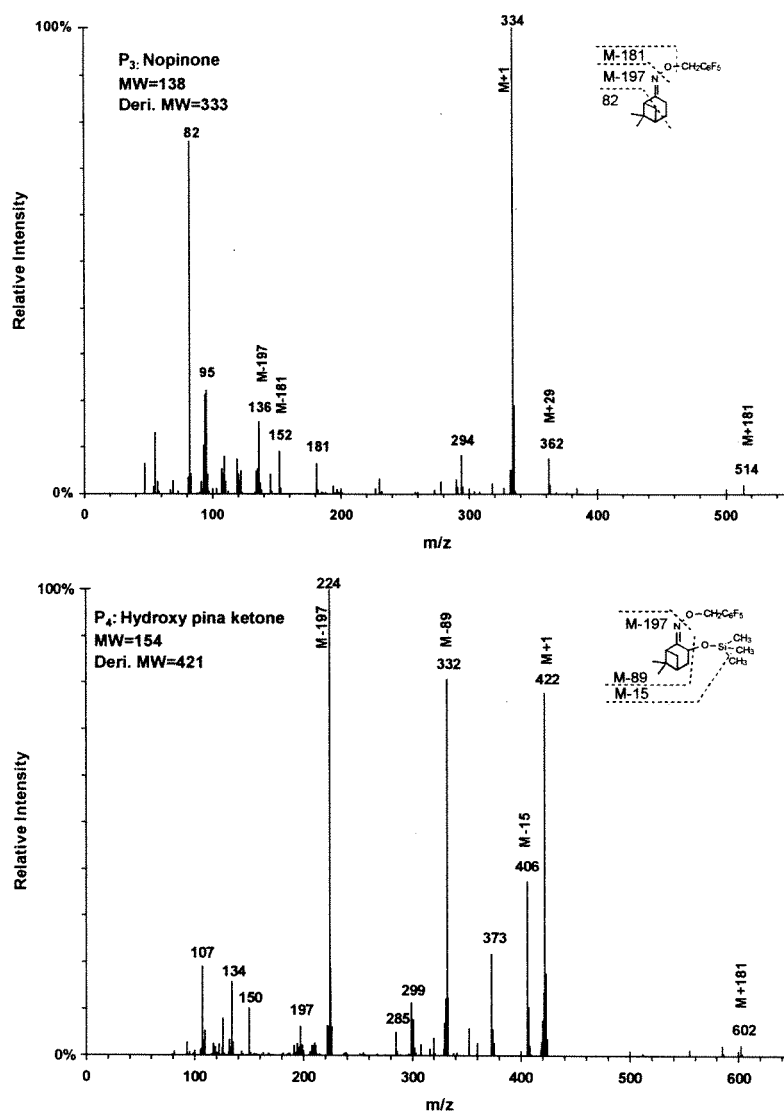


Figure A.1.2. (continued) Methane CI mass spectra for the derivatives of products from ozone oxidation of β -pinene.

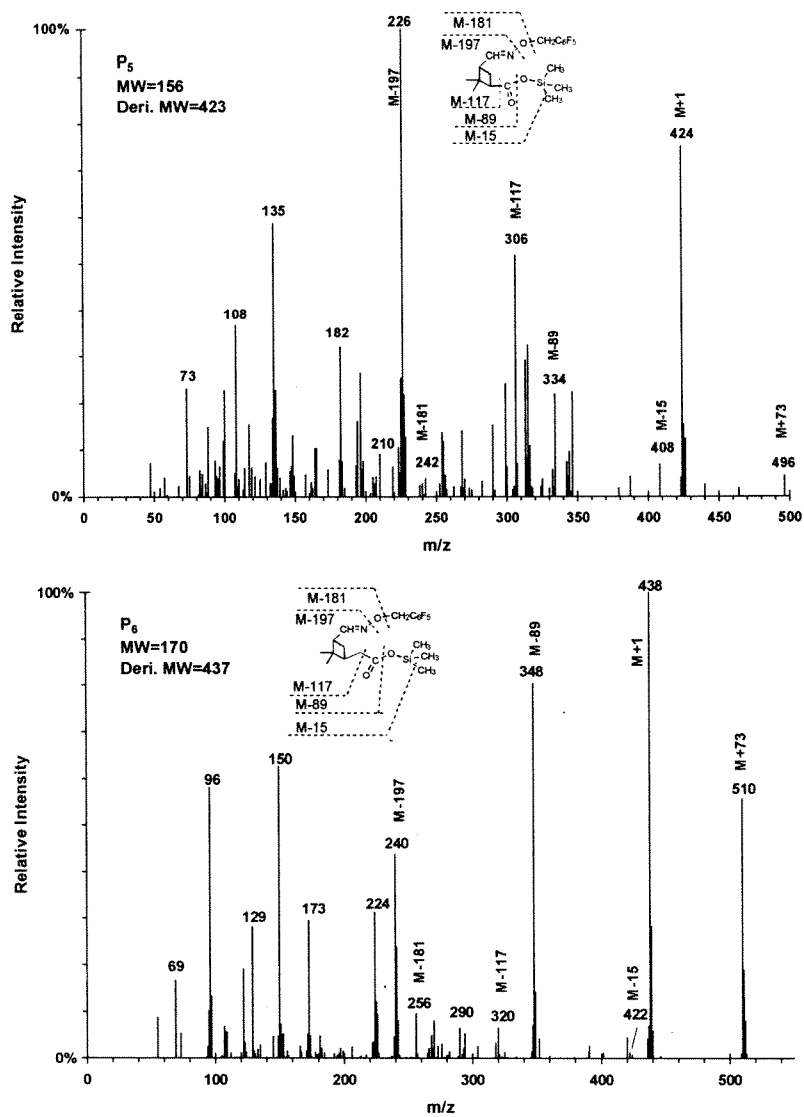


Figure A.1.2. (continued) Methane CI mass spectra for the derivatives of products from ozone oxidation of β -pinene.

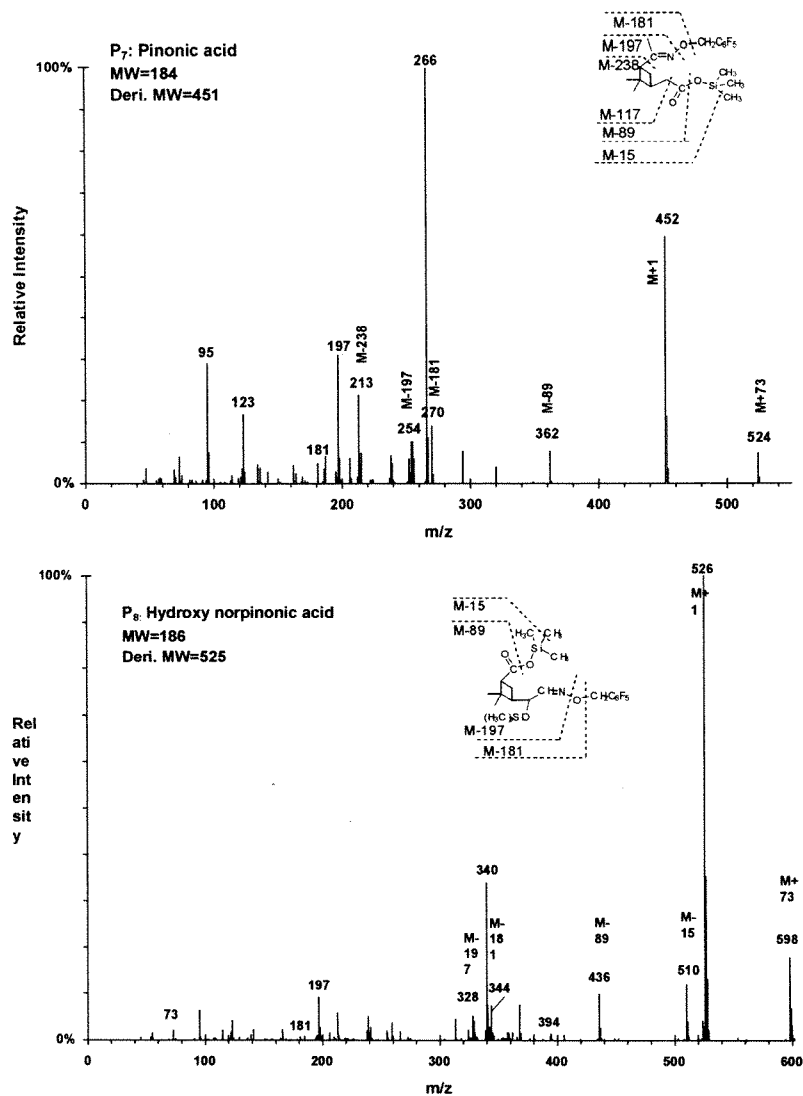


Figure A.1.2. (continued) Methane CI mass spectra for the derivatives of products from ozone oxidation of β -pinene.

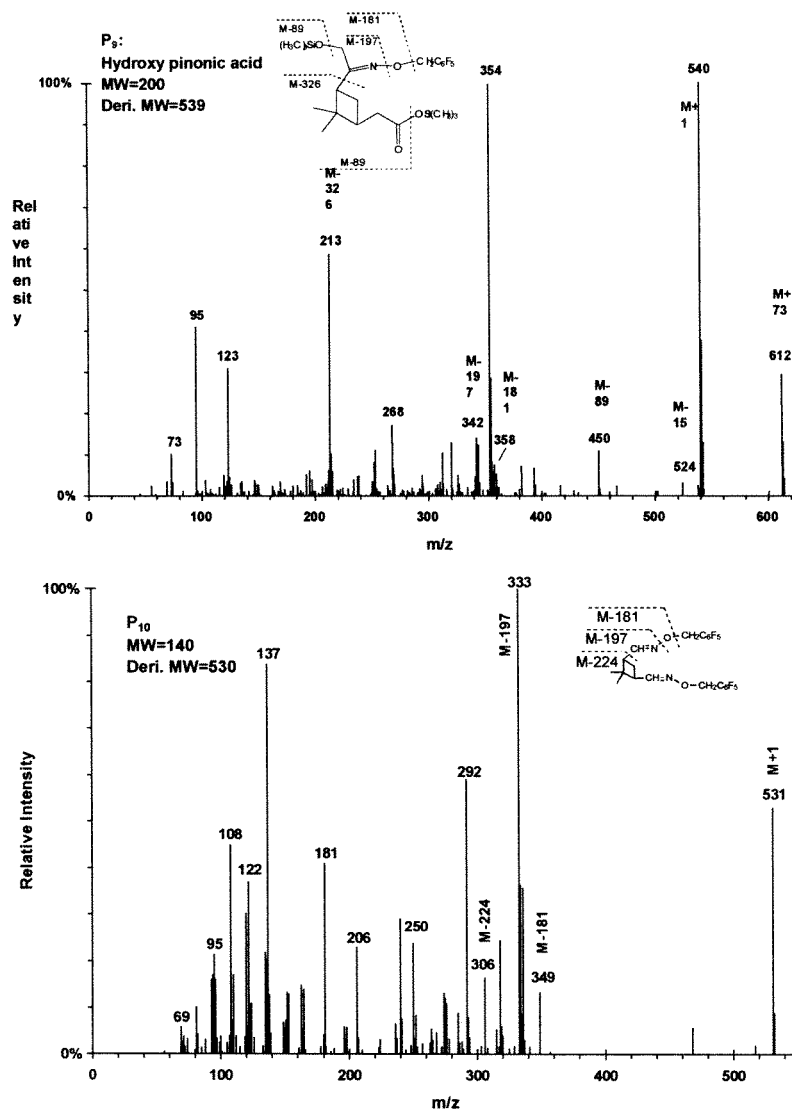


Figure A.1.2. (continued) Methane CI mass spectra for the derivatives of products from ozone oxidation of β -pinene.

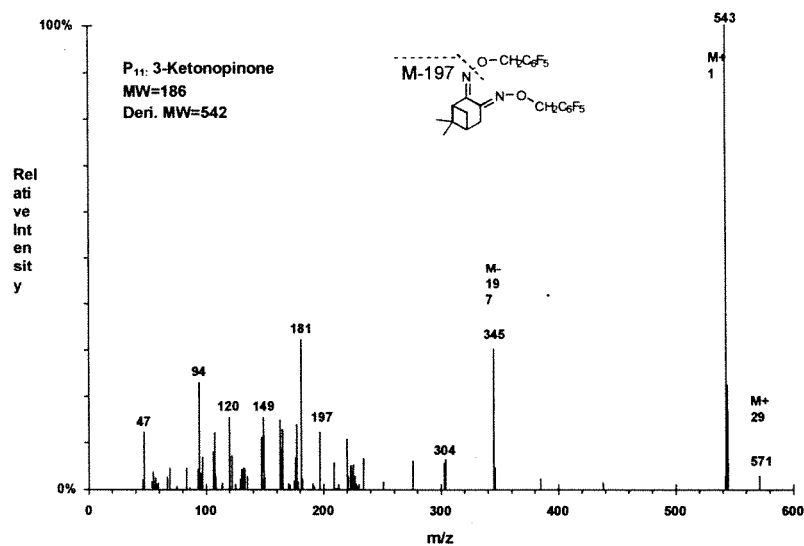


Figure A.1.2. (continued) Methane CI mass spectra for the derivatives of products from ozone oxidation of β -pinene.

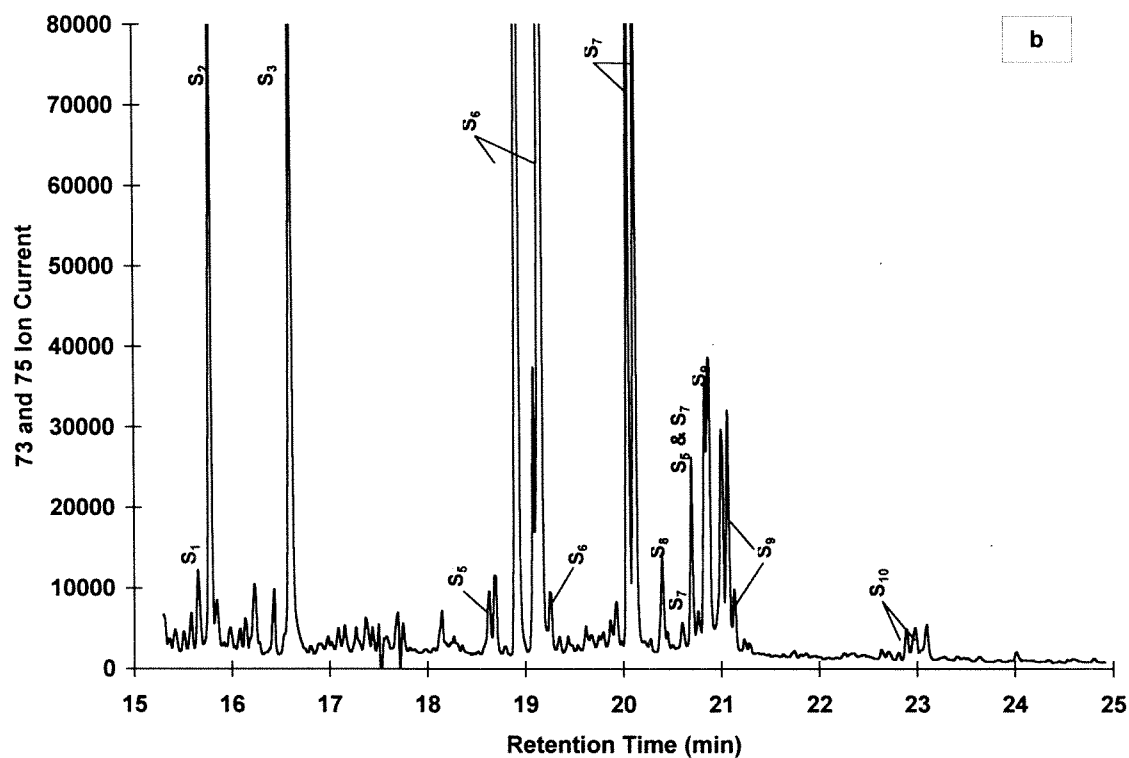
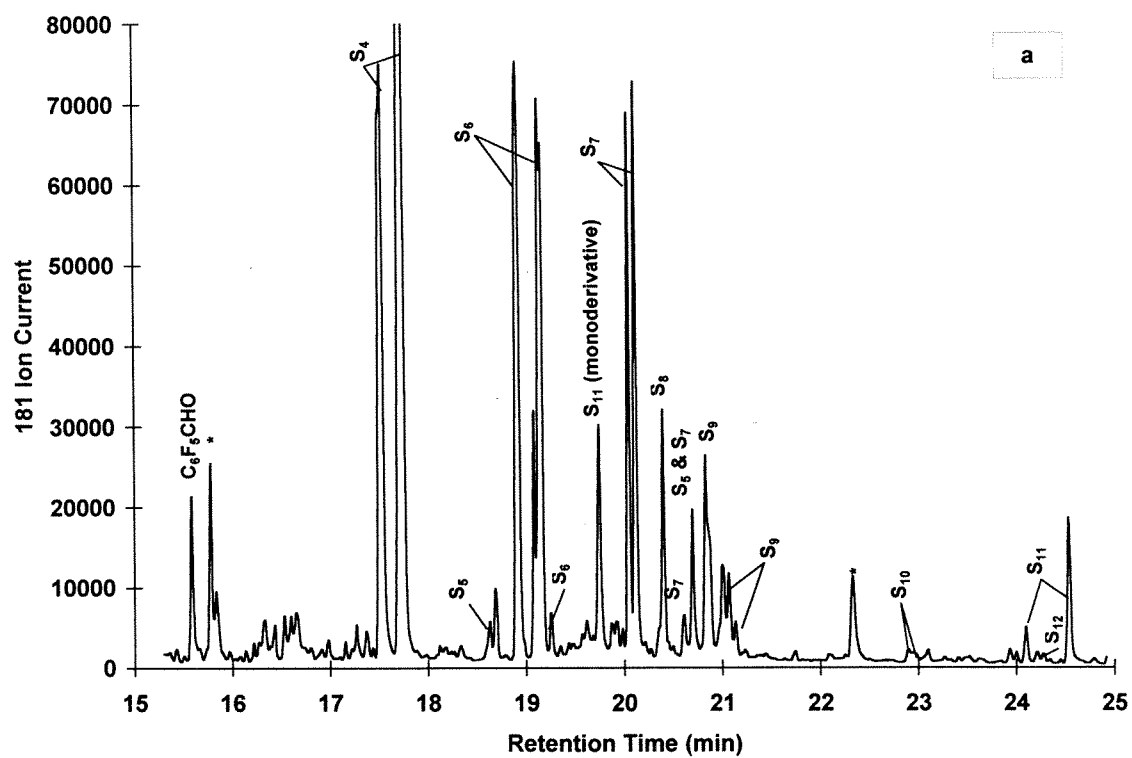


Figure A.1.3. Chromatogram of products from sabinene/O₃ reaction; see Table A.1.5 for peak identification. Top: Products containing carbonyl groups. Bottom: Products containing OH/COOH groups. (*: present in blank samples.)

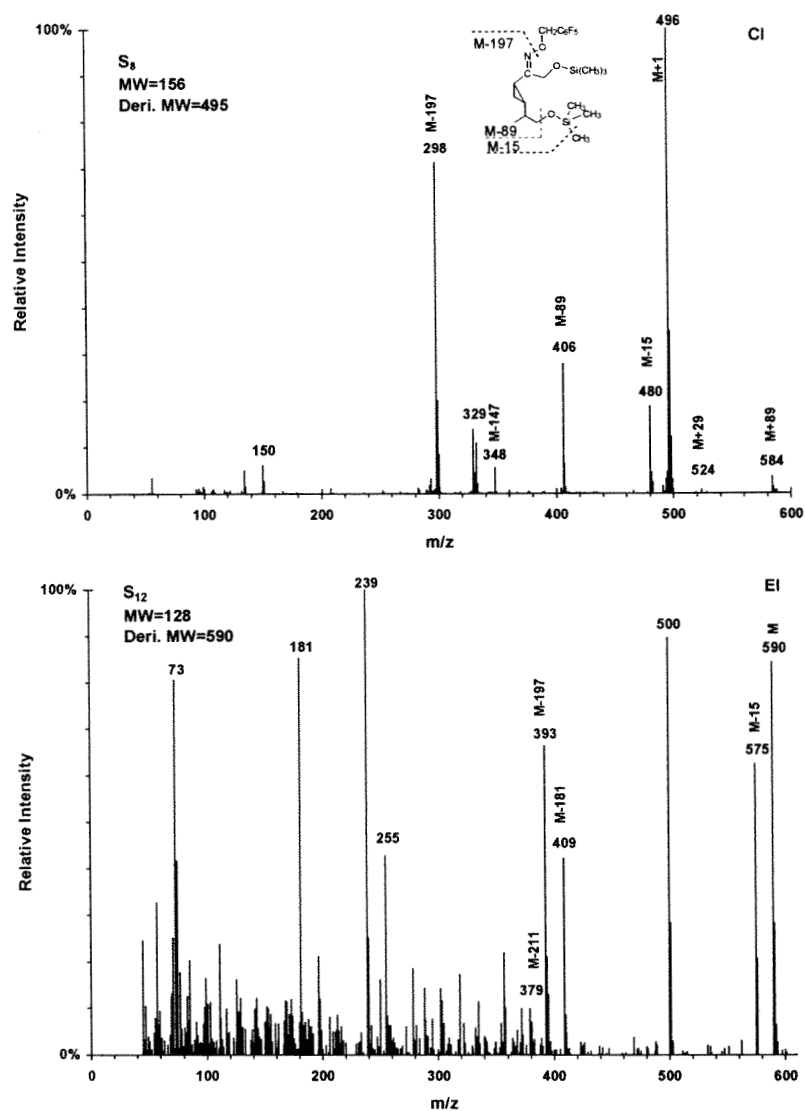


Figure A.1.4. Mass spectra for the derivatives of two products (S₈ and S₁₂) from ozone oxidation of sabinene.

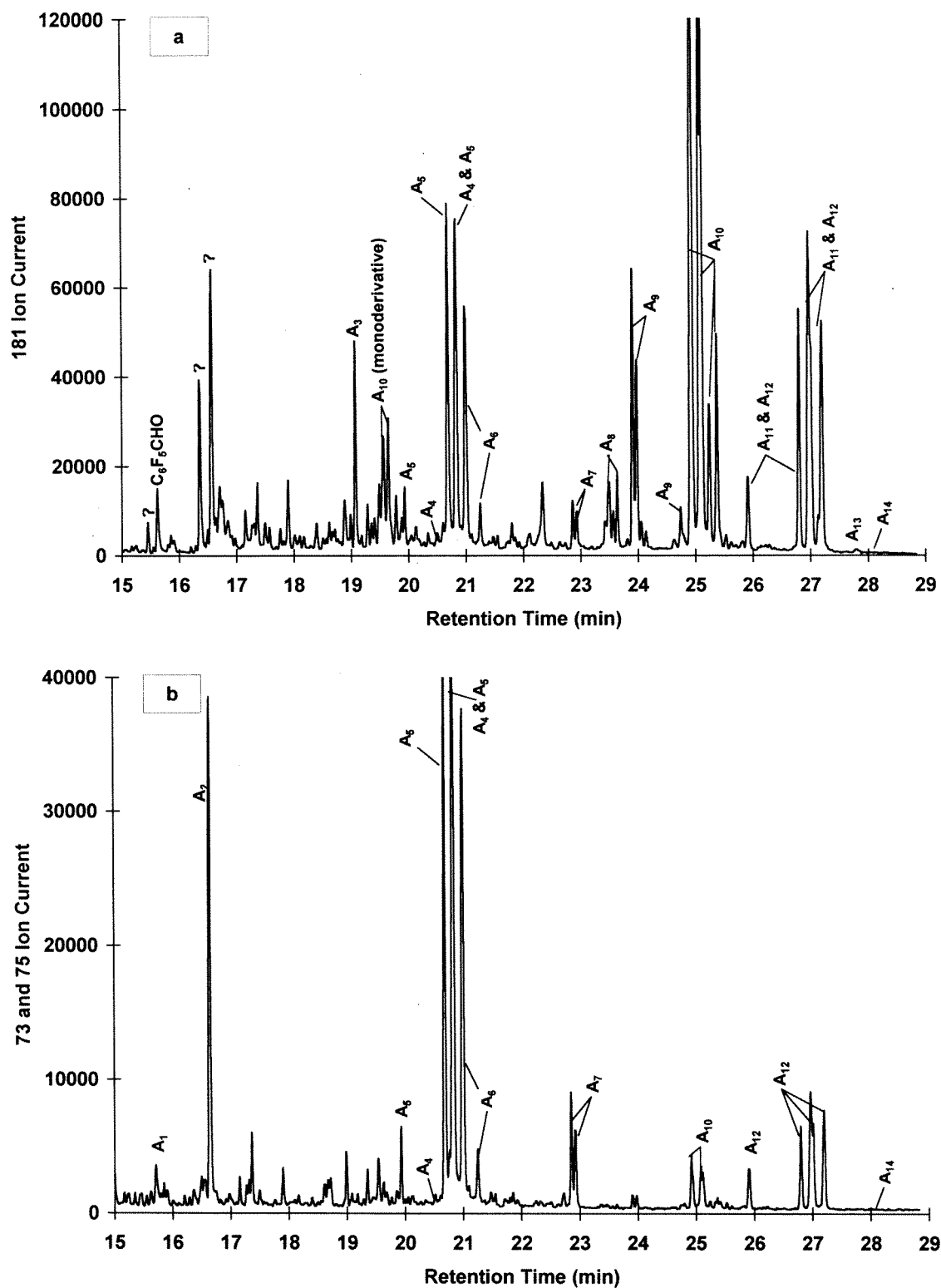


Figure A.1.5. Chromatogram of products from α -pinene/ O_3 reaction; see Table A.1.6 for peak identification. Top: Products containing carbonyl groups. Bottom: Products containing OH/COOH groups.

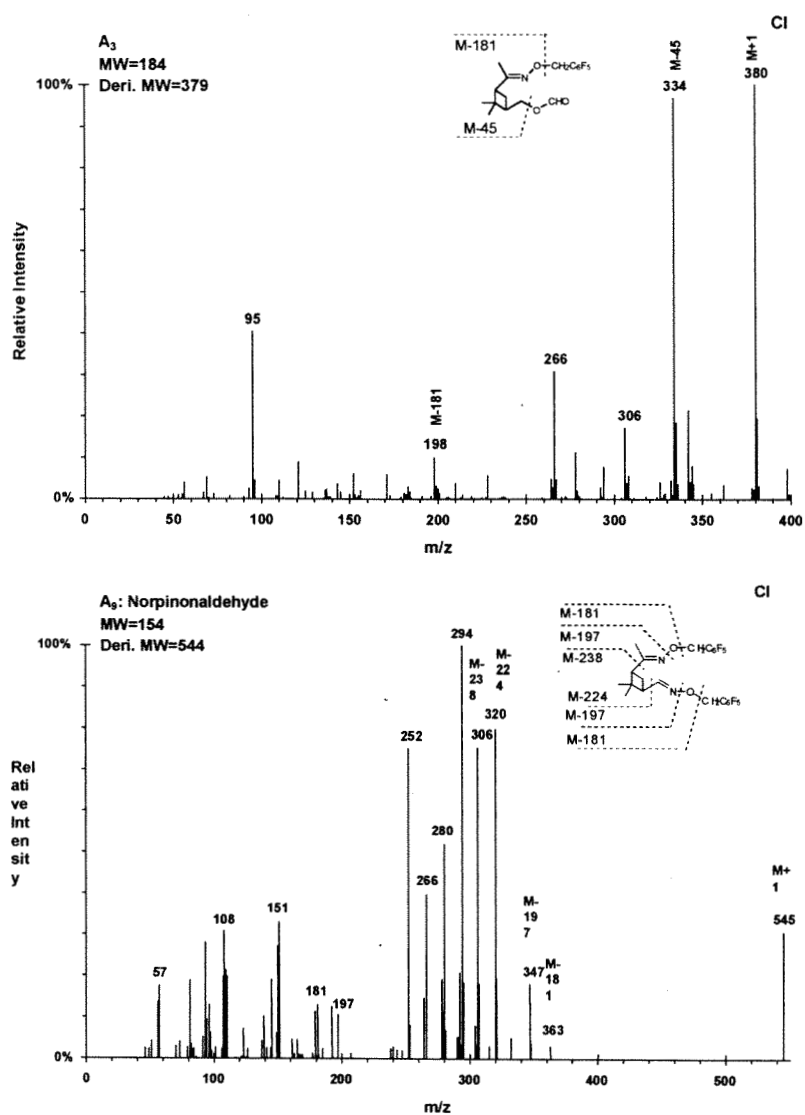


Figure A.1.6. Mass spectra for the derivatives of products from ozone oxidation of α -pinene.

Figure A.1.6. (continued) Mass spectra for the derivatives of products from ozone oxidation of α -pinene.

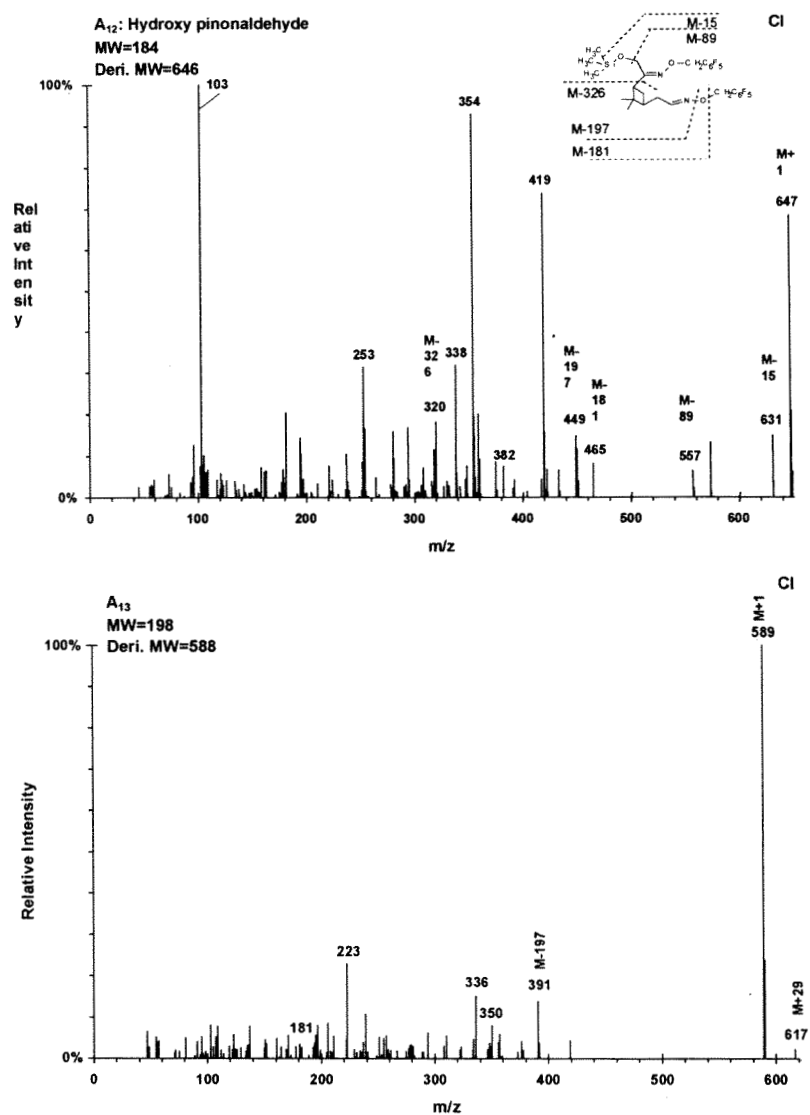


Figure A.1.6. (continued) Mass spectra for the derivatives of products from ozone oxidation of α -pinene.

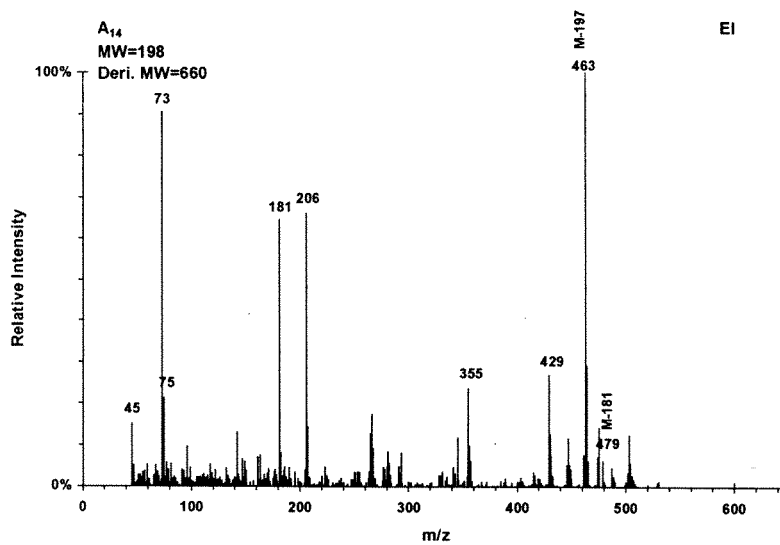


Figure A.1.6. (continued) Mass spectra for the derivatives of products from ozone oxidation of α -pinene.

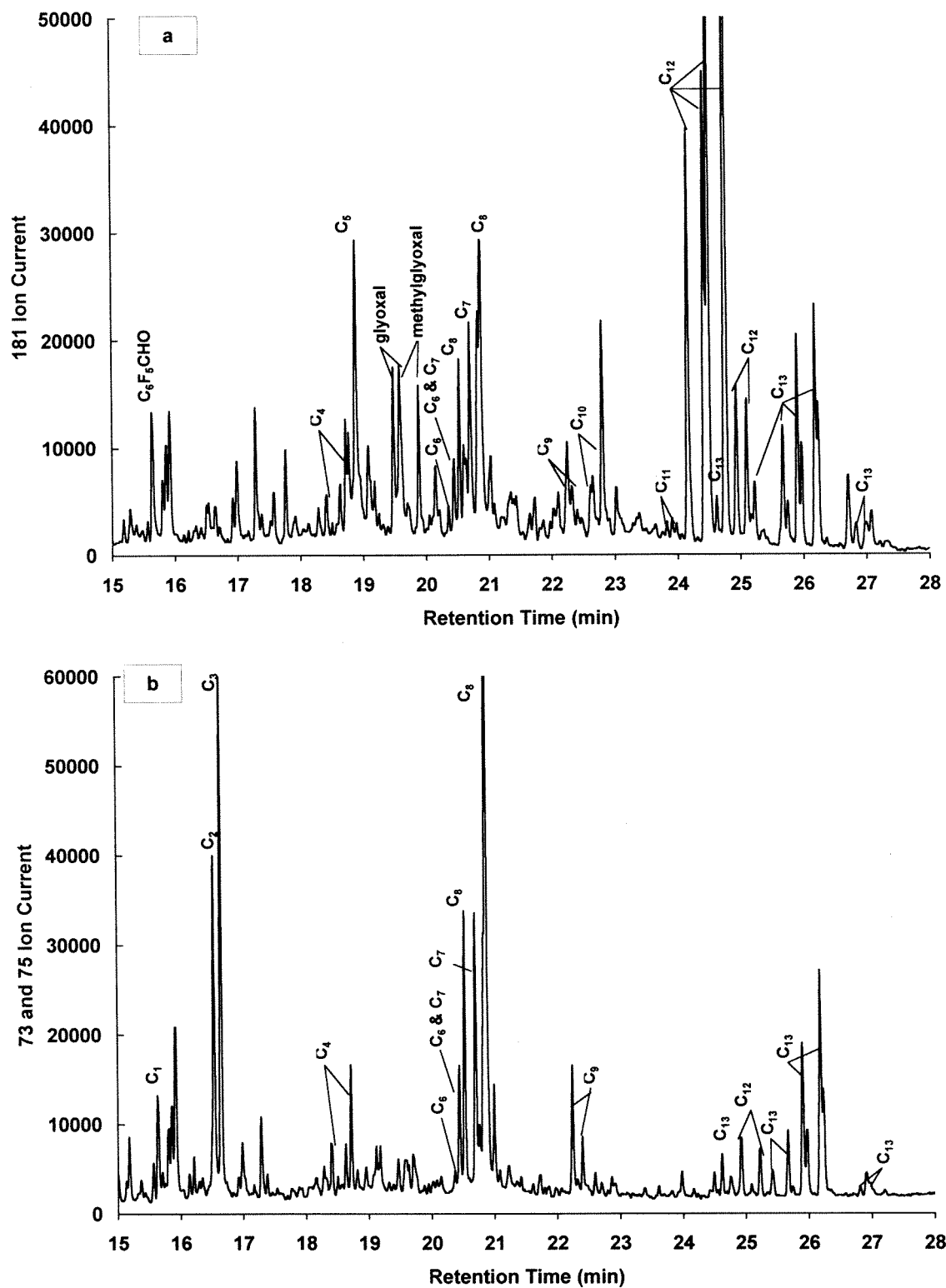


Figure A.1.7. Chromatogram of products from Δ^3 -carene/ O_3 reaction; see Table A.1.7 for peak identification. Top: Products containing carbonyl groups. Bottom: Products containing OH/COOH groups.

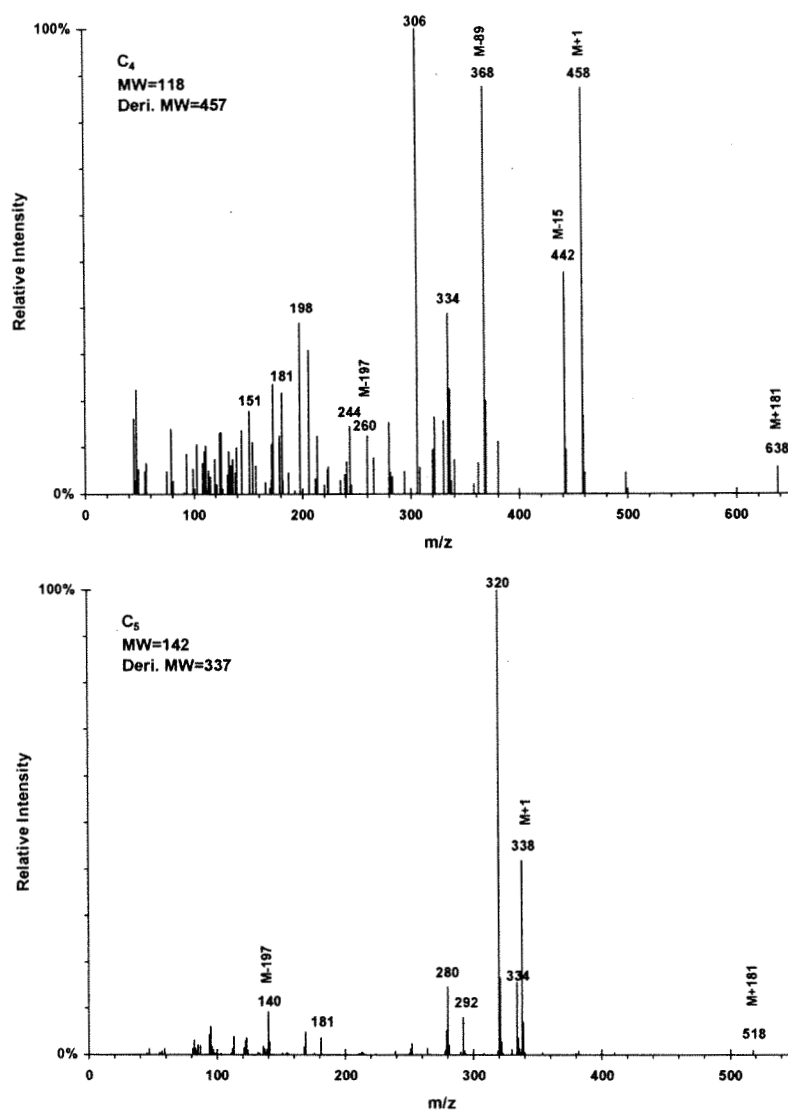


Figure A.1.8. Methane CI mass spectra for the derivatives of products from ozone oxidation of Δ^3 -carene.

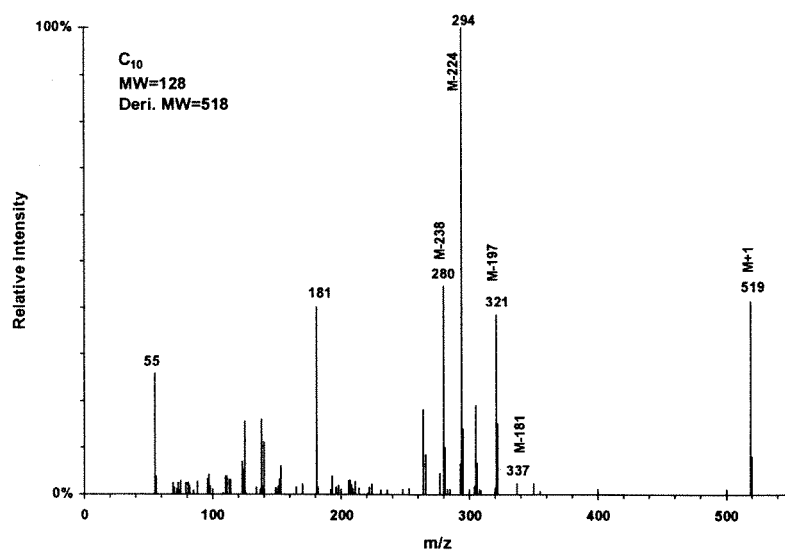


Figure A.1.8. (continued) Methane CI mass spectra for the derivatives of products from ozone oxidation of Δ^3 -carene.

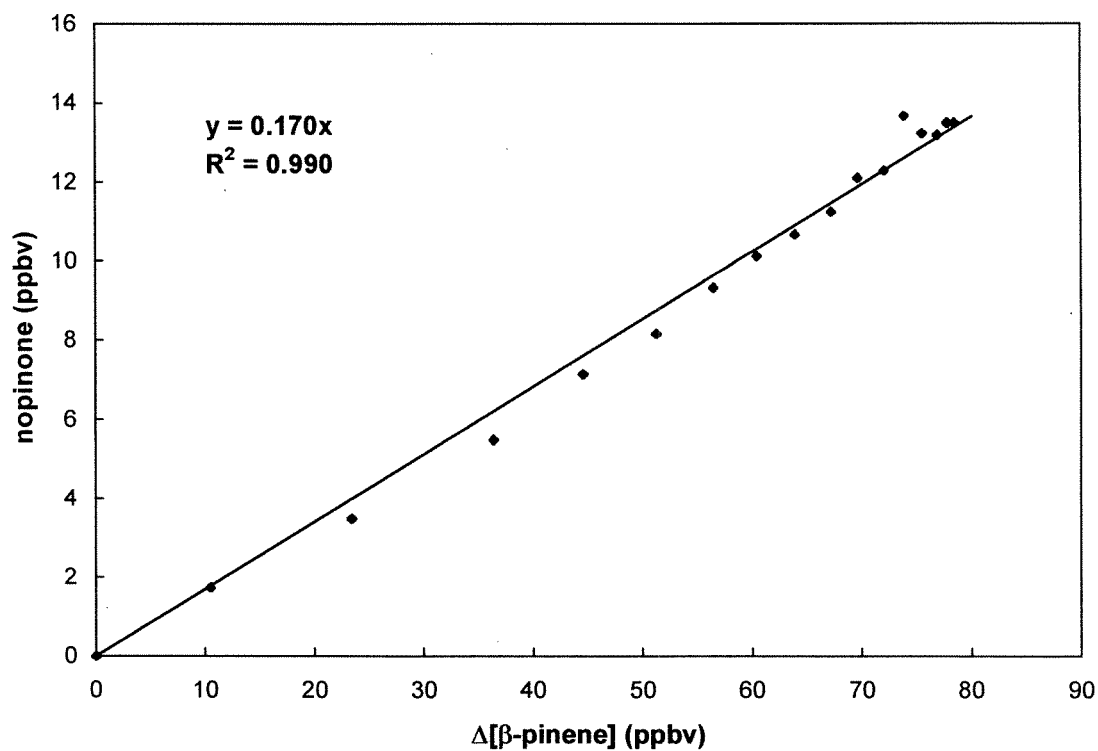


Figure A.1.9. Amount of nopinone formed versus the amount of β -pinene reacted.

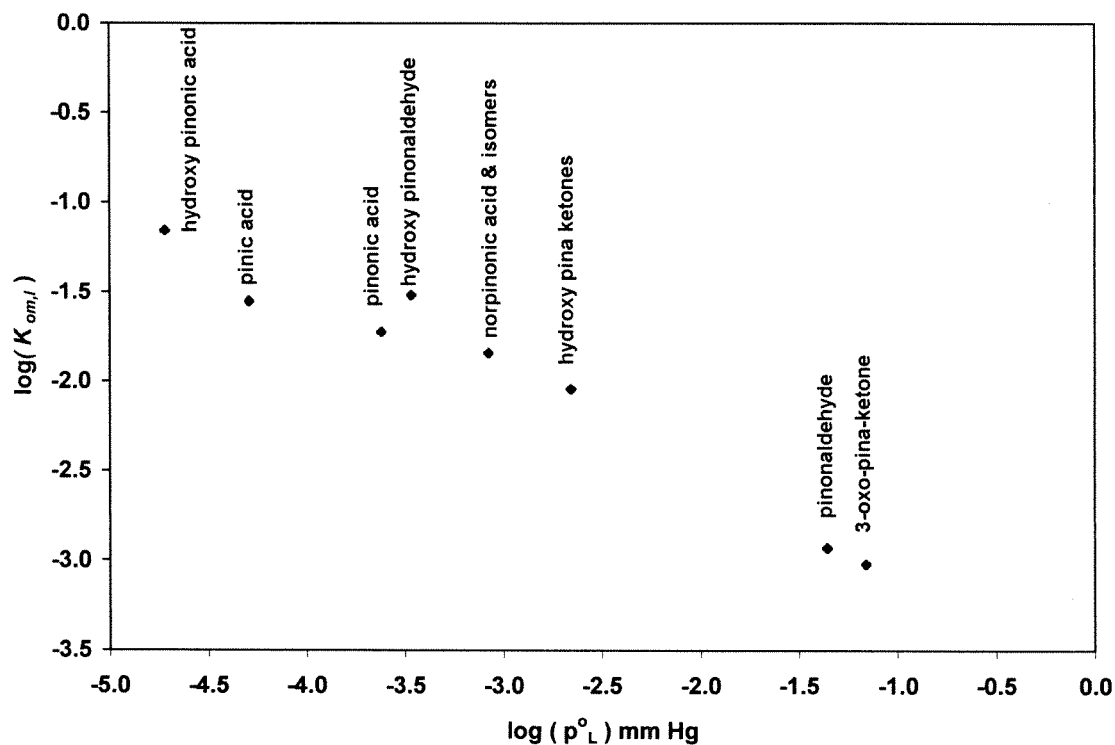


Figure A.1.10. Measured $\log(K_{om,i})$ versus estimated $\log p^\circ_L$ for the major products in the β -pinene/ O_3 and α -pinene/ O_3 systems.

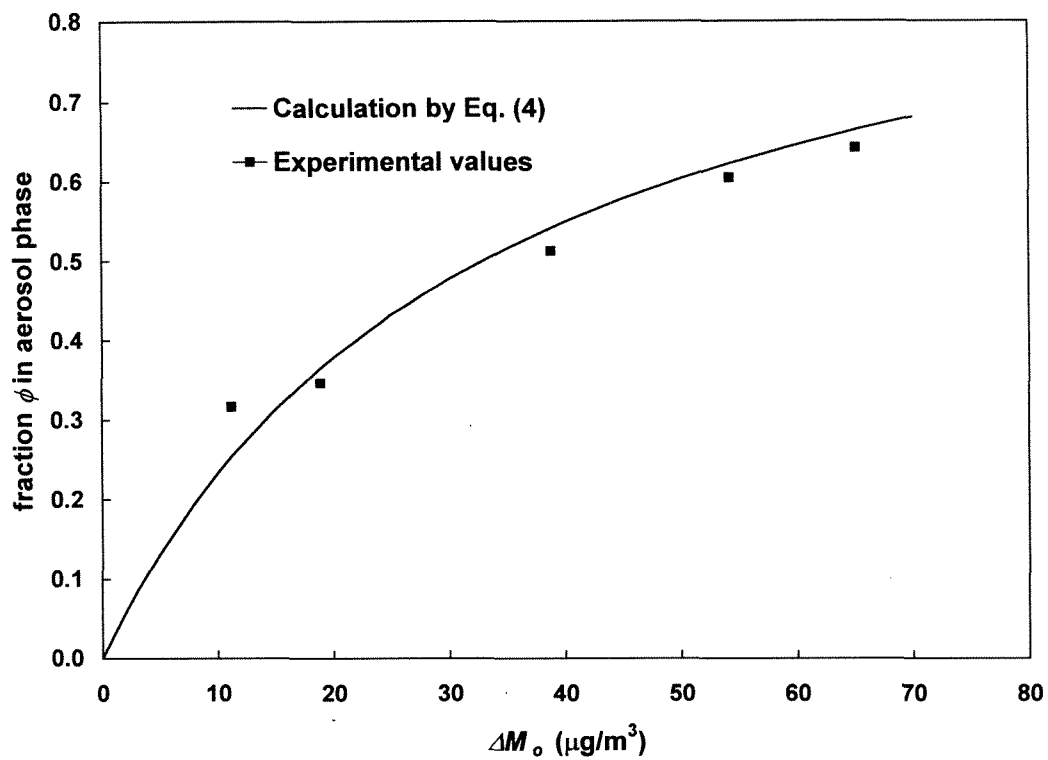


Figure A.1.11. Fraction of pinic acid in aerosol phase as a function of organic aerosol mass concentration. (The curve is generated using an average K_{om} value for pinic acid determined in all α -pinene/ O_3 and β -pinene/ O_3 experiments.)

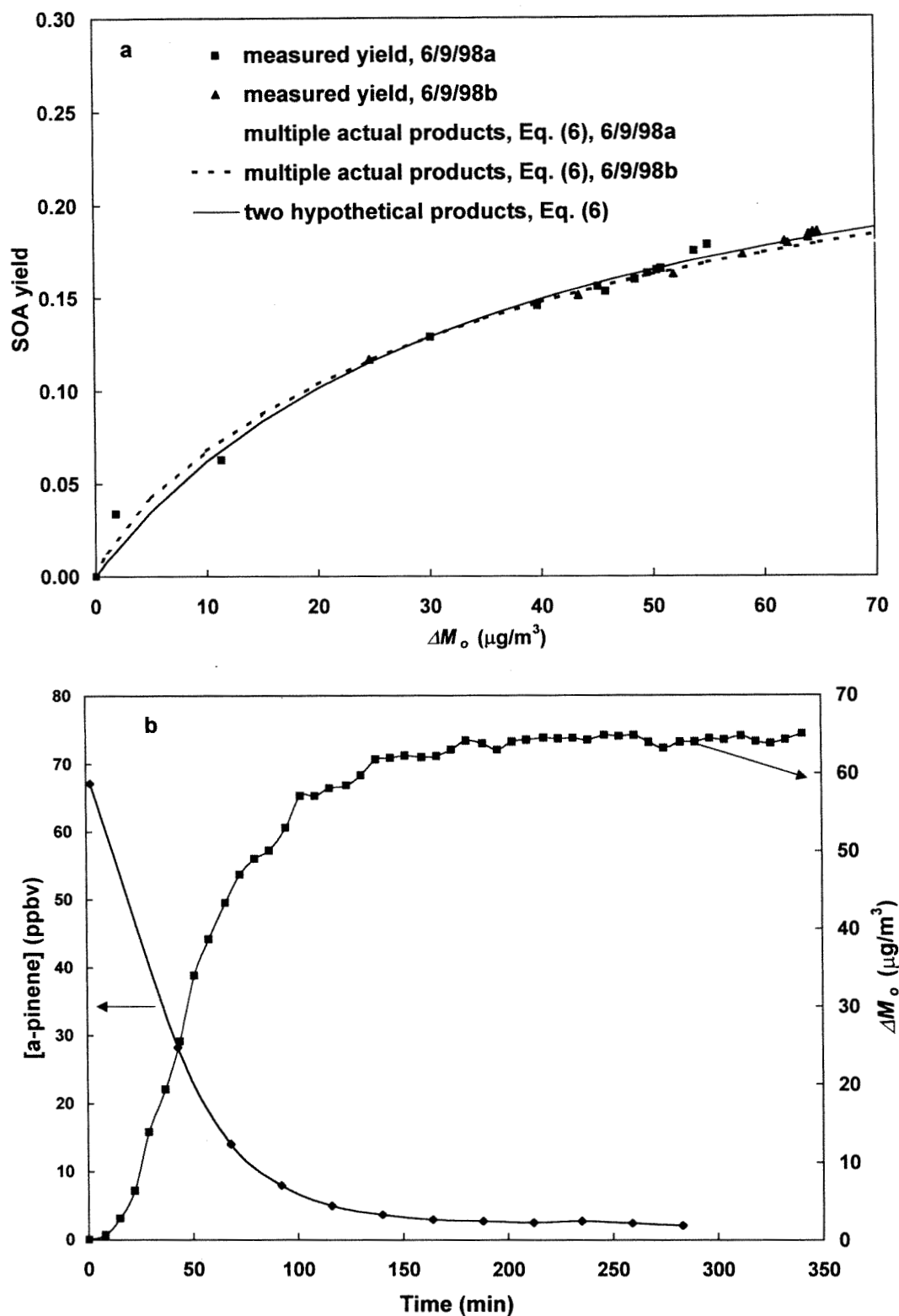


Figure A.1.12. Top: Time-dependent secondary organic aerosol yields as a function of organic aerosol mass for two α -pinene/ O_3 experiments. Bottom: α -Pinene mixing ratio and organic aerosol mass concentration as a function of time in the 6/9/98b experiment.

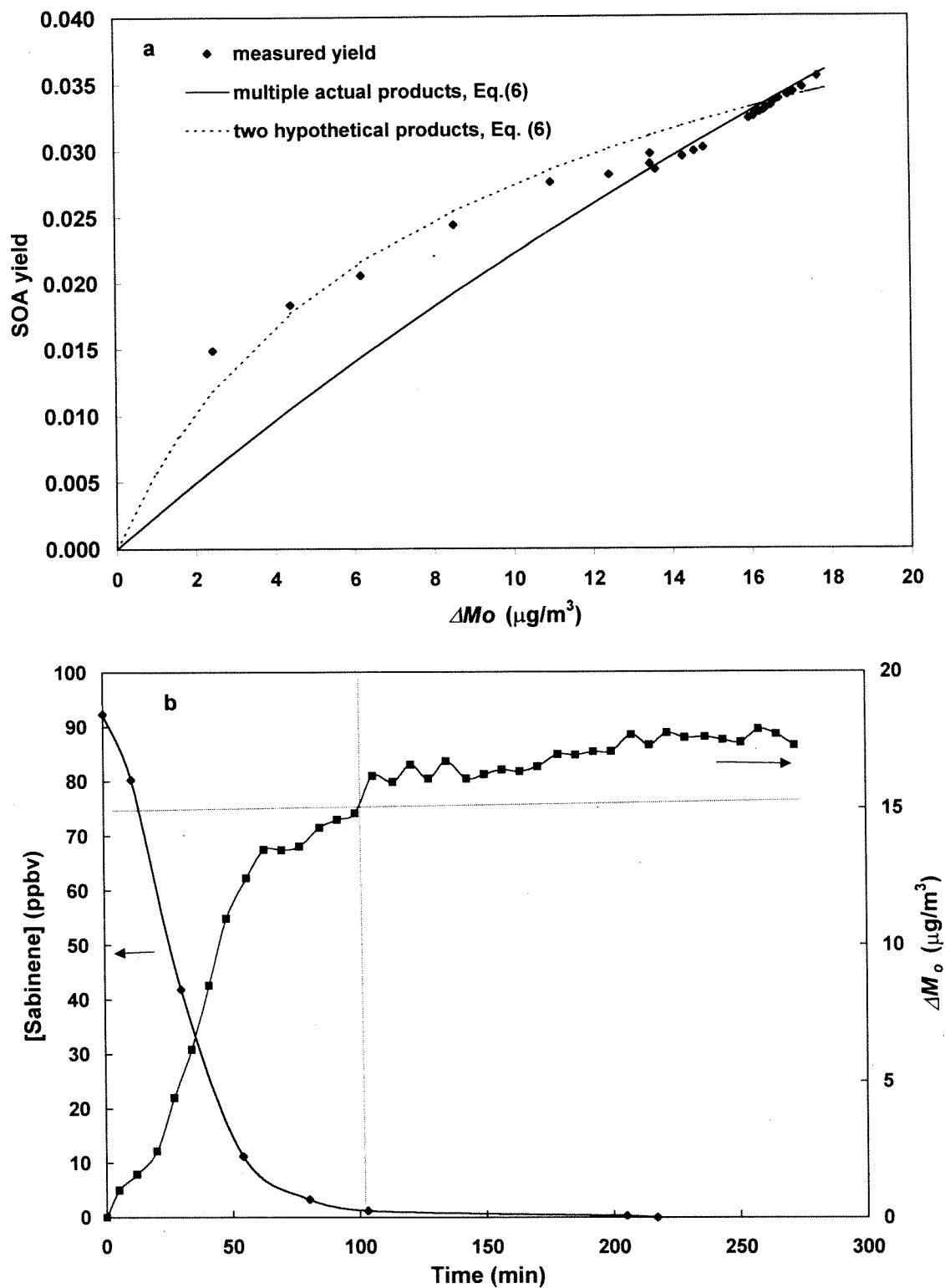


Figure A.1.13. Top: Time-dependent secondary organic aerosol yields as a function of organic aerosol mass concentration for the sabinene/ O_3 reaction. Bottom: Sabinene mixing ratio and organic aerosol mass concentration as a function of time.

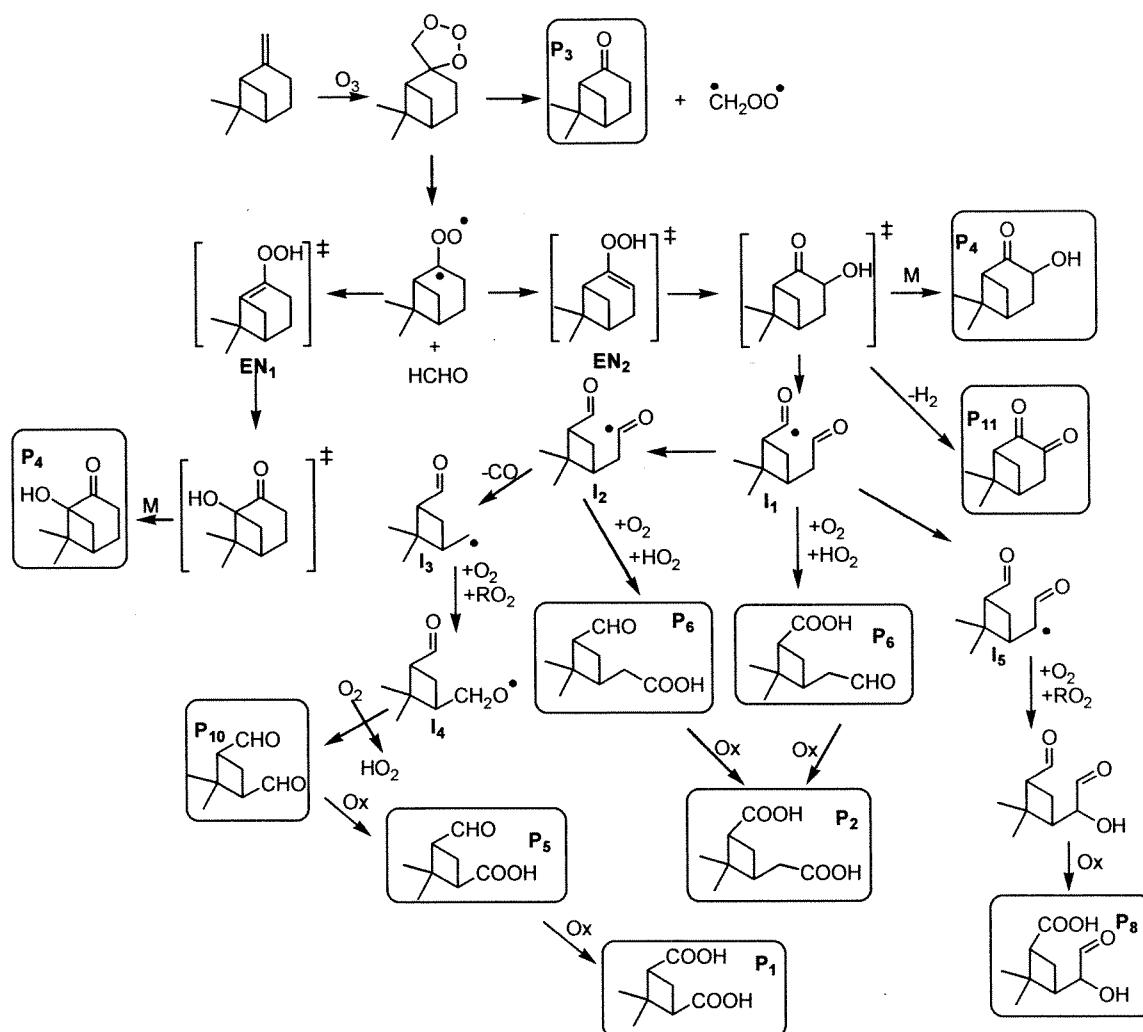


Figure A.1.14. Reaction mechanism of O_3/β -pinene reaction. (Ox denotes oxidant.)

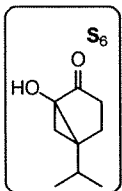


Figure A.1.15. Reaction mechanism of O₃/sabinene reaction. (Ox denotes oxidant.)

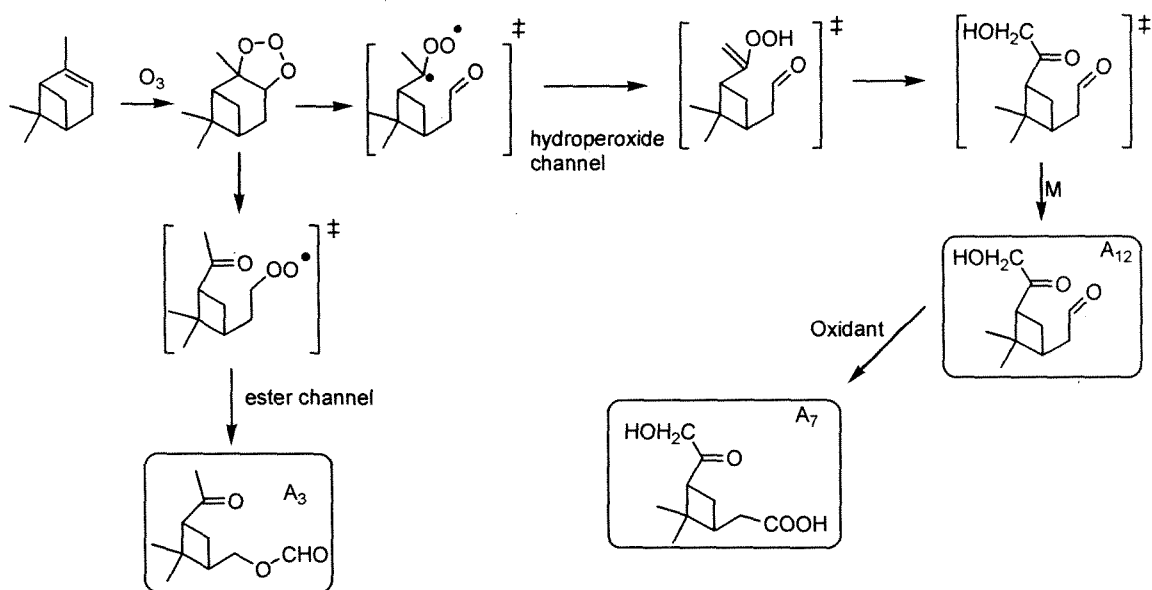


Figure A.1.16. Formation mechanism of A_3 and A_7 in the O_3/α -pinene reaction.

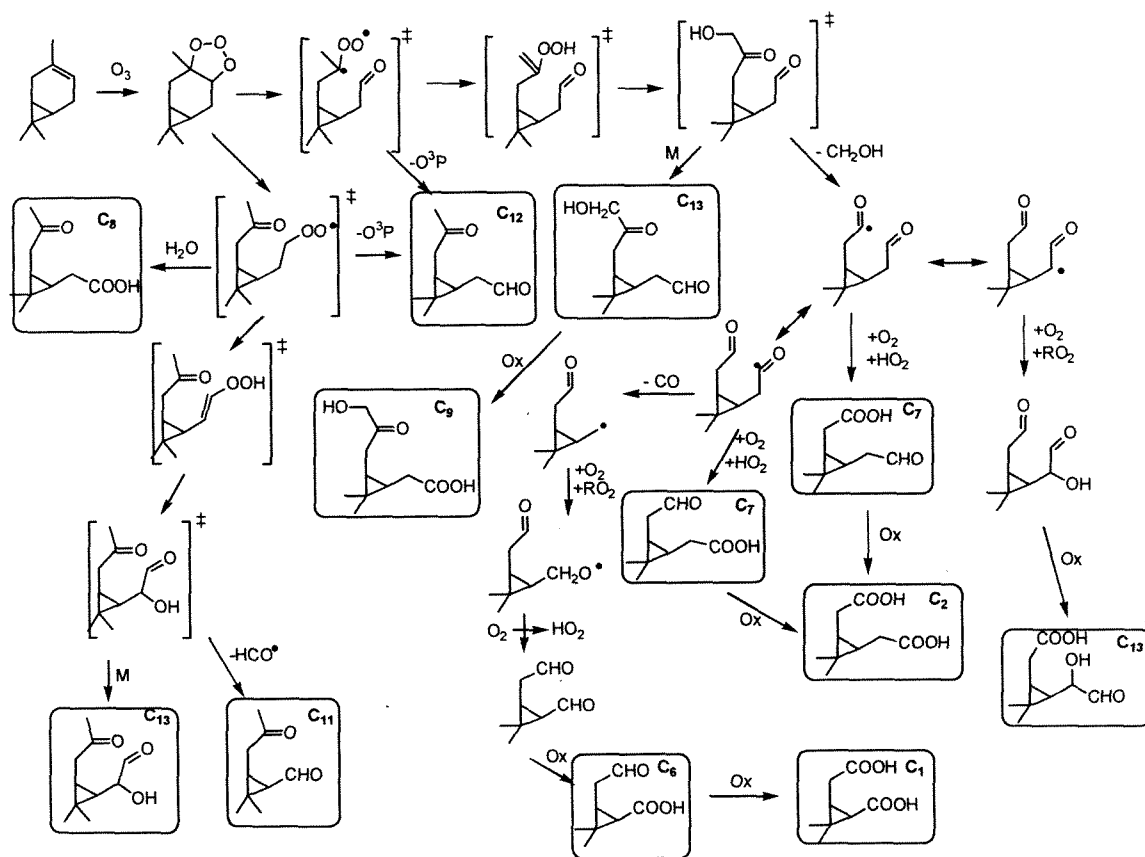


Figure A.1.17. Reaction mechanism of O_3/Δ^3 -carene reaction. (Ox denotes oxidant.)

Appendix 2**Aerosol Formation in the Cyclohexene-Ozone System**

M. Kalberer, J. Yu, D. R. Cocker, R. C. Flagan, and J. H. Seinfeld

A.2.1 Introduction

Volatile organic compounds, when photooxidized in the atmosphere, can lead to products that have sufficiently low vapor pressure to partition between the gas and aerosol phases. The fraction of organic particulate matter arising from this path is referred to as secondary organic aerosol (SOA). Parent organic compounds that, upon oxidation, lead to SOA generally contain six or more carbon atoms. While overall yields of SOA have been measured in the laboratory, investigation of aerosol composition at the molecular level have only recently begun to resolve an appreciable fraction of SOA. Molecular identification of SOA is difficult because atmospheric oxidation pathways of $\geq C_6$ compounds lead to a relatively large number of products that are generally highly polar, complicating their analysis. Cyclohexene, a cyclic alkene that is known to produce aerosol upon oxidation, was, in fact, one of the first organic compounds investigated for its aerosol-forming potential. Hatakeyama et al. (1) identified pentanedial, 5-oxo-pentanoic acid, glutaric acid, hexanedial, 6-oxo-hexanoic acid, and adipic acid as SOA products of cyclohexene oxidation. Gaseous compounds measured included formic acid, pentanal, pentanedial, and hexanedial. Since no actual aerosol measurements were performed in that study, there is no information as to what fraction of the total particle mass was identified. In a later study, Izumi et al. (2) measured the aerosol yield of cyclohexene in the presence of ozone and OH radicals in the cyclohexene concentration range between 0.5 and 5 ppm but determined only the total carbon and nitrogen content of the aerosol particles. Grosjean et al. (3) measured gas-phase products of the cyclohexene-ozone reaction, in the presence of an OH scavenger (cyclohexane), and found pentanal as a principal oxidation product.

The goal of the present paper is to revisit the cyclohexene-ozone system.

Cyclohexene-ozone has been selected as a model system because it has been intensively studied, gas-phase products are well-characterized, and a reasonable amount is known about reaction mechanisms in the system. Although cyclohexene is not likely to be an important precursor for secondary organic aerosol in the ambient atmosphere, the cyclohexene-ozone system is highly relevant for its use as a model system that is relatively well understood, rather than for its importance as a major aerosol precursor. We seek molecular identification of gas- and aerosol-phase products, using recently developed methods of derivatization and mass spectrometric detection. Such data will, in the future, serve as a basis for evaluating the ability to predict SOA formation from first principles; that is, if all the semi-volatile oxidation products of a parent hydrocarbon were known, together with their physical properties, such as their vapor pressures, then the yield of SOA from that parent molecule could be predicted for any given set of conditions.

A.2.2 Experimental

A.2.2.1 Smog chamber experiments.

Most of the experimental procedures associated with the Caltech outdoor smog chamber have been described previously (4-6), and only a brief summary is given here. Reactant concentrations and general experimental conditions for the cyclohexene-O₃ system are given in Table A.2.1. Experiments were performed in the dark in two outdoor Teflon chambers of about 22 m³ volume each. The temperature for all experiments was maintained at 298 K (\pm 2 K). Before the reactants were introduced into the chambers, (NH₄)₂SO₄ seed aerosol, of mean diameter of approximately 100 nm, was injected, at a

number concentration of about 10^4 cm^{-3} . Particle number and size measurements were performed with a differential mobility analyzer (Model 3071, TSI, St. Paul, MN) and a condensation nucleus counter (Model 3760, TSI, St. Paul, MN). To prevent OH oxidation by OH generated in alkene- O_3 reactions, CO was added as an OH-scavenger (see for example Gutbrod et al. (7)), at levels (268 to 1040 ppm) sufficient to ensure that >95 % of any OH generated was scavenged. (The current experiments were not designed to measure OH yield from the cyclohexene- O_3 reaction.) Samples for gas- and particle-phase analysis were taken after the hydrocarbon was essentially consumed. The mixing ratio of cyclohexene was measured with a Hewlett Packard 5890 GC/FID. All experiments were carried out under dry conditions ($\text{RH} < 5\%$), so the dependence of product levels on aerosol water was not addressed.

A.2.2.2 Gas and particle sampling.

Since many reaction products are present in both gas and particle phases, the sampling system consisted of a series of two annular denuders (University Research Glassware, Chapel Hill, NC) to remove the gaseous reaction products, followed by a Teflon coated quartz fiber filter (Pallflex, Putnam, CT), which collected all particles. The first denuder is 40 cm long, and the second is 20 cm long. Both denuders consist of 5 annular channels with 2 mm spacing between channels. An additional denuder was placed behind the filter to trap compounds that might volatilize from the filter during sampling. The gaseous concentration of a compound was calculated from the sum of the amounts found in the first two denuders, and the particle phase concentration was determined from the amounts found on the filter and the third denuder. Samples were taken at a flow rate of 25 l min^{-1} for 1 hour resulting in a total sampling volume of 1.5 m^3 .

We evaluated particle loss to the denuders and found it to be less than 5% by mass.

Regarding artifacts from blowing off a compound from a denuder to the gas phase, our experiments showed that two denuders retain more than 99.4% of all compounds with the exception of pentanedial, for which the retention was 95%. The composition of secondary aerosols may include artifacts from filter absorption of gas-phase species that evade denuder collection. The contribution from this effect can be estimated for 1,4-butanedial, the most volatile product detected in the aerosol phase. The first denuder has a collection efficiency for 1,4-butanedial of 92% (Table A.2.2); the two denuders then have a combined collection efficiency of 99.4% for this compound. If the 0.6% of gaseous 1,4-butanedial that escaped collection on the denuders was retained on the filter, this amounted to $0.6\% \times 0.45\% = 0.0027\%$ of the 1,4-butanedial gas-phase yield. The measured aerosol-phase yield of 1,4-butanedial was 0.05% (to be presented subsequently). Thus, only 5% ($0.0027/0.05$) of the 1,4-butanedial collected on the filter can be attributed to artifact. Further details about denuder coating and preparation are given by Yu et al. (4).

A.2.2.3 Sample treatment and analysis.

Following elution of the denuders with a dichloromethane/acetonitrile/hexane mixture and extraction of the filter in a soxhlet apparatus (dichloromethane/acetonitrile mixture), the samples were derivatized with PFBHA (O-(2,3,4,5,6-pentafluorobenzyl)hydroxy amine) and BSTFA (N,O-bis (trimethylsilyl)-trifluoroacetamide). The derivatization reactions convert polar into less polar compounds, i.e., carbonyl groups react with PFBHA to form oxime derivatives and carboxyl and hydroxyl groups react with BSTFA to form trimethylsilyl derivatives. Sample analysis was

performed with a Varian Star 3400/Saturn 2000 gas chromatograph/mass spectrometer in electron ionization and chemical ionization mode. The gas used in the CI mode was methane. Samples were separated in a RTX-5MS column (Restek, Bellefonte, PA).

Most compounds identified were quantified, either with an authentic standard or with surrogate compounds of similar structure. Calibration mixtures that included all standards were produced at five concentrations in the range of 10 to 50 ng μl^{-1} . Compound specific ions or, in the case of surrogates, mass fragments typical for the functional group were used for quantification of the different compounds. Surrogates were chosen to have the same type and number of functional groups and the same carbon number, if possible. Since the compounds with surrogates were quantified with mass fragments typical for the functional groups, the number of functional groups was important for selection of a surrogate compound.

Recovery experiments to account for losses during sampling were performed by spiking standard mixtures with known amounts of all standard compounds on the denuders and filters. The denuder collection efficiency, defined by the amount of a given compound collected by the two denuders preceeding the filter, is shown for each compound in the cyclohexene- O_3 system in Table A.2.2. The collection efficiency was > 91% for all compounds, except for pentanal. Because it is expected that pentanal should exist exclusively in the gas-phase, the amount of pentanal found on the filter and on the denuder behind the filter was considered to be part of the gas-phase fraction. Because analytes can be lost to extraction vessels and by evaporation during rotary evaporation, “recovery” refers to the fraction of a compound that is recovered at the end of the treatment process.

A.2.3 Results and Discussion

A.2.3.1 Aerosol yield.

Figure 1 shows cyclohexene and total particle mass concentrations for experiment 5/13/99a; this behavior is typical of all experiments. Cyclohexene was almost completely consumed within the first two hours, and the organic particle mass increased correspondingly. Typical aerosol size distributions before the start of the experiment and after particle growth ceased are shown in the insert in Figure A.2.1. The volume of organic aerosol material produced, ΔM_o , was determined from the two size distributions, after accounting for wall losses of particles.

For a wide variety of parent VOCs, the fractional aerosol yield by mass that is Y as a function of ΔM_o , can be fit by assuming two empirical oxidation products (5, 8). Fractional aerosol yields for the six cyclohexene- O_3 experiments are given in Table A.2.1. Parameters (5, 8) of the two-component best fit correlation to these data are $\alpha_1 = 0.36$, $\alpha_2 = 0.32$, $K_{om,1} = 0.009 \text{ m}^3 \mu\text{g}^{-1}$ and $K_{om,2} = 0.001 \text{ m}^3 \mu\text{g}^{-1}$.

A.2.3.2 Identification of products.

Identified products in the cyclohexene- ozone system are given in Table A.2.3. In the mass spectrometer, derivatized compounds fragment in a characteristic way, as described by Yu et al. (6) and LeLacheur et al. (9). Compounds with a carbonyl functional group are identified by the mass m/z 181, and those with a carboxylic or hydroxy group show a typical mass fragment at m/z 73 and m/z 75. In addition, the fragments at m/z M-15, M-73, M-89 and M-117 (M-117 is a characteristic ion only for carboxyl groups, not for hydroxyl groups), which denote a loss of $[\text{CH}_3]$, $[\text{Si}(\text{CH}_3)_3]$,

$[\text{OSi}(\text{CH}_3)_3]$ and $[\text{C}(\text{O})\text{OSi}(\text{CH}_3)_3]$ from the derivatized molecule, respectively, were used in identification. In the CI mode the fragment M-89 was often stronger compared to EI mode spectra, where M-117 was often prominent. Also the molecular ion and the adduct ion, M+1 and M+73, were often detected in the CI mode spectra. The fragment m/z 147 was always associated with compounds with two carboxyl or hydroxyl groups, and m/z 117 ($\text{C}(\text{O})\text{OSi}(\text{CH}_3)_3$) was prominent in spectra of compounds with only one carboxylic group. For compounds with carbonyl groups, the mass fragment M-197, which results from a loss of $[\text{OCH}_2\text{C}_6\text{F}_5]$ from the derivatized molecule, was generally used for identification in the EI mode mass spectrum along with the molecular ion in the CI mode spectrum.

Figure A.2.2a shows the m/z 181 ion chromatogram of a filter sample indicating all nine compounds identified in the cyclohexene- O_3 system with a carbonyl group, and Figure A.2.2b shows the m/z 73+75 ion chromatogram of the same sample with all 12 compounds identified containing a carboxylic and/or hydroxyl group. In total, 17 compounds were identified; for eight of which an authentic standard was available, the others identified tentatively by their mass spectra (see Table A.2.4).

Three dialdehydes, 1,4-butanedial, 1,5-pentanedial, and 1,6-hexanedial were found in both the particle and gas phases. Of these, an authentic standard was available only for 1,5-pentanedial; the two others were tentatively identified by comparing their mass spectra with that of 1,5-pentanedial. The EI spectra give compound specific information, i.e., for carbonyl compounds a strong peak at m/z M-197. The spectra of the compounds identified as 1,4-butanedial and 1,6-hexanedial showed prominent peaks at m/z 279 and 307, respectively, which are -14 and +14 mass units ($-\text{CH}_2-$ group)

compared to the M-197 peak of 1,5-pentanedial. In addition, the CI spectra showed the molecular ion peaks (M+1) of the two compounds (i.e., m/z 477 for the 1,4-butanedial derivative and m/z 505 for the 1,6-hexanedial derivative). The retention time supports the identification, i.e., 0.98 minutes earlier than that of 1,5-pentanedial for 1,4-butanedial and 0.9 minutes later for 1,6-hexanedial. 1,5-Pentanedial was quantified with compound-specific ions, whereas 1,4-butanedial and 1,6-hexanedial were quantified using the carbonyl specific m/z 181 (see Table A.2.4).

Three oxo-alkanoic acids, 4-oxo-butanoic acid, 5-oxo-pentanoic acid, and 6-oxo-hexanoic acid, were identified in both the gas and particle phases. An authentic standard was available only for 4-oxo-butanoic acid; however, the two other compounds could be identified, similar to the dialdehydes, by comparing their mass spectra with that of 4-oxo-butanoic acid. Molecular peaks, as well as characteristic fragments, were found. Again the M-197 fragments typical for carbonyls were prominent for 5-oxo-pentanoic acid and 6-oxo-hexanoic acid at $m/z + 14$ and $m/z + 28$, compared to the spectrum of 4-oxo-butanoic acid. Fragments also characteristic for the carboxyl group (i.e., M-15 and M-89) were found in both compounds. Again, the retention time supports the identification as 5-oxo-pentanoic acid and 6-oxo-hexanoic acid (see Table A.2.4). For quantification, m/z 73+75+181 using the surrogates 4-oxo-pentanoic acid and 5-oxo-hexanoic acid, respectively, were used for 5-oxo-pentanoic acid and 6-oxo-hexanoic acid. 4-Oxo-butanoic acid was quantified with the compound-specific ions.

All five dicarboxylic acids identified, oxalic acid, malonic acid, succinic acid, glutaric acid, and adipic acid, were verified with authentic standards and were quantified with compound-specific ions (Table A.2.4).

Four different compounds with a hydroxyl functional group were tentatively identified, hydroxy pentanoic acid, hydroxy glutartaric acid, hydroxy adipic acid, and 4-hydroxy-1-butanol. The compound occurring in the chromatogram at 11.04 min has been tentatively identified as hydroxy pentanoic acid. In the CI spectrum the molecular ion, m/z 262, was visible, as well as the adduct $M+73$, which is typical for compounds with a derivatized carboxyl or hydroxyl group. In the EI mode the spectrum showed a strong peak at mass m/z 247, which is the typical $M-15$ fragment observed for all carboxyl and hydroxyl compounds, assuming m/z 262 is the molecule ion as found under CI conditions. This molecular mass can be attributed theoretically to three different compounds in this context, i.e., succinic acid, hexanediol, and hydroxy pentanoic acid. Standards were available for the first two compounds; however, their retention times did not match with the peak at 11.04 min. Glutaric acid was used as a surrogate to quantify the amounts of hydroxy pentanoic acid using the ions m/z 73 and 75.

Hydroxy glutartaric acid was similarly identified by rationalizing the mass spectrum occurring at 14.7 min in the chromatogram. The CI spectrum showed again a prominent peak at m/z $M+73$ and at m/z $M+1$, although the latter was rather weak. In the EI mode spectrum the corresponding fragments, m/z 349 ($M-15$), m/z 247 ($M-117$) and m/z 147, were found. 3-Hydroxy-3-methyl-glutaric acid was used as a surrogate to quantify the amounts of hydroxy glutartaric acid using the ions m/z 73+75.

The peak at 15.90 min retention time showed a similar spectrum to that for hydroxy glutaric acid, except that all relevant mass fragments were shifted by 14 mass units towards higher masses; mass unit 14 is typically assigned to a $-CH_2-$ group, and

thus this compound was tentatively identified as hydroxy adipic acid and quantified with 3-hydroxy-3-methyl-glutaric acid as surrogate.

The peak at 15.05 min was characterized by the presence of m/z 181 and m/z 73+75, indicating that the compound has a carbonyl as well as a carboxyl or hydroxyl group. The CI spectrum shows weak peaks at m/z 356 and m/z 340 and the base peak at m/z 266, which were assigned to $M+1$, $M-15$ and $M-89$, respectively, of 4-hydroxy-1-butanal. In the EI spectrum the fragment m/z 158 ($M-197$) strengthened the identification of this peak as 4-hydroxy-1-butanal. For quantification, the surrogate 4-oxo-butanoic acid was used. Pentanal, found only in the gas phase, was identified and quantified with an authentic standard.

At a retention time of 15.96 min, 5-oxo-pentyl formate was tentatively identified. In the CI spectrum the molecule ion (m/z 325) was prominent with 16% relative intensity. The main peak in the CI spectrum was m/z 280 ($M-45$), corresponding to the loss of formate from the molecule. In addition, the fragment $M-197$, prominent in the CI spectrum, and m/z 181, specially strong in the EI spectrum, both typical for carbonyls, supported the identification. 5-Oxo-pentyl formate was the only compound identified that was not quantified, since no appropriate standard was available.

A.2.3.3 Quantification of reaction products.

The molecular yield of cyclohexene- O_3 reaction products in the gas and particulate phases and the total yield are given in Table A.2.5. The largest single yield was measured for pentanal at 17%. This agrees with that reported by Grosjean et al. (3) of 16% and by Hatakeyama et al. (1) of 17%. The two other groups of compounds with high molar yields are dicarboxylic acids and oxo-carboxylic acids, at about 22% and 16%,

respectively. Among the dicarboxylic acids, oxalic acid, malonic acid, and glutaric acid are the most abundant, whereas succinic acid and adipic acid were found in smaller quantities. All three oxo-carboxylic acids (4-oxobutanoic acid, 5-oxopentanoic acid, 6-oxohexanoic acid) were formed in about equal amounts (4 - 7%). Dialdehydes and hydroxylated compounds were produced in only minor amounts. The overall average carbon yield, both gas and particle phase, of the experiments was about 47% (see Table A.2.5); that is, only about one-half of the carbon atoms originally present in the cyclohexene were recovered in the 16 compounds quantified in this study. Much of the missing carbon can likely be attributed to volatile products that could not be identified with the technique used in this study. For example, Hatakeyama et al. (1) found significant amounts of CO, CO₂, HCOOH, and C₂H₂. If one assumes that for all compounds with fewer than six carbon atoms, corresponding compounds with one or two carbon atoms were produced, the carbon balance increases to about 62%.

The average distribution of aerosol composition is shown in Figure A.2.3. Total particle mass was calculated from the measured increase of the particle diameter using a density of the organic mass of $\rho = 1.4 \text{ g cm}^{-3}$, which is the weighted average of the densities of the individual compounds listed in Table A.2.5. Di-carboxylic acids contribute about 41% of the aerosol mass. The two hydroxylated dicarboxylic acids, hydroxy glutaric acid and hydroxy adipic acid, contribute about one-third to the aerosol mass (38%). Although their overall molar reaction yields are rather small (3.5%), they contribute significantly to the particle mass because of their low vapor pressures. About 17% of the particle mass consists of oxo-carboxylic acids; dialdehydes account for only a small amount, about 1.1%.

By summing all the individual compounds, the average total aerosol mass was 104% of the volume calculated from the DMA size measurements based on an estimated aerosol density of 1.4 g cm^{-3} . This agreement between the two independent methods indicates that the entire aerosol mass has been accounted for on a molecular level, subject to uncertainties inherent in the chemical analysis and the assumed particle density.

A.2.3.4 Cyclohexene-ozone reaction mechanism

The initial reaction between cyclohexene and ozone is the well-established addition of ozone to the double bond leading to the energy-rich Criegee biradical (Figure A.2.4a) (10). Loss of CO_2 from the Criegee biradical leads to the formation of pentanal (b), the most abundant identified reaction product (Figure A.2.4b). The Criegee biradical can also react with water and by subsequent loss of H_2O_2 and H_2O lead to 1,6-hexanediol (c) and 6-oxo-hexanoic acid (d), respectively. Adipic acid (e) might be formed by oxidation of 6-oxo-hexanoic acid, although an explicit mechanism for this reaction is not obvious (Figure A.2.4c). Similarly, we speculate that other acid products, h, i, n, o, p, q, are formed from their corresponding aldehyde precursors.

Intramolecular isomerization of the Criegee biradical leads to an excited intermediate (f) and by subsequent loss of CH_2O can lead to 1,5-pentanedial (g), which is oxidized to 4-oxo-pentanoic acid (h) and further to glutaric acid (i) (Figure A.2.4d). The intermediate (f), however, can also lead to the C_4 compounds identified in this study as outlined in Figure A.2.4e. This reaction chain involves the cleavage of a C-C bond of the intermediate alkoxy radical (j), which leads either to a C_4 alkyl radical (k) or the C_5 compound 1,5-pentanedial (g). After reaction with O_2 and HO_2 , the alkyl radical (k) is converted to a second alkoxy radical (l), which can react to 1,4-butanediol (m) and by

further oxidation to 4-oxo-butanoic acid (n) and succinic acid (o). Another pathway the intermediate alkoxy radical (l) can undergo is a cleavage and subsequent reaction to malonic (p) and oxalic acid (q) (see Figure A.2.4f).

A possible reaction mechanism for the formation of hydroxy-adipic acid is shown in Figure A.2.4g. After an initial H abstraction from adipic acid, the reactions with O_2 and HO_2 lead to the formation of hydroxy adipic acid. The path of formation of hydroxy glutaric acid is thought to be equivalent to that leading to hydroxy-adipic acid. CO was present in the reaction chamber, which should have scavenged about 95% of the OH radicals generated in the cyclohexene- O_3 reaction. It is not clear whether the formation of hydroxy-glutaric acid and hydroxy-adipic acid (molar yields: 1.6 and 0.9%, respectively) was a result of unscavenged OH radicals or whether another reaction mechanism is responsible for the formation of these two compounds.

The Criegee biradical can undergo reaction with aldehydes to produce ozonides (11, 12) (Figure A.2.5a). Since different aldehydes are present as reaction products, formation of ozonides is likely. No ozonides were detected; however, a possible reason for which might be their decomposition during sample treatment. PFBHA is a primary amine that can react with ozonides leading to an aldehyde and an acid (13) (Figure A.2.5b). The occurrence of the relatively high vapor pressure particle-phase aldehydes and acids might actually be a result of ozonide decomposition products. While another possibility could be thermal decomposition of ozonides during the soxlet extraction of the filter samples, which was performed at about 70°C, at temperatures below 100°C the decomposition reactions are probably too slow to contribute to a significant loss for the ozonides (14). We do not exclude the possibility that products of relatively high

volatility, such as hexanedial and pentanedial, were present in the aerosol phase. Even if the presence of these relatively high vapor pressure compounds in the aerosol phase resulted from experimental artifacts, they represent only about 4% of the aerosol mass and therefore do not compromise the general results of this study.

A.2.4 References

- Bailey, P.S. *Ozonation in organic chemistry*, Academic Press, New York, 1978.
- Bauld, N.L., Thompson, J.A., Hudson, C.E., and Bailey, P.S. *J. Am. Chem. Soc.* **1968**, *90*, 1822.
- Ellam, R.M., and Padbury, J.M. *Chem. Comm.* **1971**, 1094.
- Griffin, R.J., Cocker, D.R., Flagan, R. C., and Seinfeld, J.H. *J. Geophys. Res.* **1999**, *104*, 3555.
- Grosjean, E., Grosjean, D., and Seinfeld, J.H. *Environ. Sci. Technol.* **1996**, *30*, 1038.
- Gutbrod, R., Meyer, S., Rahman, M.M., and Schindler, R.N. *Int J. Chem. Kinet.* **1997**, *29*, 717.
- Hatekayama, S., Tanonaka, T., Weng, J., Bandow, H., Takagi, H., and Akimoto, H. *Environ. Sci. Technol.* **1985**, *19*, 935.
- Hull, L.A., Hisatsune, I.C., and Heicklen, J., *J. Phys. Chem.* **1972**, *76*, 2659.
- Izumi, K., Murano, K., Mizuochi M., and Fukujama, T. *Environ. Sci. Technol.* **1988**, *22*, 1207.
- LeLacheur, R.M., Sonnenberg, L.B., Singer, P.C., Christman R.F., and Charles, M.J. *Environ. Sci. Technol.* **1993**, *27*, 2745.
- Loan, L.D., Murray, R.W., and Story, P.R. *J. Am. Chem. Soc.* **1965**, *87*, 737.
- Odum, J. R., Hoffmann, T., Bowman, F., Collins, D., Flagan, R. C., and Seinfeld, J. H.

Environ. Sci. Technol. **1996**, 30, 2580.

Yu, J., Cocker, D.R., Griffin, R.J., Flagan, R.C., and Seinfeld, J.H. *J. Atmos. Chem.* **1999**, 34, 207.

Yu, J., Flagan, R.C., and Seinfeld, J.H. *Environ. Sci. Technol.* **1998**, 32, 2357.

Table A.2.1. Experimental conditions.

Experiment	O ₃ (init.) [ppb]	Cyclohexene (initial) [ppb]	Cyclohexene (final) [ppb] ^a	Δ Cyclo- hexene [ppb]	ΔM_o ^b [$\mu\text{g}/\text{m}^3$]	Yield ^c [%]
5/13/99 a	539	131	1.3	130	43	9.6
5/13/99 b	388	87	2.5	85	36	12.3
5/17/99 a	634	186	2.8	183	126	20.0
5/17/99 b	415	120	3.2	117	43	10.7
5/19/99 a	203	48	4.2	44	14	9.3
5/19/99 b	1011	137	0 ^d	137	36	7.6

^a concentration when denuder/filter sampling began.

^b ΔM_o = based on SEMS measurements, assumed $\rho=1.4 \text{ g}/\text{cm}^3$, see text.

^c Yield = $\Delta M_o / \Delta \text{Cyclohexene}$.

^d below detection limit.

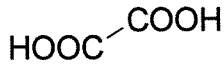
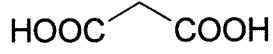
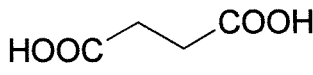
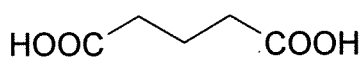
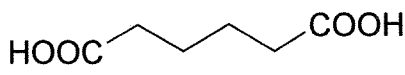
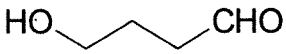
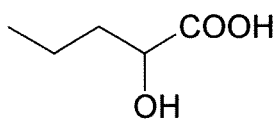
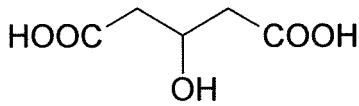
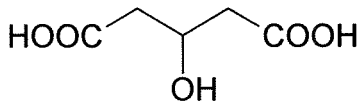
Table A.2.2. Denuder collection efficiencies for individual cyclohexene/ozone reaction products.

reaction product	denuder collection efficiency ^a
oxalic acid	0.95 ±0.02
malonic acid	0.98 ±0.01
succinic acid	0.96 ±0.02
adipic acid	0.98 ±0.01
glutaric acid	0.99 ±0.01
4-hydroxy-1-butanal	0.91±0.08 ^b
hydroxy pentanoic acid	0.99 ±0.01
hydroxy glutaric acid	0.95 ±0.02
hydroxy adipic acid	0.93 ±0.02
6-oxo-hexanoic acid	0.98 ±0.03
5-oxo-pentanoic acid	0.99 ±0.01
4-oxo-butanoic acid	0.98 ±0.01
1,6-hexanedial	0.99 ±0.01
1,5-pentanedial	0.98 ±0.02
1,4-butanedial	0.92 ±0.06
Pentanal	0.77 ±0.18

^a Denuder collection efficiencies for individual products are calculated using six sets of samples.

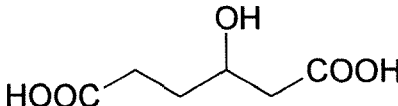
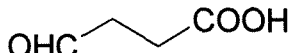
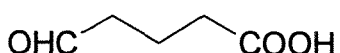
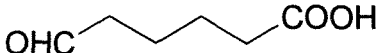
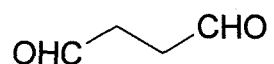
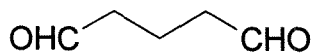
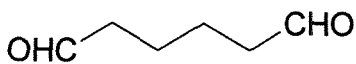
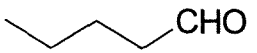
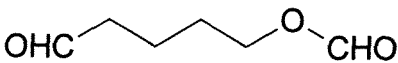
^b Only 5 data points.

Table A.2.3. Chemical structures of products of the cyclohexene-ozone reaction.

Compound	Structure	Molecular Weight	Molecular weight of derivative ^a
oxalic acid		90	234
malonic acid		104	248
succinic acid		118	262
glutaric acid		132	276
adipic acid		146	290
4-hydroxy-1-butanal		88	355
2-hydroxy pentanoic acid		118	262
3-hydroxy glutaric acid		148	364
3-hydroxy adipic acid		162	378

^aMolecular weight for derivative is for full derivatization of all the possible functional groups in the molecule.

Table A.2.3. Chemical structures of products of the cyclohexene-ozone reaction continued

Compound	Structure	Molecular Weight	Molecular Weight of Derivative ^a
3-hydroxy-adipic acid		162	378
4-oxo-butanoic acid		102	369
5-oxo-pentanoic acid		116	383
6-oxo-hexanoic acid		130	397
1,4-butanedial		86	476
1,5-pentanedial		100	490
1,6-hexanedial		114	504
pentanal		86	281
5-oxo-pentyl formate		116	383

^aMolecular weight for derivative is for full derivatization of all the possible functional groups in the molecule.

Table A.2.4. Chemical compounds used as standards or surrogates for quantification.

Compounds found in samples	Standard or surrogates	Quantification ions	Retention time [min]	Density [g/cm ³]	Surrogate for density
oxalic acid	oxalic acid	219	8.533	1.9	
malonic acid	malonic acid	233	9.931	1.619	
succinic acid	succinic acid	247	11.082	1.572	
glutaric acid	glutaric acid	261	12.348	1.424	
adipic acid	adipic acid	275	13.748	1.36	
4-hydroxy-1-butanal	4-oxo-butanoic acid	73,75,181	14.983	0.817	butanal
hydroxy pentanoic acid	3-OH-3-methylglutaric acid	73,75	11.39	0.9391	pentanoic acid
hydroxy glutaric acid	3-OH-3-methylglutaric acid	73,75	14.716	1.424	glutaric acid
hydroxy adipic acid	3-OH-3-methylglutaric acid	73,75	15.817	1.36	adipic acid
4-oxo-butanoic acid	4-oxo-butanoic acid	354,188,172	16.014		
5-oxo-pentanoic acid	4-oxo-pentanoic acid	73+75+181	17.049	0.9391	pentanoic acid
6-oxo-hexanoic acid	5-oxo-hexanoic acid	73+75+181	18.149	0.93	
1,4-butanedial	1,5-pentanedial	181	20.284	0.817	butanal
1,5-pentanedial	1,5-pentanedial	309,293	21.166	0.8095	pentanal
1,6-hexanedial	1,5-pentanedial	181	21.149	0.8139	hexanal
pentanal	pentanal	181	11.698	0.8095	

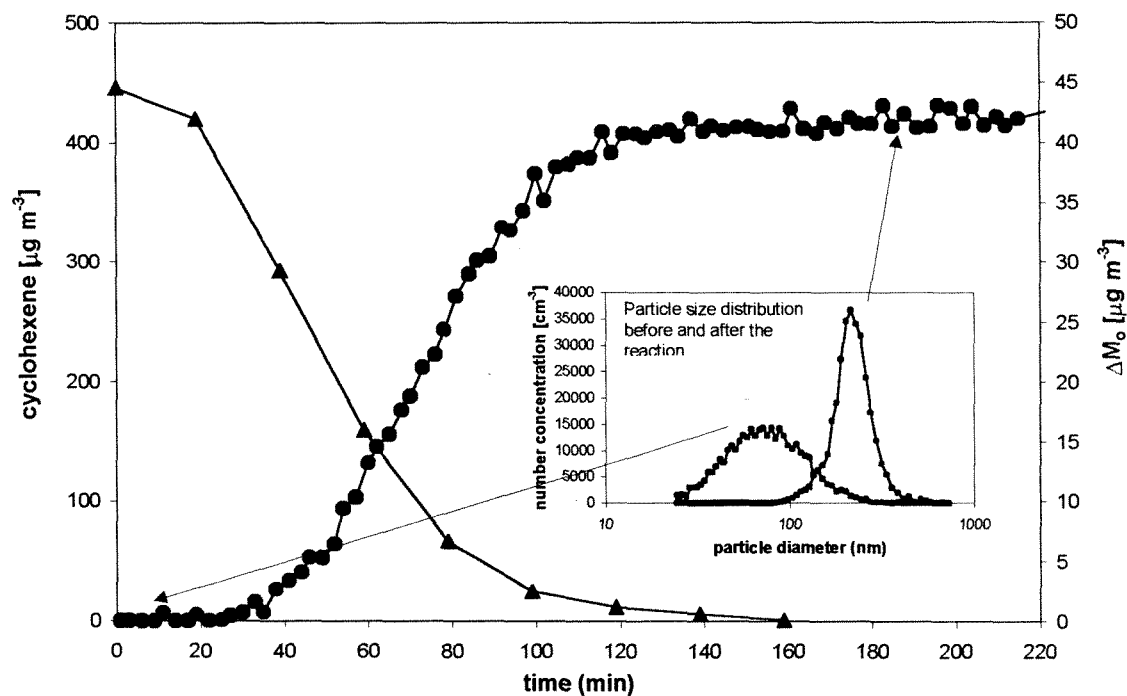


Figure A.2.1. Cyclohexene and total aerosol mass concentration ΔM_0 as a function of time. As the cyclohexene concentration decreases with time, the organic aerosol mass increases correspondingly. The organic aerosol mass ΔM_0 is calculated from the difference of the aerosol size distributions at the beginning and end the reaction and at the end, as shown in the insert.

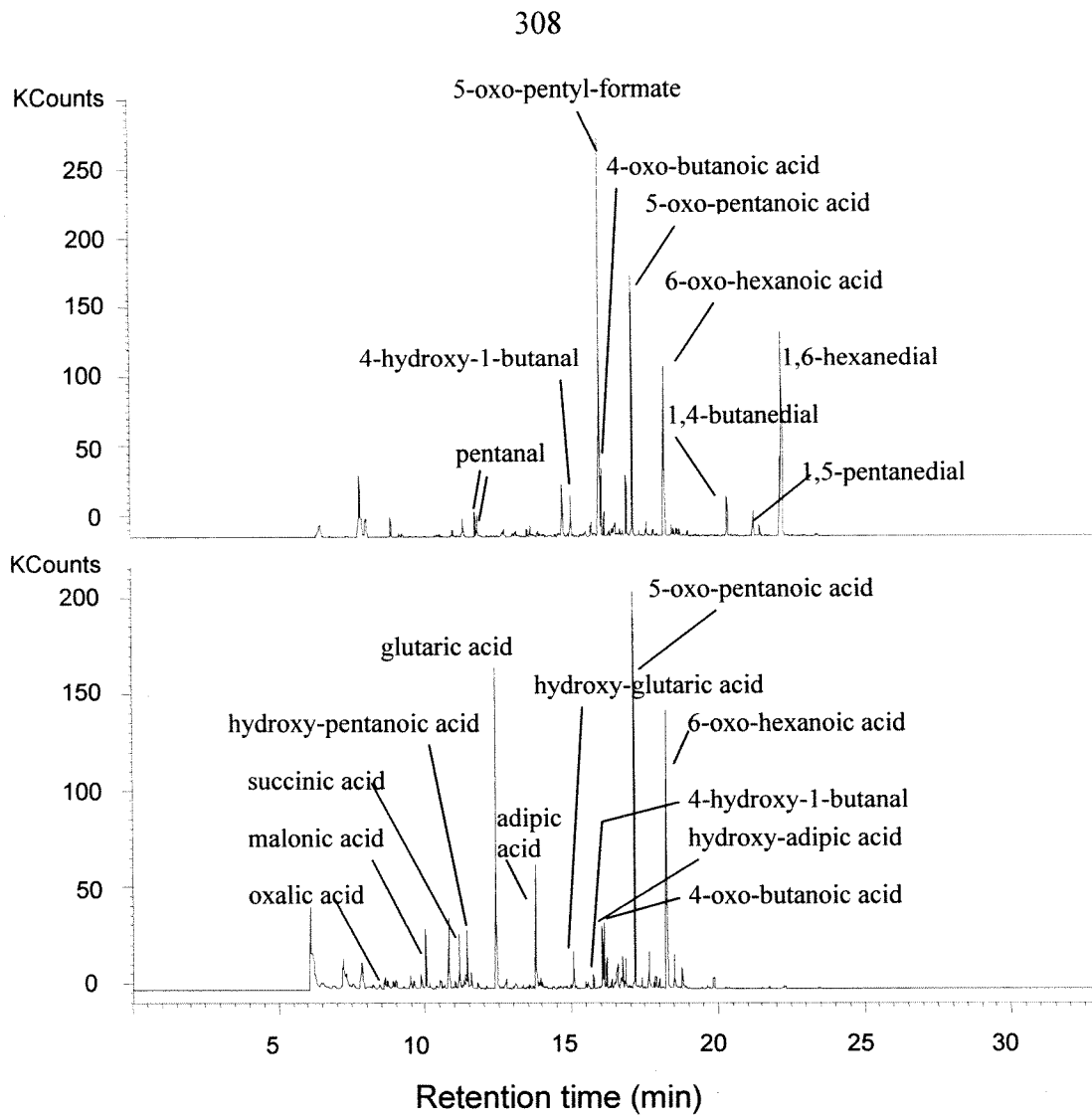


Figure A.2.2. Chromatogram of a filter sample. (a) m/z 181 chromatogram showing all carbonyl compounds identified; (b) m/z 73+75 chromatogram showing the compounds with a carboxylic and/or hydroxy functional group.

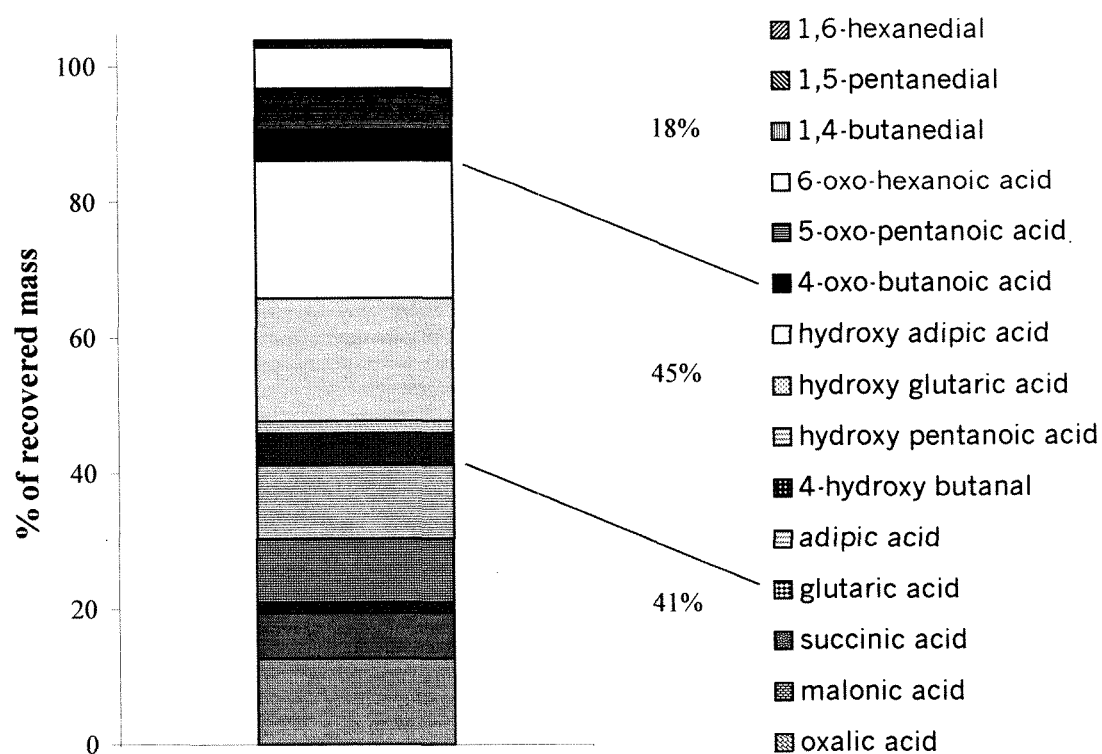


Figure A.2.3. Molecular distribution of the particle composition. 104% of the particle mass could be resolved on a molecular level assuming a weighted particle density of 1.4 g cm^{-3} .

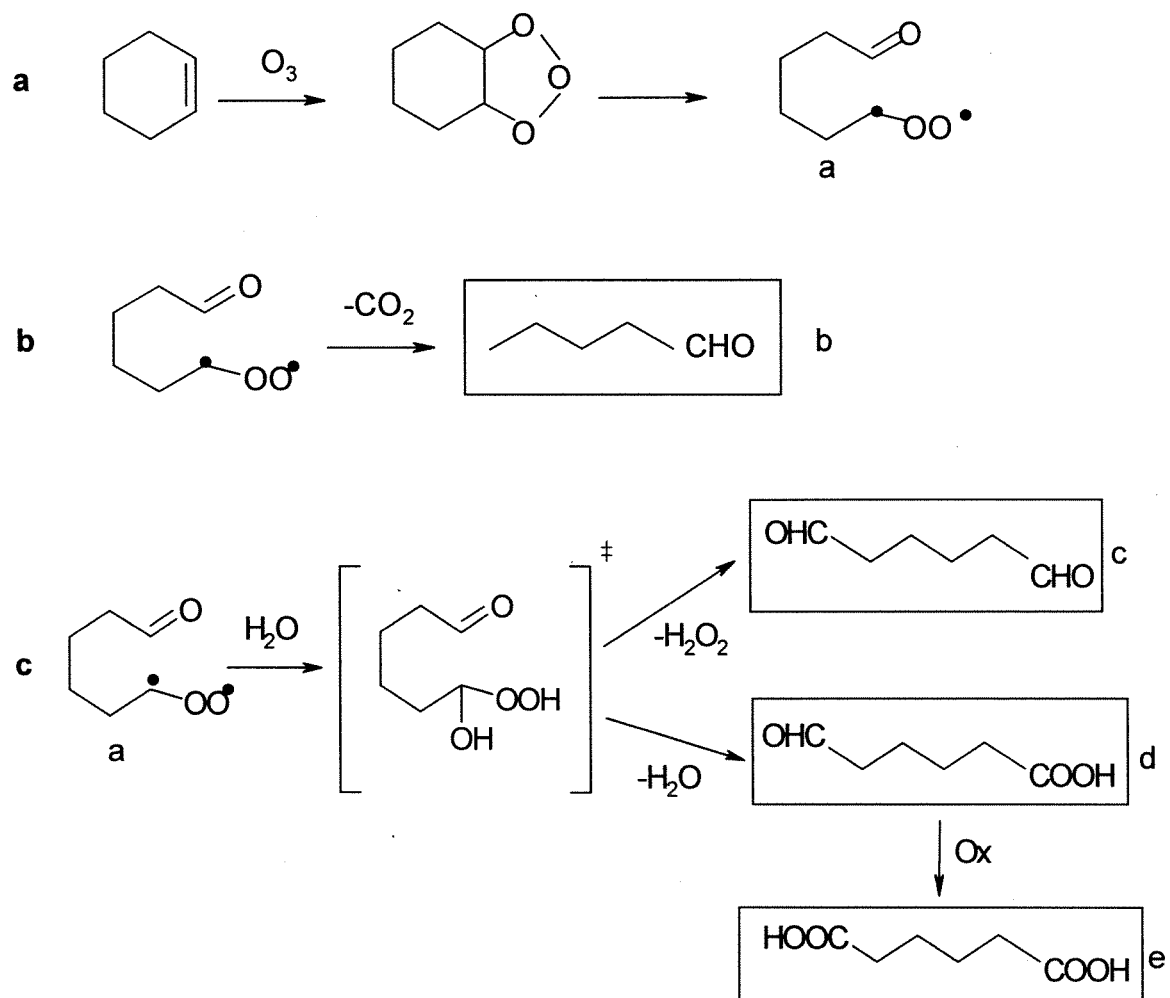


Figure A.2.4. (a)-(g) Proposed reaction mechanism of the cyclohexene-ozone reaction leading to the products observed in this study. For details see text. The combined mass of all individual compounds is 104% of the mass determined from DMA measurement, based on an assumed aerosol density of 1.4 g cm^{-2} .

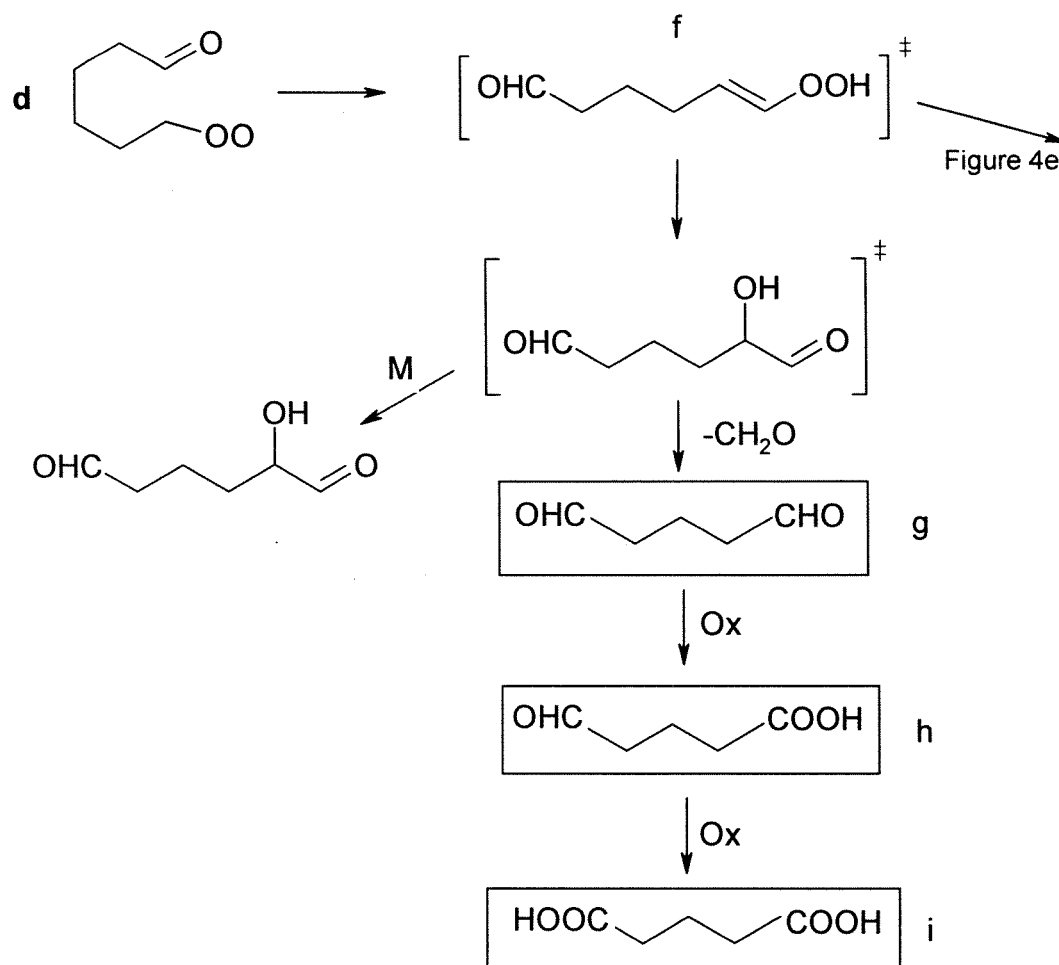


Figure A.2.4 continued. (a)-(g) Proposed reaction mechanism of the cyclohexene-ozone reaction leading to the products observed in this study. For details see text. The combined mass of all individual compounds is 104% of the mass determined from DMA measurement, based on an assumed aerosol density of 1.4 g cm^{-2} .

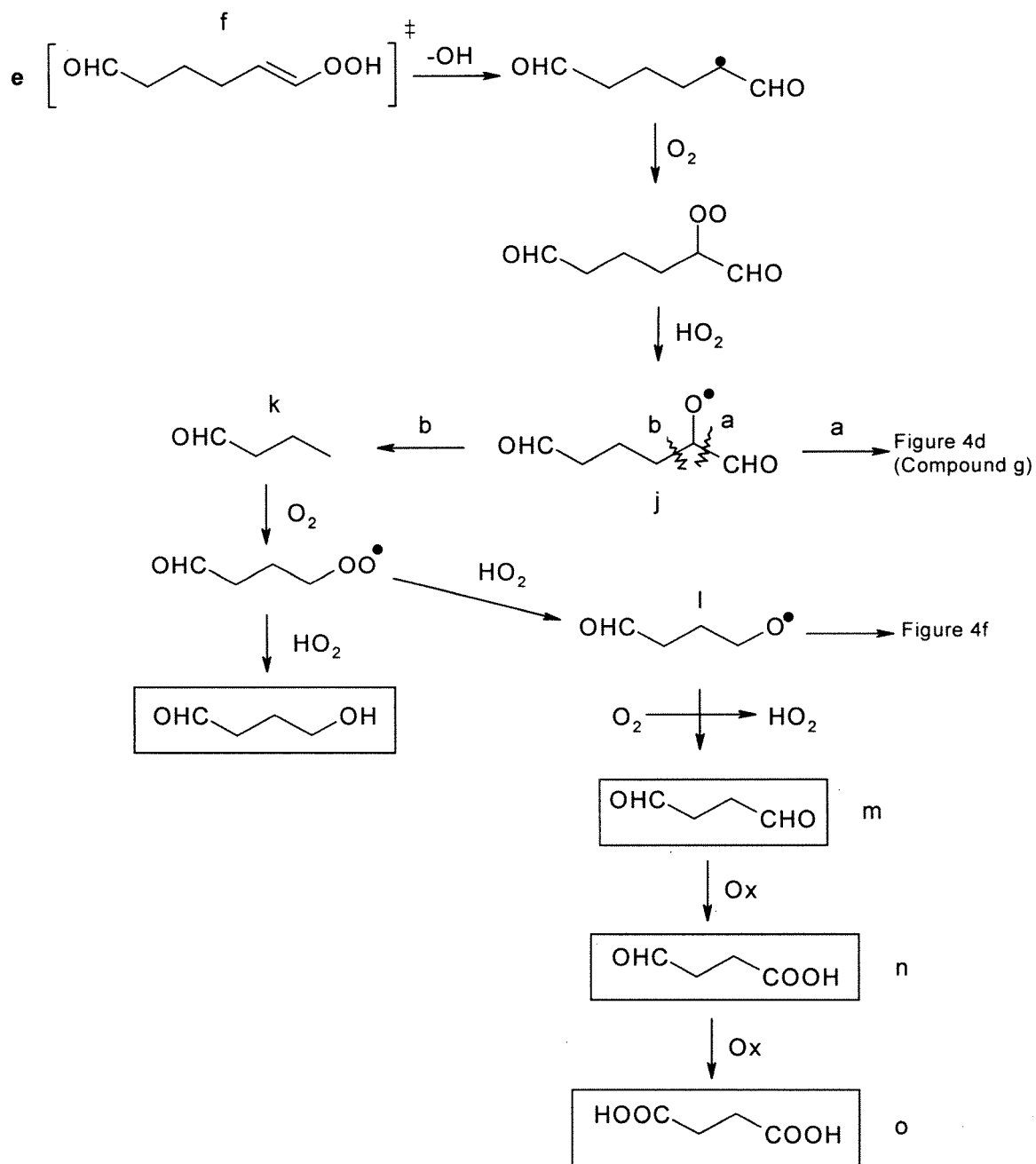


Figure A.2.4 continued. (a)-(g) Proposed reaction mechanism of the cyclohexene-ozone reaction leading to the products observed in this study. For details see text. The combined mass of all individual compounds is 104% of the mass determined from DMA measurement, based on an assumed aerosol density of 1.4 g cm^{-2} .

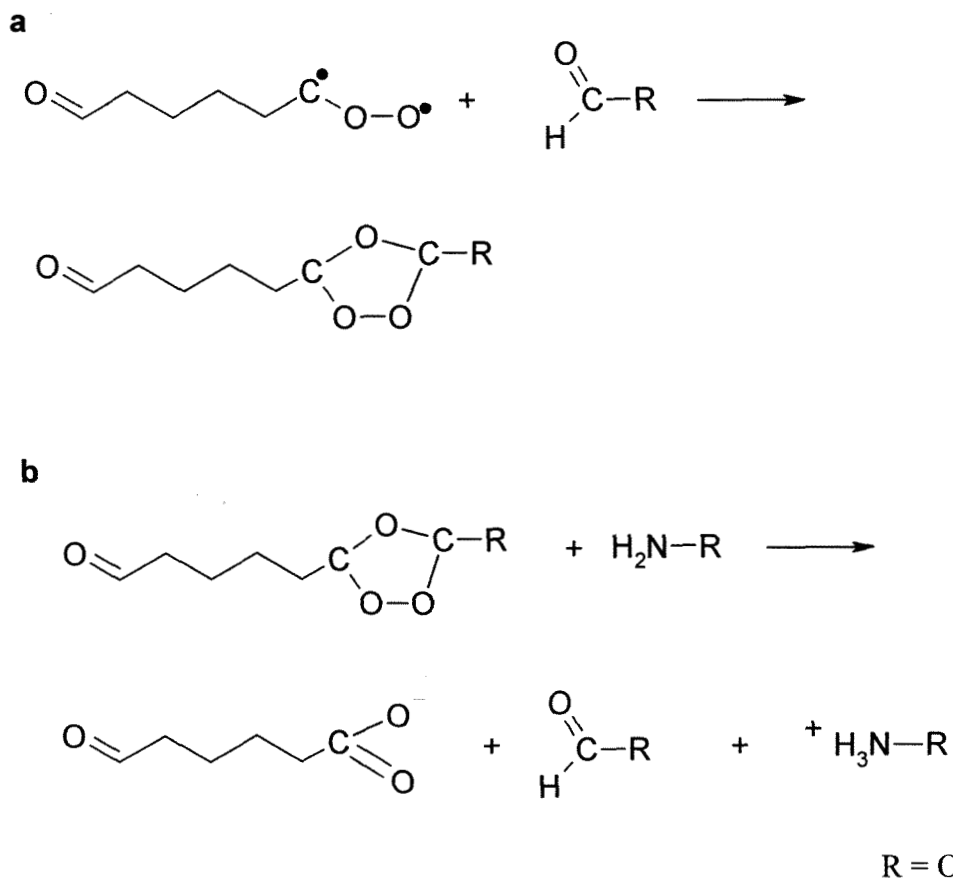


Figure A.2.5. (a) The Criegee biradical can react with aldehydes to a second ozonide.

(b) Ozonides, like the reaction product of (a), might react with the derivatization agent

PFBHA, a primary amine, to form an aldehyde and an acid.

Appendix 3

Observation of Gaseous and Particulate Products of Monoterpene

Oxidation in Forest Atmospheres

Reference: J. Yu, R.J. Griffin, D.R. Cocker III, R.C. Flagan, J.H. Seinfeld, and P.

Blanchard, *Geophys. Res. Lett.*, 26, 1145-1148, 1999.

Abstract

Atmospheric oxidation of biogenic hydrocarbons, such as monoterpenes, is estimated to be a significant source of global aerosol. Whereas laboratory studies have established that photochemical oxidation of monoterpenes leads to aerosol formation, there are limited field studies detecting such oxidation products in ambient aerosols. Drawing on prior results of monoterpene product analysis under controlled smog chamber conditions, we have identified organic aerosol components attributable to monoterpene oxidation in two forest atmospheres, Kejimikujik National Park, Nova Scotia, Canada, and Big Bear, San Bernardino National Forest, California, U.S.A. The major identified aerosol products derived from α -pinene and β -pinene oxidation include pinic acid, pinonic acid, norpinonic acid and its isomers, hydroxy pinonaldehydes, and pinonaldehyde, concentrations of which in the aerosol phase are in the sub ng m⁻³ range. Identification of oxidation products in atmospheric aerosol samples serves as direct evidence for aerosol formation from monoterpenes under ambient conditions.

A.3.1 Introduction

The atmospheric aerosol-forming potential of biogenic hydrocarbons was noted as early as 1960 [Went, 1960], and laboratory studies have established that atmospheric oxidation of monoterpenes and sesquiterpenes leads to aerosol formation [Hoffmann *et al.*, 1997; Griffin *et al.*, 1999]. Production of biogenic secondary organic aerosols on a global basis is estimated to range between 30 and 270 Tg year⁻¹, a magnitude comparable to the production of biogenic and anthropogenic sulfate aerosols [Andreae and Crutzen, 1997].

Monoterpenes are important constituents of aerosol-forming biogenic compounds [Griffin *et al.*, 1999]. Despite numerous field measurements of gas-phase monoterpenes [e.g., Roberts *et al.*, 1983; Zimmerman *et al.*, 1988; Clement *et al.*, 1990; Biesenthal *et al.*, 1998], there are few field studies in which their oxidation products have been measured. Recent advances in analytical methods have now made it possible to detect and identify such secondary organic aerosol components, which generally have multiple polar oxygenated functional groups [Yu *et al.*, 1998; 1999]. Ambient measurements of biogenic hydrocarbon oxidation products in the atmospheric aerosol provide the link that establishes the importance of this source to global tropospheric aerosol. We present here measurements of monoterpene-derived aerosol components in two forest atmospheres, Kejimikujik National Park, Nova Scotia, Canada, and San Bernardino National Forest, California, U.S.A.

A.3.2 Ambient Sampling and Analysis

The measurement site in Kejimikujik National Park (44°26' N, 62°12' W) is situated in the Atlantic province of Nova Scotia. The park is in a forest consisting of a mixture of two-thirds coniferous and one-third deciduous trees [Bottenheim *et al.*, 1994]. Ambient mixing ratios of α -pinene and β -pinene were determined on-line using a Hewlett-Packard GC/MS [Biesenthal *et al.*, 1998]. Aerosol samples were collected in July, 1996, over a period of two to three days at a flow rate of 10 L min⁻¹ on 47 mm quartz fiber filters. Since the aerosol samples were collected in a field campaign that did not include characterizing semivolatile organics as one of its goals, adequate sampling devices were not implemented to minimize sampling artifacts for semivolatiles. Collection of two filter samples analyzed in this work commenced on July 5 and July 8,

based on a sampled air volume of 26.94 and 44.72 m³, respectively. The diurnal temperature during the sampling period ranged from 11 to 21°C, and the relative humidity from 13% to 50% [Leaitch *et al.*, 1999].

The measurement site in the San Bernardino National Forest is located in Big Bear Valley (34°13' N, 116°49' W), CA, at an elevation of 2150 meters. Lodgepole pines, pinion pines, oaks, and Douglas firs are major tree species in this area. Hourly measurements of gas-phase monoterpenes were achieved by collecting 300 L of air on Tenax tubes, and were then analyzed by a Hewlett-Packard GC/MS following thermal desorption using a Tekmar AeroTrap Desorber 6000. Two types of aerosol sampling devices were deployed, one consisting of one or two denuders followed by a Teflon impregnated glass fiber filter, and the other one consisting of two 47 mm filters--a Teflon impregnated glass fiber filter followed by a glass fiber filter. Two sampling trains were set up for each type of sampling device. The sampling train with two denuders was used to quantify denuder collection efficiency. Samples were collected from 19:00 PDT Aug. 31 to 13:00 PDT Sep. 1, 1998, at a flow rate of 22 L min⁻¹. The back filter in the two-filter set-up was used for assessing filter adsorption of gaseous semivolatile organics. Ambient temperature during the sampling period varied from 18 to 32°C, and relative humidity ranged from 20% to 59%.

Denuder samples were extracted on-site, and all samples were stored at 0°C before analysis. The procedure for extraction, subsequent processing, and analysis of denuder and filter samples has been described elsewhere [Yu *et al.*, 1999]. The extracts of denuder and filter samples were derivatized by (2,3,4,5,6-pentafluorobenzyl) hydroxy amine (PFBHA) and N, O-bis (trimethylsilyl)-trifluoroacetamide. By this procedure,

carbonyl functional groups of the oxidation products were converted into oximes, and carboxyl and hydroxyl function groups were converted into trimethylsilyl (TMS) groups. The resulting derivatives were then analyzed by GC/MS, using both electronic ionization (EI) and chemical ionization (CI) modes for identification and quantification. Blank filters in both studies were treated and analyzed following the same procedures applied to the sample filters. Quantification of products for which authentic standards do not exist was achieved by using surrogate compounds that have the same functional groups and approximate carbon numbers [Yu *et al.*, 1999].

A.3.3 Results and Discussion

A.3.3.1 Identification of Monoterpene Oxidation Products

Oxidation products of α -pinene and β -pinene in the ambient samples were identified by comparing GC chromatograms and mass spectra of the ambient samples with those obtained from controlled chamber experiments. Table A.3.1 lists the chemical structures of the monoterpene oxidation products observed.

Established products from oxidation of α -pinene and β -pinene include pinic acid, norpinic acid, pinonaldehyde, norpinonaldehyde, hydroxy pinonaldehydes, pinonic acid, norpinonic acid, hydroxy pinonic acid, hydroxy pina ketones, and nopinone. An unidentified product (denoted X_1), having two carbonyl groups and a molecular weight of 198 as determined from its EI and CI mass spectra, is observed in both laboratory generated aerosol in the α -pinene/ O_3 system and ambient aerosols at both sites. Besides oxidation products derived from α -pinene and β -pinene, a compound denoted X_2 , detected in samples from both sites, is identified as a C_9 dioxo mono-carboxylic acid, having a molecular weight of 186. Figure A.3.1 displays the CI mass spectrum for the

PFBHA and TMS derivative of this compound X₂. The molecular weight and some structural information can be determined from the mass spectrum [Yu *et al.*, 1998].

Ozone oxidation of limonene could lead to the formation of a C₉ dioxo mono-carboxylic acid, 3-acetyl-6-oxo-heptanoic acid, as illustrated in Figure A.3.2 [Horie *et al.*, 1994; Neeb *et al.*, 1997]. The mass spectrum shown in Figure A.3.1 is consistent with that expected for this compound.

A.3.3.2 Kejimikujik Samples

Table A.3.2 lists mixing ratios of three monoterpenes and concentrations of various monoterpene oxidation products in the aerosol phase in two filter samples collected in Kejimikujik National Park. All the identified oxidation products are detected at the sub-nanogram m⁻³ level. The presence of monoterpene oxidation products in filter samples correlates with the observation that aerosol volume increased with the decrease in α -pinene and β -pinene during the same sampling period at this same site [Leaitch *et al.*, 1999].

A.3.3.3 Big Bear Samples

Table A.3.3 lists the mixing ratios of six monoterpenes and the concentrations of various monoterpene oxidation products detected in both the gas and aerosol phases in the San Bernardino National Forest of California. The denuder/filter set-up at this site allowed simultaneous determination of semi-volatile compounds in both gas and particulate phases. Species collected by the denuder represent those in the gas phase. Denuder collection efficiencies for the products in Table A.3.3 range from 0.88 to 1.0. Gas-phase concentrations as determined from denuder samples have been corrected for the denuder collection efficiency for each product. As evident in Table A.3.3, the

monoterpene oxidation products at this site predominately exist in the gas phase. A number of oxidation products were detected solely in the gas phase due to either their high volatility (e.g., nopinone, hydroxy pinones, and norpinonaldehyde) or to such a low concentration in the air that the amount partitioned to the aerosol phase is below detection limit (e.g., norpinonic acid and hydroxy pinonic acid).

Comparison of filter samples in the presence and absence of a denuder in front of the sampling train indicates that the filter-only technique suffers a positive sampling artifact. Semivolatile products are also detected on the back filter in the filter-only set-up, which is evidence for filter adsorption of gaseous semivolatile organics. Concentrations obtained via the filter-only technique are 120%-137% higher than those obtained using the denuder/filter sampling device for sampling conditions employed at the Big Bear site. *McDow and Huntzicker* [1990] observed a significant increase of positive artifact with decreasing filter face velocity for a quartz fiber filter. They estimated that at low organic carbon concentrations, the correction factor due to adsorption could exceed 50% at a sampling face velocity of 40 cm s^{-1} . Considering the lower face velocity ($\sim 20 \text{ cm s}^{-1}$), the positive artifact observed at the Big Bear site is in general agreement with the results of *McDow and Huntzicker* [1990]. Therefore, the filter-only technique is not adequate for measurements of biogenic oxidation products in the aerosol phase. Concentrations derived from the two Kejimikujik filter samples likely overestimate the actual aerosol concentrations for this reason.

A.3.4 Comparison with Prior Field Studies

Previous field measurements of particulate-phase terpene oxidation products have been limited to pinonaldehyde, pinonic acid, and nopinone. A recent study has also

measured ambient concentrations of pinic acid and norpinonic acid [Kavouras *et al.*, 1999]. Yokouchi and Ambe [1985] measured pinonaldehyde concentrations of 2-3 ng m⁻³ in aerosol samples collected in the cedar forest at Kiyosumi and in the pine forest at Tsukuba in Japan in summer time. Satsumabayashi *et al.* [1990] detected pinonaldehyde at 30 ng m⁻³ and 100 ng m⁻³ at two mountainous sites in central Japan. Calogirou *et al.* [1997] observed pinonaldehyde near Ispra, Italy, at 90 ng m⁻³ using DNPH-coated cartridges. Since an ozone scavenger was used in this study, which also collected particles, this concentration reflects that in the gas-phase. Kavouras *et al.* [1998] reported aerosol concentrations for pinonic acid, nopinone, and pinonaldehyde ranging from 9-140, 0.3-13.2, and 0.17-32.1 ng m⁻³, respectively, at a forest site in Portugal. In the most recent study, Kavouras *et al.* [1999] deployed a denuder/filter sampling device to measure monoterpene oxidation products in both gas and aerosol phases in a conifer forest located in Pertouli in Central Greece. They reported diurnal particulate concentrations for pinonic acid, pinic acid, norpinonic acid, pinonaldehyde, and nopinone to be 1.0-25.7, 0.4-4.4, 0.2-5.4, 0.2-1.2, and 0-0.4 ng m⁻³, respectively. In this study, simultaneous measurements of Aitken nuclei also provided evidence that the photooxidation products from biogenic precursors play a role in forming new particles.

Considering the many factors influencing concentrations of aerosol-phase monoterpene oxidation products, the wide variability of ambient concentrations among the six studies is not surprising. Pinonaldehyde, for example, was measured in all six studies with concentrations ranging from under detection limit to 100 ng m⁻³. Concentrations of precursor monoterpenes and atmospheric oxidants govern formation rate of the products. The higher mixing ratios of α -pinene (0-3.2 ppbv) and β -pinene (0-

1.4 ppbv) may partly account for the more plentiful oxidation products in the aerosol phase in the study of *Kavouras et al.* [1999]. The aerosol-phase fraction of a semi-volatile organic compound, such as any of the monoterpene oxidation products, is known to be controlled by available organic aerosol mass and the compound's gas-aerosol partitioning coefficient, which, in turn, is a function of temperature and the overall aerosol chemical composition [*Odum et al.*, 1996; *Jang et al.*, 1997; *Jang and Kamens*, 1999; *Yu et al.*, 1999]. Besides these factors intrinsic to aerosol formation, sampling artifacts can also introduce variability in the reported concentrations. For example, as noted earlier, the filter-only technique suffers a positive artifact from adsorption of gas-phase semi-volatiles onto the filter surface, whereas volatilization of aerosol-phase semi-volatiles introduces a negative artifact, which depends on sampling rate and filter area [*McDow and Huntzicker*, 1990]. In addition, a number of products (e.g., pinonaldehyde and norpinonic acid) do not have available commercial standards, and different surrogate compounds have been used to estimate their concentrations.

A.3.5 Conclusions

We have detected in two forest atmospheres a number of gas- and aerosol-phase products from oxidation of α -pinene and β -pinene, including pinic acid, norpinic acid, pinonic acid, norpinonic acid and its isomers, pinonaldehyde, norpinonaldehyde, hydroxy pinonaldehydes, hydroxy pinonic acid, and nopinone. In addition, a C₉ dioxo carboxylic acid, detected at both sites, is postulated to be 3-acetyl-6-oxo-heptanoic acid, a product expected from ozone oxidation of limonene. Identification of monoterpene oxidation products in aerosol samples serves as direct evidence for aerosol formation from monoterpenes under ambient conditions.

A.3.6 References

- Andreae, M. O., and P.J. Crutzen, Atmospheric aerosols: Biogeochemical sources and role in atmospheric chemistry, *Science*, 276, 1052-1055, 1997.
- Biesenthal, T.A., J.W. Bottenheim, P.B. Shepson, and P.C. Brickell, The chemistry of biogenic hydrocarbons at a rural site in eastern Canada, *J. Geophys. Res.*, 103, 25,487-25,498, 1998.
- Bottenheim, J.W., A. Sirois, K.A. Brice, and A.J. Gallant, Five years of continuous observation of PAN and ozone at a rural location in Eastern Canada, *J. Geophys. Res.*, 99, 5333-5352, 1994.
- Calogirou, A., M. Duane, D. Kotzias, M. Lahaniati, and B.R. Larsen, Polyphenylenesulfide NOXON, an ozone scavenger for the analysis of oxygenated terpenes in air, *Atmos. Environ.*, 13, 2741-2751, 1997.
- Clement, B., M.L. Riba, R. Leduc, M. Haziza, and L. Terres, Concentration of monoterpenes in a maple forest in Quebec, *Atmos. Environ.*, 24A, 2513-2516, 1990.
- Griffin, R.J., D.R. Cocker, R.C. Flagan, and J.H. Seinfeld, Organic aerosol formation from the oxidation of biogenic hydrocarbon., *J. Geophys. Res.*, 104, 3555-3568, 1999.
- Hoffmann, T., J.R. Odum, F. Bowman, D. Collins, D. Klockow, R.C. Flagan, and J.H. Seinfeld, Formation of organic aerosols from the oxidation of biogenic hydrocarbons, *J. Atmos. Chem*, 26, 189-222, 1997.
- Horie, O., P. Neeb, S. Limbach, and G.K. Moortgat, Formation of formic acid and organic peroxides in the ozonolysis of ethene with added water vapor, *Geophys. Res. Lett.*, 21, 1523-1526, 1994.

- Jang, M., and R.M. Kamens, Newly characterized products and composition of secondary aerosols from the reaction of α -pinene with ozone, *Atmos. Environ.*, **33**, 459-474, 1999.
- Jang, M., R.M. Kamens, K.B. Leach, and M.R. Strommen, A thermodynamic approach using group contribution methods to model the partitioning of semivolatile organic compounds on atmospheric particulate matter, *Environ. Sci. Technol.*, **31**, 2805-2811, 1997.
- Kavouras, I.G., N. Mihalopoulos, and E.G. Stephanou, Formation of atmospheric particles from organic acids produced by forests, *Nature*, **395**, 683-686, 1998.
- Kavouras, I.G., N. Mihalopoulos, and E.G. Stephanou, Formation and gas/particle partitioning of monoterpenes photooxidation products over forests, *Geophys. Res. Lett.*, **26**, 55-58, 1999.
- Leaith, W.R., J.W. Bottenheim, T.A. Biesenthal, S.M. Li, P.S. K. Liu, K. Asalien, H. Dryfhout-Clark, F. Hopper, and F. Brechtel, A case study of gas-to-particle conversion in an eastern Canadian Forest, *J. Geophys. Res.*, **104**, 8095-8111, 1999.
- McDow, S.R., and J.J. Huntzicker, Vapor adsorption artifact in the sampling of organic aerosol: Face velocity effects, *Atmos. Environ.*, **24A**, 2563-2571, 1990.
- Neeb, P., F. Sauer, and O. Horie, Formation of hydroxymethyl hydroperoxide and formic acid in alkene ozonolysis in the presence of water vapor, *Atmos. Environ.*, **31**, 1417-1423, 1997.
- Odum, J.R., T. Hoffmann, F. Bowman, D. Collins, R.C. Flagan, and J.H. Seinfeld, Gas/particle partitioning and secondary organic aerosol yields, *Environ. Sci. Technol.*, **30**, 2580-2585, 1996.

- Roberts, J.M., F.C. Fehsenfeld, D.L. Albritton, and R.E. Sievers, Measurement of monoterpene hydrocarbons at Niwot Ridge, Colorado, *J. Geophys. Res.*, 88, 667-678, 1983.
- Satsumabayashi, H., H. Kurita, Y. Yokouchi, and H. Ueda, Photochemical formation of particulate dicarboxylic acids under long-range transport in Central Japan, *Atmos. Environ.*, 24A, 1443-1450, 1990.
- Went, F.W., Blue hazes in the atmosphere, *Nature*, 187, 641-643, 1960.
- Yokouchi, Y., and Y. Ambe, Aerosols formed from the chemical reaction of monoterpenes and ozone, *Atmos. Environ.*, 19, 1271-1276, 1985.
- Yu, J., R.C. Flagan, and J.H. Seinfeld, Identification of products containing -COOH, -OH, and -C=O in atmospheric oxidation of hydrocarbons, *Environ. Sci. Technol.*, 32, 2357-2370, 1998.
- Yu, J., D.R. Cocker III, R.J. Griffin, R.C. Flagan, and J.H. Seinfeld, Gas-phase ozone oxidation of monoterpenes: Gaseous and particulate products, *J. Atmos. Chem.*, 104, 3555-3568, 1999.
- Zimmerman, P.R., J.P. Greenberg, and C.E. Westberg, Measurement of atmospheric hydrocarbons and biogenic emission fluxes in the Amazon boundary layer, *J. Geophys. Res.*, 93, 1407-1416, 1988.

Table A.3.1. Monoterpene oxidation products detected at forest sites.

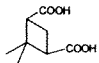
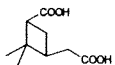
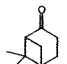
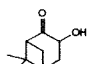
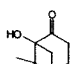
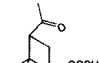
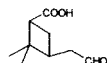
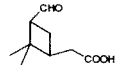
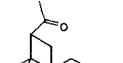
Name	Structure	note
<hr/>		
$C_8H_{12}O_4$		
norpinic acid		a, b
MW=172		
<hr/>		
$C_9H_{14}O_4$ *		
pinic acid		c, d
MW=186		
<hr/>		
$C_9H_{14}O$ *		
nopinone		e, f
MW=138		
<hr/>		
$C_9H_{14}O_2$		
hydroxy pina		e, f
ketones		
MW=154		
<hr/>		
$C_9H_{14}O_3$		
norpinonic acid		a, d
& its isomers		
MW=170		
<hr/>		
$C_{10}H_{16}O_3$ *		
pinonic acid		g, d
MW=184		
<hr/>		

Table A.3.1. (continued) Monoterpene oxidation products detected at forest sites.

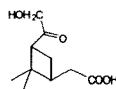
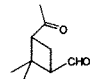
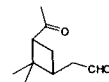
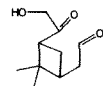
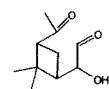
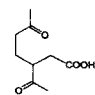
Name	Structure	note
<hr/>		
$C_{10}H_{16}O_4$		
hydroxy		a, h
pinonic acid		
MW=200		
<hr/>		
$C_9H_{14}O_2$		
norpinonaldehyde		g, f
MW=154		
<hr/>		
$C_{10}H_{16}O_2$		
pinonaldehyde		g, d
MW=168		
<hr/>		
$C_{10}H_{16}O_3$		
hydroxy		g, d
pinonaldehydes		
MW=184		
<hr/>		
X_1	two carbonyl	g, d
MW=198	groups	
<hr/>		
X_2	e.g.	
$C_9H_{14}O_4$		i, d
MW=186		
<hr/>		

Table A.3.1. (continued) Monoterpene oxidation products detected at forest sites.

* identification confirmed with an authentic standard.

^a known product of O₃ oxidation of α -pinene and β -pinene.

^b detected in Kejimikujik samples.

^c known product of O₃ oxidation of α -pinene, β -pinene, sabinene and Δ^3 -carene.

^d detected in Kejimikujik and Big Bear samples.

^e known product of O₃ oxidation of β -pinene.

^f detected in Big Bear denuder samples.

^g known product of O₃ oxidation of α -pinene.

^h detected in Big Bear denuder and filter samples.

ⁱ possible product of O₃ oxidation of limonene.

Table A.3.2. Monoterpene oxidation products in filter samples collected in Kejimikujik National Park, Nova Scotia.

monoterpene				conc. (ng m ⁻³)	
mixing ratio (pptv)		product			
	960705 ^a	960708 ^a		960705 ^a	960708 ^a
α -pinene	88-283	147-642	norpinic acid ^b	0.34	0.34
β -pinene	69-401	209-864	pinic acid	0.48	0.59
camphene	60-442	156-561	norpinonic acid	0.24	0.04
			& its isomers ^c		
			pinonic acid	0.39	0.13
			pinonaldehyde ^d	0.19	0.08
			hydroxy	0.12	ND ^e
			pinonaldehydes ^c		
			X ₁ ^d	0.12	0.13
			X ₂ ^c	0.19	0.13

^a Dates when aerosol samples commenced.

^b Quantified using the calibration factor and recovery for pinic acid.

^c Quantified using the calibration factor and recovery for pinonic acid.

^d Quantified using the calibration factor and recovery for 5-methyl-cyclohexane-1,3-dione.

^e Not detectable.

Table A.3.3. Gaseous and particulate monoterpene oxidation products in samples collected in San Bernardino National Forest, California.

monoterpene					
mixing ratio (pptv)		product	conc.(ng m ⁻³) ^a		
range	avg.		gas	aerosol	
α -pinene	22 - 119	63	pinic acid	11.5	0.5
β -pinene	16 - 111	50	norpinonic acid & its isomers	12.3	ND ^b
limonene	13 - 63	27	pinonic acid	202.4	0.8
camphene	7 - 76	36	norpinonaldehyde	4.7	ND
Δ^3 -carene	2 - 21	10	pinonaldehyde	280	1.0
junipene	0 - 8	5	hydroxy pinonaldehydes	16.8	0.5
		X ₁	3.3	0.2	
		X ₂	17.8	0.8	
		hydroxy pinonic acid	9.0	ND	
		hydroxy pina ketones	18.0	ND	
		nopinone & isomers ^c	132.9	ND	

^a average values of two samples.

^b Not detectable.

^c Possible isomers include primary carbonyl products from ozone oxidation at the external C=C bond in limonene and camphene.

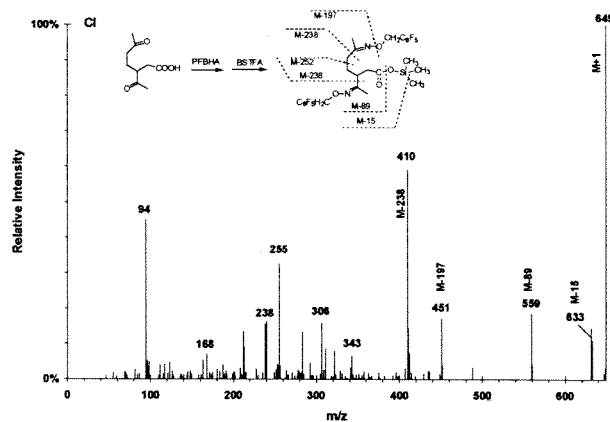


Figure A.3.1. Chemical ionization mass spectrum for the derivative of a C₉ dioxo carboxylic acid compound detected in aerosol samples.

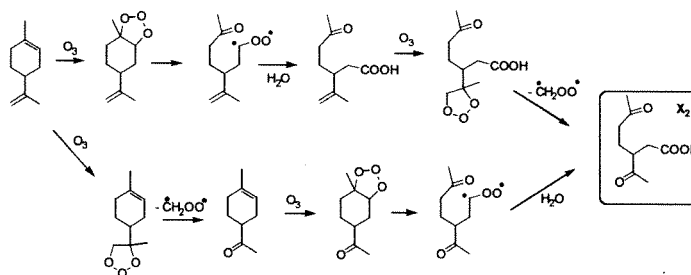


Figure A.3.2. Formation pathways for a C₉ dioxo carboxylic acid product from oxidation of limonene.

Appendix 4**Estimate of Global Atmospheric Organic Aerosol from Oxidation of
Biogenic Hydrocarbons**

Reference: R.J. Griffin, D.R. Cocker III, J.H. Seinfeld, and D. Dabdub, *Geophys. Res. Lett.*, 26, 2721-2724, 1999.

A.4.1 Introduction

Biogenic hydrocarbons emitted by vegetation play an important role in the chemistry of the urban- and regional-scale atmosphere [Fehsenfeld *et al.*, 1992]. These compounds are among the most reactive in the atmosphere as measured by their reaction rate constants with ozone (O_3) and the hydroxyl (OH) and nitrate (NO_3) radicals [Atkinson *et al.*, 1995; Shu and Atkinson, 1995; Atkinson, 1997]. Biogenic hydrocarbons contribute to tropospheric ozone formation in regions of extensive vegetation [Chameides *et al.*, 1988; Roselle *et al.*, 1991] and yield relatively non-volatile secondary oxidation products that form aerosols [Hoffmann *et al.*, 1997; Griffin *et al.*, 1999].

The aerosol-forming potential of biogenic hydrocarbons was first noted by Went [1960]. However, a quantitative understanding of aerosol formation from these molecules was lacking until recently [Hoffmann *et al.*, 1997; Griffin *et al.*, 1999]. Griffin *et al.* [1999] investigated the predominant aerosol-forming compounds emitted by vegetation [Arey *et al.*, 1991, 1995; Guenther *et al.*, 1994, 1996; König *et al.*, 1995], the majority of which are monoterpenes that apparently function as defensive agents against herbivory [Lerdau, 1991]. Understanding the aerosol-forming potential of these compounds is imperative to assess the contribution of biogenically derived aerosol to regional particulate levels and the global aerosol burden.

Lioussé *et al.* [1996] included formation of organic aerosol from biogenic precursors in their global study of carbonaceous aerosols; they employed a constant aerosol yield of 5% for all biogenic species except isoprene, which does not form aerosol upon oxidation. Based on previous chamber data, Andreae and Crutzen [1997] provided an estimate of the global amount of aerosol formed annually from biogenic precursors of

30 to 270 Tg yr⁻¹. Recent work has expanded greatly the understanding of secondary organic aerosol (SOA) formation beyond that available to *Andreae and Crutzen* [1997]. Accounting for new data on the aerosol-forming potential of biogenic organics, spatially and temporally resolved, compound-specific global emissions profiles, and the nonlinear nature of SOA formation allows for a sharpening of this estimate.

A.4.2 Secondary Organic Aerosol Formation

Experiments investigating the aerosol-forming potential of 14 biogenic compounds have been described previously [*Hoffmann et al.*, 1997; *Griffin et al.*, 1999]. SOA forms through adsorptive and/or absorptive condensation or nucleation of products of gas-phase hydrocarbon oxidation [*Pankow*, 1994; *Odum et al.*, 1996]. The SOA yield, Y , defined as the dimensionless ratio of the mass concentration of SOA formed, ΔM_o , to the mass concentration of the parent hydrocarbon reacted, measures the aerosol-forming potential of a compound. Gas-aerosol partitioning of oxidation products depends on the mass concentration of an absorbing organic phase. As a result, Y is a function of the final equilibrium organic mass concentration of this absorbing phase, M_o ($\mu\text{g m}^{-3}$). For the experiments considered, M_o equals ΔM_o as the absorbing medium is generated completely by the parent hydrocarbon oxidation. The relationship between Y and M_o is

$$Y = M_o \sum_i \left(\frac{\alpha_i K_{om,i}}{1 + K_{om,i} M_o} \right) \quad (\text{A.4.1})$$

where α_i is the mass-based stoichiometric yield of oxidation product i and $K_{om,i}$ ($\text{m}^3 \mu\text{g}^{-1}$) is the gas-particle equilibrium coefficient that describes the partitioning of oxidation

product i between the absorbing organic aerosol phase and the gas phase [Pankow, 1994; Odum *et al.*, 1996]. Yield data for over 30 individual aromatic and biogenic parent hydrocarbons have been fit to equation (A.4.1) on the basis of a two-product model, that is, by parameters α_1 , α_2 , $K_{om,1}$, and $K_{om,2}$ [Odum *et al.*, 1996, 1997; Hoffmann *et al.*, 1997; Griffin *et al.*, 1999]. Many products capable of partitioning into the aerosol phase are formed during the atmospheric oxidation of such hydrocarbons [Yu *et al.*, 1998].

However, the remarkably close fit of yield data to equation (A.4.1) for the compounds studied indicates that two generic products approximate well the stoichiometry and volatility of the final product mix. While yield scales linearly with M_o in the range of atmospheric applicability (small M_o), experiments must be performed over the entire range of organic mass concentrations to obtain the yield parameters for each parent hydrocarbon (See Table A.4.1.). Calculated yields are also shown in Table A.4.1 for values of M_o between 5 and 40 $\mu\text{g m}^{-3}$. These yields encompass the range of 5-40% used by Andreae and Crutzen [1997].

A.4.3 Individual Oxidant Contributions to Aerosol Formation

The unsaturated carbon-carbon bonds inherent to the monoterpene structure induce a high level of reactivity with OH, NO₃, and O₃. At NO_x levels characteristic of chamber photooxidation experiments, NO₃ contributes significantly to oxidation if a sufficient amount of NO₃ forms prior to complete consumption of the hydrocarbon by OH and O₃. Of the compounds of interest, this is the case only for α -pinene, β -pinene, Δ^3 -carene, and sabinene.

In remote areas, NO₃ concentrations are expected to be very low as there is little impact from anthropogenic NO_x sources. Therefore, in order to extrapolate smog

chamber data to ambient conditions for these four bicyclic alkenes, the contribution of NO_3 to chamber aerosol formation must be removed from that measured. To do so, the amount of parent hydrocarbon that reacted with each oxidant in each experiment must be determined. Despite the complexity of the gas-phase chemistry in these experiments, it is possible to simulate hydrocarbon consumption patterns using the SAPRC90b chemical mechanism of *Carter* [1990].

In order to assess the importance of each oxidant to aerosol formation for the bicyclic alkenes, experiments in which either O_3 or NO_3 was the only available oxidant (a scavenger was used to consume any OH formed in the O_3 -alkene reaction) were performed in the dark, but at daytime temperatures. On the basis of the resulting yield information for single-oxidant systems and the gas-phase simulations, it is possible to determine the amount of organic aerosol formed from reaction with each oxidant in full-photooxidation experiments [*Hoffmann et al.*, 1997; *Griffin et al.*, 1999]. By subtracting the NO_3 contribution, yield parameters for aerosol formation in the absence of NO_3 for bicyclic alkenes have been developed (Table A.4.1).

In order to extrapolate chamber data to the ambient, it is important to determine if the relative hydrocarbon oxidation by OH and O_3 observed in the chamber is consistent with that expected in the ambient. Global average estimates of 50 ppbv for O_3 and 2.6×10^6 molecules cm^{-3} for OH do lead to relative hydrocarbon consumption patterns similar to those observed in the smog chamber for bicyclic alkenes [*Griffin et al.*, 1999] (Table A.4.2). Therefore, we assume that relative consumption patterns for the other biogenic parent compounds studied in the chamber will approximate those expected in the ambient. Because the hydrocarbon oxidation consumption patterns seen in

experiments are similar to those derived using global-average oxidant concentrations, further oxidation of first-generation products in the chamber should mimic appropriately such reactions occurring in the ambient. *Yu et al.* [1998] have shown evidence of these reactions in our chamber. Thus, it can be assumed that the aerosol yield parameters in Table A.4.1 can be used to describe ambient aerosol formation even though experimental conditions do not mimic exactly ambient conditions in all situations. While it is expected that aerosol yield will decrease with increasing temperature, there are currently no quantitative data available to describe this phenomenon. Therefore, the parameters given here (derived for an average temperature of 310K) are used in all cases. Given that the majority of biogenic emissions occur in hot, tropical regions, this assumption may not induce a large amount of error.

A.4.4 Compound-Specific Emissions Inventory for Biogenic Compounds

Because the biogenic species considered exhibit a wide range of SOA yields, it is necessary to assess global-scale emissions of the most important monoterpenes and other reactive volatile organic compounds (ORVOC) in order to estimate the amount of global, biogenically derived SOA formed annually. The global emissions of monoterpenes and ORVOC have been estimated by ecosystem [*Guenther et al.*, 1995]. By determining the predominant plant species associated with these ecosystems and identifying and quantifying the specific monoterpene and ORVOC emissions from these individual species [*Arey et al.*, 1991, 1995; *Guenther et al.*, 1994, 1996; *König et al.*, 1995], the contributions of individual compounds to emissions of monoterpenes or ORVOC on a global scale can be inferred (Table A.4.3). Less important compounds are grouped with others expected to have similar aerosol-forming potentials.

By applying the contributions of each species listed in Table A.4.3 to the emissions in each $5^\circ \times 5^\circ$ horizontal cell in a global model, a compound-specific and temporally and spatially resolved emissions profile for monoterpenes and ORVOC is established. These emissions are converted to concentration units by using appropriate reactive layer heights specific to each compound. These heights are derived from an estimate of vertical eddy diffusivity [Seinfeld and Pandis, 1998] and appropriate time scales inferred from reaction rate constants and OH and O_3 concentrations simulated by IMAGES [Müller and Brasseur, 1995]. IMAGES oxidant concentrations are given for specific times and, if needed, are scaled by factors ranging from 3 to 10 to reflect values at times when oxidation, and therefore aerosol formation, is expected to be maximum [Mount *et al.*, 1997]. Because biogenic emissions are given as hourly averages for each month, diurnal oxidant concentration is neglected, and each scaled value is used for an entire day. Vertical cells are thus defined by increasing values of the scale heights for the compounds of interest. For example, the lowest three-dimensional cell, in which all compounds are present and well mixed, has a height equal to the scale height of the most reactive compound. The second cell will then extend from the top of the first cell to the scale height of the second most reactive compound. In this second cell, all compounds except the most reactive are present. This development of vertical cell heights is extended until the scale height of the least reactive compound is reached. These vertical cell heights are derived for each surface cell since OH and O_3 levels vary spatially. For simplicity, ground level concentrations of OH and O_3 are used. NO_3 is assumed not to contribute to oxidation.

Since the formation of organic aerosol depends on the relative amounts of monoterpenes and ORVOC emitted, a second emissions scenario was constructed by using the other major biogenic inventory of *Guenther et al.* [1995]. In the second scenario, emissions of each species in each cell were found simply by using the ratio of emission values predicted by *Müller* [1992] and *Guenther et al.* [1995] (See Table 3.3.). The major difference between these two estimates is that *Guenther et al.* [1995] predict almost three times as much ORVOC emission as *Müller* [1992]. *Andreae and Crutzen* [1997] considered an annual emissions rate of 300-500 Tg C yr⁻¹, which is greater than that predicted by *Müller* [1992] and essentially equal to that predicted by *Guenther et al.* [1995] (See Table A.4.3.).

A.4.5 Global Aerosol Formation from Biogenic Hydrocarbons

Individual α_i and $K_{om,i}$ values have been shown to simulate the amount of SOA formed from mixtures as complex as evaporated gasoline [*Odum et al.*, 1997]. M_{oT} , the mass concentration of SOA formed from the oxidation of the mixture of n hydrocarbons, can be found by solving

$$\sum_j^n \left[\Delta \text{HC}_j \sum_i \left(\frac{\alpha_{i,j} K_{om,i,j}}{1 + K_{om,i,j} M_{oT}} \right) \right] = 1 \quad (\text{A.4.2})$$

where ΔHC_j is the concentration of parent compound j reacted. To estimate the M_{oT} in each cell from biogenic compounds, equation (A.4.2) is used with the yield parameters from Table A.4.1 and the daily biogenic concentrations derived in each cell. The yield parameters of sabinene were used for ten-carbon, bicyclic terpenoid ketones because each

species exhibits an exocyclic double bond. Yield parameters for aromatics with multiple methyl groups were employed for aromatics [Odum *et al.*, 1997]. First, the compounds listed in Table A.4.1 and these aromatics and ketones are considered. If the left-hand side is greater than unity for M_{OT} equal to zero, equation (A.4.2) is solved iteratively to find the appropriate M_{OT} for the cell of interest. (Otherwise, M_{OT} is set to zero for that cell.) In the non-zero cases, additional SOA formation from straight-chain olefins and carbonyls is considered. For these two classes, a flat yield of 5% is assumed for SOA formation [Wang *et al.*, 1991]. The concentration of SOA formed in each cell is thus calculated on a daily basis, converted to mass using cell volume, and summed spatially to provide the global daily amount of SOA formed. At the end of each day, it is assumed that the SOA is released to the free troposphere. The amount of SOA generated from the oxidation of biogenic species annually is found by summing the results of each day of the year.

Using the emissions profiles of both Guenther *et al.* [1995] and Müller [1992] to account for possible differences in the distribution between monoterpenes and ORVOC, the estimated range of global biogenically derived SOA is 13-24 Tg yr⁻¹. In the absence of additional information, the best estimate can be taken as the average, 18.5 Tg yr⁻¹. The range estimated here is likely a lower bound since products of biogenic oxidation will partition to primary organic aerosol mass and anthropogenic SOA.

The majority of this biogenically derived SOA will be formed in forested regions. However, because of their extensive conversion to aerosol, biogenic hydrocarbons can also contribute substantially to aerosol burdens in any areas with significant vegetation. On average, if a one-week lifetime is assumed, the predicted burden of SOA from biogenic oxidation is 0.36 Tg, which is slightly less than but of the same order of

magnitude as the predicted burdens for primary carbonaceous aerosols from biomass and fossil fuel burning [Lioussse *et al.*, 1996]. This burden is smaller than those predicted for sea salt, soil dust, and sulfate aerosols but is the same order of magnitude as those predicted for black carbon, nitrate, and ammonium aerosols [Tegen *et al.*, 1997; Adams *et al.*, 1999].

A.4.6 References

- Adams, P.J., J.H. Seinfeld, and D.M. Koch, Global concentrations of tropospheric sulfate, nitrate, and ammonium aerosol simulated in a general circulation model, *J. Geophys. Res.*, *104*, 13,791-13,823, 1999.
- Andreae, M.O., and P.J. Crutzen, Atmospheric aerosols: Biogeochemical sources and role in atmospheric chemistry, *Science*, *276*, 1052-1058, 1997.
- Arey, J., D.E. Crowley, M. Crowley, M. Resketo, and J. Lester, Hydrocarbon emissions from natural vegetation in California's South Coast Air Basin, *Atmos. Environ.*, *29*, 2977-2988, 1995.
- Arey, J., A.M. Winer, R. Atkinson, S.M. Aschmann, W.D. Long, C.L. Morrison, and D.M. Olszyk, Terpenes emitted from agricultural species found in California's Central Valley, *J. Geophys. Res.*, *96*, 9329-9336, 1991.
- Atkinson, R., Gas-phase tropospheric chemistry of organic compounds, 1, Alkanes and alkenes, *J. Phys. Chem. Ref. Data*, *26*, 215-290, 1997.
- Atkinson, R., J. Arey, S.M. Aschmann, S.B. Corchnoy, and Y.H. Shu, Rate constants for the gas-phase reactions of *cis*-3-hexen-1-ol, *cis*-3-hexenylacetate, *trans*-2-hexenal, and linalool with OH and NO₃ radicals and O₃ at 296 ± 2K and OH radical formation yields from the O₃ reactions, *Int. J. Chem. Kinet.*, *27*, 941-955, 1995.

Carter, W.P.L., A detailed mechanism for the gas-phase atmospheric reactions of organic compounds, *Atmos. Environ.*, *24A*, 481-518, 1990.

Chameides, W.L., R.W. Lindsay, J. Richardson, and C.S. Kiang, The role of biogenic hydrocarbons in urban photochemical smog: Atlanta as a case study, *Science*, *241*, 1473-1475, 1988.

Fehsenfeld, F., et al., Emissions of volatile organic compounds from vegetation and the implications for atmospheric chemistry, *Global Biogeochem. Cycles*, *6*, 389-430, 1992.

Griffin, R.J., D.R. Cocker III, R.C. Flagan, and J.H. Seinfeld, Organic aerosol formation from the oxidation of biogenic hydrocarbons, *J. Geophys. Res.*, *104*, 3555-3567, 1999.

Guenther, A., et al., A global model of natural volatile organic compound emissions, *J. Geophys. Res.*, *100*, 8873-8892, 1995.

Guenther, A., L. Otter, P. Zimmerman, J. Greenberg, R. Scholes, and M. Scholes, Biogenic hydrocarbon emissions from southern African savannas, *J. Geophys. Res.*, *101*, 25,859-25,865, 1996.

Guenther, A., P. Zimmerman, and M. Wildermuth, Natural volatile organic compound emission rate estimates for U.S. woodland landscapes, *Atmos. Environ.*, *28*, 1197-1210, 1994.

Hoffmann, T., J.R. Odum, F. Bowman, D. Collins, D. Klockow, R.C. Flagan, and J.H. Seinfeld, Formation of organic aerosols from the oxidation of biogenic hydrocarbons, *J. Atmos. Chem.*, *26*, 189-222, 1997.

- König, G., M. Brunda, H. Puxbaum, C.N. Hewitt, S.C. Duckham, and J. Rudolph, Relative contribution of oxygenated hydrocarbons to the total biogenic VOC emissions of selected mid-European agricultural and natural plants, *Atmos. Environ.*, 29, 861-874, 1995.
- Lerdau, M.T., Plant function and biogenic terpene emission, in *Trace Gas Emissions by Plants*, edited by T.D. Sharkey, et al., pp. 121-134, Academic Press, Inc., San Diego, 1991.
- Liousse, C., J.E. Penner, C. Chuang, J.J. Walton, H. Eddleman, and H. Cachier, A global three-dimensional model study of carbonaceous aerosols, *J. Geophys. Res.*, 101, 19,411-19,432, 1996.
- Mount, G.H., F.L. Eisele, D.J. Tanner, J.W. Brault, P.V. Johnston, J.W. Harder, E.J. Williams, A. Fried, and R. Shetter, An intercomparison of spectroscopic laser long-path and ion-assisted *in situ* measurements of hydroxyl concentrations during the Tropospheric OH Photochemistry Experiment, fall 1993, *J. Geophys. Res.*, 102, 6437-6455, 1997.
- Müller, J.F., Geographical distribution and seasonal variation of surface emissions and deposition velocities of atmospheric trace gases, *J. Geophys. Res.*, 97, 3787-3804, 1992.
- Müller, J.F., and G.P. Brasseur, IMAGES - a 3-dimensional chemical-transport model of the global troposphere, *J. Geophys. Res.*, 100, 16445-16490, 1995.
- Odum, J.R., T.P.W. Jungkamp, R.J. Griffin, R.C. Flagan, and J.H. Seinfeld, The atmospheric aerosol-forming potential of whole gasoline vapor, *Science*, 276, 96-99, 1997.

- Odum, J.R., T. Hoffmann, F. Bowman, D. Collins, R.C. Flagan, and J.H. Seinfeld, Gas/particle partitioning and secondary organic aerosol yields, *Environ. Sci. Technol.*, **30**, 2580-2585, 1996.
- Pankow, J.F., An absorption model of gas/particle partitioning of organic compounds in the atmosphere, *Atmos. Environ.*, **28**, 185-189, 1994.
- Roselle, S.J., T.E. Pierce, and K.L. Schere, The sensitivity of regional ozone modeling to biogenic hydrocarbons, *J. Geophys. Res.*, **96**, 7371-7394, 1991.
- Seinfeld, J.H., and S.N. Pandis, *Atmospheric Chemistry and Physics: From Air Pollution to Climate Change*, John Wiley and Sons, Inc., New York, 1998.
- Shu, Y., and R. Atkinson, Atmospheric lifetimes and fates of a series of sesquiterpenes, *J. Geophys. Res.*, **100**, 7275-7281, 1995.
- Tegen, I., P. Hollrig, M. Chin, I. Fung, D. Jacob, and J. Penner, Contribution of different aerosol species to the global aerosol extinction optical thickness: Estimates from model results, *J. Geophys. Res.*, **102**, 23,895-23,915, 1997.
- Wang, S.-C., S.E. Paulson, D. Grosjean, R.C. Flagan, and J.H. Seinfeld, Aerosol formation and growth in atmospheric organic/NO_x systems - I. Outdoor smog chamber studies of C₇- and C₈- hydrocarbons, *Atmos. Environ.*, **26A**, 403-420, 1992.
- Went, F.W., Blue hazes in the atmosphere, *Nature*, **187**, 641-643, 1960.
- Yu, J., R.C. Flagan, and J.H. Seinfeld, Identification of products containing -COOH, -OH, and -C=O in atmospheric oxidation of hydrocarbons, *Environ. Sci. Technol.*, **32**, 2357-2370, 1998.

Table A.4.1. Aerosol yield parameters for biogenic organics.

Parent	α_1	α_2	$K_{om,1}$	$K_{om,2}$	Yield
Δ^3 -Carene	0.057	0.476	0.063	0.0042	2.3-10.9%
β -Caryophyllene	1.000	N/A	0.0416	N/A	17.2-62.5%
α -Humulene	1.000	N/A	0.0501	N/A	20.0-66.7%
Limonene	0.239	0.363	0.055	0.0053	6.1-22.8%
Linalool	0.073	0.053	0.049	0.0210	1.9-7.3%
Myrcene ¹	0.100	0.275	0.513	0.0032	7.6-12.7%
Ocimene	0.045	0.149	0.174	0.0041	2.4-6.0%
α -Pinene ²	0.038	0.326	0.171	0.0040	2.4-7.8%
β -Pinene	0.113	0.239	0.094	0.0051	4.2-13.0
Sabinene	0.060	0.376	0.406	0.0038	4.7-10.6%
α - & γ -Terpinene	0.091	0.367	0.081	0.0046	3.4-12.7%
Terpinene-4-ol	0.049	0.063	0.159	0.0045	2.3-5.2%
Terpinolene	0.046	0.034	0.185	0.0024	2.3-4.4%

¹These values are an estimate as only two experiments were performed. ²SOA formation by NO₃ oxidation is negligible [Griffin *et al.*, 1999].

Table A.4.2. OH and O₃ oxidation patterns for bicyclic alkenes.

Parent	Chamber		Global Average	
	O ₃	OH	O ₃	OH
Δ^3 -Carene	18.0%	82.0%	16.2%	83.8%
α -Pinene	41.1%	58.9%	42.5%	57.5%
β -Pinene	12.6%	87.4%	8.0%	92.0%
Sabinene	16.9%	83.1%	25.2%	74.8%

Table A.4.3. Estimated species contributions to global emissions.

MONOTERPENES		ORVOC	
Monoterpene ¹	Contribution	ORVOC ²	Contribution
α -Pinene	35%	Terpenoid	9%
β -Pinene	23%	C ₇ -C ₁₀ <i>n</i> -	7%
Limonene	23%	Aromatics	6%
Myrcene	5%	Sesquiterpenes	5%
Sabinene	5%	Terpenoid Ketones	4%
Δ^3 -Carene	4%	Higher Olefins	1%
Ocimene	2%		
Terpinolene	2%		
α - & γ -Terpinene	1%		

¹*Guenther et al.* [1995] estimate a total monoterpene emission rate of 127 TgC yr⁻¹; *Müller* [1992] estimates 147 Tg yr⁻¹. ²Only those capable of forming aerosol are included; *Guenther et al.* [1995] estimate an ORVOC emission rate of 260 TgC yr⁻¹; *Müller* [1992] estimates 94 Tg yr⁻¹